Characterising the stress response of the heart in Heart Failure with Preserved Ejection Fraction using Magnetic Resonance Imaging and Spectroscopy

ROSHAN XAVIER

Exeter College
University of Oxford

A thesis submitted in partial fulfilment of the requirements for the degree of Doctor of Philosophy in Medical Sciences

DECLARATION

This thesis is entirely my own work unless otherwise indicated. It has not been submitted, either wholly or substantially, for another degree at this university, or for a degree at any other institution. I have acknowledged assistance from colleagues and collaborators where relevant.

The word count, not including references, abstract, diagrams, tables and front matter is 30,367.

ABSTRACT

Heart failure with preserved ejection fraction (HFpEF) is growing to be one of the most significant contributors to morbidity and mortality in the 21st century with increasing unmet need as the population ages and the prevalence of metabolic diseases increase. Numerous clinical trials have demonstrated heterogeneity in effect suggesting the existence of different endotypes of HFpEF. Given symptoms often arise only during exercise, further research into exercise responses of such endotypes and the biology that underpins them is necessary. Moreover, given the likely alterations in cardiac metabolism induced by many of the contributory risk factors, study of cardiac energetics and substrate utilisation may provide new therapeutic targets.

In chapter 3, I evaluate the exercise responses of HFpEF compared to older controls using multi-modality exercise imaging and the underlying molecular milieu using aptamer-based proteomics performed on plasma acquired following exercise. I then examine the heterogeneity within HFpEF and compare 2 groups dichotomised by an LV ejection fraction greater or lower than 60%. Here, I demonstrate that $HFpEF_{EF>60}$ is characterised by smaller hearts with reduced stroke volume and cardiac output at rest despite increased LVEF. They exhibit impaired cardiac contractile reserve and reduced functional capacity. Plasma proteomics following exercise reveals both commonalities and distinct abnormalities within each HFpEF endotype when compared to controls. While the $HFpEF_{EF<60}$ group exhibit additional perturbations in extracellular matrix, RNA processing, signalling and inflammatory pathways, both endotypes exhibit alterations in lipid metabolism.

In chapter 4, myocardial energetics in HFpEF is studied in greater detail using ^{31}P phosphorus spectroscopy and saturation transfer techniques to measure PCr/ATP and CK activity alongside exercise CMR and echocardiography. CK flux is shown to be impaired in HFpEF and both CK flux and the forward rate constant at rest are shown to be linked to a number of metrics of cardiac function at rest and during exercise, ultimately being linked to cardiac output during exercise.

In chapter 5, the effect of altering substrate provision and utilisation is examined. Intralipid administration results in impaired cardiac energetics and CK flux without any major changes in cardiac function. In contrast, ketonaemia results in improved

systolic and diastolic function with preservation of energetics, potentially increased ATP delivery and afterload reduction. Substrate switching to glucose results in minimal effects in comparison.

Overall, the data demonstrates that exercise responses are diminished in HFpEF and likely underlie symptoms during daily exertion. Different haemodynamic endotypes exist with distinct morphology, exercise reserve and plasma proteomic signatures. Impairment in ATP delivery is seen in HFpEF with strong associations with cardiac function at rest and stress. Substrate switching is capable of altering this in both positive and detrimental ways indicating that myocardial metabolism is a therapeutic target in HFpEF.

PUBLICATIONS and ABSTRACTS

Publications

1. **Exploring cardiovascular involvement in IgG4-related disease: a case series approach with cardiovascular magnetic resonance**
   JA Henry, R Xavier, E Selvaraj, M Burrage, KE Thomas, E Lukaschuk, Q Zhang, VM Ferreira, SK Piechnik, S Neubauer, OJ Rider, EL Culver, AJM Lewis.
   Heart, 2025

Presented abstracts

1. **Exercise CMR and proteomic characterization of HFpEF across the spectrum of LV ejection fraction**
   R Xavier, SM Ng, J Pan, PM Arvidsson, JJ Miller, FE Mózes, L Valkovič, J Rayner, WD Watson, M Rigolli, M Fronheiser, S Neubauer, AJM Lewis, OJ Rider
   Early Career Award winning presentation – Translation session SCMR 2025

2. **HFpEF with resting LVEF >60% exhibit a distinct exercise response and circulating proteome to HFpEF with LVEF <60%**
   R Xavier, SM Ng, J Pan, JJ Miller, FE Mózes, L Valkovič, J Rayner, M Rigolli, M Fronheiser, S Neubauer, OJ Rider, AJM Lewis
   American Heart Association Nov 2024

3. **Investigating the role of the right ventricle in HFpEF using exercise CMR**
   R Xavier, SM Ng, J Pan, JJ Miller, FE Mózes, L Valkovič, J Rayner, M Rigolli, M Fronheiser, S Neubauer, AJM Lewis, OJ Rider
   Global CMR (SCMR/EACVI) 2024 Oral Presentations session

4. **Novel endotypes in HFpEF identified using exercise stress CMR and machine learning**
   R Xavier, SM Ng, J Pan, JJ Miller, FE Mózes, L Valkovič, J Rayner, M Rigolli, M Fronheiser, S Neubauer, OJ Rider, AJM Lewis
   Global CMR (SCMR/EACVI) 2024 Rapid Fire Abstract session.

ACKNOWLEDGEMENTS

The work that led to the thesis would not have been possible without the aid and support of a number of colleagues and organisations.

First and foremost, I would like to thank my supervisors Prof Oliver Rider, Dr Andrew Lewis and Prof Stefan Neubauer for their invaluable guidance and support throughout the period of study. I would also like to extend special thanks to Dr Sher May Ng and Dr Jiliu Pan with whom I co-ran nearly all the study visits and were instrumental to carrying out the experiments. A number of other colleagues and collaborators at both OCMR and in other departments and institutions also provided valuable input into this work including Prof Ladislav Valkovič, Dr Ferenc Mózes, Dr William Watson, Dr Jennifer Rayner, Dr Jack Miller, Dr Per Arvidsson, Dr Matthew Fronheiser and Dr Marzia Rigolli. I also owe thanks to the entire team at OCMR including all the research fellows, research nurses, clinical and administrative staff who have unwaveringly offered their help throughout.

I would like to thank the funding bodies including the excellent collaborative partnership established between the University of Oxford and Bristol Myers Squibb through means of a fellowship as well as funding from the British Heart Foundation. The patients who generously provided their time and effort were critical to this endeavour.

Finally, I would like to thank my wife Chandni whose own commitment and work ethic has been inspirational and my parents for their continuous support and encouragement throughout these last few years and long before.

Table of Contents

List of Tables

List of figures

List of abbreviations

6MWT	6-minute Walk Test
ACAT	Acetyl-CoA Acetyltransferase
ACBP	Acyl-CoA Binding Protein
ACE	Angiotensin Converting Enzyme
ACS	Acyl-CoA Synthetase
ADP	Adenosine Diphosphate
AF	Atrial Fibrillation
AGAT	Arginine-Glycine Amidino Transferase
AHP	Adiabatic Half-passage Pulse
AMARES	Advanced Method for Accurate, Robust and Efficient Spectral Fitting
AMP	Adenosine Monophosphate
ARNi	Angiotensin Receptor/Neprilysin Inhibitor
ATP	Adenosine Triphosphate
BCAA	Branched Chain Amino Acid
BCAT	Branched Chain Amino-Transaminase
BCKA	Branched Chain α-Keto-Acid
BCKDH	Branched Chain α-Keto-Acid Decarboxylase
BDH	βOHB dehydrogenase
BMI	Body Mass Index
BNP	B-type Natriuretic Peptide
βOHB	Beta - Hydroxybutyrate
BP	Blood Pressure

BSA	Body Surface Area
C4	Complement component 4
CK	Creatine Kinase
CKD	Chronic Kidney Disease
CMR	Cardiac Magnetic Resonance
CO	Cardiac Output
CPT	Carnitine Palmitoyl Transferase
CS	Coronary Sinus
CSI	Chemical Shift Imaging
CVP	Central Venous Pressure
DAG	Diacylglycerol
DANTE	Delayed Alternating with Nutation for Tailored Excitation
DBP	Diastolic Blood Pressure
DCM	Dilated Cardiomyopathy
DLCO	Diffusion Capacity for Carbon Monoxide
DNA	Deoxyribonucleic acid
DOCP	Desoxycorticosterone Pivalate
DPG	Diphosphoglycerate
DPP	Dipeptidyl Peptidase
DRESS	Depth Resolved Surface coil Spectroscopy
ECG	Electrocardiogram
EDTA	Ethylenediamin Tetra-acetic Acid
EDV	End Diastolic Volume
EF	Ejection Fraction

ELISA	Enzyme-Linked Immuno-Sorbent Assay
ERR	Estrogen Related Receptor
ESC	European Society of Cardiology
ESV	End Systolic Volume
ETC	Electron Transport Chain
FABP	Fatty Acid Binding Protein
FAD	Flavin Adenine Dinucleotide
FAO	Fatty Acid Oxidation
FAT	Fatty Acid Translocase
FC	Fold Change
FDR	False Discovery Rate
FEV	Forced Expiratory Volume
FFA	Free Fatty Acid
FID	Free Induction Decay
FOV	Field of View
FVC	Forced Vital Capacity
G6P	Glucose-6-Phosphate
GAMT	Guanidinoacetate Methyltransferase
GDF	Growth differentiation factor
GE	General Electric
GLP	Glucagon Like Peptide
GLS	Global Longitudinal Strain
GLUT	Glucose Transporter
HIF	Hypoxia Inducible Factor

HLA	Horizontal Long Axis
HMG-CoA	Hydroxymethylglutaryl-CoA
HMGCL	Hydroxymethylglutaryl-CoA Lyase
HMGCS2	Hydroxymethylglutaryl-CoA Synthase 2
HOMA-IR	Homeostatic Model Assessment for Insulin Resistance
HR	Heart Rate
IGF	Insulin-like Growth Factor
ILR1	Interleukin Receptor 1
IR	Inversion Recovery
KCCQ	Kansas City Cardiomyopathy Questionnaire
KCO	Carbon Monoxide Transfer Coefficient
LA	Left Atrium
LAEDV	Left Atrial End Diastolic Volume
LAEF	Left Atrial Emptying Fraction
LAESV	Left Atrial End Systolic Volume
LCFA	Long Chain Fatty Acid
LDH	Lactate Dehydrogenase
LV	Left Ventricle
LVEDP	Left Ventricular End Diastolic Pressure
LVEDV	Left Ventricular End Diastolic Volume
LVEF	Left Ventricular Ejection Fraction
LVESV	Left Ventricular End Systolic Volume
LVH	Left Ventricular Hypertrophy
LVM	Left Ventricular Mass

LVSV	Left Ventricular Stroke Volume
MAP	Mean Arterial Pressure
MCT	Mono-Carboxylate Transporter
MPC	Mitochondrial Pyruvate Carrier
MRI	Magnetic Resonance Imaging
MRS	Magnetic Resonance Spectroscopy
NAD	Nicotinamide Adenine Dinucleotide
NADPH	Nicotinamide Adenine Dinucleotide Phosphate
NEFA	Non-Esterified Fatty Acid
NHS	National Health Service
NMR	Nuclear Magnetic Resonance
NTproBNP	N-terminal pro-B-type natriuretic peptide
NYHA	New York Heart Association
PASP	Pulmonary Artery Systolic Pressure
PC	Phase Contrast
PCr	Phosphocreatine
PCWP	Pulmonary Capillary Wedge Pressure
PDH	Pyruvate Dehydrogenase
PDK	Pyruvate Dehydrogenase Kinase
PEA	Proximity Extension Assay
PGC1	PPAR Gamma Coactivator
PH	Pulmonary Hypertension
PPA	Phenylphosphonic Acid
PPAR	Peroxisome Proliferator Activated Receptor

PVR	Pulmonary Vascular Resistance
RA	Right Atrium
RAAS	Renin-Angiotensin-Aldosterone System
RAEDV	Right Atrial End Diastolic Volume
RAEF	Right Atrial Emptying Fraction
RAESV	Right Atrial End Systolic Volume
REC	Research Ethics Committee
RFU	Relative Fluorescence Unit
RNA	Ribonucleic Acid
ROS	Reactive Oxygen Species
RPP	Rate Pressure Product
RV	Right Ventricle
RVEDV	Right Ventricular End Diastolic Volume
RVEF	Right Ventricular Ejection Fraction
RVESV	Right Ventricular End Systolic Volume
RVSV	Right Ventricular Stroke Volume
SAR	Specific Adsorption Rate
SBP	Systolic Blood Pressure
SCOT	Succinyl-CoA:3-oxoacid CoA transferase
SERCA	Sarcoplasmic/Endoplasmic Reticulum Calcium ATPase
SGLT	Sodium-dependent Glucose Cotransporter
SLAM	Spectroscopy with Linear Algebraic Modelling
SSFP	Steady State Free Precession
SST	Serum Separator Tube

STEAM	Stimulated Echo Acquisition Mode
SV	Stroke Volume
TAG	Triacylglyercol
TAPSE	Tricuspid Annular Plane Systolic Excursion
TCA	Tricarboxylic acid
TE	Echo Time
TNF	Tumour Necrosis Factor
TNFR1	Tumour Necrosis Factor Receptor
TR	Repetition Time
UK	United Kingdom
USA	United States of America
VA	Alveolar Volume
VENC	Velocity Encoding
VLA	Vertical Long Axis
VLDL	Very Low Density Lipoprotein
VO2	Oxygen consumption
XBP1	X-box-binding protein

CHAPTER 1: INTRODUCTION

1.1 HEART FAILURE WITH PRESERVED EJECTION FRACTION – AN OVERVIEW

Heart failure with preserved ejection fraction (HFpEF) is increasing in both incidence and prevalence in the western world and accounts for half of newly diagnosed cases of heart failure[1]. This mirrors a rise in the ageing population, obesity, diabetes and hypertension. Despite having a similarly poor prognosis to heart failure with reduced ejection fraction (HFrEF), therapeutic options remain scarce in comparison[2]. There is an unmet need for novel medicines as well as biomarkers to assist in their development in HFpEF.

1.1.1 The pathophysiology of HFpEF at a macroscopic level

HFpEF can be defined as the inability of the heart to provide adequate cardiac output without a pathological rise in left ventricular filling pressures in the presence of a left ventricular ejection fraction >50%[3]. This results in symptoms such as dyspnoea along with pulmonary and peripheral congestion.

The gold standard test for HFpEF is invasive haemodynamic exercise testing. Pulmonary capillary wedge pressures (PCWP) of ≥15mmHg at rest or ≥25mmHg on exercise are thresholds at which HFpEF is diagnosed[4]. Exercise testing is particularly important in the early stages of HFpEF where natriuretic peptides may not be elevated. However, this carries risks and is not available in many centres. Therefore, it is not mandated for most patients in clinical guidelines[5]. Probability based scoring methods used clinically include the HFA-PEFF and H_2FPEF scores. However, the ability of low scores to exclude HFpEF in dyspnoeic patients is limited with a large proportion missed[6].

Unlike HFrEF where the resulting symptoms and congestion appear to rely heavily on an activated neurohormonal system regardless of aetiology, understanding the pathophysiology of HFpEF has been much more challenging. There are a number of roads to the clinical syndrome of HFpEF with contributions from multiple comorbidities leading to distinct phenotypes[7].

Relationship between the heart and lung vasculature

In the normal heart, the response of the myocardium to varying loads is described by the Frank-Starling mechanism. An increase in the load on the left ventricle prior to systole leads to an increase in ventricular work. This is described as the left ventricular pre-load and in the absence of significant mitral stenosis is equivalent to the left atrial and pulmonary venous pressures at the end of diastole.

Starling also described the net flow of fluid across the capillary wall[8]. The gradient between the hydrostatic pressure within the capillary and the lower pressure in the surrounding interstitial fluid provides the main driver for the transudation of fluid. Counterbalancing this gradient is the colloid osmotic pressure within the capillary, driven by albumin in particular. This is higher than that of the interstitium and tends to keep fluid within the capillary. The balance of the forces changes along the capillary wall.

In normal physiology, transudation across the capillary wall into the interstitium occurs continuously. However, the capillary wall is relatively impervious to fluid and tightly apposed to the alveolar membrane. The lymphatic system drains excess fluid preventing any impairment of gas exchange and breathlessness.

The development of pulmonary oedema

In HFpEF, the Frank-Starling curve moves down and to the right[9]. In order to produce an equivalent level of cardiac work to that of a normal heart, a higher filling pressure is necessary. This results in a concomitant rise in the pressure within the left atrium and pulmonary capillaries. The capillary wall tension is proportional to the pressure and the radius of the capillary wall and there is an increase in the rate of transmural filtration. If this exceeds the ability of the lymphatic system to clear the fluid, then it starts to accumulate in the airspaces of the lungs. Seminal experiments in dogs have demonstrated that beyond a critical left atrial pressure, there is an almost linear correlation between the rise in left atrial pressure and the development of pulmonary congestion[10]. In order to protect against pulmonary oedema, capillary permeability may be reduced in chronic heart failure as an adaptive response[11].

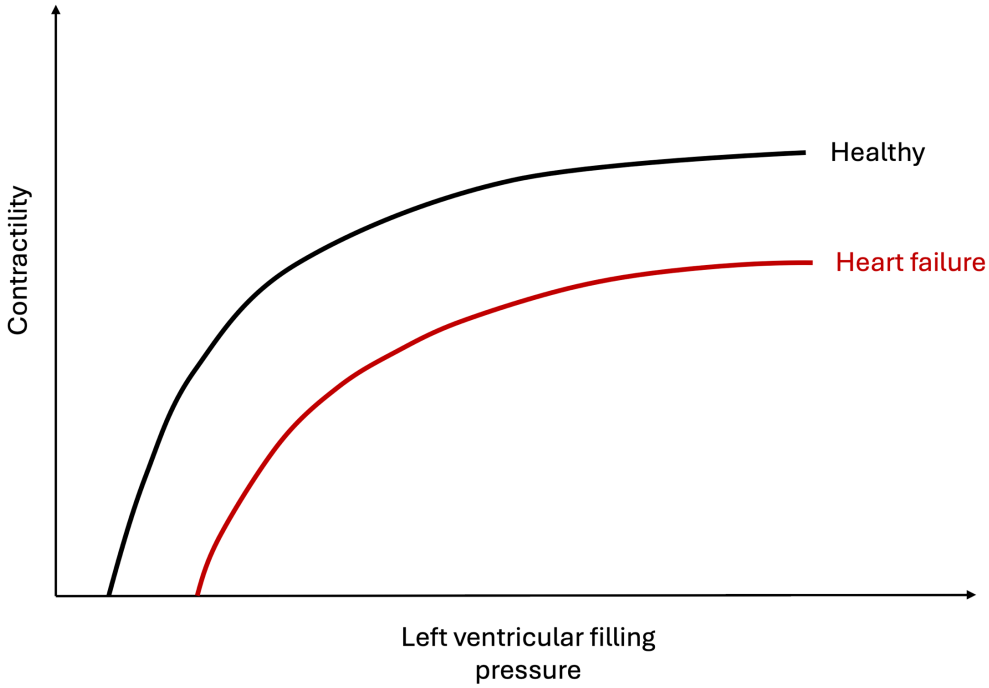

Figure 1: Frank-Starling curves in healthy hearts and those with HFpEF

Lymphatic system in pulmonary oedema

The lymphatic system plays a crucial role in the development of pulmonary oedema in heart failure. Thoracic duct lymph flow rates have been demonstrated to be increased up to 8 fold in decompensated heart failure patients[12]. Despite this, there is insufficient lymphatic clearance.

There are 2 important factors responsible for this – local resistance at the thoracic duct-jugular vein junction and central venous pressure. Experiments in sheep have demonstrated that when left atrial pressure is elevated, there is increased accumulation of pulmonary fluid when the systemic venous pressure is also elevated[13]. In addition, structural and molecular alterations have also been demonstrated in the lymphatics of skin in HFpEF patients resulting in reduced clearance of interstitial fluid - suggesting systemic involvement of the lymphatic system.

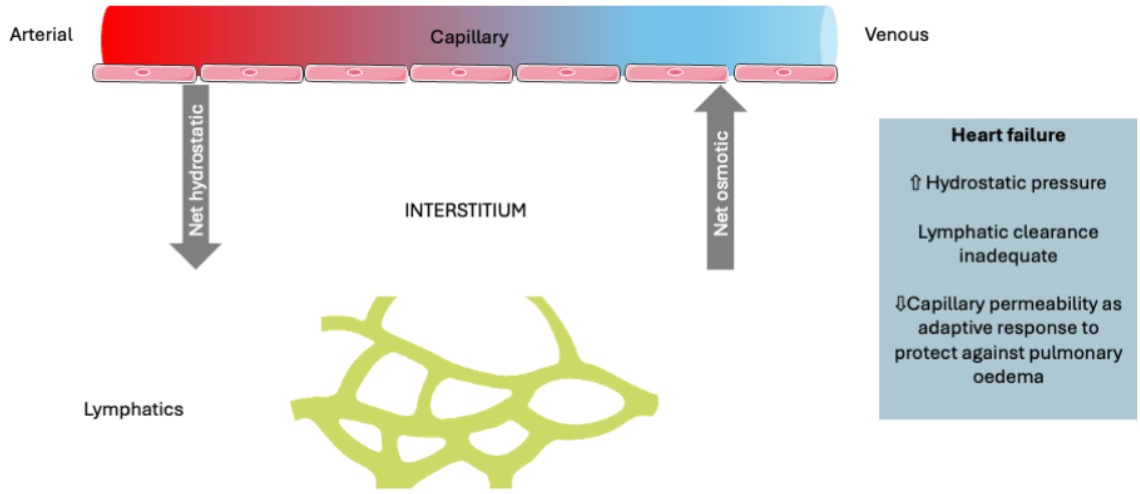

Figure 2: Capillary fluid filtration and clearance

On the arterial side, the hydrostatic pressure exceeds the osmotic pressure leading to net fluid filtration into the interstitium. On the venous side, the osmotic pressure exceeds the hydrostatic pressure leading to fluid reabsorption. The lymphatic system clears the excess fluid in the interstitium from this process and drains into the systemic venous circulation. In heart failure, there is increased hydrostatic pressure resulting in interstitial congestion beyond the capacity of the lymphatic system to clear. There is adaptive reduction in capillary permeability as a protective measure.

Impairments in left ventricular systolic and diastolic reserve

While at first glance, the systolic function in HFpEF may appear to be normal there are indicators of systolic dysfunction present even at rest. This includes subtle impairments in resting longitudinal systolic function which can be measured by tissue doppler and strain techniques on echocardiography and may confer adverse prognosis[14,15]. But it is upon exertion that the systolic abnormalities in HFpEF are truly revealed. There is thought to be an inability to contract down to a lower end systolic volume (ESV) and a failure to increase stroke volume in response to increased demand[16]. This reduction in systolic reserve leads to a blunted increase in cardiac output[17]. The resultant lower cardiac power output reserve is also associated with lower peak VO2, poorer biventricular systolic dysfunction during exercise and related to increased mortality and HF events[18].

The inability to contract down to a lower ESV also contributes directly to impaired early diastolic suction during exercise. In normal physiology, this suction effect is critical to respond to increases in venous return and depends on the speed of LV relaxation, the mitral annular motion, untwisting and the ESV[19-21]. Apart from this

dynamic part of diastole, the very earliest part of diastole is characterised by isovolumic relaxation. In HFpEF the rate of decay of pressure in this phase is reduced[22]. During exercise, this becomes even more pronounced with higher heart rates. Finally, passive diastolic stiffness of the LV also contributes to elevated filling pressures. In keeping with this, E_{ed} (end-diastolic elastance) has been shown to be increased in HFpEF[23]. Whilst traditionally thought to be secondary to elevated collagen within the extracellular matrix, the importance of the myocyte itself including the sarcomeric molecule titin has been highlighted[24]. Ultimately, left atrial pressures must go up to overcome the diastolic impairment and fill the ventricle.

Atrial dysfunction

In the early stages of HFpEF, the left atrium compensates for LV diastolic dysfunction through its reservoir, conduit and booster functions. Left atrial contraction is important to achieve LV filling in HFpEF, particularly during exercise[25]. Disease progression is characterised by LA remodelling, dilatation and loss of contractile reserve[26]. Reduction in left atrial compliance leads to increased pressure which is then transmitted to the pulmonary vascular bed[27]. Worsening atrial dysfunction in the form of bi-atrial myopathy is linked to blunted exercise cardiac output reserve with increasing central venous pressure and associated with poorer morbidity and mortality[28].

Eventually patients may develop electrical instability leading to the development of atrial fibrillation. Initially, this may be paroxysmal, followed by progression to persistent AF[29]. This further impairs compliance and mechanics. In comparison to sinus rhythm, AF leads to diminished exercise capacity in HFpEF despite similar heart rate augmentation[30]. Finally, it is associated with right atrial and right ventricular dysfunction[31].

The right ventricle, pulmonary hypertension and impaired pulmonary arterial-right ventricular coupling

Right ventricular dysfunction is frequently present in HFpEF and is associated with death and hospitalisation[32]. Similarly, pulmonary hypertension (PH) is common in HFpEF and predicts mortality[33]. This is partly caused by left atrial pressure being transmitted to the pulmonary vasculature leading to pulmonary venous

hypertension. This is termed post-capillary PH. In order to maintain a normal transpulmonary gradient (Mean pulmonary artery pressure – PCWP), there is a proportionate increase in pulmonary pressures.

Yet, this does not wholly account for the severity of PH in HFpEF. There is evidence for remodelling within the whole pulmonary vascular bed from the arteries and small vessels through to the veins[34]. This results in increased pulmonary vascular resistance (PVR) in some patients leading to combined pre- and post-capillary pulmonary hypertension[35].

This manifests itself in abnormal right ventricular-pulmonary arterial coupling (i.e. the RV systolic response to increased afterload) and is associated with exertional pulmonary oedema[36,37]. Consequentially, right ventricular failure occurs. This is unmasked only during exercise in the initial stages, but progressively becomes apparent at rest[38].

In support of this, end-systolic elastance as a load-independent marker of contractility and the RV stiffness constant β are elevated in HFpEF at rest[39]. There is also an increase in the end-diastolic pressure volume relationship which mirrors that of the LV. This contrasts with healthy individuals, where the RV exhibits significant contractile reserve and a three-fold increase in lusitropic reserve[40]. Ventricular-arterial coupling as defined by the ratio of the end-systolic elastance and the arterial elastance is preserved at all stages of exercise in controls.

In addition to invasive pressure-volume loop analysis, there are alternative non-invasive methods of measuring RV-PA coupling using imaging. Stress echocardiography derived measures such as a TAPSE/PASP have been able to predict exercise-related pulmonary hypertension in HFpEF[41]. There has also been suggestion that in those patients with an abnormal exercise pulmonary vascular resistance, impaired RV longitudinal strain is present on CMR[42]. In addition the RV stroke volume/ESV ratio provides an estimate of RV-PA coupling which can be readily measured using CMR[43].

Furthermore, right-atrial : right-ventricular coupling is also likely to be of importance[44]. Resting RV filling is compensated by increased right atrial booster function and greater filling in late diastole. The right atrial conduit function appears

to be linked to functional impairment. A rise in right atrial pressure also occurs and is likely to reflect HFpEF severity due to inter-atrial interaction rather than purely a measure of RV dysfunction[45].

In addition to these, secondary tricuspid regurgitation is often present and contributes to further congestion[46]. This may occur either as a result of RV remodelling and dilatation consequent to pulmonary hypertension or atrial remodelling as a result of atrial fibrillation. This results in a functional mechanism of regurgitation with the leaflets pulled apart from each other and is a therapeutic target for surgery or trans-catheter based therapies.

Pericardial restraint and ventricular interdependence

Total cardiac volume can increase due to right ventricular and left atrial enlargement where LV volumes are normal or due to biventricular dilatation in the context of obesity[47]. In addition, obesity is characterised by increased epicardial adipose tissue which further increases the overall volume within the pericardium[48]. Within the pericardium, this acts to increase coupling with the heart, promoting ventricular interdependence. Here, the increased right heart volume acts to impede left ventricular filling, leading to an increase in LV filling pressures. 20-40% of the LV cavity pressure may be related to this[49]. These features are exacerbated during exercise with elevated pulmonary pressures and right heart dilatation[50]. Approaches using surgical pericardiotomy have demonstrated an attenuated increase in PCWP on volume loading demonstrating the contribution of this component in a subtype of HFpEF[51].

Vascular dysfunction

Hypertension is extremely common in HFpEF and is a significant pathophysiological contributor. Calcium deposition, ageing, pro-inflammatory cytokines and endothelial dysfunction leads to stiffening of the aorta[52]. This results in unfavourable ventricular-arterial coupling and increases afterload. Over time, this promotes concentric remodelling, hypertrophy and impaired diastolic function[53]. There is also inadequate vasodilatory reserve seen in some patients during exercise, leading to impaired dynamic ventricular-arterial coupling and blunted exercise capacity[54].

Myocardial ischaemia

Myocardial ischaemia can be caused directly by hypertension through a supply-demand mismatch and a rise in LV filling pressures reducing the coronary perfusion gradient. Moreover, both epicardial and microvascular disease can contribute to HFpEF. Epicardial coronary disease portends a lower ejection fraction and increased mortality[55]. In addition, coronary microvascular dysfunction has been proposed to be a major driver of HFpEF and is seen in up to 75% of patients[56]. This could be driven by endothelial inflammation, reducing nitric oxide availability[57]. In addition, coronary microvascular rarefaction has also been demonstrated[58].

Peripheral skeletal muscle contributors

Exercise intolerance in HFpEF is not caused exclusively by cardiac abnormalities. There is a 40% reduction in peak oxygen consumption (VO2peak) in HFpEF[59]. Whilst this is partly due to attenuated cardiac output increase, there is also a significant reduction in arterio-venous oxygen reserve[60]. The skeletal muscle structure and function is thought to be different in HFpEF, containing fewer slow-twitch Type I myofibres[61]. In comparison with HFrEF and controls, there is also evidence of reduced muscle strength despite similar chronological age[62]. Anaemia and iron deficiency is also frequently present, affecting oxygen-carrying capacity[63,64].

Abnormalities in lung function

Pulmonary disease often co-exists with HFpEF, partly due to shared risk factors such as smoking. Both obstructive and restrictive spirometric abnormalities are associated with HFpEF and a reduction in both FEV1 and FVC is associated with incident HFpEF[65]. While obstructive defects may be explained by smoking and associated chronic obstructive pulmonary disease, restrictive lung defects are not. Abnormal respiratory mechanics can occur with obesity, a frequent comorbidity and may contribute to restrictive physiology and symptoms.

In addition to spirometric abnormalities, patients with HFpEF have been found to have impaired lung diffusing capacity (DLCO) at rest and during exercise due to a combination of lower alveolar-capillary membrane conductance and pulmonary capillary blood volume[66-68]. Pulmonary vascular remodelling is known to occur in

heart failure due to sustained increases in pressure and is associated with a reduction in lung diffusing capacity[34].

1.1.2 Molecular pathophysiology of HFpEF within the myocardium

The current paradigm of the molecular underpinnings of HFpEF involves a pro-inflammatory state induced by a combination of metabolic comorbidities and excess haemodynamic load[69]. This impacts upon collagen homeostasis, fibrosis and stiffness with interactions among these at multiple levels.

Inflammation, changes in the extra-cellular matrix and myocardial fibrosis

Numerous comorbidities can contribute to inflammation including metabolic ones such as diabetes and obesity, but many others such as hypertension with the resultant haemodynamic load and kidney disease may also contribute. A number of circulating biomarkers such as TNFR1 (Tumour Necrosis Factor Receptor 1), interleukins and GDF-15 (Growth Differentiation Factor 15) are thought to mediate this link[70]. This now forms a therapeutic target of interest with a clinical outcomes trial of an anti-IL-6 antibody now under way[71].

In conjunction with pro-inflammatory signalling, profibrotic signalling also contributes to the development of HFpEF. Recruitment of pro-fibrotic cells including activated macrophages and T-cells promote procollagen processing and fibre assembly. This relies on migration assisted by vascular cell adhesion proteins. In addition, fibroblasts are activated to become matrix-synthesising and collagen cross-linking enzymes reduce degradation.

Oxidative-nitrosative stress

The pro-inflammatory state results in increased nitric oxide synthesis in cardiomyocytes. This results in reduced X-box-binding protein 1 (XBP1) levels, affecting the unfolded protein response and endoplasmic reticular stress[72]. In addition, oxidative stress which commonly arises from many HFpEF-associated comorbidities results in reactive oxygen species (ROS) formation through enzymes such as NADPH oxidase. ROS can alter the properties of many kinases such as protein kinase A/G and key proteins such as SERCA, ryanodine receptor 2 and the sarcomeric proteins resulting in altered excitation-contraction coupling[73].

Alterations in sarcomeric properties

Titin, a large protein which acts as a molecular spring in the sarcomere has been implicated in HFpEF. From left ventricular biopsy specimens, alterations in phosphorylation of titin by protein kinases have been linked to increased myocardial stiffness in those with HFpEF and hypertension[24]. In comparison, on RV biopsy specimens, patients with HFpEF and obesity demonstrate depressed sarcomere function as demonstrated by a reduction in systolic force-Ca dependence, but a lesser degree of passive stiffening in comparison to those with HFpEF related to hypertension[74].

Metabolism

Impairments in myocardial metabolism have been demonstrated in HFpEF with likely significant contributions from underlying comorbidities. This topic is dealt with in subsequent sections within this chapter.

Overall, these pathophysiological mechanisms are all tied together by a process of metabolic inflammation. These extend to the periphery but are not covered here.

1.2 APPROACHES TO PHENOTYPING HFpEF

With increasing recognition of heterogeneity within HFpEF, multiple different approaches to phenotyping have been taken to identify specific groups who may benefit from tailored therapies. Clinical phenotyping represents the simplest approach to this[75]. The relative contribution of multiple comorbidities including ageing, hypertension, obesity, diabetes, atrial fibrillation, anaemia, and kidney disease can give rise to HFpEF phenotypes with different characteristics requiring therapies moulded to the major contributors.

Imaging techniques have also been used to phenotype HFpEF further[76]. Echocardiography is the first port of call to look for structural and morphological abnormalities associated with HFpEF. It can be used to detect subtle abnormalities in the LV or the LA and estimate the probability of high pulmonary pressures or left ventricular filling pressures[77]. In particular, stress echocardiography is able to detect abnormalities which are only unmasked during exercise. CMR, a more precise

modality is able to quantify myocardial mass, myocardial fibrosis and evaluate strain[78].

Molecular and genetic profiling of HFpEF enables better understanding of the key orchestrators leading to the manifestation of HFpEF[79]. Examination of biomarkers relevant to HFpEF range from well-established cardiac specific markers including BNP and troponin through to specific biomarkers of fibrosis, inflammation and those of comorbidities. Approaches to this have included proteomic studies on a number of different platforms, transcriptomics, genome-wide association studies and micro-RNA analysis.

The haemodynamic basis of HFpEF, particularly during exercise has been highlighted recently. There has been recognition of differences in a number of parameters such as stiffness, contractility and exercise stroke volume reserve between different groups with HFpEF and is described in greater detail in the subsequent section.

Finally, with advances in computational technology the vast array of data that can potentially be compiled for each individual patient from the above approaches can be consolidated through the use of machine learning techniques[80]. Multiple studies have attempted this using clinical data and blood biomarkers combined with machine learning and cluster-mapping[81-83]. A recent Japanese study involved applying latent class analysis clustering techniques to commonly available demographic, clinical, laboratory and echocardiography data to distinguish phenogroups, looking for discriminatory pathophysiological biomarker signatures for each of these groups and identifying differential drug responses[84-86]. With increasing adoption of these techniques at the point of drug discovery, they are also likely to find their way into clinical practice.

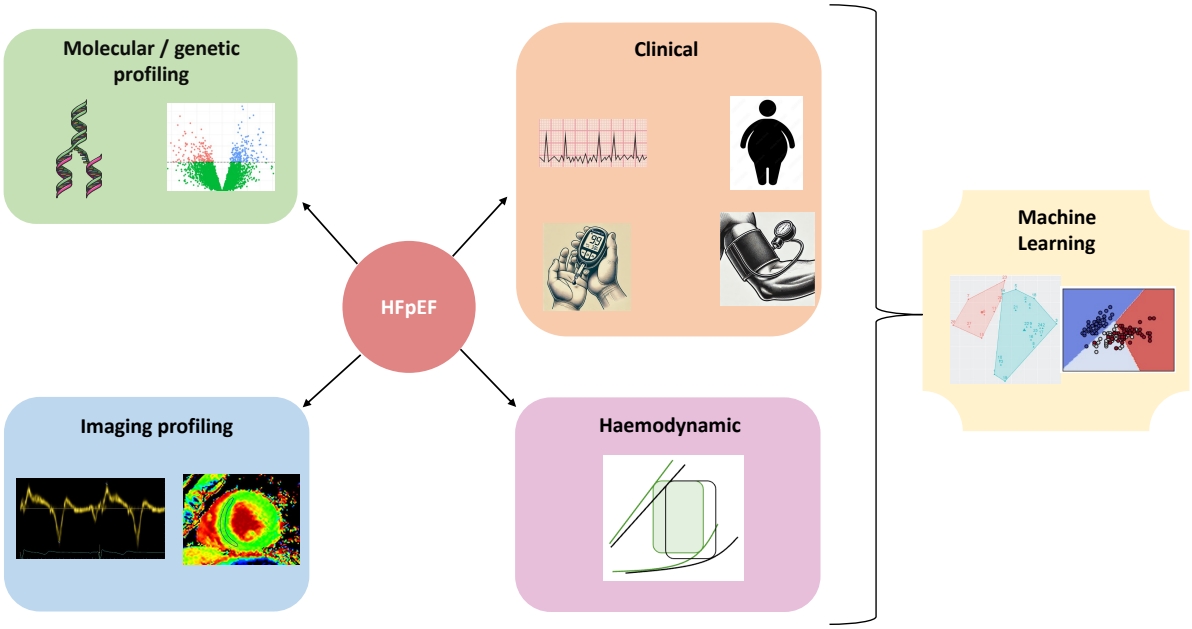

Figure 3: Approaches to phenotyping HFpEF

1.2.1 Haemodynamic phenotypes in HFpEF

While the LVEF has guided the distinction between HFrEF and HFpEF for many decades, there has been recent interest in the haemodynamics of those who fall within the HFpEF umbrella. Imaging characteristics of HFpEF varies from those with subtle depression of LV systolic function through to hyperdynamic ventricles with supra-normal LV ejection fraction. This degree of heterogeneity is likely to have had a significant role to play in the differential effects of multiple conventional heart failure therapies. This includes RAAS inhibitors, but also more recently developed therapies such as SGLT2 (Sodium-dependent Glucose Cotransporter 2) inhibitors, with therapies such as ARNIs, spironolactone and empagliflozin showing greater benefit in those with a lower LVEF[87-89].

In a study where a group of HFpEF patients were dichotomised into those with LVEF 50-60% vs those >60%, the higher EF group were noted to have small LV volumes with higher baseline contractility (measured by end-systolic elastance) and diastolic stiffness (measured by the β constant)[90]. Despite similar stroke volumes at rest, there was a decrease in the stroke volume in this group on exertion with greater increases in filling pressure. The extracellular volume fraction measured on MRI was higher in the LVEF 50-60% group however, with an increase in myocardial fibrosis on biopsy.

In another invasive study, there were similar increases in diastolic stiffness with a leftward shifted end-diastolic pressure volume relationship in the higher LVEF groups where cut-offs of both 57% and 65% were used[91].

There is likely to be a significant underlying genetic predisposition to the supranormal EF phenotype with heart failure developing subsequently following environmental triggers. A UK bio-bank based study used a genetic risk score for the presence of a supranormal LVEF in the general population and demonstrated an association with higher mortality and underdiagnosed heart failure[92]. In another study of those without significant cardiovascular disease, supranormal LVEF was also associated with impaired coronary flow and heart rate reserve suggesting microvascular and autonomic dysfunction[93,94]. This appears to also be the case in other cardiac pathologies. In a cohort of patients receiving transcatheter valve replacements for aortic stenosis, those with an LVEF >65% had poorer outcomes[95].

Characterisation of the differences between these different phenotypes of HFpEF is of great interest due to a signal of poorer prognosis in those with higher LVEF with increased mortality and risk of heart failure hospitalisation[96]. This effect is particularly pronounced in women with supra-normal EF[96,97]. In addition, therapies such as ARNis cause greater degrees of adverse effects such as hypotension in those with higher LVEF[98]. Specific therapies will need to be developed in this group given the paucity of therapeutic options. To enable this, a more developed understanding of the molecular biology of different phenotypes such as through the use of precision technologies such as multi-omic profiling will be necessary.

1.3 PROTEOMICS APPROACHES IN CARDIOVASCULAR DISEASE

The human proteome is thought to contain at least 20,000 proteins[99]. Proteins provide excellent targets to study as potential biomarkers given their stability and abundance in comparison to other targets such as RNA. There are 2 ways in which to examine the proteome – targeted or untargeted. Untargeted approaches are particularly useful in identifying novel biomarkers and pathways of interest and tend to look at a larger number of proteins. However, this raises the possibility of false discovery due to multiple hypothesis testing. The alternative is to use targeted approaches where proteins known to be involved in pathways relating to a specific disease are interrogated which reduces the chance of false discovery. However, this runs the risk

of missing relevant pathways which may not have been previously known to be linked. The major techniques used to quantify proteins in samples in an unbiased manner are mass spectrometry-based techniques, antibody-based methods and aptamer-based quantification[100].

Techniques in proteomic quantification

The ability of different techniques to quantify the proteome varies. Mass spectrometry based techniques involve ionisation of a sample[101]. The mass analyser is then able to separate ions by the mass-to-charge ratios. The ionisation spectra provides information allowing identification of the chemical structure from which mapping of the peptide fragments making up a protein is achieved. The major limitation of the technique is that it can detect only the most abundant few hundred proteins. Alternative approaches limit throughput. The inability to scale this technique results in a diminished ability to identify potentially important biomarkers of lower abundance.

In contrast, antibody-based techniques have higher sensitivity to detect proteins with lower concentrations. This relies on recognition and binding of specific epitopes on a protein using antibodies with high affinity. Often, this requires a second antibody to ensure specificity. This is used in most clinical laboratories due to the relative ease of use for single-analyte tests, such as ELISA (Enzyme-Linked Immuno-Sorbent Assay). However, on its own, this cannot be scaled due to cross reactivity of secondary antibodies. Proximity extension assays have been used to combat these shortcomings[102]. The sample is incubated with dual antibodies which bind to nearby epitopes. DNA oligonucleotide sequences are used to label these antibodies which due to their proximity leads to hybridisation. This is then extended and amplified by adding a DNA polymerase. Subsequent quantification using PCR (polymerase chain reaction) is directly proportional to the initial concentration of the target. This has proven to be scalable with limited intra- and inter-assay variability[103]. This technique is now able to quantify up to 5400 proteins in commercial streams (Olink Proteomics, Uppsala, Sweden).

Aptamer-based techniques have recently been developed to improve scalability and throughput[104]. Aptamers are oligonucleotide-based affinity reagents which can be amplified and detected easily using PCR and hybridisation arrays. Commercial

multiplex platforms such as SomaScan (Somalogic Inc., Boulder, Colorado, USA) which use modified aptamers called SOMAmers (Slow Off-rate Modified Aptamer) can assay up to 11000 proteins. These oligonucleotides can fold into different shapes with specific affinity to protein targets. When samples are incubated with these, equilibrium binding occurs between the targets and fluorophore-tagged SOMAmers. This is followed by multiple 'catch' and wash steps. The final SOMAmer-protein complexes are isolated from the reagent and quantified by hybridisation-based DNA quantification. The relative fluorescence of each SOMAmer reflects the relative amount of the target protein within the sample.

There are multiple advantages to the aptamer approach. As they don't have cross-interference due to immune responses as antibody-based methods do, it is highly scalable and there is no theoretical limit to the targets which can be quantified. It is also highly sensitive and allows quantification over a larger range from the most abundant to relatively scarcely abundant proteins[105]. However, there are still some limitations to this method[106]. They can bind to off-target proteins with high affinity[107]. In addition, the epitope that it binds to may not be clear and thus it may bind to different isoforms of the same protein. There is also the possibility that single nucleotide polymorphisms lead to single amino acid changes which alter the affinity of binding.

Proteomics in HFpEF

The field of proteomics holds promise in understanding the pathophysiology of cardiovascular disease including HFpEF, the distinctions between phenotypes and responses to drugs. Computational models from machine learning techniques can predict the development of disease and prognosis.

Early studies sought to characterise HFpEF in comparison to the other phenotypes of heart failure - HFrEF and HFmrEF. An aptamer-based approach has suggested enrichment for proteins involved in growth factor signalling, humoral immunity and angiogenesis in HFpEF[108]. Further studies have allowed for distinctions to be drawn between HFpEF with different comorbidity profiles.

In a study using a targeted approach, increases in plasma levels of proteins relating to volume expansion (adrenomedullin), fibrosis (thrombospondin-2) and inflammation

(galectin-9, tumour necrosis factor-related apoptosis-inducing ligand receptor 2 and CD4) were seen in obese HFpEF patients compared to non-obese HFpEF and control patients with many linked to mortality[109]. In an untargeted aptamer-based study using samples from clinical trials, a lipocalin called ApoM emerged as a potential mediator of poor prognosis in HFpEF patients with diabetes in comparison to those without diabetes[110]. Proteomics may also be able to distinguish differences between men and women as has been shown to be the case in coronary microvascular dysfunction in HFpEF[111].

An approach using plasma proteomic scores to explain different aspects of impairment in cardiac haemodynamics and peripheral abnormalities has also been explored[112]. In this study, proteomic signatures of multiple variables such as peak VO2, PCWP/CO, peak CO and peak PVR were developed using ridge regression. The signature of peripheral O_2 extraction was distinct from these with proteins linked to multiorgan health (kidney, liver, muscle, adipose tissue) being implicated. Despite a symptomatic control population who demonstrated impaired peripheral O_2 extraction, the signatures of peak oxygen uptake and PCWP/CO slope were associated with incidence of HFpEF in a Framingham Heart Study cohort.

Beyond understanding the pathophysiology of HFpEF, such data can also be used to predict the development of HFpEF along with prognosis. Studies in larger cohorts of patients with more extensive proteomic coverage using both aptamer-based and PEA (Proximity Extension Assay) panels have demonstrated the ability to predict incident HFpEF and HFrEF[113,114]. Proteomic studies have also looked at markers of frailty and the incidence of heart failure[115]. In a study of patients recruited to the PARAGON-HF trial, multiple proteins relating to metabolic, coagulation and extracellular matrix regulatory pathways were related to poorer prognosis in HFpEF[116]. A study based on a subset of HFpEF patients enrolled in the TOPCAT (Treatment of Preserved Cardiac Function Heart Failure with an Aldosterone Antagonist Trial) produced a machine-learning derived model which could predict death and heart failure hospitalisation based on plasma biomarkers[117].

Using such information is not limited to understanding the mechanisms underlying HFpEF or predicting its development or prognosis however. It can also be used to understand how putative medicines can affect the pathways involved and who would

most benefit. An example is the use of proteomic panels to determine the effects of an anti-inflammatory drug targeting myeloperoxidase which demonstrated downregulation of a number of biomarkers associated with adverse prognosis in HFpEF cohorts[118].

Other-omics approaches have also been studied in HFpEF. A targeted metabolomics approach revealed associations with fibrosis, oxidative stress, impaired lipid metabolism and an inflammatory state[119]. Models combining metabolite data compared favourably with NT-pro BNP in predicting a clinical diagnosis of HFpEF[120]. Targeted sphingolipidomics demonstrated that levels of circulating ceramide 16:0 and 18:0 were associated with death or heart failure hospitalisation in the TOPCAT trial[121]. A multi-omic approach incorporating genomics, transcriptomics, proteomics and metabolomics holds great promise to better diagnose and prognosticate HFpEF, develop medicines targeted to the affected pathways and match the therapeutic options to individual phenotypes[122].

1.4 MYOCARDIAL ENERGETICS IN HFpEF

ATP, creatine and the creatine kinase system

The CK (Creatine Kinase) reaction acts as the major spatial and temporal buffer for high energy phosphate metabolism in the myocardium[123].

$$MgADP^{-} + PCr^{2-} + H^{+} <_{k-1}^{k1}> MgATP^{2-} + Cr$$

In a healthy heart, ATP levels are maintained even during stress. However, mitochondrial oxidative phosphorylation can be too slow to respond immediately to replete ATP in this scenario. Phosphocreatine (PCr) is smaller and less charged than ATP. This facilitates easier diffusion from the mitochondria to regions of use. In addition, it can accumulate to higher levels (~20 mM compared to 10 mM of ATP in the healthy human heart)[124]. The CK reaction is able to provide ATP about 10-fold faster than other means of ATP synthesis at rest and 3-5-fold during stress[125].

One of the key features of the CK reaction is compartmentalisation. The mitochondrial CK isoform (mtCK) is an octamer which accounts for up to 35% of creatine kinase in the myocardium and is localised to the inner mitochondrial membrane in close relationship with the ANT (Adenine Nucleotide Translocator)[126]. Here, following the production of ATP from oxidative phosphorylation, it catalyses the creation of phosphocreatine from ATP. The resultant formation of ADP keeps the ATP/ADP ratio low, thus reducing the energy required for ATP synthesis. In addition, keeping concentrations of ADP high stimulates mitochondrial oxidative phosphorylation.

The cytosolic form of CK is formed of a combination of 2 subunits – either M (muscle-type) or B (brain-type). Of these, the CK-MM isoform accounts for the bulk of all CK (65%) in the heart. These are found in close association with consumers of ATP in the heart such as sarcoplasmic/endoplasmic reticulum calcium (SERCA) ATPase and myosin ATPase. Here, it favours the transfer of phosphorus from PCr to ADP to form ATP. This helps keep cytosolic ADP levels low resulting in a higher ATP/ADP ratio. In turn, there is an increase in the Gibbs free energy of hydrolysis from the ATPase reactions (ΔG_{ATP}) resulting in more energy per mole of ATP to perform work. The free creatine then travels to the mitochondria and stimulates respiration[127].

Cardiomyocytes do not synthesise creatine. This necessitates uptake against a large concentration gradient via a specific creatine transporter (CrT) which also takes in $2Na^+$ and $1Cl^-$ ions[128]. This circulating creatine is obtained either from dietary sources or produced from processing of arginine and glycine sequentially in the kidney and liver via the actions of arginine-glycine amidinotransferase (AGAT) and guanidinoacetate methyltransferase (GAMT).

It is worth noting that the CK system is not the only phospho-transfer system. The adenylate kinase system accounts for about 15% of phospho-transfer activity in the heart. It catalyses the following reaction.

$$2MgADP^- \rightleftharpoons MgATP^{2-} + AMP^{2-} + Mg^{2+}$$

It is particularly useful during metabolic stress such as during ischaemia and provides an alternative mechanism to provide ATP and produce AMP[129]. This stimulates AMP Kinase to conserve energy by shutting down pathways with high levels of consumption. Glycolytic flux also accounts for around 5% of phosphotransfer[130]. Finally, while simple cytosolic diffusion of ADP and ATP is also possible, this is heavily restricted in cardiomyocytes, particularly in the case of ADP prohibiting this as a primary mechanism to provide ATP[131].

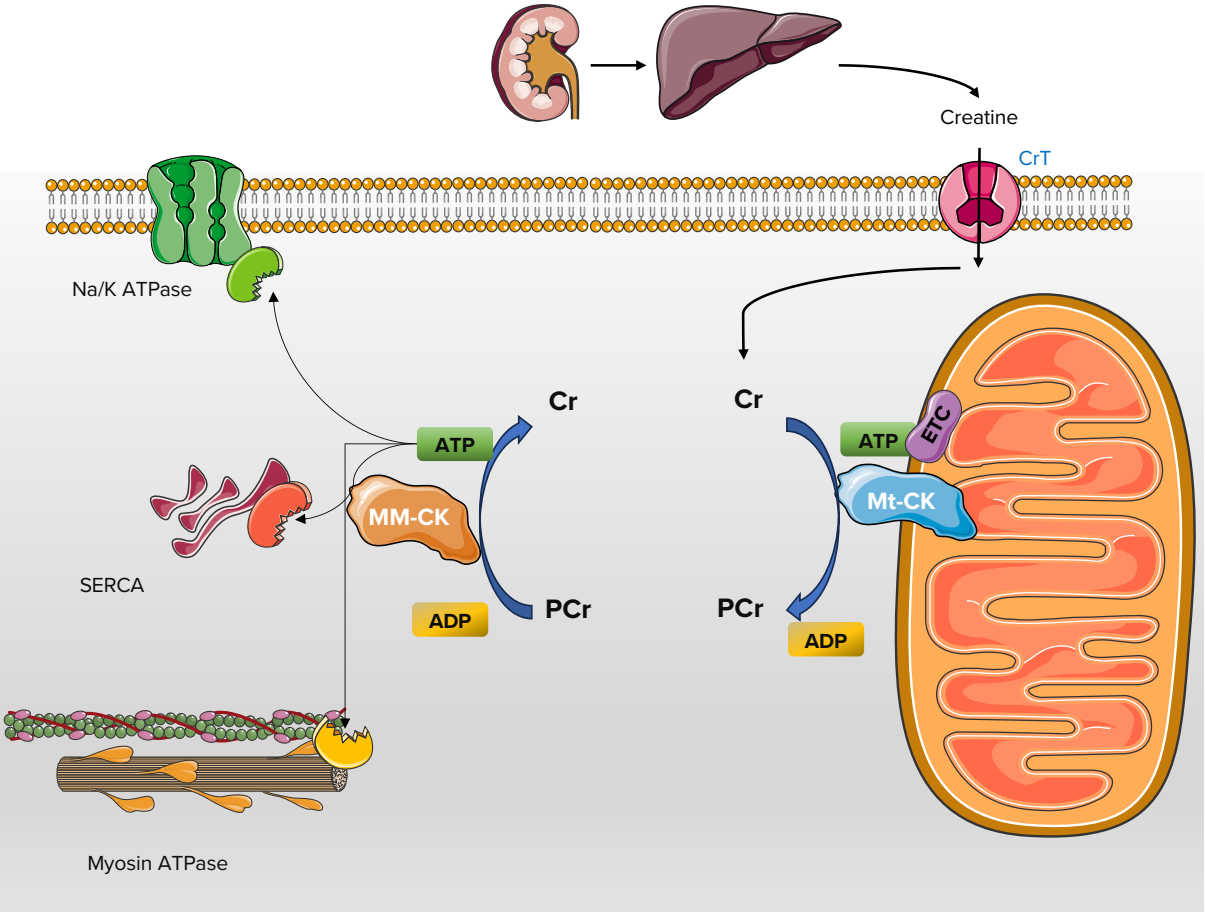

Figure 4: The creatine kinase system in the cardiomyocyte

CrT: Creatine transporter, ATP: Adenosine Triphosphate, ADP: Adenosine Diphosphate, Cr: Creatine, ETC: Electron Transport Chain, PCr: Phosphocreatine, Mt-CK: Mitochondrial Creatine Kinase, MM-CK: Muscle-type Creatine Kinase, SERCA: Sarcoplasmic/Endoplasmic Reticulum Calcium ATPase, Na/K ATPase: Sodium-potassium pump ATPase. Figure created using graphics from Servier.

PCr/ATP ratio

The most widely used non-invasive, in vivo measure of the overall cardiac energetic status is the PCr/ATP ratio derived from ^{31}P Magnetic Resonance Spectroscopy (MRS). As described above, ATP levels are maintained in the face of increased demands through means of greater production. But where this cannot be achieved, ATP levels are kept steady through transfer from PCr by the CK system and a subsequent fall in its concentration leads to a lower ratio of the peak heights of PCr to ATP. While absolute quantification of the metabolites rather than the relative ratio would be preferable, this is challenging to achieve in humans.

This technique when applied in HFrEF has demonstrated reduced PCr/ATP which in turn has been linked to mortality in non-ischaemic cardiomyopathy[132]. This fall has

also been shown to extend to HFpEF and it has been hypothesised that a lower energetic reserve in HFpEF may underlie the worsening of left ventricular relaxation and a failure to improve contraction during exercise [133,134]. Over a spectrum of diastolic dysfunction extending from diabetes, through to HFpEF and severe dysfunction in cardiac amyloidosis, the reduction in PCr/ATP ratio has also been linked to the development of pulmonary oedema[135].

The impairment in energetic state is likely to precede the development of overt HFpEF and manifests in linked comorbidities as diastolic abnormalities develop. Diastolic dysfunction in hypertensive heart disease has been linked to lower PCr/ATP ratios at both rest and during atropine-dobutamine stress[136]. Impaired high energy phosphate metabolism has also been associated with diastolic dysfunction in asymptomatic, normotensive patients with obesity or type 2 diabetes[137-140].

It is worth noting that the ratio can be a limited measure of cardiac reserve in advanced heart failure where the ATP concentration also drops driven by a reduction in the adenine pool[141]. This could lead to pseudo-normalisation in the PCr/ATP ratio in some cases due to a fall in the concentrations of both[142]. Interestingly in a study by Starling *et al*, patients with restrictive cardiomyopathy i.e. diastolic dysfunction, but a preserved ejection fraction had levels of ATP, adenine nucleotides and NAD even lower than that of dilated cardiomyopathy.

The creatine kinase system in heart failure and HFpEF

A limitation of the PCr/ATP ratio is that it does not consider the continuous recycling of metabolites. Using CK flux as a measure of the energetic status of the heart enables us to incorporate both metabolite concentrations and enzyme activity. While direct measurements of CK activity can only be performed on biochemical assays, measurements of CK flux in vivo can be performed using ^{31}P-NMR magnetization saturation transfer techniques, although only in a summative fashion, without distinguishing between activity in different compartments. The pseudo-first order unidirectional forward rate constant kf ($k_{PCr \rightarrow ATP}$) is derived and the product with [PCr] provides an estimate of CK forward flux. This is described in greater detail in the Methods section.

The creatine kinase reaction has been relatively well studied in HFrEF. In dilated cardiomyopathy as well as in left ventricular hypertrophy, a 30-50% reduction in CK flux has been demonstrated, even where myocardial ATP levels were normal[125,143]. This correlates with impaired cardiac mechanical work in heart failure[144]. Finally, it has also been demonstrated that CK flux is an independent predictor of cardiovascular events in heart failure[145].

In contrast, there have been no studies examining the CK reaction in human HFpEF. Creatine is the most extensively extracted metabolite in HFpEF, underlining its importance to cardiac metabolism[146]. Impairment of the CK system could be a potential contributor in multiple ways to the pathophysiology underlying HFpEF. Firstly, studies in animal models have indicated that a stepwise reduction in CK activity through irreversible inhibitors leads to a proportional decrease in contractile reserve and results in an increase in end-diastolic pressure[147,148]. This could be through an inability to meet the free energy of hydrolysis requirements of SERCA ATPase. In addition, the CK system is thought to keep cytosolic ADP concentrations low, which in turn allows a higher energy of ATP hydrolysis. As the 'energy reserve' for the ΔG_{ATP} from hydrolysis compared to the energy required for SERCA is the lowest for all ATPases, a reduction in the ATP/ADP ratio leading to reduced free energy of hydrolysis could contribute to diminished SERCA activity and impaired relaxation.

The mitochondrial CK system is also likely to be important. Transgenic overexpression of the mtCK isoform resulted in attenuation of pathological hypertrophy induced by both transverse aortic constriction and adrenergic stimulation in a murine model, and this was dependent on the availability of creatine[149]. In comparison, overexpression of cytosolic CK did not achieve the same[150]. This demonstrates the important role of mtCK in regenerating ADP in the mitochondria. However, overexpression of cytosolic CK leads to increased CK flux, improved resting and stress contraction and prolonging survival in mouse hearts demonstrating the importance of both isoforms[150]. Moreover, the failure to maintain a low cytosolic ADP concentration due to reduced CK flux led to impaired diastolic function in hypertrophied rat hearts[151]. While not directly demonstrated in human studies, the above studies provide an indication as to how manipulating CK activity could affect the ability to perform cardiac work without a pathological rise in filling pressures.

While data in HFpEF is not available, myocardial energetics in associated comorbidities have been characterised in more detail. Despite a lower PCr/ATP, patients with obesity maintain similar CK flux to controls without obesity at rest by virtue of a higher k_f[152]. However, on application of dobutamine stress, they are unable to augment CK flux in the manner of controls and this is associated with reduced systolic reserve. This high k_f returns to normal with weight loss along with a normalisation of PCr/ATP. This demonstrates the potential of obesity to modify the energetic phenotype in heart failure and this has been studied in HFrEF. The presence of obesity in DCM results in an apparent 'pseudo-normalisation' of CK flux compared to the reduction seen in DCM without obesity[153]. Weight loss in this group also results in a fall in ATP delivery rate.

Pressure overload is a common contributor to the pathophysiology of HFpEF, usually through means of arterial hypertension, but also sometimes in conjunction with less than severe aortic stenosis. The presence of hypertensive LVH results in a 35% reduction in PCr levels with stable ATP levels[143]. While k_f is normal in LVH, it is halved where HF co-exists suggesting that the kinetics of phospho-transfer is intimately involved in the transition to heart failure. CK flux progressively decreases relative to the control group, driven by a lower PCr/ATP ratio in those with LVH, but with a further decrease in those with heart failure due to the additive effect of a lower k_f. It must be noted that the heart failure group in this study spanned both HFrEF and HFpEF. The effects of pressure overload have also been studied in aortic stenosis. This demonstrates reduction in resting CK flux even at the moderate stenosis stage with preserved LV systolic function, driven primarily by reduction in PCr/ATP with a stable CK k_f[154].

1.5 CARDIAC METABOLISM IN THE NORMAL HEART

The heart relies on oxidation of metabolic substrates with oxidative phosphorylation accounting for 95% of ATP generation. These include fat, glucose, ketone bodies, lactate and amino acids. This process relies on multiple sequential steps - cellular uptake of substrate followed by its oxidation in the mitochondria and entry into the Krebs cycle. This generates reducing agents and shuttling of electrons resulting in an electrochemical proton gradient. The gradient drives the production of ATP from ADP.

In the normal heart, the major source of energy is free fatty acid oxidation, accounting for up to 80% in the fasting state[155]. The remainder is provided by metabolism of glucose with smaller contributions from other substrates. However, the healthy heart exhibits flexibility in substrate selection depending on the available substrate within the bloodstream. This may occur in relation to the feeding state with increased glucose availability postprandially as opposed to relatively more fatty acid availability in the fasting state. It is also capable of altering this in response to various stimuli. For example, it can increase its utilisation of glucose in response to exercise[156].

Fatty acid metabolism

Free fatty acids (FFA) are supplied to the heart albumin-bound in the blood. Alternatively, they are produced following hydrolysis of triacylglycerols (TAG) in chylomicrons or very low-density lipoproteins (VLDL). Uptake depends on the concentration of FFA within the plasma and transport through the cell membrane is facilitated by CD36/Fatty Acid Translocase (FAT) and Fatty Acid Binding Proteins (FABP).

Once inside the myocyte, they undergo esterification to produce fatty acyl-CoA (coenzyme A). They may then enter the mitochondria to act as substrate or they may be diverted to production of TAG stores within the cell. However, they can also be diverted to the production of reactive lipid species such as ceramides and diacylglycerol (DAG).

Long-chain fatty acids enter the mitochondrion through the action of carnitine palmitoyl transferase 1 (CPT-1) which transfers the fatty acid moiety to carnitine, thus forming long chain acylcarnitine. Once inside the mitochondrion, the fatty acid group is transferred back to CoA and subsequently undergoes beta-oxidation. This produces acetyl-CoA, thus entering the Krebs cycle.

Fatty acid metabolism is tightly regulated through a variety of mechanisms. Firstly, CPT-1 is inhibited by malonyl CoA which acts as a negative feedback mechanism[157]. It is produced by acetyl CoA carboxylase and degraded by malonyl CoA decarboxylase. The $FAD/FADH_2$, $NAD^+/NADH$ and mitochondrial acetyl-CoA/CoA ratios all influence fatty acid metabolism. Additionally, peroxisome proliferator activated receptors (PPARs) and estrogen related receptors (ERRs) are

also key players through transcriptional regulation of oxidative enzyme expression. This is key in the heart's ability to select between substrates. Despite producing the largest yield of ATP per 2 carbon moiety, fatty acids are less oxygen efficient, requiring more oxygen than glucose to do so.

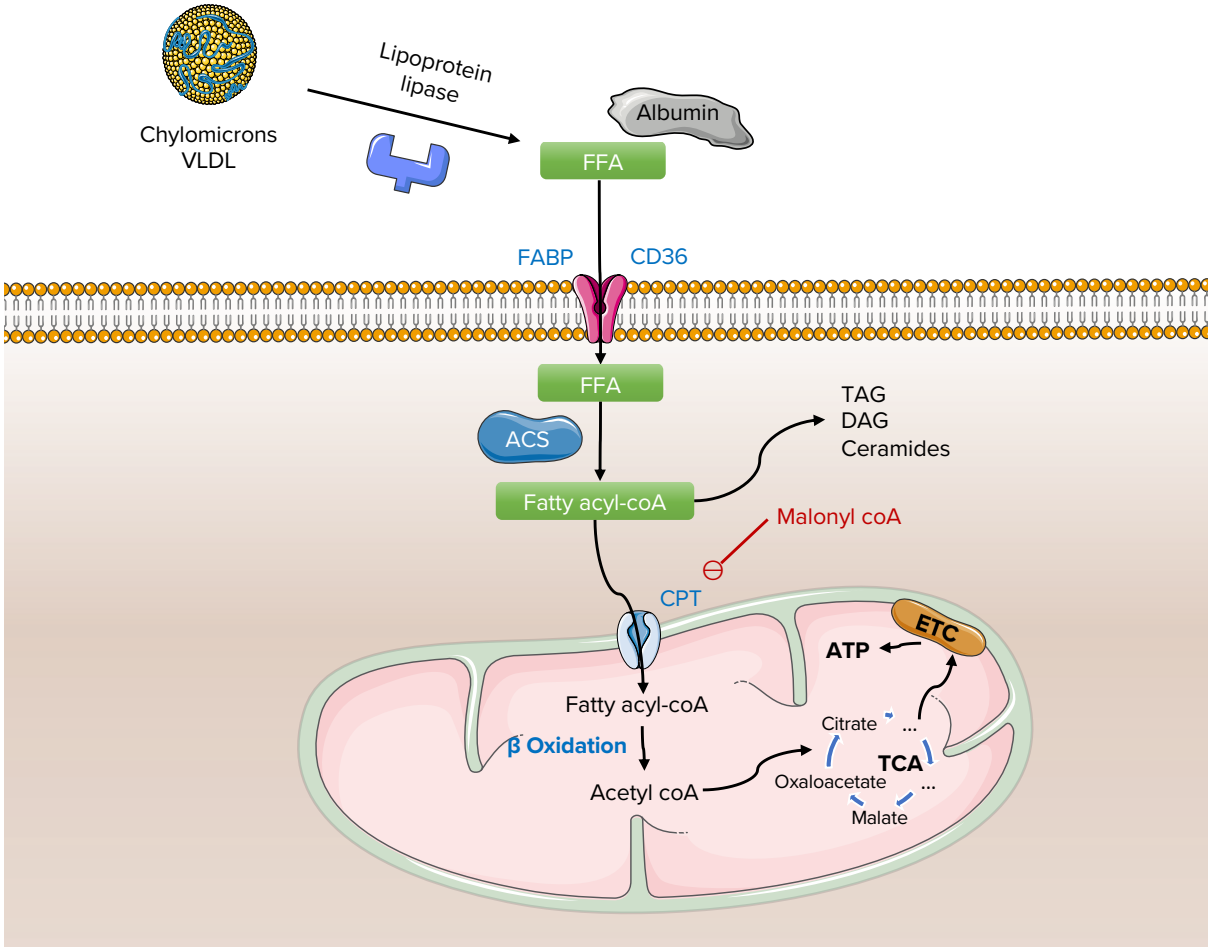

Figure 5: Fatty acid metabolism in a cardiomyocyte

FFA: Free fatty acid, VLDL: Very Low Density Lipoprotein, FABP: Fatty Acid Binding Protein, CD36: Also known as fatty acid transporter, ACS: Fatty acyl-CoA synthetase, TAG: Triacylglycerol, DAG: Diacylglycerol, CPT: Carnitine Palmitoyltransferase, ETC: Electron Transport Chain, ATP: Adenosine Triphosphate, TCA: Tricarboxylic acid cycle. Figure created using graphics from Servier.

Glucose metabolism

Uptake of glucose into the myocyte is dependent on the gradient across the plasma membrane and occurs via the insulin independent GLUT-1 and insulin sensitive GLUT-4 transporters. GLUT-4 translocation to the cell membrane is increased in

response to insulin, exercise and ischaemia[158,159]. In contrast, an increase in plasma free fatty acid availability reduces uptake[160].

Glucose can be metabolised to produce ATP through anaerobic glycolysis and oxidation of the resultant pyruvate. Upon entry into the cell, there are 2 potential paths. It could be diverted to the polyol pathway and formation of sorbitol and fructose. A greater proportion undergoes phosphorylation by hexokinase to glucose 6-phosphate. From here, it has several possible fates – undergo glycolysis to form pyruvate, conversion to glycogen or enter the pentose phosphate and hexosamine biosynthetic pathways. Pyruvate can either be converted to lactate or enter the mitochondrion through the mitochondrial pyruvate carrier (MPC). It then enters the Krebs cycle following conversion to acetyl-CoA by pyruvate dehydrogenase (PDH) or less frequently, by carboxylation to the intermediates oxaloacetate or malate.

In addition to uptake, additional regulation of glucose use occurs during glycolysis with 3 rate limiting steps catalysed by the enzymes hexokinase, phospho-fructo-kinase-1 and pyruvate kinase. The first commits glucose to the cell, the second to glycolysis and the last to generation of ATP during glycolysis. Insulin secretion following carbohydrate ingestion results in activation of hexokinase to stimulate glucose use[161].

Following glycolysis, flux through the rate-limiting PDH enzyme is related to the rate of myocardial glucose uptake. The increase in the ratio of NADH/NAD^+ and acetyl-CoA/free CoA can activate PDH kinase (PDK) which in turn, inhibits PDH. The heart switches to carbohydrate metabolism during times of stress due to the ability to generate ATP through anaerobic glycolysis. HIF-1 is a key player in response to hypoxia, by stimulating glycolysis and activating PDK[162]. Oxidation of a glucose molecule can generate 31 molecules of ATP while only consuming 12 oxygen atoms. This yields a phosphorus: oxygen (P:O) ratio of 2.58. In comparison, 105 ATP molecules are generated for 46 oxygen atoms on oxidation of palmitate (P/O ratio 2.33). It has been demonstrated in humans that activation of free fatty acid metabolism during stress results in increased myocardial oxygen consumption with the opposite occurring with inhibition[163]. Therefore the increase in myocardial oxygen efficiency with glucose metabolism means that it is theoretically beneficial for the body to switch

to glucose metabolism during times of stress, although this has not been conclusively proven in human studies.

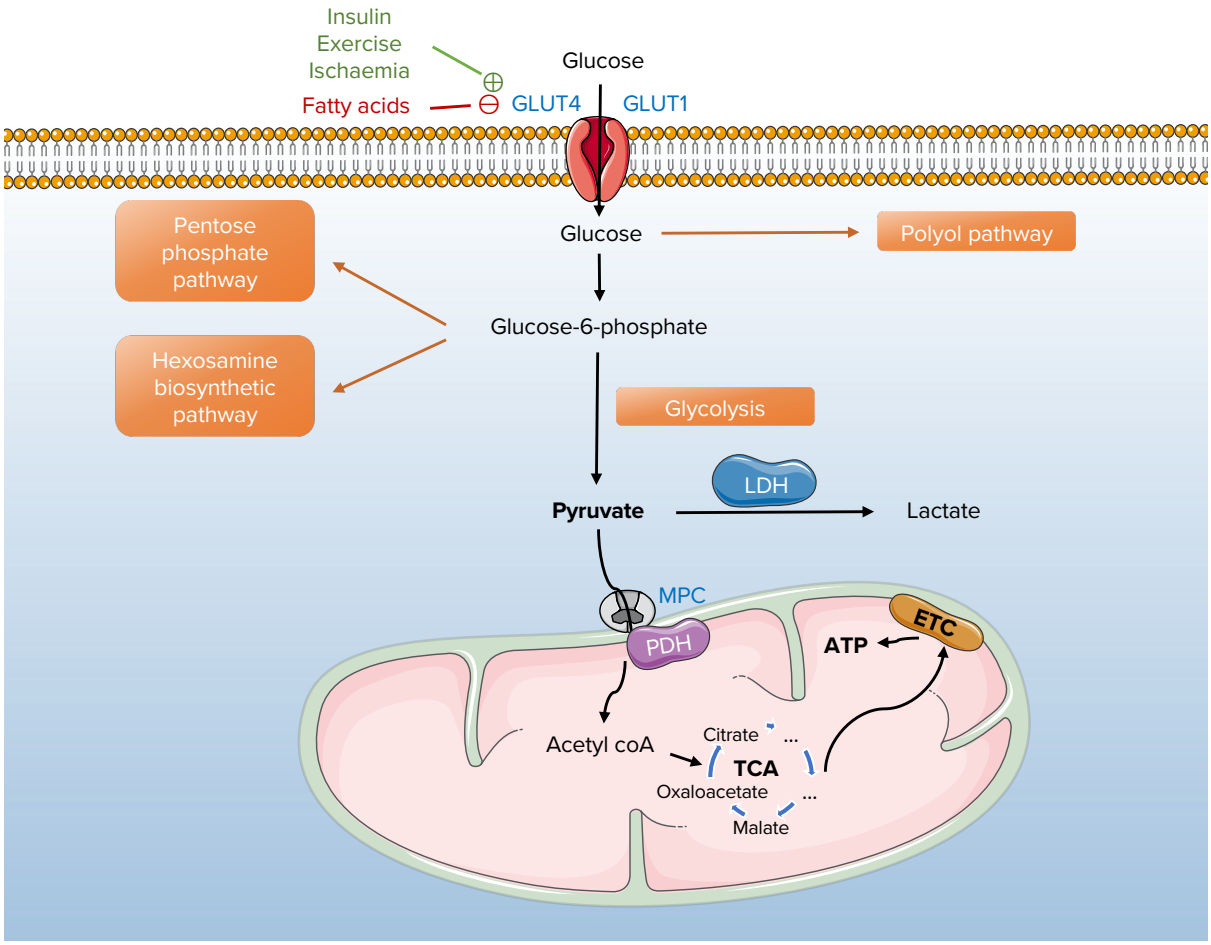

Figure 6: Glucose metabolism in a cardiomyocyte

GLUT: Glucose transporter, LDH: Lactate Dehydrogenase, PDH: Pyruvate Dehydrogenase, MPC: Mitochondrial Pyruvate Carrier, ETC: Electron Transport Chain, ATP: Adenosine Triphosphate, TCA: Tricarboxylic acid cycle. Figure created using graphics from Servier.

Ketone metabolism

In recent years, ketone bodies have been recognised as an important substrate. They are produced in the liver and are particularly abundant during nutritional and physiological stress including long-term starvation, pregnancy, and high-fat diets[164]. These include acetoacetate, β-hydroxybutyrate (βOHB) and acetone. Acetone is inactive from a metabolic perspective and undergoes excretion through the urine or exhalation.

Synthesis of ketone bodies occurs from excess beta-oxidation of circulating non-esterified fatty acids. While extrahepatic organs such as the heart and kidney can produce ketone, the liver is the only organ which can contribute significantly to circulating ketone levels in most contexts. The excess aceto-acetyl-CoA and acetyl-CoA derived from over-abundant fatty acid oxidation is then converted to 3-hydroxymethylglutaryl-CoA (HMG-CoA) by the enzyme 3- hydroxymethylglutaryl-CoA synthase 2 (HMGCS2) in what is the flux-limiting step committing to ketogenesis. The HMG-CoA is then cleaved by HMG-CoA lyase to acetyl-CoA and acetoacetate. βOHB dehydrogenase associated with the inner mitochondrial membrane controls the NAD^+/NADH dependent redox equilibrium between acetoacetate and βOHB[165].

Acetoacetate and βOHB are released into the plasma by monocarboxylate transporters (MCT1 and 2). Uptake by the myocytes is also carried out by MCT in a saturable process dependent on the plasma concentration. βOHB is the major ketone body utilised by the heart and is transported into the mitochondria where it is oxidised by βOHB dehydrogenase (BDH-1) to acetoacetate. This is then converted to aceto-acetyl -CoA by succinyl-CoA:3-oxoacid CoA transferase (SCOT) in a succinyl-CoA coupled, fate-committing reaction. Subsequent action of thiolases such as acetyl-CoA acetyltransferase (ACAT1) produces acetyl-CoA which enters the TCA cycle. The exclusion of SCOT from hepatocyte mitochondria ensures net export of ketone bodies by the liver.

Generally, ketones account for about 5% of the energy supply of the heart, however this is increased during starvation. During fasting, the decrease in insulin and rise in glucagon levels promote lipolysis and ketone production. At circulating levels of 2mM, βOHB could become a significant metabolic fuel for oxidation as demonstrated in animal models[166]. For reference, the level of ketones during extreme fasting (75-250kcal intake/day) rises from 1mM on day 1 to 2mM on day 3 and 5mM by day 12, suggesting that maintenance by dietary fasting is not feasible long term[167]. In comparison, provision of exogenous ketone ester supplementation results in ~3mM circulating levels and increased fractional extraction in both control and HFrEF hearts, demonstrating the ability of the heart to enhance uptake depending on availability[168]. Fatty acid uptake and oxidation is inhibited by ketones[169], as is glucose uptake[170]. Theoretically, ketone bodies produce ATP with a P:O ratio of 2.5. Therefore, in relation

to oxygen efficiency, they are more efficient than fatty acids, but less efficient than glucose.

Lactate metabolism

Lactate can provide energy in conditions where circulating levels increase. Cellular uptake is performed by a monocarboxylic anion transporter (MCT). Lactate dehydrogenase (LDH) converts this to pyruvate which then enters the TCA cycle.

Amino acid metabolism

Amino acid oxidation is also capable of ATP supply to the heart and generally accounts for <2% of production. Of these, branched chain amino acid (BCAA) oxidation is particularly well characterised. Firstly, mitochondrial branched chain amino-transaminase (BCATm) catalyses a reversible transamination to a branched chain α-keto-acid (BCKA)[171]. This is then followed by oxidative decarboxylation of the BCKA by mitochondrial branched-chain α-keto-acid decarboxylase (BCKDH). This process can either generate acetyl-CoA for the TCA cycle or succinyl-CoA for anaplerosis. Phosphorylation of BCKDH inhibits activity, whereas dephosphorylation activates it.

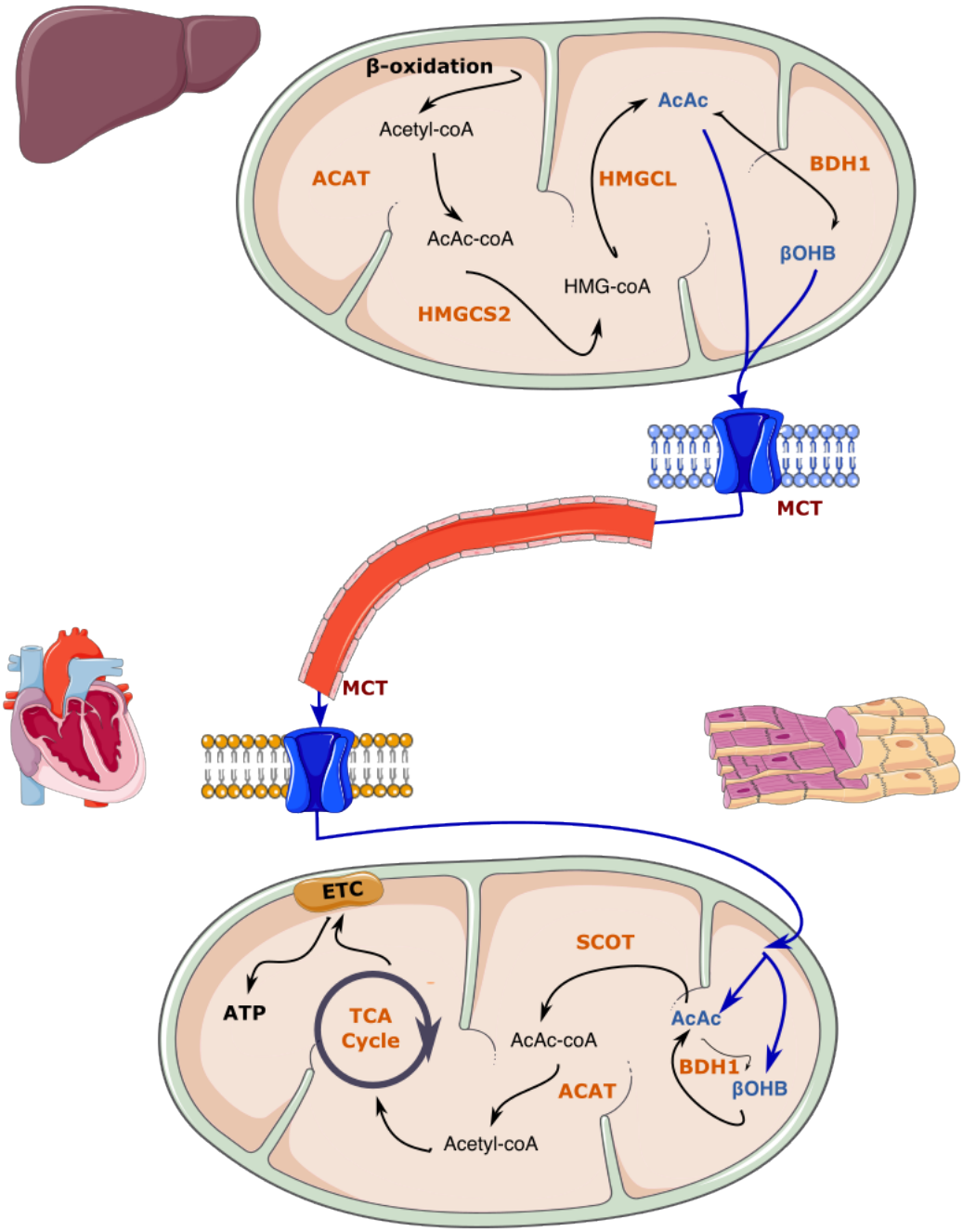

Figure 7: Ketone production and metabolism

MCT: Mono-carboxylate transporter, AcAc: Acetoacetate, βOHB: β-hydroxybutyrate, HMG-CoA: 3-hydroxymethylglutaryl-CoA, ACAT: acetyl-CoA acetyltransferase, HMGCS2: 3- hydroxymethylglutaryl-CoA synthase 2, HMGCL: HMG-CoA lyase, BDH: βOHB dehydrogenase, TCA: Tricarboxylic acid cycle, ETC: Electron Transport Chain, ATP: Adenosine Triphosphate. Figure created using graphics from Servier.

1.6 CARDIAC METABOLISM IN HFpEF

In a similar manner to HFrEF, there is impaired cardiac energetics in HFpEF. Over time, there has also been a transition from hypertensive disease being the primary clinical driver of HFpEF towards a cardiometabolic phenotype driven by obesity and diabetes and frequently, all of them together.

The limitations of animal models

A paucity of appropriate experimental models has resulted in a more limited characterisation of cardiac metabolism in HFpEF in comparison to HFrEF. Volume and pressure overload models without a reduction in ejection fraction, as well as models of diastolic dysfunction in the form of obesity and type 2 diabetes form the majority of studies. However, the heterogenous contribution of many or all of these metabolic factors as well as aging has meant that recapitulating a representative HFpEF model has been challenging. More recently, advanced models using 'three hits' have been developed to help remedy this[172]. Examples include combining obesity (high-fat diet), hypertension due to desoxycorticosterone pivalate (DOCP) or Angiotensin II and aging[173,174]. This results in models which demonstrate clinical features of HFpEF such as myocardial hypertrophy, fibrosis and pulmonary congestion. However, the applicability of these models to the disease remains uncertain.

Human studies

There are few studies in humans focusing specifically on HFpEF. The impact of the most prominent risk factors for HFpEF such as diabetes, obesity and hypertension have been more extensively studied. These are thought to contribute to energetic remodelling in HFpEF.

Type 2 diabetes has long been recognised to lead to asymptomatic diastolic dysfunction and is associated with the subsequent development of heart failure[175,176]. It is a state of insulin resistance, leading to reduced glucose uptake and oxidation[177]. In contrast, there is a substrate shift towards fatty acids with increased circulating plasma levels, uptake and oxidation[178,179] while demonstrating impaired diastolic function[180]. In patients with diabetes, there may be greater efficiency of ATP use with enhanced free fatty acid provision rather than glucose. This results in

reduced CK flux whilst maintaining an unchanged PCr/ATP ratio with improved LV systolic function and cardiac work[181].

Obesity, one of the other major contributors to HFpEF also exhibits insulin resistance leading to lower glucose uptake and oxidation. There are higher levels of lipolysis and FFA release from adipose tissue resulting in an increase in PPARα expression. This leads to a compensatory increase in uptake. Yet, it is thought there is a mismatch with oxidation. This results in lipotoxicity due to intramyocardial accumulation of diacylglycerols, ceramides and triglycerides. The degree of obesity is also linked to upregulation of genes involved in ATP synthesis and transport in HFpEF in comparison to donor controls[182].

Hypertension in contrast is associated with downregulation of fatty acid oxidation and enhanced glucose use[183,184]. Atrial fibrillation, another frequent comorbidity in HFpEF also demonstrates increased uptake of glucose in the atria which normalises following return to sinus rhythm[185].

Recent studies in HFrEF have suggested that increasing fatty acid oxidation could be beneficial where the LV systolic function is impaired. Administration of intralipid results in an increase in LVEF and improvement in PCr/ATP[186]. A separate study linked an increase in fatty acid uptake to the reverse remodelling seen with cardiac resynchronisation therapy[187]. Whether these beneficial effects of fatty acids are present in HFpEF is yet to be tested.

INDIVIDUAL SUBSTRATE UTILISATION IN HFpEF AND THERAPEUTIC TARGETS

Fatty acids in HFpEF

The role of fatty acid oxidation (FAO) in HFpEF is uncertain. Diabetes and obesity leads to increased fatty acid availability. But there is contradictory data on levels of FAO in HFpEF. An animal model which reproduced obesity, glucose intolerance, hypertension with LVH and diastolic dysfunction suggested that FAO provides the bulk of the ATP production with suppression of insulin-promoted stimulation of glucose oxidation[188]. However, this has not been borne out in available human studies. In the non-fasted state, there appears to be reduced fatty acid use with an

increase in protein catabolism[146]. Additionally, quantities of myocardial medium and long chain acylcarnitines are lower in HFpEF despite similar plasma levels to controls[189]. This is paired with reduced gene expression of multiple proteins involved in fatty acid uptake and regulating metabolism. The ratio of plasma acylcarnitine/carnitine as a marker of inefficient fatty acid oxidation is linked to cardiac event rates in HFpEF[190].

It is likely that even if there were possible upregulation in fatty acid oxidation, it is insufficient to prevent accumulation of excessive lipid content in the myocardium. Such intracardiac accumulation is thought to play an important role in the pathogenesis of cardiometabolic HFpEF. Cytosolic fatty acids can either be directed to enter the mitochondria following the action of CPT or they can be esterified and stored as myocardial triglyceride or other metabolites such as ceramides. In the healthy heart, the triglyceride levels are low in comparison to the rate of free fatty acid uptake (~3mg/g tissue)[191]. These levels are thought to be tightly controlled and dysregulation in these conditions is thought to lead to lipotoxicity, predisposing to HFpEF[192]. In human cardiac proton spectroscopy studies, there is increased myocardial triglyceride content in HFpEF, particularly in women[193]. This is associated with reduced diastolic strain rate in HFpEF and subclinical diastolic dysfunction and with impaired peak oxygen consumption on exercise testing[133,194]. Putative mechanisms for such effects include the generation of reactive oxygen species, mitochondrial dysfunction and altered calcium handling[192].

Glucose metabolism in HFpEF

Animal models have provided conflicting data. As alluded to above, many of the metabolic models have suggested a greater role for fatty acid oxidation. This contrasts with studies based on LVH/hypertensive models of HFpEF. Animal studies in the 1990s indicated an increased contribution of glycolysis to ATP production in LV hypertrophy with no change in glucose oxidation compared to control hearts[195]. More recent studies have demonstrated an increase in glycolysis with uncoupling of glycolysis from glucose oxidation in a hypertensive model of HFpEF[196].

Targeted metabolomics in the myocardium of human patients with HFpEF show increased glucose levels with increased GLUT1 expression [197]. Despite this, there is

down-regulation of hexokinase, phosphofructokinase and phosphoglycerate kinase leading to reduced glucose-6-phosphate, fructose 1,6 – bisphosphonate and 3-phosphoglycerate. This suggests proximal downregulation of glycolysis. Moreover, there is a 5-fold increase in glycogen content which is likely related to downregulation of glycogen phosphorylase which converts glycogen to G6P. These changes were not explained by the presence of obesity or diabetes.

Interestingly, the levels of myocardial pyruvate are noted to be high despite a reduction in pyruvate kinase. This may be explained by the increased extraction of pyruvate and lactate[146]. Uptake of pyruvate into the mitochondria may be impaired due to reduced expression of MPC with a reduction in downstream TCA metabolites seen. Overall, the increase in glycolytic end-products is likely to represent inefficiency in proceeding to the mitochondrial TCA cycle and oxidative phosphorylation.

An alternative fate for pyruvate is conversion to aspartate. There is increasing evidence to suggest that increased glucose utilisation is necessary to promote aspartate biosynthesis in LVH[198,199]. This is essential for nucleotide synthesis and downstream RNA and protein synthesis to increase LV mass. Preserving FAO maintains catabolic metabolism, preventing hypertrophy in these models.

Overall, despite greater glucose uptake, there appears to be a likely decrease in glucose oxidation and glycolysis with greater extraction of pyruvate from the arterial circulation. It is possible that a predominant LVH phenotype could exhibit different glucose utilisation to a metabolic syndrome predominant phenotype, although not all of this may relate to ATP synthesis but instead could serve to increase LV mass.

Ketones in HFpEF

There has been increasing interest in the role of ketones as an alternative fuel in heart failure in response to downregulation of fatty acid and glucose metabolism. Much of the work has been focused on HFrEF however with limited studies in HFpEF.

In earlier studies of patients with LV hypertrophy secondary to aortic stenosis, there was increased cardiac uptake of ketone bodies in comparison to controls[200]. In patients with diabetes, a similar observation has been made, thought to be a compensatory measure to the reduction in glucose uptake[201].

In an unfasted state, there is no increase in circulating levels of ketone bodies in HFpEF, although there is possibly extraction of acetoacetate across the heart[120,146]. While myocardial ketone bodies are increased in HFrEF this is not the case in HFpEF[189]. In addition, C4-OH beta-hydroxybutyryl was significantly lower in HFpEF myocardium compared to HFrEF or controls suggesting that ketone metabolism is not upregulated, at least in those with high levels of obesity. However, this does not necessarily exclude the ability to take up and utilise ketone bodies when levels are high.

There are multiple animal studies which raise promise of a beneficial effect of ketones in HFpEF. The administration of βOHB improved diastolic function and attenuated cardiac inflammation and fibrosis in mice models of HFpEF[173,202]. Further, ketone ester treatment appeared to attenuate ventricular hypertrophy, atrial enlargement and lung congestion[203]. Interestingly, the combination of an SGLT-2 inhibitor with ketone ester treatment for 12 weeks resulted in a synergistic improvement in diastolic function and cardiac ATP levels compared to either alone.

Recently, a randomised, double blind crossover study performed by Gopalasingam et al in patients with HFpEF and type 2 diabetes demonstrated that acute administration of oral ketone ester results in an increase in cardiac output with a modest reduction in PCWP of 1mmHg at rest[204]. During peak exercise there was a greater reduction in PCWP of 5mmHg with an increase in stroke volume. This demonstrated a favourable acute haemodynamic effect of ketonaemia.

There are limited studies looking at the effects of ketones on myocardial energetics and have primarily been performed in healthy participants with none in HFpEF. Administration of a ketone ester in healthy participants did not result in a change in cardiac PCr/ATP or skeletal muscle metabolic parameters although unlike HFpEF there is no energetic deficit to correct[205].

Metabolism as a therapeutic target in HFpEF

Approaches to reduce fatty acid oxidation and increase glucose oxidation have represented the bulk of the therapeutics targeting metabolism in heart failure with a longer history in HFrEF than HFpEF. Trimetazidine, a partial fatty acid oxidation inhibitor, did not improve myocardial energetics, exercise haemodynamics or functional indices in HFpEF[206]. In another study, ranolazine appeared to reduce PCWP and LVEDP, although at the expense of a small reduction in cardiac output, but with no change in cardiopulmonary exercising testing or relaxation parameters measured invasively or on echocardiography[207].

The converse approach, i.e. increasing fatty acid oxidation has also been tested. In a randomised trial of L-carnitine in patients with HFpEF there was improvement in diastolic parameters and left atrial remodelling on echocardiography[208]. The effects of increasing ketone body usage have yet to be tested in human studies of HFpEF, but trials are underway.

1.7 RESEARCH RATIONALE

The aim of the work within this thesis is to address a number of knowledge gaps within our understanding of HFpEF.

Firstly, there has been greater recognition of the importance of endotypes in HFpEF with different degrees of contractility, stiffness and haemodynamic responses to exercise stress. It is highly likely that there are differences in the systemic molecular signature that either predispose to or represent a consequence of these endotypes. However, this has not been studied previously with only limited characterisation of the myocardium having been performed. In addition, given that there are limitations in exercise reserve in many patients with HFpEF a greater understanding of the change in the molecular milieu with exercise could provide therapeutic targets.

Secondly, given the metabolic insults present in many of the comorbidities which predispose to HFpEF an energetic component to its development is likely with PCr/ATP known to be impaired. There have been no studies which have examined ATP delivery through the CK system in HFpEF. With conflicting data from studies within these comorbidities, it is not known whether there is a unifying energetic phenotype of HFpEF or if it is a result of impaired ATP delivery or inefficiency of use.

Finally, given that the evidence so far indicates abnormal substrate utilisation in HFpEF and the selection of substrate is key to ATP production and efficiency, it represents a potential therapeutic target. The effects of substrate switching in HFpEF on myocardial energetics, ATP delivery and function are not known and would inform development of metabolic therapies.

1.8 AIMS OF THE THESIS

1.8.1 To characterise exercise responses of HFpEF and elucidate endotypes with different haemodynamic properties during exercise stress

In Chapter 3, I characterise the effects of exercise stress within HFpEF in comparison to controls using multiple modalities including multi-parametric CMR, echocardiography, lung function tests and functional assessment. From here, the endotypes of HFpEF as defined by haemodynamics, i.e. LVEF 50-60% and LVEF >60% are compared to each other. In order to gain greater insight into the differences in molecular milieu which underlies HFpEF and its endotypes, a comparison of the plasma proteome with the control proteome is performed following exercise stress.

1.8.2 To understand changes in the myocardial energetic state and creatine kinase kinetics in HFpEF and its relationship to cardiac function

In Chapter 4, I examine the myocardial energetic state as measured by PCr/ATP and creatine kinase flux in HFpEF using ^{31}P phosphorus spectroscopy and saturation transfer techniques. Specifically, comparison is made to age-matched controls to account for natural changes which occur in asymptomatic individuals as they age. The relationships of these with exercise stress response are explored using magnetic resonance and echocardiography.

1.8.3 To examine the effects of substrate switching using fat, glucose and ketones on the energetics and function of the heart in HFpEF

In Chapter 5, I examine the effects of substrate manipulation on cardiac energetics and function in HFpEF using multi-parametric CMR and echocardiography. In addition to rest, whole-heart stress responses to exercise are also characterised.

CHAPTER 2: METHODS

2.1 Ethical approval

Ethical approval for all studies outlined in this thesis was provided by the South Central – Oxford C Research Ethics Committee and carried out in accordance with institutional procedures and the principles of the Declaration of Helsinki. The specific approvals for the work in each chapter are detailed below:

Novel endotypes in heart failure:	REC reference 13/SC/0376
Myocardial energetics in HFpEF:	REC reference 13/SC/0376
Substrate selection in HFpEF:	REC reference 18/SC/0170

2.2 Statistical analysis

Statistical analysis and visualisation was performed using Prism Version 10.3.0 (Graphpad holdings, San Diego, USA) and RStudio 2023.06.01 (Posit, Boston, USA).

Data are presented as mean ± standard deviation unless otherwise specified. Two-tailed testing was performed for statistical analysis. The presence of a normal distribution of data for unpaired data or for the differences in the case of paired data was established using a Shapiro-Wilk test. Student's t-test or one-way ANOVA was performed for continuous variables with normal distributions. For other continuous data, non-parametric tests were performed – Wilcoxon signed rank tests for paired and Mann-Whitney U tests for unpaired continuous data. Repeated-measures ANOVA was performed where data from the same participants were recorded over more than 2 time points. Tukey post-hoc correction was performed for pair-wise comparisons in this instance. Categorical data were assessed using the Chi-Square test. Pearson correlation was performed when data were normally distributed and Spearman's rank correlation tests when they were not. The significance threshold was set at a p-value <0.05.

The statistical methods employed for proteomics analysis and any additional methods are detailed in the relevant chapters.

2.3 Magnetic Resonance Spectroscopy

All magnetic resonance studies including proton imaging and spectroscopy was performed on a Siemens Prisma 3 Tesla scanner (Siemens Healthcare, Erlangen, Germany).

2.3.1 ^{31}P DRESS Magnetic Resonance Spectroscopy

Phosphorus spectra were acquired in a fasting state through the use of a depth resolved surface coil spectroscopy (DRESS) technique[209]. This method was chosen for the study in Chapter 3 based on availability of ^{31}P techniques at the point of study commencement.

A dual-tuned surface ^{1}H/^{31}P coil (butterfly coil for ^{1}H, 11cm loop for ^{31}P, Rapid Biomedical GmbH, Rimpar, Germany) was placed over the heart with the subject lying supine and moved to the isocentre of the scanner. Optimal positioning of the coil was ensured by acquiring the locations of cod-liver oil phantoms in addition to the phenylphosphonic acid (PPA) fiducial attached to the coil. Free induction decay inversion recovery (IR-FID) experiments were performed with increasing inversion delay (50-1500ms) with the 50ms experiments repeated at 50 and 75V in order to assess coil loading effects and measure the flip angle at the fiducial reference.

Proton localisers were used to place a single, large voxel parallel to the coil to provide a slice-selective excitation pulse, ensuring maximal coverage of the myocardium including the septum with a field of view of 200 x 200 x 20mm. 2 saturation bands of 30mm thickness were placed to suppress skeletal muscle signal and a further saturation band was placed over the liver. To ensure uniform excitation of the spectral peaks, the radiofrequency pulse was centred by subtracting 250Hz from the observed frequency of the phosphocreatine (PCr) peak, placing it between the γ and α-ATP peaks[210]. This allows the excitation bandwidth to include β-ATP through to the phospho-monoesters. 300 averages were acquired.

Spectra were analysed using the OXSA toolbox within MATLAB (Mathworks, Natick, MA, USA)[211]. The locations of the cod liver capsules and fiducial were manually identified and used in combination with the inversion recovery experiments to calculate the variation in flip angle from coil loading effects. Pre-processing including baseline correction was applied initially, followed by fitting

of the spectral peaks using the AMARES (Advanced Method for Accurate, Robust and Efficient Spectral Fitting) program[212]. Using prior knowledge, peaks for phosphocreatine, 3 ATP peaks (α, β, γ), 2,3-diphosphoglycerate and phosphodiesters were fitted using Lorentzian line shapes. Correction for blood contamination was performed by subtracting part of the 2,3-DPG signal from each of the ATP amplitudes[210]. Following correction for the effects of partial saturation, the final PCr/ATP ratio was calculated as the ratio of the corrected values of PCr/the average of the ATP peaks. Co-efficient of variation was assessed using the Cramer-Rao lower bounds, providing an indication of the signal to noise ratio in the sample and the quality of spectral fit. All spectra were assessed for inclusion in the final dataset by a blinded second assessor with expertise in MR spectroscopy.

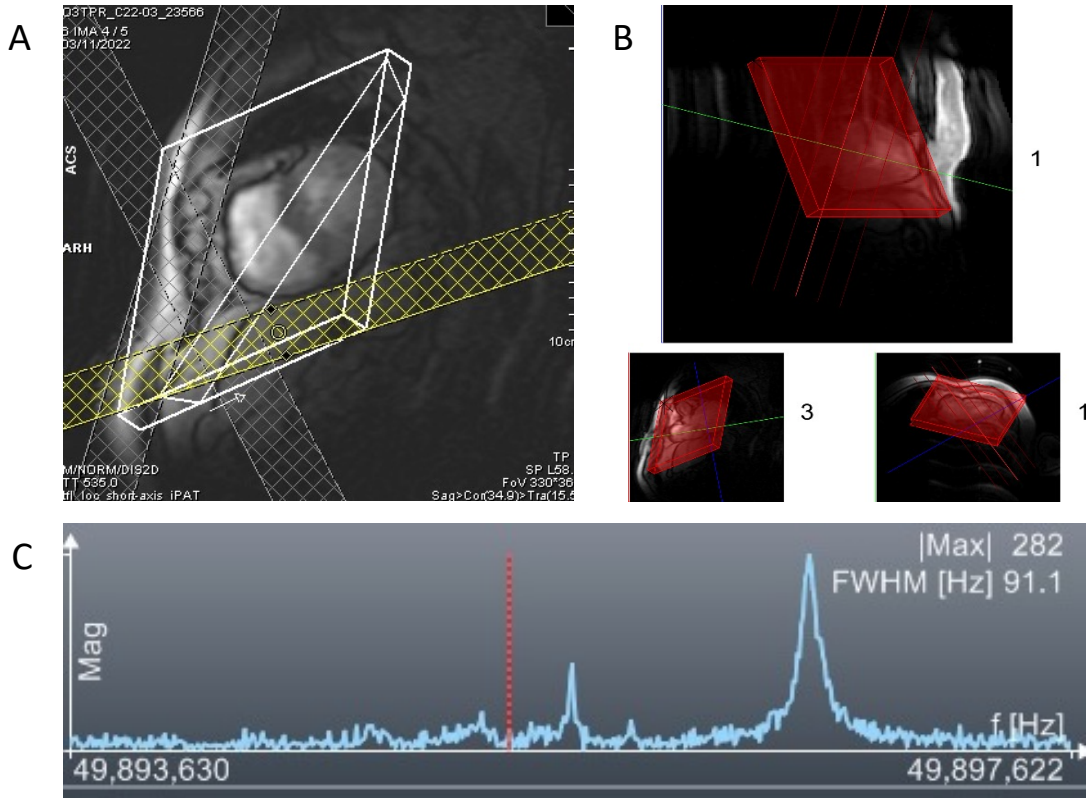

Figure 8: A: Placement of the DRESS voxel with saturation bands across the skeletal muscle and liver**. B:** Appearance of the voxel in the Matlab interface **C:** Selection of the centre-frequency 250Hz away from the PCr peak (the 2nd tallest peak in the middle of the figure) on the Siemens SyngoMR console.

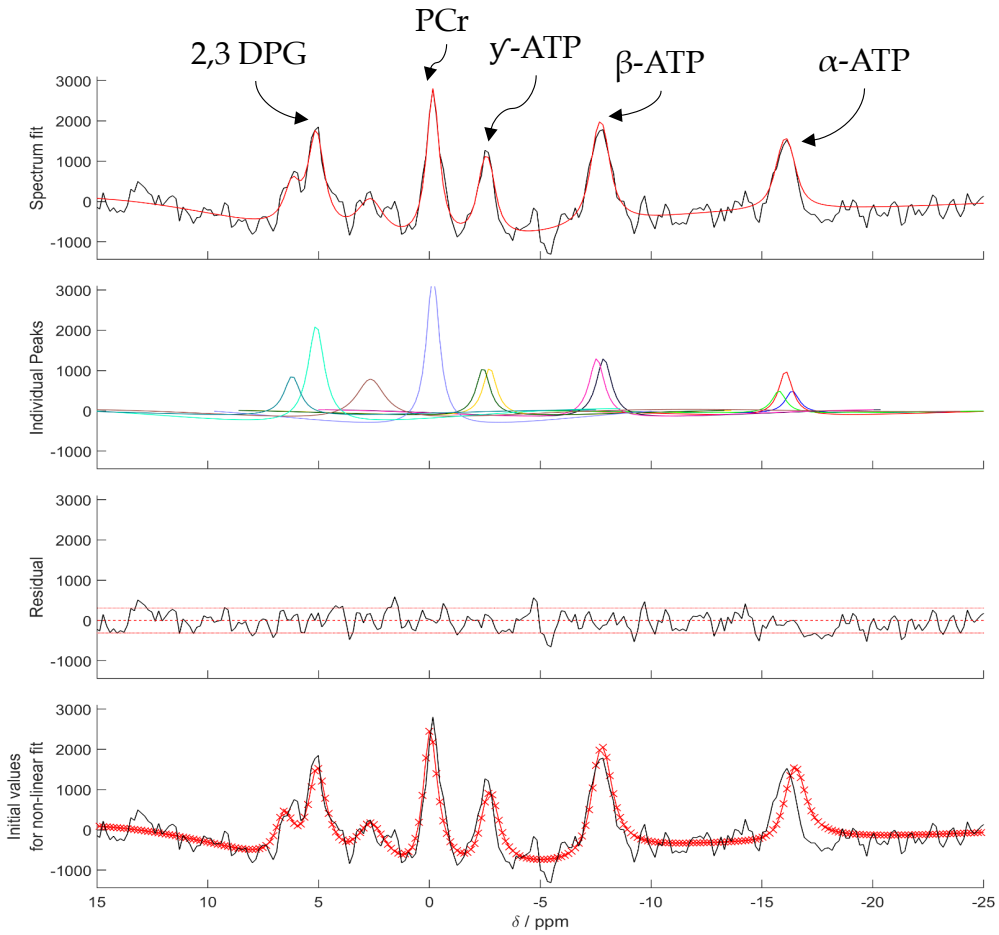

Figure 9: Example spectral fit of ^{31}P DRESS using the OXSA Matlab analysis package

2.3.2 ^{31}P 3D Chemical Shift Imaging (CSI) Spectroscopy

This technique was used when the relevant coils became available for use prior to the studies in Chapters 4, and 5 as there is a more extensive body of literature underpinning its use in cardiac studies compared to DRESS. Initial studies were performed with patients lying prone on the coil. Part-way through the study, due to loss of signal from the coil, the study subsequently used a multi-layer coil for which the subjects were scanned supine.

The prone coil used was a Siemens 1.5T Heart/Liver coil which was adapted for use on the Prisma and consisted of a large (26x28cm) ^{1}H transmit-receive and ^{31}P transmit outer element in addition to a loop (12x15cm)/butterfly (23x12cm) pair to receive ^{31}P signals. For supine studies, a custom-made ^{31}P multi-layer coil (PulseTeq Ltd., Chobham, United Kingdom) was used. In both cases, the subjects were positioned so that the heart lay at the centre of the coil. Proton localisers were used

to ensure appropriate positioning of the coil over the left ventricle by checking the position of cod liver oil phantoms relative to the heart.

Free-induction decay inversion recovery experiments were performed with increasing inversion delays with the frequency centred over the PPA fiducial. For the supine coil, this was performed in a manner similar to that described in 2.3.1 and for the prone coil consisted of inversion delays between 50-4000ms.

The parameters of the 3D acquisition-weighted chemical shift imaging (CSI) were as follows – acquisition matrix size 16x16x8 and field of view 240x240x200mm with a voxel size of 5.6 ml. HLA, VLA and short-axis localisers were used to position the matrix, with voxels aligned with the interventricular septum. Saturation bands were placed over the skeletal muscle and liver to avoid contamination. The centre-frequency was set to -250Hz from the PCr frequency in order to uniformly excite the phosphorus peaks of interest as in 2.3.1. The acquisition was non-gated with a TR of 720ms and TE 2.3ms and lasted approximately 9 minutes.

Analysis was performed using an in-house Matlab script as described in 2.3.1. Reconstruction was performed using the SLAM method which has been validated for use at 3T and 7T[213,214]. Here, voxels covering the myocardium were selected and the signal averaged to produce a PCr/ATP ratio following blood and saturation correction. Where this was not possible, 2 individual voxels at the interventricular septum adjacent to each other were selected and the PCr/ATP ratio averaged.

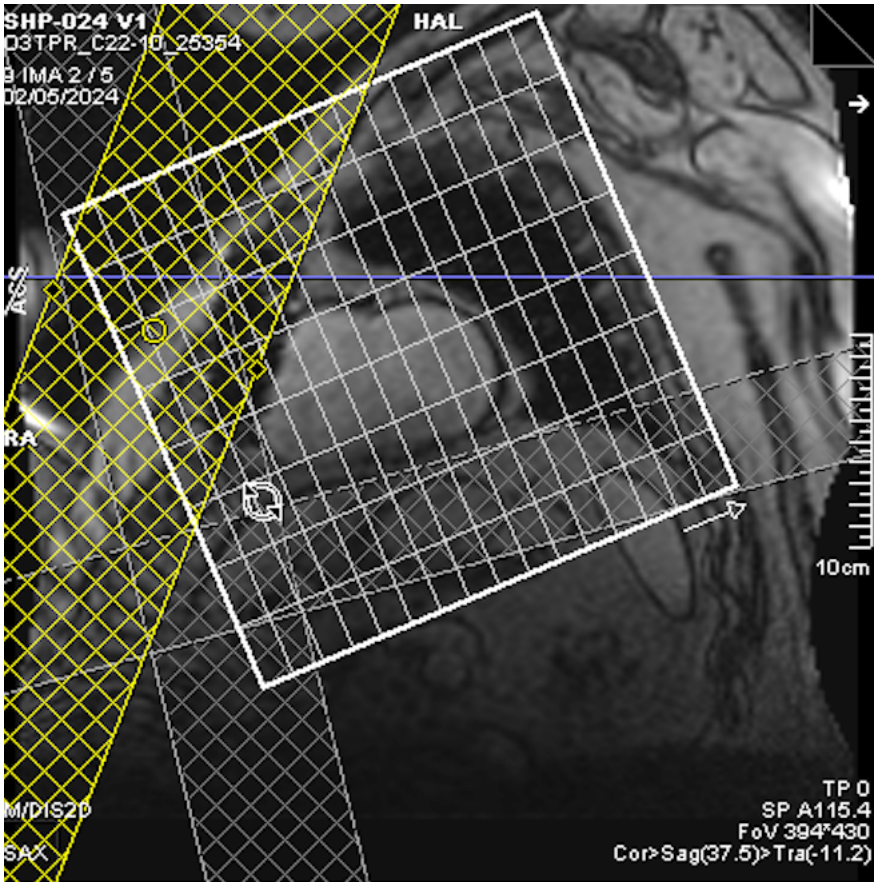

Figure 10: Illustrative placement of the 3D CSI matrix with a voxel placed directly over the interventricular septum on the Siemens MR console

2.3.3 ^{31}P Triple Repetition Saturation Transfer (TRiST)

The creatine kinase equilibrium is expressed as:

$$MgADP^{-} + PCr^{2-} + H^{+} <_{k-1}^{k1}> MgATP^{2-} + Cr$$

which can be represented as a simpler, 2-site exchange:

$$PCr <_{kr}^{kf}> \gamma ATP$$

Here k_f is the unidirectional pseudo first order rate constant of the forward i.e. ATP producing direction, while k_r is that of the reverse PCr producing direction. Flux in either direction can be calculated by multiplying the concentration of the constant by [PCr].

Saturating the γ-ATP resonance peak results in a corresponding fall in the height of the PCr peak, enabling calculation of k_f.

$$k_f = \frac{1}{T'_{1,PCr}} \cdot \left(1 - \frac{M'_{0,PCr}}{M_{0,PCr}}\right)$$

where $M'_{0,PCr}$ = the magnetisation of PCr when γ-ATP is saturated (fully relaxed, equilibrated), $M_{0,PCr}$ = the magnetisation of PCr when γ-ATP is not saturated, $T'_{1,PCr}$ = the apparent T_1 of PCr when γ-ATP is saturated. In order to achieve this, the TRiST sequence was used and is described below[215].

The subjects were scanned supine. A custom-made ^{31}P multi-layer coil (PulseTeq Ltd., Chobham, United Kingdom) was placed over the left ventricle axially and centred in the scanner. ^{1}H gradient echo localisers acquired using the body coil were used to ensure appropriate positioning of the multi-layer coil over the left ventricle while checking the position of cod-liver oil phantoms and the PPA fiducial. Transverse and sagittal localisers were obtained. Using these, the 1D CSI matrix (160 x 160 x 160mm) was placed with voxels parallel to the coil, with approximately 2 voxels outside the body, 2 covering the skeletal muscle and the remainder covering the heart.

Four sequences were consecutively run with 16 phase encoding steps to allow depth-selection.

1) Short TR sequence with no saturation
2) Short TR sequence with γ-ATP saturation
3) Long TR sequence with γ-ATP saturation
4) Short TR sequence with a 'control' saturation pulse targeted on the other side of the PCr peak, in the opposite direction to the γ resonance at an equivalent distance.

For the very first acquisition, the centre frequency is set by subtracting 70Hz from the PCr peak, although this acquisition is not localised to the heart and is thus biased towards the skeletal muscle peaks. The centre frequency was set for the

remainder from the first sequence by placing it exactly halfway between the PCr and γ-ATP peaks in the most apical cardiac voxel to account for subtle differences in PCr and ATP chemical shift frequencies between cardiac and skeletal muscle.

The sequence uses adiabatic half-passage (AHP) pulses to achieve 90° excitation regardless of the distance from the coil (which affects B1 transmit strength) provided the adiabatic threshold is reached[216]. The maximal transmit voltage of the coil of approximately 165V was used for all AHP pulses. A modified DANTE (Delayed Alternating with Nutation for Tailored Excitation) pulse was applied for saturation (duration 0.1ms, inter-pulse delay 0.25ms) with a saturation voltage of 25V as this was sufficient to suppress γ-ATP and avoid underestimation of k_f. The control pulse accounts for off-target, spill-over saturation onto the PCr peak.

Post-processing was performed using a dedicated Matlab based tool. The most apical cardiac voxel without skeletal muscle contamination was used to maximise signal to noise. Where necessary, other voxels were selected for use when judged to be of sufficient quality by a second, blinded operator with expertise who also reviewed all datasets.

Table 1: TRiST acquisition parameters

Sequence	Selective saturation	Averages	TR (s)	Duration (min)	Measured parameters
1	None	2	15	9	$M_{0,PCr}$, $M_{0,\gamma ATP}$
2	γATP	18	1.5	10	$M'_{1.5s,PCr}$
3	γATP	8	9.5	22	$M'_{9.5s,PCr}$
4	Control	2	15	9	M^{Ctrl}_{PCr}, $M^{Ctrl}{}_{\gamma ATP}$

This provides input into calculations for k_f.

$$M_{0,PCr} = \frac{M'_{1.5s,PCr}}{1 - e^{\frac{-1.5s}{T_1'}}}$$

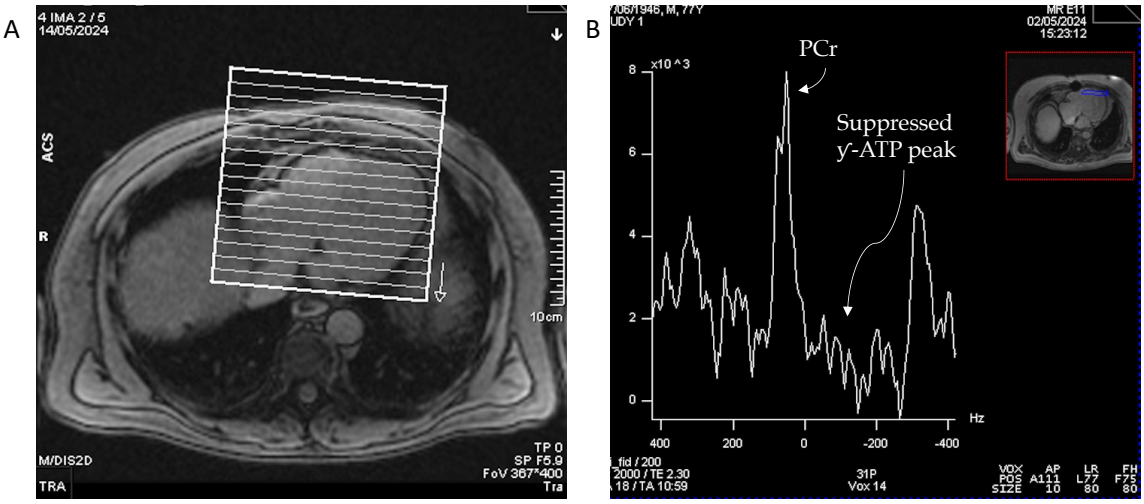

Figure 11: A: Positioning of voxels across the myocardium. **B:** Suppression of the γ-ATP peak at the apical cardiac voxel as viewed on the Siemens console

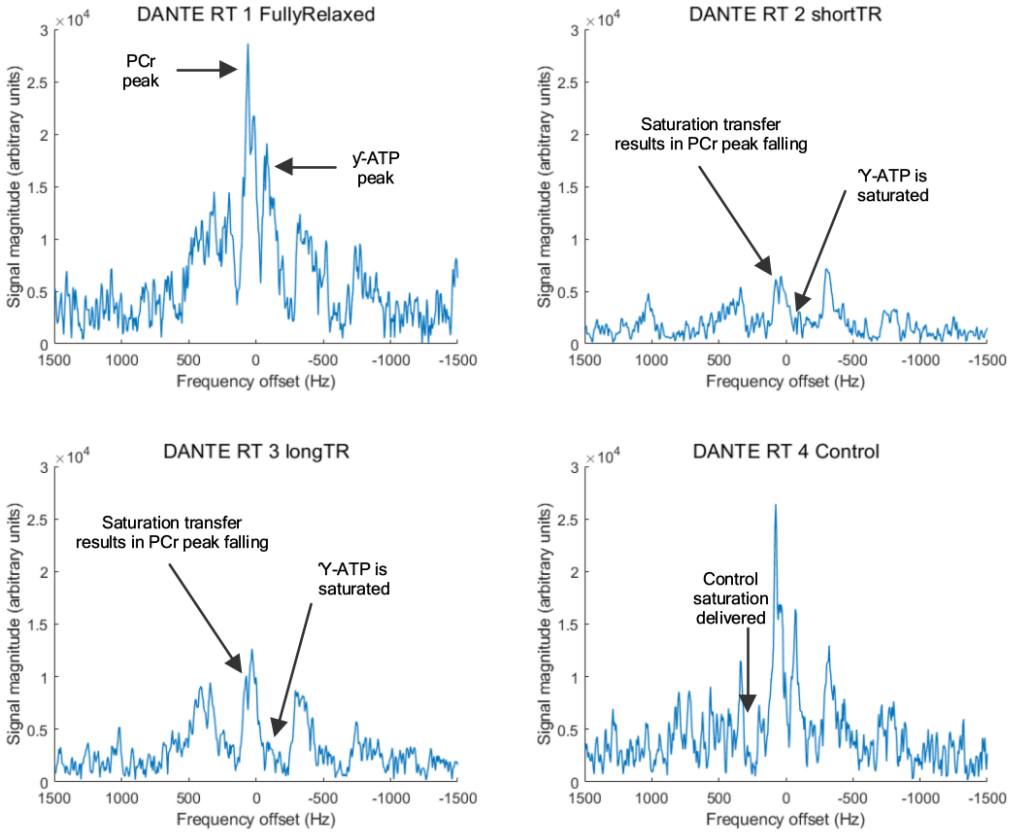

Figure 12: TRiST spectra from a participant with HFpEF at 3T

This demonstrates the fall in the PCr peak amplitude due to saturation transfer following application of the DANTE pulse to γ-ATP.

2.3.4 ^{1}H Proton Spectroscopy

In order to quantify myocardial triglyceride content, ^{1}H Proton Spectroscopy was performed supine using a water-suppression cycling STEAM (Stimulated Echo Acquisition Mode) sequence as described previously[217]. SSFP cine images were used for planning. A voxel with a volume of 32 x 18 x 18mm^3 was placed in the mid-ventricular septum to reduce the risk of contamination from epicardial fat. B_0 shimming was performed using an adjust volume of 40 x 30 x 26mm^3 during a breath-hold and adequate field homogeneity confirmed. Spectra were acquired with and without water suppression in mid-diastole during end-expiration to minimise cardiac motion.

Post-processing was performed using an in-house MATLAB script.

Myocardial triglyceride content was calculated as a percentage relative to water signal.

$$\frac{Sum\ of\ lipid\ signal\ amplitudes}{Water\ signal\ amplitude} \times 100\%$$

Where the lipid signals detected are -CH_2- @ 1.3 ppm, -CH_3 @ 0.9 ppm.

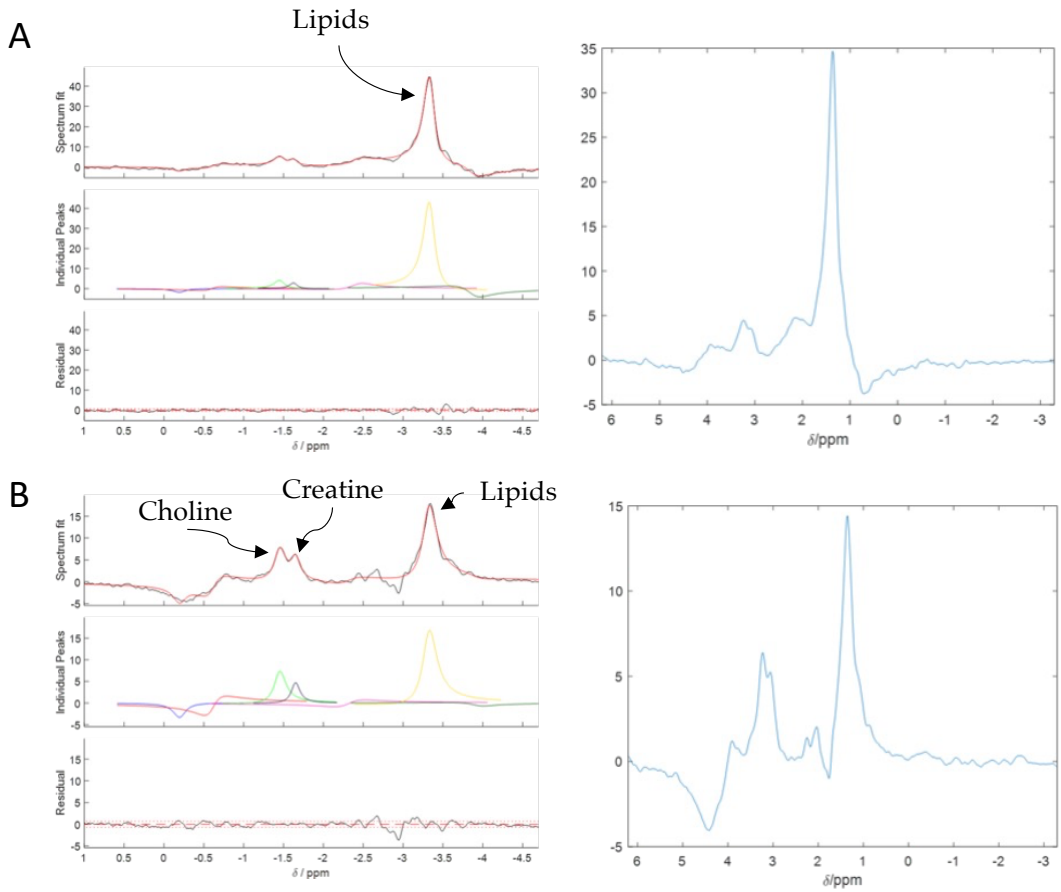

Figure 13: A: Spectral fitting of ^{1}H spectroscopy in a participant with HFpEF. **B:** Spectral fitting in a healthy control with a substantially smaller lipid peak.

2.4 Cardiac Magnetic Resonance Imaging

2.4.1 Cardiac volumes and function

This was performed supine. A 24-channel spine matrix and 18 channel body surface coil was used to enable parallel imaging. Following standard planning, long axis images at rest were acquired at breath-hold using a balanced steady state free precession (bSSFP) sequence with typical parameters as follows with adjustments depending on patient features - slice thickness 8mm, TE 1.2ms, TR 42ms, flip angle 40°, field of view (FOV) 400mm, matrix size 192 in the frequency encoding direction. Retrospective gating was used in sinus rhythm, with prospective gating used for irregular rhythms.

A short-axis stack covering the atria and ventricles were acquired with the patient free breathing, using a 4x accelerated, compressed sensing modified bSSFP real-time sequence. Typical sequence parameters were as follows with adjustments

based on patient factors and SAR (specific adsorption rate) limitations – TR 47ms, TE 1.1ms, FOV 400x360mm², slice thickness 8mm, flip angle 40-45° with a matrix size of 160 in the frequency encoding direction. Typical spatial resolution was 1.8x1.8mm, with 25-35 cardiac phases. This sequence was repeated following 5 minutes of exercise stress to acquire free breathing, short axis images. Long-axis imaging was performed during exercise using the same sequence.

Post-processing was performed offline using CVI42 (version 5.13, Circle Cardiovascular Imaging Inc, Calgary, Canada). Endocardial and epicardial contours were drawn in a semi-automated fashion, enabling calculation of LV mass, ejection fraction and strain. Endocardial borders were delineated through a full cardiac cycle to produce LV diastolic filling curves. Atrial borders were manually contoured on short-axis slices.

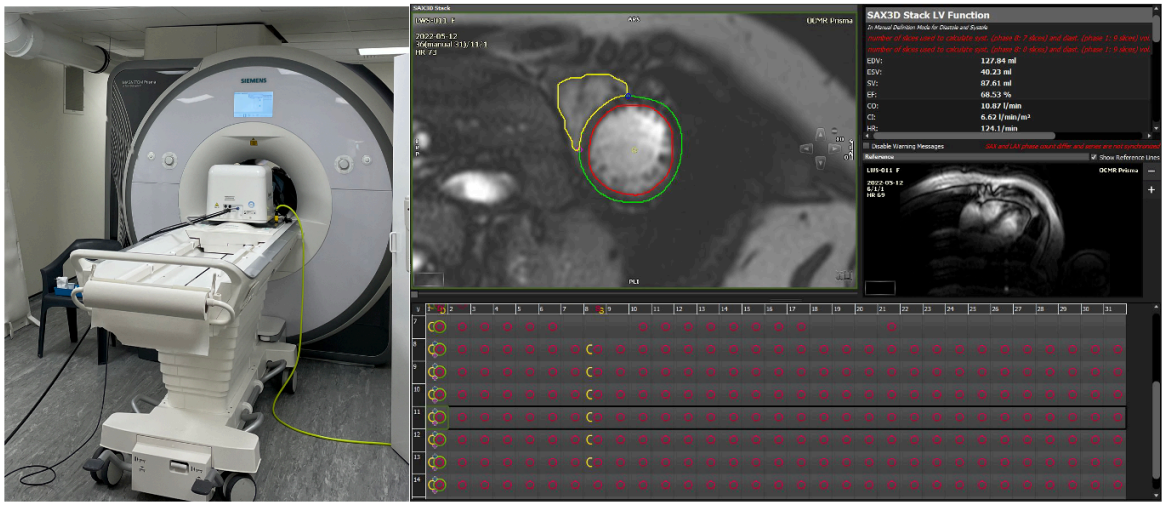

Figure 14: The left-hand panel demonstrates a participant in the scanner undergoing the ergometer protocol. The right-hand panel shows semi-automated whole cardiac cycle contouring

2.4.2 Coronary sinus flow

The participant who underwent paired coronary sinus – radial artery sampling as described later also underwent coronary sinus flow assessment during the MR study. A cine of the coronary sinus in short axis was acquired following planning from localisers. A non-breath-hold averaging sequence was performed during rest and during exercise. VENC was set to 60 cm/s at rest and 120 cm/s during exercise.

2.4.3 Exercise stress

Steady state exercise at a fixed, sub-maximal workload of 35W was performed for 6 minutes using an MR conditional stepper ergometer (Cardio Step, Ergospect GmbH, Austria). This allows for supine exercise in the MR scanner with the heart remaining at the isocentre of the bore, thus enabling high quality imaging.

2.5 Echocardiography

Assessment of diastolic function was carried out using a GE Vivid I system (GE Healthcare, Chicago, USA). 2D images were acquired for assessment of cardiac wall thickness, function and chamber size. Colour doppler and continuous wave doppler assessment was performed to assess for significant valvular disease and to measure the tricuspid regurgitant velocity. Pulse wave doppler and tissue doppler were used to assess markers of LV filling pressure. Right ventricular function was assessed using M-mode and tissue doppler imaging. The assessments were repeated during sub-maximal 35W exercise using a pedalling ergometer (Magnetrainer, 3D Innovations, Colorado, USA) at approximately 5 minutes, to coincide with the acquisition of the real-time cine CMR imaging. This was performed supine to match that of the MR exercise as there are differences in cardiac haemodynamics in comparison to upright exercise[218].

2.6 Lung Function Tests

Lung function tests were conducted using a Vyntus™ one pulmonary function system (Vyaire Medical Inc., Chicago, USA). Baseline spirometry was performed at a minimum in duplicate and the best attempt recorded. Gas exchange was measured using DLCO and was recorded in duplicate with the best attempt recorded. The test gas was composed of 0.28% carbon monoxide, 21% oxygen, 0.28% methane (tracer) with nitrogen forming the remainder. The measurements were repeated following 6 minutes of 35W exercise using an ergometer.

2.7 Blood Samples

2.7.1 Sample preparation for proteomic analysis in Chapter 3

Blood samples were collected at rest and immediately following 6 minutes of exercise. BD-vacutainer SST (Serum Separator Tube) and K_2EDTA (Ethylenediamin tetra-acetic acid) were used for serum and plasma preparation respectively. The Serum SST tubes were analysed in the Oxford University Hospitals Biochemistry laboratory for NT-pro BNP and Troponin I.

Sample preparation for proteomic analysis was carried out by immediate centrifugation as previously described[219]. Initially, the sample was centrifuged at 1.3g for 12 minutes. The supernatant was transferred to a tube without additive and then centrifuged again at 2.5g for 15 minutes. The resulting supernatant was immediately aliquoted and stored at -80°C.

Samples were then transferred for proteomic quantification using a commercial pipeline, Somascan 7K (Somalogic Inc., Boulder, Colorado, USA). This platform uses a multiplex, modified aptamer-based assay[104]. In brief, aptamers are chemically modified short single-stranded oligonucleotides, which bind with high affinity to proteins and the Somascan assay uses aptamers with slow-off rate kinetics. The resulting Somamer reagent concentration is quantified by microarray hybridisation which in turn is directly proportional to the amount of target protein. The assay quantified up to 7000 proteins, which maximised the ability to detect differences in a large number of pathways in an unbiased manner.

Data is reported in relative fluorescence units (RFU) rather than absolute concentrations and reflect relative protein quantity, particularly in the context of making comparisons across groups. These are also normalised to a diverse, healthy adult population by calculating the ratio of the reference and measured RFUs. We undertook a comparison of NT-proBNP RFU obtained using this method with a reference standard (Oxford University Hospital biochemistry laboratory) using bloods drawn at the same time during stress. This demonstrated excellent correlation between them ($r=0.86$, $p<0.0001$). Excluding the 2 outliers with the highest NT-proBNP values in the reference measurement improved this to $r=0.92$ ($p<0.0001$) and is likely to reflect the effects of the normalisation algorithms within

Somascan and also the dilution over which the sample is assayed. This suggests that any detected differences in SomaScan RFU values are likely to represent true biological variation in the sample set.

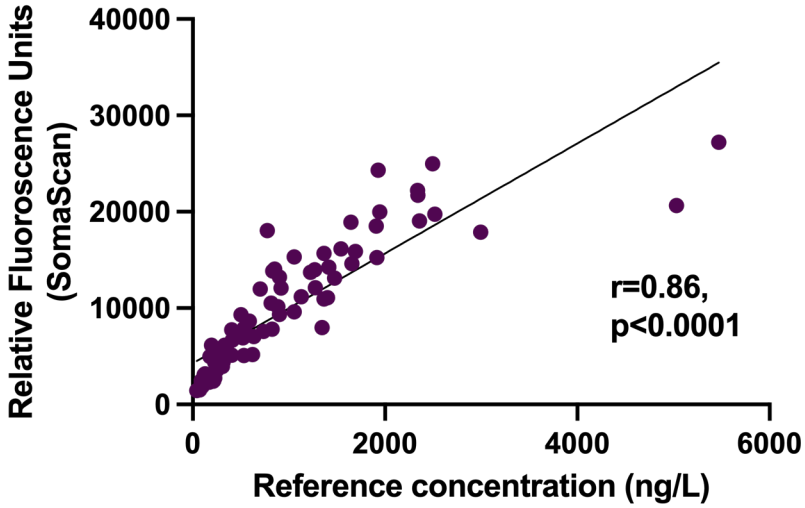

Figure 15: NT-proBNP correlation analysis of SomaScan measured relative fluorescence units vs the reference concentration at stress

2.7.2 Sample preparation for laboratory analysis in the Substrate selection in HFpEF study

Serum samples for the Substrate selection study were centrifuged for 10 minutes at 4°C at 4000rpm. The supernatant was then transferred to sample vials and stored at -80°C prior to analysis at the Oxford University Hospitals NHS Foundation Trust.

2.8 Anthropomorphic measurements

Anthropomorphic measurements

The height and weight of participants were measured using a digital weighing scale and body mass index (BMI) and body surface area (BSA) were calculated (Mosteller formula). Waist and hip circumference were measured.

Blood pressure

Brachial blood pressure was measured using an automated, oscillometric cuff. During MRI this was measured using an MR400 device (Philips, Best, Netherlands). During echocardiography and lung function assessments, this was measured using an automated machine (Carescape V100, GE Healthcare, Chicago, USA).

Electrocardiogram (ECG)

A digital 12 lead ECG was performed using a digital Cardiovit FT-1 (Schiller, Baar, Switzerland).

Six minute walk test (6MWT)

This was performed with the participants walking at a relatively fast pace they felt comfortable with along a 30m circuit. If exercise tolerance was limited by non-cardiac reasons, this was recorded and excluded for analysis.

2.9 Substrate Manipulation

2.9.1 Hyperinsulinaemic-euglycaemic clamp

A hyperinsulinaemic-euglycaemic clamp was employed to enhance glucose uptake into cardiomyocytes whilst maintaining euglycaemia at approximately the baseline glucose level[220]. Fast-acting insulin (Actrapid, Novo Nordisk, Denmark) and 20% dextrose were used in this protocol. 2 cannulae were inserted into large veins in the ante-cubital fossa in each arm. In one of the arms, both insulin and dextrose infusions were run simultaneously through a three-way tap. The other cannula was used to draw venous blood samples at regular intervals. Blood glucose was measured using a point-of-care testing device (Freestyle Optium Neo™, Abbott Diabetes Care, UK). A loading regimen was used as described below with each step being performed in sequence for 1 minute until the steady-state constant rate was reached.

63.8 mU/m^2/min	1 minute
56.8 mU/m^2/min	1 minute
50.6 mU/m^2/min	1 minute
45.1 mU/m^2/min	1 minute
40.1 mU/m^2/min	1 minute
35.7 mU/m^2/min	1 minute
31.8 mU/m^2/min	1 minute
31.8 mU/m^2/min	1 minute

25.2 mU/m^2/min	1 minute
22.5 mU/m^2/min	1 minute
20 mU/m^2/min	Remainder of the study visit

A modification was specified in the protocol if the clamp was administered to a patient with a history of diabetes mellitus where the loading as well as the steady state rate at the end of loading was doubled. At 4 minutes, an infusion of 20% dextrose was commenced at a rate of 2 mg/kg/min. At 10 minutes, a venous blood sample was drawn and the rate of the dextrose infusion was altered according to the venous glucose level. For the first hour, this process was repeated every 5 minutes until the glucose level stabilised. Subsequently, this was repeated where opportune in the research MRI and echo protocol. An in-house Microsoft Excel spreadsheet provided by the Oxford Centre for Diabetes, Endocrinology and Metabolism was used for adjustment of dextrose infusion rates.

2.9.2 Intralipid

Intralipid 20% (Frasenius Kabi, United Kingdom) primarily provides long-chain triglycerides (16-18 carbons) including linoleic, oleic and palmitic acids in addition to phospholipids. This was infused at a rate of 60 ml/hour. While the protocol specified simultaneous infusion of intravenous heparin given at 0.4 U/kg/hour, all participants randomised to this group were already on therapeutic anticoagulation and hence this was omitted due to safety concerns.

2.9.3 Ketone ester

Ketone ester (TdeltaS, Delaware, USA) was ingested orally at a dose of 0.6 mg/kg. A dose intermediate to 0.5 mg/kg and 0.75 mg/kg used in a number of previous studies was chosen to offset the relatively lengthy nature of the research imaging protocol (approximately 4 hours) while maintaining adequate ketosis throughout. Simultaneous slow crystalloid infusion was given using 0.9% Sodium chloride at 60 ml/hour to avoid additional substrates found in other balanced crystalloids and account for any haemodynamic effect caused by intravenous infusion in the other substrate arms. A baseline blood ketone level was measured using a point of care testing device capable of measuring β-Hydroxybutyrate levels (Freestyle Optium

Neo™, Abbott Diabetes Care, UK). A measurement was made at 30 minutes post ingestion prior to commencing the MRI protocol and additional measurements were made at an opportune time during the protocol. This was repeated for willing participants in the presence of either intralipid or the hyperinsulinaemic euglycaemic clamp.

2.10 Paired arterial-coronary sinus sampling

1 participant from the ketone group was invited to take part in a study to establish fractional extraction of metabolites in the fasting state at rest and exercise with comparison made following administration of ketone ester and saline.

Radial arterial access was established under local anaesthetic using a 3F arterial catheter (Vygon, Swindon, UK). Coronary sinus access was established following axillary vein puncture under fluoroscopy. A Worley coronary sinus sheath was inserted and right atrial pressures were measured. A CASII catheter was passed through this to sample blood from the coronary sinus.

Initial simultaneous sampling from the radial artery and coronary sinus were made at rest in a fasting state. Sampling was repeated following 6 minutes of exercise at 35W using an ergometer mounted on the catheter laboratory table. Ketone ester was administered in addition to 0.9% sodium chloride and both rest and exercise sampling was repeated after 30 minutes.

CHAPTER 3: NOVEL ENDOTYPES OF HFpEF AND THEIR PROTEOMIC SIGNATURES

ABSTRACT

Background

Given symptoms occur during exercise in much of HFpEF, understanding whole-heart cardiac responses to exercise will help link these to impaired functional capacity. Moreover, given there are heterogenous responses to medicines in key phase 3 trials in HFpEF, there are likely to be intrinsically different endotypes within HFpEF with potentially different exercise responses.

Methods

Patients with HFpEF (n=64) and controls of similar age (n=16) underwent multi-parametric CMR including whole-heart real-time sub-maximal exercise CMR (35W for 6 minutes) using an MR-conditional ergometer and assessment of myocardial energetics and steatosis. They also underwent lung-function tests to measure gas exchange, 6-minute walk test to assess functional capacity and completed a KCCQ (Kansas City Cardiomyopathy Questionnaire) to quantify symptom burden. Plasma was acquired immediately following 6 minutes of exercise and aptamer based proteomic profiling was performed for 7289 proteins. Differential abundance and pathway analysis was performed using Bioconductor packages in RStudio. Following an initial analysis looking at responses within HFpEF as a whole compared to healthy controls, unsupervised K-means clustering was performed to identify key differences within HFpEF. On the basis of this, a comparison of HFpEF with LVEF>60% (n=46) is made to HFpEF with LVEF 50-60% (n=18) in a similar vein.

Results

At rest, HFpEF and control groups have similar sized ventricles, LV systolic function and cardiac output. The HFpEF cohort exhibited an impairment in exercise-induced contractile reserve leading to a reduced stroke volume and cardiac output during exercise. However, there was marked heterogeneity in responses and cardiac morphology within HFpEF compared to controls. Unsupervised k-means

clustering identified 2 groups which differed in resting LVEF and ventricular size who went on to exhibit different exercise responses. On this basis a comparison between HFpEF with LVEF>60% and 50-60% was performed.

Compared to $HFpEF_{EF<60}$, $HFpEF_{EF>60}$ had lower LV (LVEDVi 64.8 ± 14.7 vs 93.6 ± 17.1 ml/m^2, p<0.0001) and RV volumes (RVEDVi 67.7 ± 16.6 vs 93.6 ± 21.5, ml/m^2, p<0.0001) at rest with the expected higher LVEF (65.2 ± 3.2 vs 55.2 ± 2.6%). During exercise, $HFpEF_{EF>60}$ had attenuated systolic augmentation (LVEF +3.1 ± 4.9 vs +5.5 ± 3.6 %, p=0.03), lower cardiac index (4.5 ± 1.1 vs 5.2 ± 1.3 L/min/m^2, p=0.048) and lower 6-minute walk distance (348 ± 95 vs 401 ± 76m, p=0.04). Both groups demonstrated alterations in lipid metabolism pathways on plasma proteomics analysis with the $HFpEF_{EF>60}$ group also demonstrating changes in extracellular matrix, RNA processing and inflammatory pathways.

Conclusions

There is significant heterogeneity within HFpEF in terms of exercise responses suggesting the presence of endotypes. There are marked morphological differences between $HFpEF_{EF>60}$ and $HFpEF_{EF<60}$ at rest with the former demonstrating smaller biventricular volumes and higher LVEF but lower cardiac output. While exercise responses of both HFpEF groups are impaired compared to controls, there is greater impairment of systolic reserve in the higher EF group and overall diminished stress cardiac output which is linked to functional impairment. There are perturbations in whole-body lipid metabolism common to both, which could be a potential therapeutic target.

3.1 Introduction

HFpEF is a condition characterised by blunted systolic and diastolic reserve during exercise, resulting in impaired augmentation of cardiac output and the development of lung congestion during exercise. However, characterisation of HFpEF physiology as well as heterogenous treatment effect in both successful and failed phase 3 clinical trials have indicated the presence of different endotypes of HFpEF. These are likely to respond differently to medicines, but also may have different degrees of functional impairment and potentially prognosis. Multiple approaches have been attempted to pheno-group HFpEF including classification using LVEF, through to using multi-parametric models.

Understanding the molecular biology underpinning them is paramount to understanding these endotypes. Plasma proteomics represents an accessible way to measure this at a whole-body level. Given that HFpEF is in effect a systemic disease characterised by peripheral abnormalities such as impaired oxygen extraction in addition to myocardial abnormalities, this will provide a more comprehensive overview. Thus far, all approaches have used samples obtained at rest. Analysis of the plasma proteome at stress may provide greater insight given that patients experience symptoms at stress.

In this chapter, I will aim to characterise initially the haemodynamic abnormalities in HFpEF during exercise stress compared to controls and the differences in the stress proteome between them.

Then, I will identify endotypes within HFpEF on the basis of haemodynamic changes and compare these to each other as well as to controls.

3.2 Methods

Inclusion criteria for patients with HFpEF:

- Willing and able to give informed consent to the study
- Male or female, age >18 years
- Heart failure symptoms
- LVEF ≥ 50% on echocardiography
- Clinical diagnosis of HFpEF made in a secondary/tertiary care level Cardiology clinic
- No clinical suspicion of amyloidosis

Exclusion criteria for patients with HFpEF:

- Contra-indications to cardiac MRI
- Un-revascularised, obstructive/haemodynamically significant coronary artery disease (>50% stenosis or on functional test).
- More than moderate valvular heart disease or moderate aortic stenosis
- Significant underlying respiratory disease
- Prior history of systolic dysfunction with recovery
- Severe anaemia
- Severe liver disease

Inclusion criteria for controls:

- Willing and able to give informed consent to the study
- Male or female, age >60 years (to ensure similar age to HFpEF cohort)
- No cardio-pulmonary symptoms of chest pain or shortness of breath
- LVEF ≥ 57% on CMR (defined as the lower limit of normal range)
- No history of diabetes or difficult to control hypertension (more than 3 anti-hypertensive medication)

Exclusion criteria for controls:

- Contra-indications to cardiac MRI
- Any history of valvular heart disease, anaemia, respiratory or liver disease
- Any history of an LVEF below the normal range

Sixty four patients with HFpEF and sixteen controls of similar age were recruited. All participants underwent rest and exercise stress CMR, echocardiography and lung function tests. Exercise stress was performed at a steady-state fixed workload of 35W. Dyspnoea burden was assessed using the modified Borg scale. Assessment of myocardial energetics was performed using ^{31}P DRESS. They also underwent functional assessment in the form of 6-minute walk test as well as symptom burden assessment using the KCCQ questionnaire.

Plasma was acquired from blood samples taken at rest as well as immediately following 6 minutes of exercise and were analysed using a commercial aptamer-based proteomic technique. Statistical analysis was performed using RStudio with the aid of several Bioconductor packages. Differential expression was assessed using the Biobase package. Volcano plots were generated using the Enhanced Volcano package. The cluster Profiler package was used with the Reactome library for pathway overrepresentation analysis. Graphs were created using the ggplot2 package.

3.3 Results Part A: HFpEF vs Controls

3.3.1 Baseline demographics and clinical characteristics

Participants with HFpEF were slightly older (76.6 ± 5.5 vs 71.9 ± 6.2 years, p=0.004), although the mean age for both were greater than 70. There was no significant difference in sex distributions. Participants with HFpEF also had higher BMI (32.1 ± 6.2 vs 26.5 ± 3.6 kg/m², p<0.001), waist circumference (110.2 ± 16.5 vs 93.7 ± 12.3 cm, p<0.001), greater prevalence of atrial fibrillation (67 vs 0 %, p<0.001), hypertension (77 vs 44%, p=0.01), diabetes (22 vs 0%, p=0.04) and chronic kidney disease (44 vs 0%, p=0.001). Some participants in the HFpEF group also had anaemia compared to none in the control group (19 vs 0%, p=0.06).

Some participants in the control group were on antihypertensive medication, however the use of such agents was much higher in the cohort with HFpEF (Median 3 vs 0, p<0.001). None of the control group had diabetes and therefore were not on the relevant medication whereas several of the HFpEF cohort were.

The median HFA-PEFF score of participants with HFpEF was 5 which is classified as within the 'confirmed HFpEF' category within the ESC scoring system (5-6 = confirmed HFpEF, 2-4 = intermediate probability). NT-proBNP was significantly higher in this group (1146 ± 1078 vs 177 ± 106 pg/ml, p<0.001).

Table 2: Characteristics of participants - Control vs HFpEF

	Control (n=16)	*HFpEF (n=64)*	*p-value*
Age (years)	71.9 ± 6.2	76.6 ± 5.5	***0.004***
Male	7 (44%)	36 (56%)	0.37
Body Mass Index (BMI) (kg/m^2)	26.5 ± 3.6	32.1 ± 6.2	***<0.001***
Waist circumference (cm)	93.7 ± 12.3	110.2 ± 16.5	***<0.001***
Atrial fibrillation – no. (%)	0	43 (67%)	***<0.001***
Hypertension - no. (%)	7 (44%)	49 (77%)	***0.01***
Diabetes - no. (%)	0	14 (22%)	***0.04***
Chronic kidney disease – no. (%)	0	28 (44%)	***0.001***
Anaemia – no. (%)	0	12 (19%)	0.06

Table 3: HFA-PEFF score, components and key baseline characteristics of control and HFpEF participants

	Control (n=16)	*HFpEF (n=64)*	*p-value*
HFA-PEFF score	N/A	5 [4, 6]	N/A
E/E' average	7.5 ± 1.7	12.0 ± 4.5	***<0.001***
Septal e' (cm/s)	6.4 ± 1.1	6.5 ± 2.4	0.78
Lateral e' (cm/s)	9.2 ± 1.8	8.8 ± 2.9	0.60
TR velocity (m/s)	2.16 ± 0.20	2.40 ± 0.30	***0.009***
Left atrial volume index (ml/m^2)	25.5 ± 6.2	51.0 ± 21.0	***<0.001***
LV mass indexed (g/m^2)	67.5 ± 13.3	93.2 ± 28.5	***<0.001***
Relative wall thickness	0.41 ± 0.08	0.49 ± 0.10	***0.001***
NT-proBNP (ng/L)	177 ± 106	1146 ± 1078	***<0.001***
Rest LVEF CMR (%)	63.1 ± 5.1	62.4 ± 5.5	0.65
6 minute walk test distance (m)	493.5 ± 63.6	363.0 ± 92.4	***<0.0001***

Table 4: Medication at enrolment – Control vs HFpEF

	Control	*HFpEF*	*p-value*
ACE inhibitor - no. (%)	1 (6%)	18 (28%)	0.07
Angiotensin Receptor Blocker - no. (%)	2 (13%)	19 (30%)	0.16
Mineralocorticoid Receptor Antagonist - no. (%)	0	19 (30%)	***0.01***
Beta blocker - no. (%)	1 (6%)	38 (59%)	***<0.001***
Calcium Channel Blocker - no. (%)	5 (31%)	28 (44%)	0.36
Loop diuretic - no. (%)	0	33 (52%)	***<0.001***
Thiazide diuretic - no. (%)	1 (6%)	5 (8%)	0.83
Alpha-blocker - no. (%)	0	5 (8%)	0.25
No. of BP lowering drugs (including loop diuretic)	0 [0, 1]	3[2, 3]	***<0.001***
Metformin - no. (%)	0	5 (8%)	0.25
Sulfonylurea - no. (%)	0	2 (3%)	0.47
GLP-1 agonist - no. (%)	0	1 (2%)	0.61
DPP-4 inhibitor - no. (%)	0	3 (5%)	0.38
Insulin - no. (%)	0	4 (6%)	0.30

3.3.2 Ventricular volumes and function at rest and effect on cardiac output

Left ventricular volumes were similar in both groups as was LVEF at rest. LV longitudinal function on echocardiography was reduced in the HFpEF cohort (LV S' 6.7 ± 1.7 vs 8.6 ± 1.8 cm/s, p<0.001) and numerically impaired as measured by CMR (LV GLS -15.0 ± 3.5 vs -16.7 ± 3.0 %, p=0.06). Peak filling rate in early diastole was similar in both groups. Diastolic function was significantly impaired in the HFpEF cohort as measured by a raised E/E' ratio on echocardiography (12.0 ± 4.5

vs 7.5 ± 1.7, p<0.001). LV mass as directly measured on CMR (as opposed to an estimate from linear measurements on echocardiography) was similar in both groups. However, the LV mass: end diastolic volume ratio was higher in the HFpEF cohort indicating concentric remodelling (0.75 ± 0.17 vs 0.65 ± 0.11, p=0.01) which is consistent with the relative wall thickness on echocardiography (0.49 ± 0.10 vs 0.41 ± 0.08, p=0.001). LVSVi was similar, resulting in no difference in cardiac index in both groups.

Right ventricular volumes and RVEF were similar across both groups with the RV SV/ESV ratio indicating similar RV-PA coupling at rest on CMR. Similar to the LV, there was relative impairment of RV longitudinal function on echocardiography (TAPSE 20.5 ± 5.3 vs 24.0 ± 4.4 mm, p=0.001, RV S' 11.9 ± 3.1 vs 14.7 ± 3.4 cm/s, p=0.004) and CMR (RV longitudinal strain -21.2 ± 5.4 vs -24.0 ± 3.5 %, p=0.05). The estimated pulmonary artery systolic pressure was greater in the HFpEF cohort (30.4 ± 7.4 vs 21.7 ± 7.0 mmHg, p=0.002) with the TAPSE/PASP ratio as an indicator of RV-PA coupling being impaired (1.00 ± 1.07 vs 1.42 ± 1.08 mm/mmHg, p=0.006).

Table 5: Indexed volumes and function of ventricles at rest – Control vs HFpEF

	Control	*HFpEF*	*p-value*
Left ventricular end diastolic volume indexed (LVEDVi, ml/m²)	75.1 ± 9.5	72.9 ± 20.1	0.28
LV end systolic volume indexed (LVESVi, ml/m²)	27.8 ± 5.7	28.1 ± 10.7	0.51
LV ejection fraction (LVEF, %)	63.1 ± 5.1	62.4 ± 5.5	0.65
LV stroke volume indexed (LVSVi, ml/m²)	47.3 ± 6.4	44.9 ± 10.4	0.15
LV Global Longitudinal Strain (GLS, %)	-16.7 ± 3.0	-15.0 ± 3.5	0.06
LV Mass indexed (g/m²)	48.9 ± 8.6	53.4 ± 14.5	0.46
LV Mass: End diastolic volume ratio	0.65 ± 0.11	0.75 ± 0.17	***0.01***
LV peak early filling rate (EDV/s)	2.87 ± 0.94	3.29 ± 1.38	0.28
RV end diastolic volume indexed (RVEDVi, ml/m²)	77.5 ± 13.7	75.0 ± 21.4	0.22
RV end systolic volume indexed (RVESVi, ml/m²)	30.9 ± 8.1	30.5 ± 12.3	0.46
RV ejection fraction (RVEF, %)	60.8 ± 4.9	60.2 ± 6.7	0.75
RV stroke volume indexed (RVSVi, ml/m²)	46.6 ± 7.1	44.5 ± 10.8	0.46
RV longitudinal strain (%)	-24.0 ± 3.5	-21.2 ± 5.4	0.05
RV SV/ESV ratio	1.57 ± 0.33	1.59 ± 0.49	0.69

Table 6: Echocardiography parameters at rest - Control vs HFpEF

	Control	*HFpEF*	*p-value*
E/E' average (ratio)	7.5 ± 1.7	12.0 ± 4.5	***<0.001***
S' Left ventricle (cm/s)	8.6 ± 1.8	6.7 ± 1.7	***<0.001***
Tricuspid annular plane systolic excursion (TAPSE, mm)	24.0 ± 4.4	20.5 ± 5.3	***0.001***
S' Right ventricle (cm/s)	14.7 ± 3.4	11.9 ± 3.1	***0.004***
Estimated pulmonary artery systolic pressure (PASP, mmHg)	21.7 ± 7.0	30.4 ± 7.4	***0.002***
TAPSE / PASP ratio (mm/mmHg)	1.42 ± 1.08	1.00 ± 1.07	***0.006***
Left atrial volume indexed biplane (ml/m^2)	25.5 ± 6.2	51.0 ± 21.0	***<0.001***
Left ventricular mass indexed (g/m^2)	67.5 ± 13.3	93.2 ± 28.5	***<0.001***
Relative wall thickness	0.41 ± 0.08	0.49 ± 0.10	**0.001**

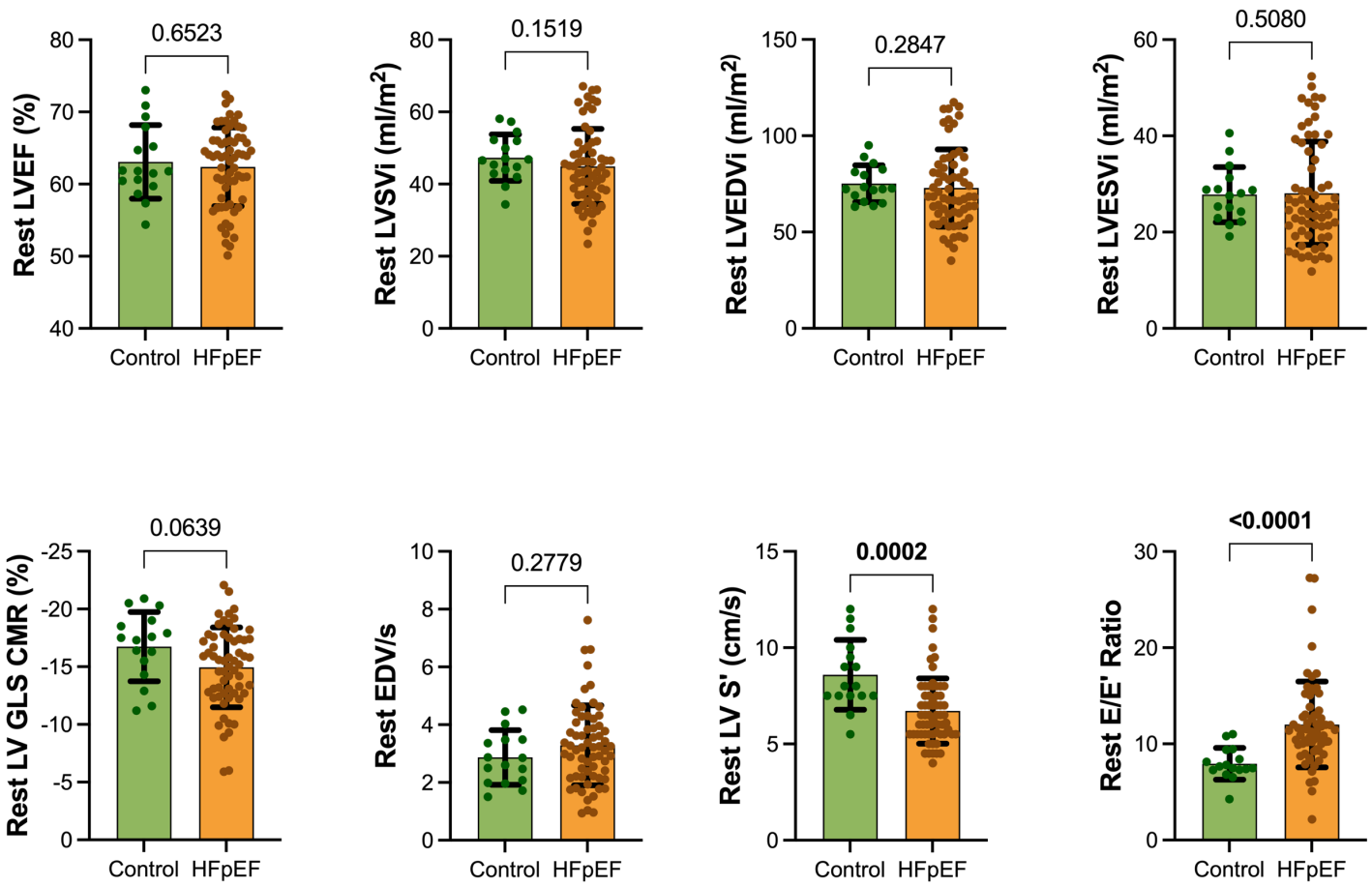

Figure 16: LV systolic and diastolic function at rest - Controls vs HFpEF

LV: Left Ventricle, EF: Ejection Fraction, SV: Stroke Volume, EDV: End Diastolic Volume, ESV: End Systolic Volume, GLS: Global Longitudinal Strain, EDV/s: Peak filling rate in early diastole normalised to the EDV, S': Mean echo S' doppler measure of longitudinal function, E/E' Ratio: Mean echo doppler measure of diastolic function

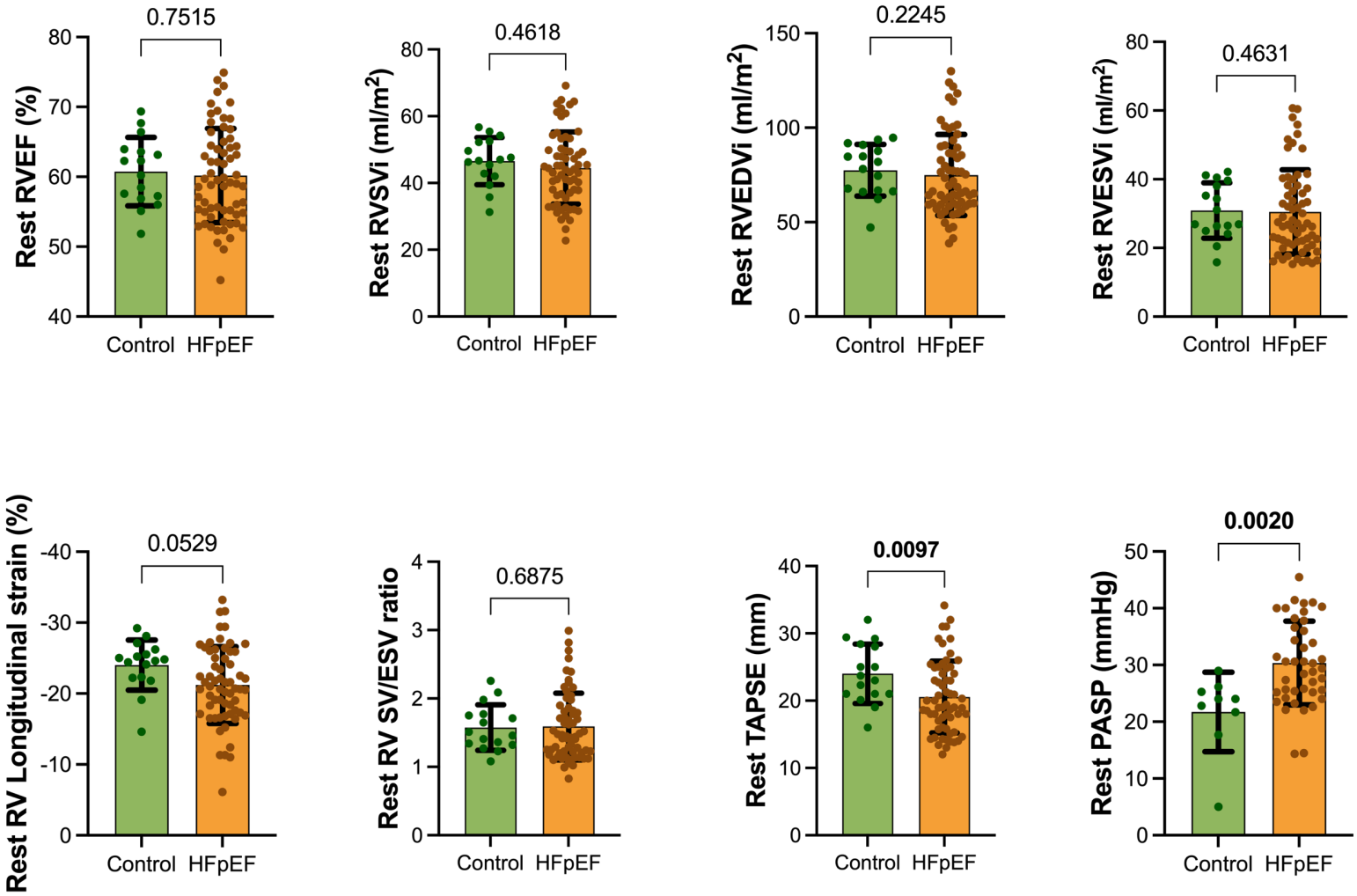

Figure 17: RV systolic function at rest - Controls vs HFpEF

RV: Right Ventricle. TAPSE and PASP measured on echocardiography. All other measurements on CMR

3.3.3 Atrial volumes and function at rest

As expected, given the current diagnostic criteria, left (LAESVi 74.8 ± 30.7 vs 54.9 ± 10.4 ml/m², p=0.0001) and right atrial volumes (RAESVi 85.4 ± 38.1 vs 58.5 ± 13.3 ml/m², p=0.01) were greater in the HFpEF cohort when measured on CMR as was left atrial volume on echocardiography. The emptying fractions of both were lower in the HFpEF cohort in the presence of a high prevalence of atrial fibrillation.

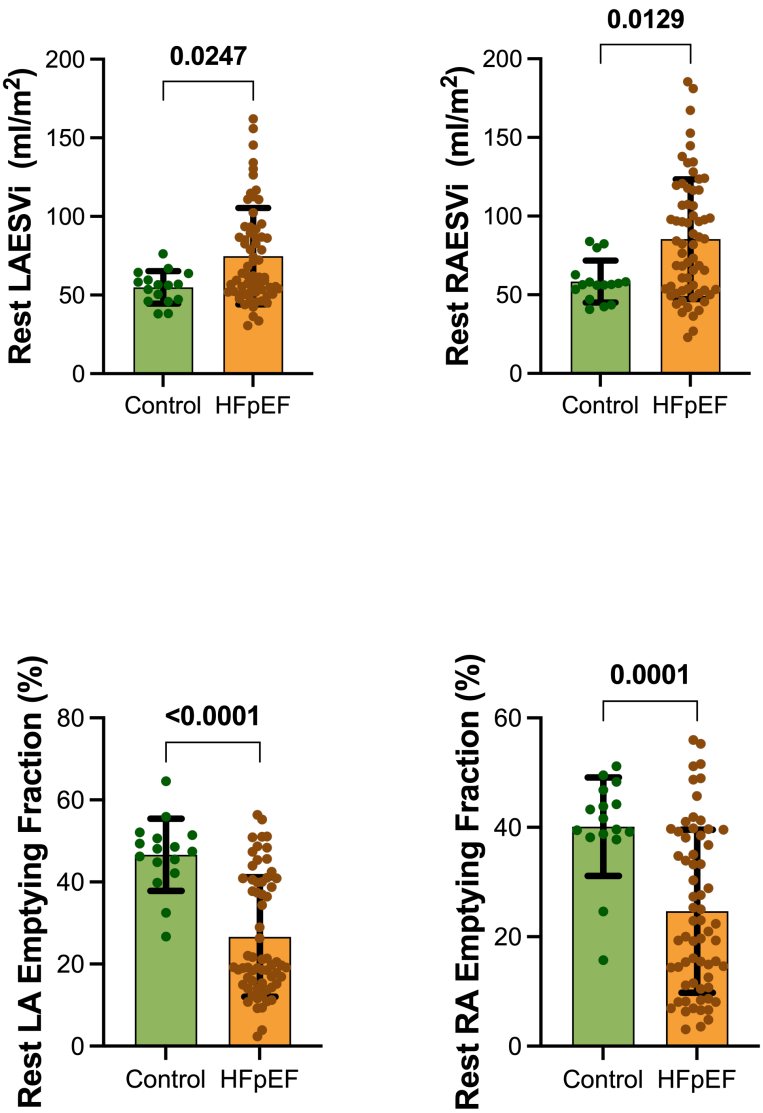

Figure 18: Atrial parameters at rest on CMR - Controls vs HFpEF
ESVi: Volume at ventricular end-systole indexed, LA: Left atrium, RA: Right atrium

Table 7: Indexed volumes and function of atria at rest - Control vs HFpEF

	Control	*HFpEF*	*p-value*
LA end diastolic volume (LAEDVi, ml/m^2)	29.7 ± 9.8	57.3 ± 30.4	***0.0001***
LA end systolic volume (LAESVi, ml/m^2)	54.9 ± 10.4	74.8 ± 30.7	***0.03***
LA emptying fraction (LAEF, %)	46.6 ± 8.8	26.6 ± 14.5	***0.0001***
Right atrial end diastolic volume (RAEDVi, ml/m^2)	35.6 ± 12.8	68.2 ± 39.2	***0.0009***
RA end systolic volume (RAESVi, ml/m^2)	58.5 ± 13.3	85.4 ± 38.1	***0.01***
RA emptying fraction (RAEF, %)	40.1 ± 9.0	24.7 ± 14.9	***0.0001***

3.3.4 Ventricular volumes and function during exercise and effect on cardiac output

In participants with HFpEF, there was a much smaller increase in LVEDVi (+2.4 ± 6.8 vs +8.6 ± 5.2 ml/m^2, p=0.001) and LVEF (+3.7 ± 4.6 vs +7.7 ± 4.4 %, p=0.003) during exercise resulting in a lower stress LVEF (66.1 ± 6.2 vs 70.8 ± 5.6 %, p=0.008) and LVSVi (49.4 ± 10.8 vs 59.2 ± 6.8 ml/m^2, p<0.001). This was paired with reduced longitudinal function (LV S' 8.3 ± 2.3 vs 10.5 ± 2.1 cm/s, p<0.001) on echocardiography. This resulted in attenuated augmentation in cardiac index (+1.85 ± 0.93 vs +3.18 ± 0.83 L/min/m^2, p<0.0001) during exercise in the HFpEF cohort by 42% and therefore a lower cardiac output (Cardiac index 4.73 ± 1.18 vs 5.98 ± 1.00 L/min/m^2, p<0.001). Diastolic function remained impaired in those with HFpEF (E/E' 12.7 ± 5.7 vs 8.5 ± 1.8, p<0.001).

In the case of the RV, there was an attenuated decrease in the RVESVi (+1.7 ± 6.7 vs -4.0 ± 5.7 ml/m^2, p=0.002) in the HFpEF cohort during exercise with a smaller increase in RVEF (+1.7 ± 6.2 vs +8.6 ± 5.3 %, p<0.001). This resulted in a lower RVEF (61.9 ± 8.6 vs 69.4 ± 5.9 %, p=0.005) and RVSVi (49.8 ± 10.9 vs 58.9 ± 7.3 ml/m^2, p=0.002). RV-PA coupling as estimated by the RV SV/ESV ratio was also lower in participants with HFpEF during exercise (1.84 ± 1.04 vs 2.38 ± 0.65, p<0.001). This

was corroborated on echocardiography with a lower TAPSE (22.0 ± 6.2 vs 28.9 ± 6.3 mm, $p<0.001$) and RV S' (14.0 ± 3.9 vs 18.2 ± 3.9 cm/s, $p=0.002$) as well as a lower TAPSE/PASP ratio (0.62 ± 0.29 vs 1.01 ± 3.44 mm/mmHg, $p=0.003$).

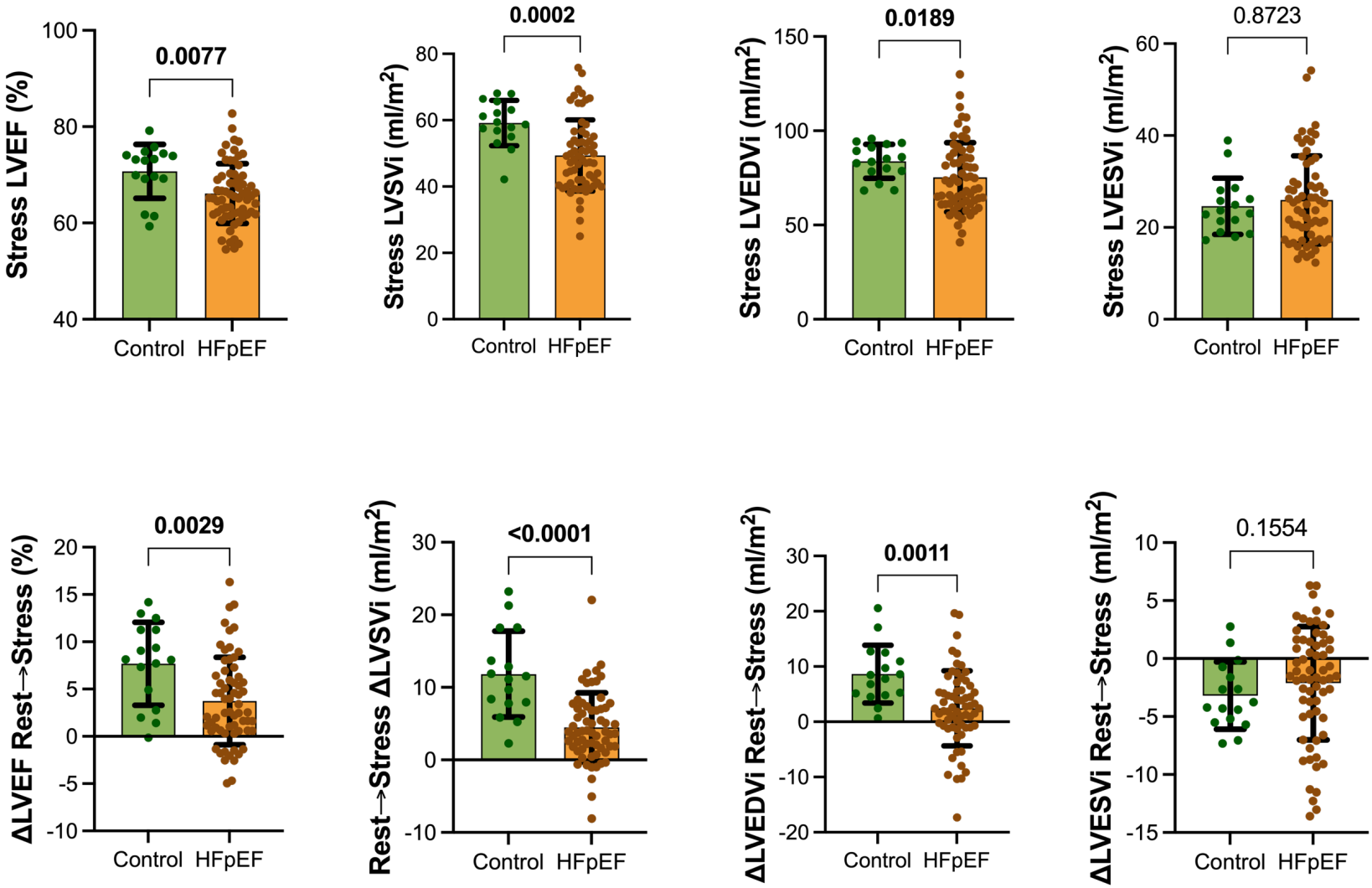

Figure 19: Stress LV function at stress and stress-induced changes on CMR - Controls vs HFpEF

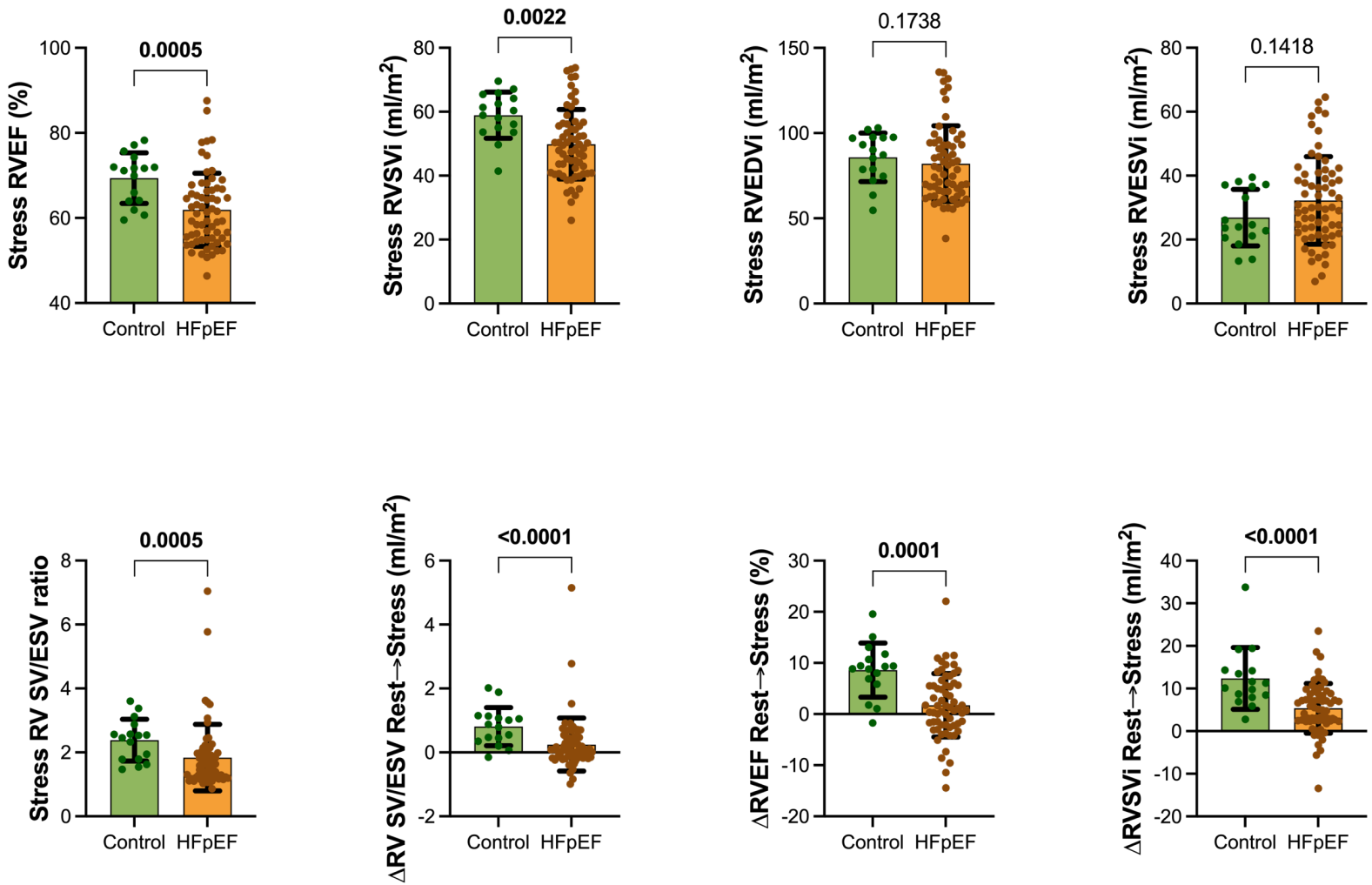

Figure 20: RV function during stress and stress-induced changes on CMR - Controls vs HFpEF

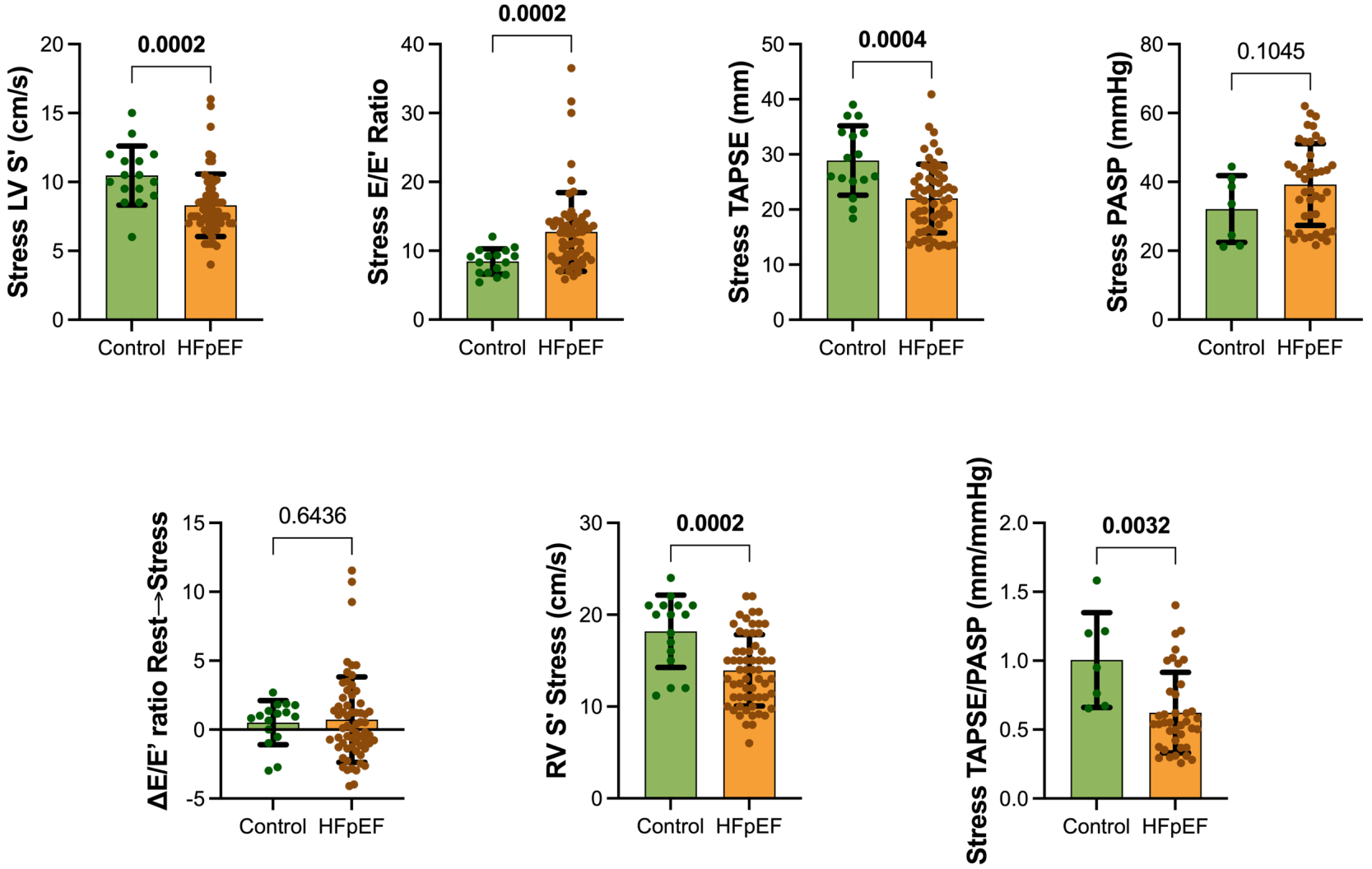

Figure 21: Echocardiography parameters on exercise - Controls vs HFpEF

Table 8: Indexed volumes and function of ventricles during exercise stress - Control vs HFpEF

	Control	*HFpEF*	*p-value*
LVEDVi (ml/m^2)	83.8 ± 9.0	75.4 ± 18.4	***0.02***
LVESVi (ml/m^2)	24.6 ± 6.1	26.0 ± 9.6	0.87
LVEF (%)	70.8 ± 5.6	66.1 ± 6.2	***0.008***
LVSVi (ml/m^2)	59.2 ± 6.8	49.4 ± 10.8	***<0.001***
LV peak early filling rate (EDV/s)	3.16 ± 1.20	3.68 ± 1.33	0.16
RVEDVi (ml/m^2)	85.8 ± 14.3	82.1 ± 22.2	0.17
RVESVi (ml/m^2)	26.9 ± 8.8	32.3 ± 13.7	0.14
RVEF (%)	69.4 ± 5.9	61.9 ± 8.6	***0.005***
RVSVi (ml/m^2)	58.9 ± 7.3	49.8 ± 10.9	***0.002***
RV SV/ESV ratio	2.38 ± 0.65	1.84 ± 1.04	***<0.001***

Table 9: Change in ventricular parameters from rest to exercise - Control vs HFpEF

	Control	*HFpEF*	*p-value*
ΔLVEDVi rest→stress (ml/m²)	+8.6 ± 5.2	+2.4 ± 6.8	***0.001***
ΔLVESVi rest→stress (ml/m²)	-3.2 ± 2.9	-2.1 ± 4.9	0.16
ΔLVEF rest→stress (%)	+7.7 ± 4.4	+3.7 ± 4.6	***0.003***
ΔLVSVi rest→stress (ml/m²)	+11.8 ± 5.9	+4.5 ± 4.8	***<0.0001***
Δpeak early filling rate (EDV/s)	+0.29 ± 1.20	+0.33 ± 1.29	0.91
ΔRVEDVi rest→stress (ml/m²)	+8.4 ± 9.9	+7.1 ± 9.1	0.49
ΔRVESVi rest→stress (ml/m²)	-4.0 ± 5.7	+1.7 ± 6.7	***0.002***
ΔRVEF rest→stress (%)	+8.6 ± 5.3	+1.7 ± 6.2	***<0.001***
ΔRVSVi rest→stress (ml/m²)	+12.4 ± 7.2	+5.4 ± 5.8	***<0.0001***
ΔRV SV/ESV ratio	+0.81 ± 0.60	+0.24 ± 0.83	***<0.001***

Table 10: Echocardiography parameters during stress - Control vs HFpEF

	Control	*HFpEF*	*p-value*
E/E′ average (ratio)	8.5 ± 1.8	12.7 ± 5.7	***<0.001***
ΔE/E′ ratio rest→stress	+0.5 ± 1.6	+0.7 ± 3.1	0.64
S′ Left ventricle (cm/s)	10.5 ± 2.1	8.3 ± 2.3	***<0.001***
TAPSE (mm)	28.9 ± 6.3	22.0 ± 6.2	***<0.001***
S′ Right ventricle (cm/s)	18.2 ± 3.9	14.0 ± 3.9	***0.002***
Estimated PASP (mmHg)	32.1 ± 9.7	39.3 ± 11.9	0.11
TAPSE/PASP ratio (mm/mmHg)	1.01 ± 3.44	0.62 ± 0.29	***0.003***

3.3.5 Atrial volumes and function during exercise

As at rest, the volumes of both right (RAESVi 97.4 ± 45.0 vs 61.3 ± 18.4 ml/m^2, p=0.003) and left (LAESVi 80.6 ± 32.5 vs 63.1 ± 10.2 ml/m^2, p=0.04) atria were higher in HFpEF with impaired emptying fractions. There was a greater increase in RAESVi in HFpEF during exercise (+12.0 ± 13.7 vs +2.9 ± 12.3 ml/m^2, p=0.02), but not in LA volume. There was no difference between the groups in how exercise affected emptying fractions.

Table 11: Atrial volumes and function at stress and exercise-induced change in these parameters - Control vs HFpEF

	Control	*HFpEF*	*p-value*
LAEDVi (ml/m^2)	32.0 ± 9.1	60.2 ± 31.1	***<0.001***
LAESVi (ml/m^2)	63.1 ± 10.2	80.6 ± 32.5	***0.04***
LAEF (%)	49.6 ± 9.3	28.1 ± 14.1	***<0.0001***
RAEDVi (ml/m^2)	31.4 ± 11.0	74.0 ± 42.3	***0.0001***
RAESVi (ml/m^2)	61.3 ± 18.4	97.4 ± 45.0	***0.003***
RAEF (%)	49.3 ± 7.4	27.9 ± 15.3	***<0.0001***
ΔLAESVi rest→stress (ml/m^2)	+8.2 ± 7.7	+5.8 ± 8.8	0.32
ΔRAESVi rest→stress (ml/m^2)	+2.9 ± 12.3	+12.0 ± 13.7	***0.02***
ΔLAEF rest→stress (%)	+3.0 ± 10.6	+1.5 ± 7.6	0.27
ΔRAEF rest→stress (%)	+9.1 ± 10.3	+3.3 ± 11.0	0.06

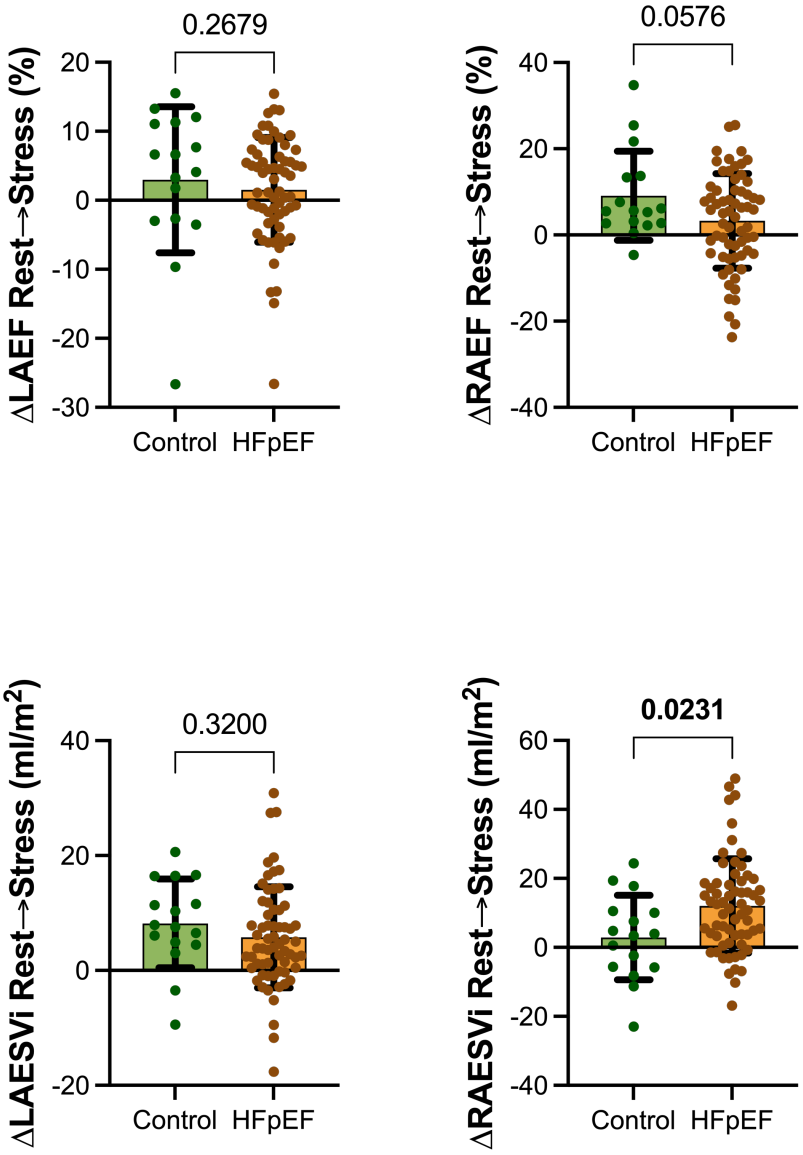

Figure 22: Changes in atrial parameters during exercise on CMR - Controls vs HFpEF

3.3.6 Cardiac output at rest and during exercise

There was no significant difference in cardiac output at rest between HFpEF and control cohorts. However, there was significant impairment in cardiac output augmentation during exercise in the HFpEF cohort (+1.85 ± 0.93 vs +3.18 ± 0.83 L/min/m², p<0.0001) which resulted in a much lower cardiac output at stress (4.73 ± 1.18 vs 5.98 ± 1.00 L/min/m², p<0.001).

Table 12: Rest and stress cardiac output - Control vs HFpEF

	Control	*HFpEF*	*p-value*
Rest Cardiac Output (L/min)	5.17 ± 1.31	5.80 ± 1.61	0.14
Rest Cardiac Index (L/min/m²)	2.80 ± 0.49	2.88 ± 0.64	0.84
Stress Cardiac Output (L/min)	10.98 ± 2.22	9.48 ± 2.67	***0.04***
Stress Cardiac Index (L/min/m²)	5.98 ± 1.00	4.73 ± 1.18	***<0.001***
ΔCardiac Index rest→stress (L/min/m²)	3.18 ± 0.83	1.85 ± 0.93	***<0.0001***

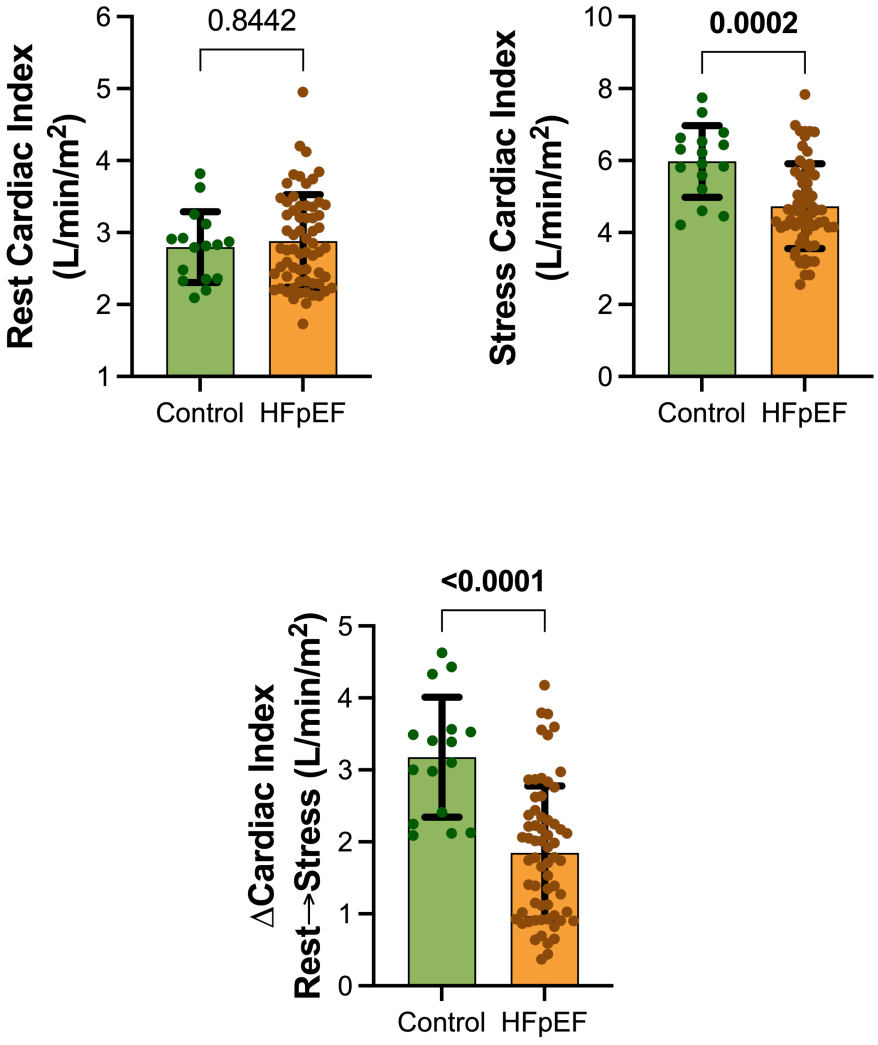

Figure 23: Rest and stress cardiac index - Control vs HFpEF

3.3.7 Lung function parameters at rest and stress

At rest, FEV1 (85.2 ± 16.9 vs 103.3 ± 10.4 %, p=0.0002) and FVC (93.2 ± 16.5 vs 113.9 ± 13.5 %, p<0.0001) were impaired in the HFpEF cohort compared to controls with a similar FEV1/FVC ratio. This was replicated during exercise with no significant changes.

The DLCO was reduced at both rest (77.2 ± 14.6 vs 93.7 ± 15.8 %, p<0.001) and exercise (86.4 ± 18.2 vs 98.4 ± 11.2 %, p=0.02) with an associated reduction in KCO at rest (90.5 ± 14.3 vs 100.7 ± 17.1 %, p=0.02), but not during exercise. Alveolar volumes were not significantly different at rest or stress.

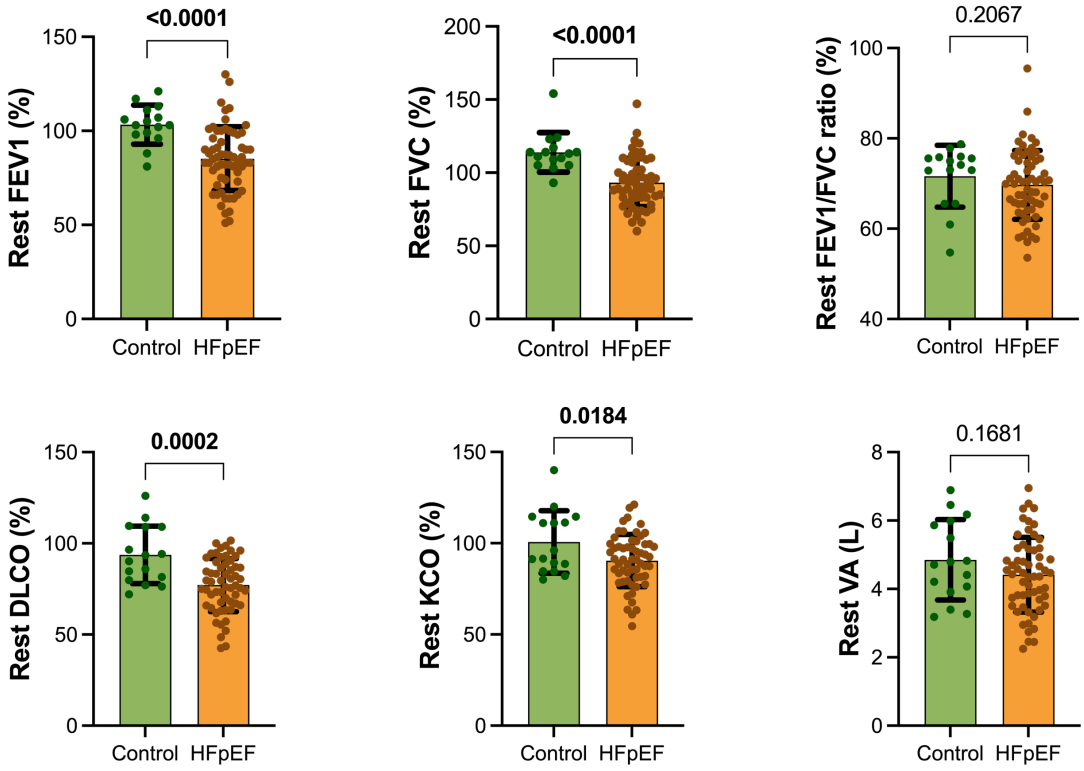

Figure 24: Lung function parameters at rest - Controls vs HFpEF
Values shown as % predicted for FEV1, FVC, DLCO and KCO

Table 13: Lung function parameters at rest - Control vs HFpEF

	Control	*HFpEF*	*p-value*
FEV1 (% predicted)	103.3 ± 10.4	85.2 ± 16.9	***0.0002***
FVC (% predicted)	113.9 ± 13.5	93.2 ± 16.5	***<0.0001***
FEV1/FVC (% ratio)	71.6 ± 6.8	69.7 ± 7.6	0.21
DLCO (% predicted)	93.7 ± 15.8	77.2 ± 14.6	***<0.001***
KCO (% predicted)	100.7 ± 17.1	90.5 ± 14.3	***0.02***
VA (L)	4.85 ± 1.18	4.42 ± 1.09	0.17

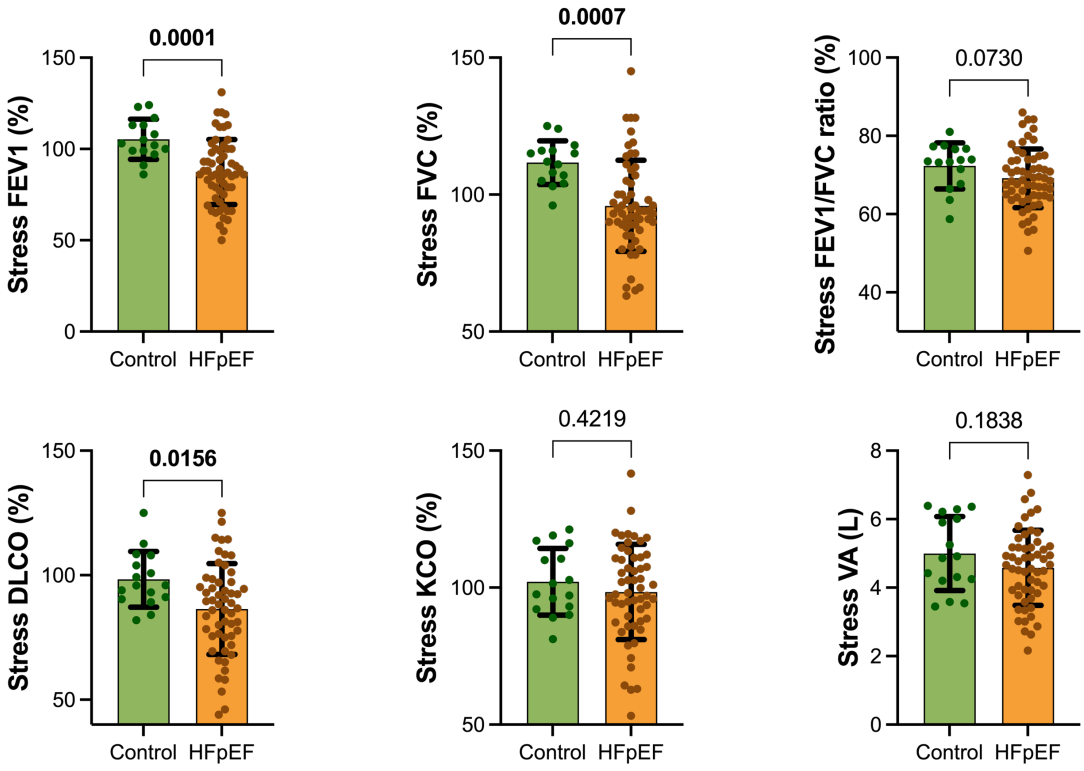

Figure 25: Stress Lung function parameters - Control vs HFpEF
Values shown as % predicted for FEV1, FVC, DLCO and KCO

Table 14: Lung function parameters following exercise - Control vs HFpEF

	Control	*HFpEF*	*p-value*
FEV1 (% predicted)	105.3 ± 11.0	87.4 ± 17.8	***0.0004***
FVC (% predicted)	111.7 ± 8.0	95.9 ± 16.7	***0.0007***
FEV1/FVC (% ratio)	72.3 ± 5.9	69.1 ± 7.5	0.13
DLCO (% predicted)	98.4 ± 11.2	86.4 ± 18.2	***0.02***
KCO (% predicted)	102.1 ± 12.2	98.4 ± 17.4	0.42
VA (L)	5.00 ± 1.08	4.58 ± 1.10	0.18

3.3.8 Myocardial energetics and triglyceride content

Compared to published normal values in healthy younger controls, the PCr/ATP ratio was reduced similarly in HFpEF as well as in older controls (1.49 ± 0.30 vs 1.53 ± 0.16, p=0.55). Myocardial triglyceride content was elevated in both cohorts (HFpEF 1.85 ± 1.40 vs Controls 2.37 ± 1.78 %, p=0.48).

Table 15: Myocardial metabolism - energetics and triglyceride content - Control vs HFpEF

	Control	*HFpEF*	*p-value*
PCr/ATP ratio	1.53 ± 0.16	1.49 ± 0.30	0.55
Myocardial triglyceride content (%)	2.37 ± 1.78	1.85 ± 1.40	0.48

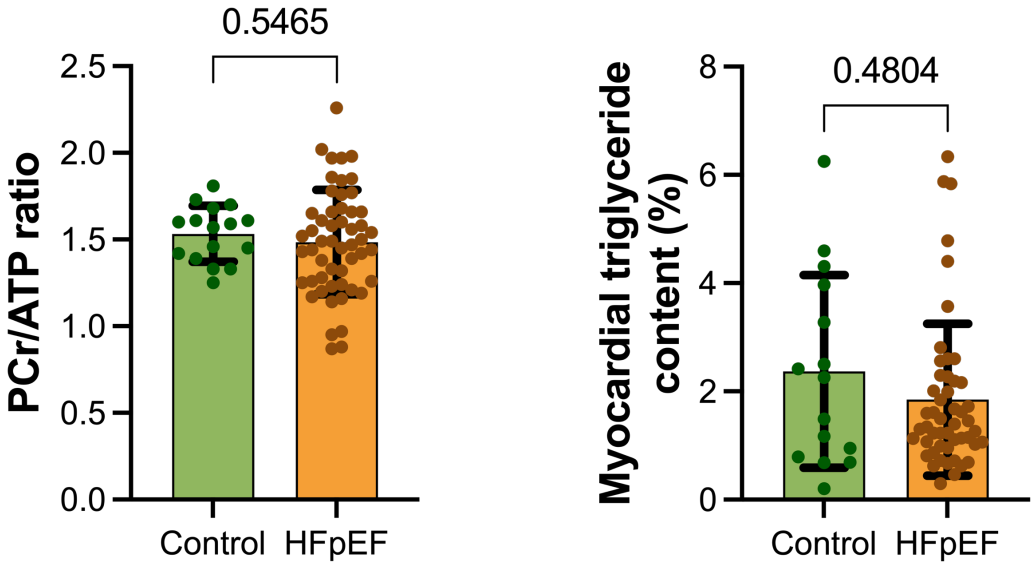

Figure 26: Myocardial metabolism - energetics and triglyceride content - Control vs HFpEF

3.3.9 Functional capacity and symptom burden

As expected, functional capacity as assessed by 6-minute walk test distance was significantly impaired in the HFpEF cohort compared to controls (363.0 ± 92.4 vs 493.5 ± 63.6 m, p<0.0001) with a greater degree of dyspnoea (Modified Borg score 2.92 ± 2.03 vs 0.47 ± 0.67, p<0.0001). They also experienced a greater degree of symptom burden as measured by a lower KCCQ clinical summary score (69.6 ± 20.1 vs 97.5 ± 4.5, p<0.0001).

Table 16: Functional capacity and symptom burden - Control vs HFpEF

	Control	*HFpEF*	*p-value*
6-minute walk test distance (m)	493.5 ± 63.6	363.0 ± 92.4	***<0.0001***
6MWT dyspnoea score (Modified Borg scale)	0.47 ± 0.67	2.92 ± 2.03	***<0.0001***
KCCQ clinical summary score	97.5 ± 4.5	69.6 ± 20.1	***<0.0001***

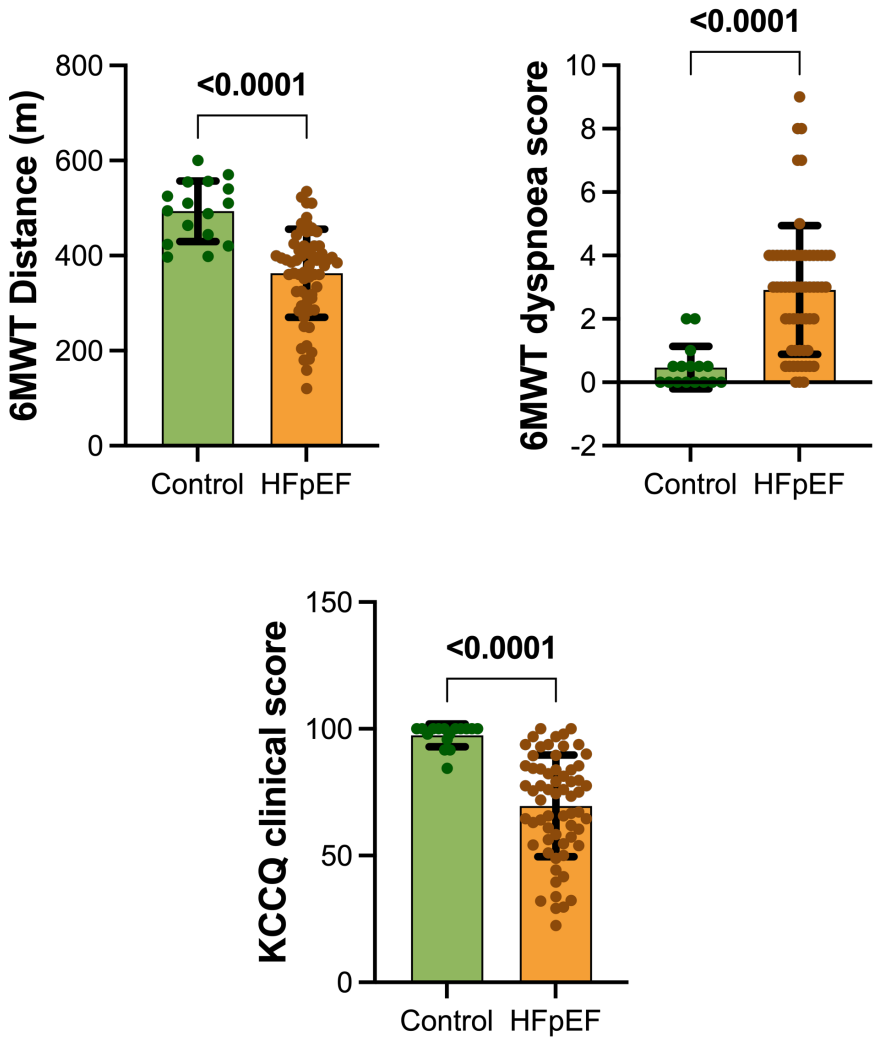

Figure 27: Functional capacity and symptom burden - Control vs HFpEF

3.3.10 Analysis of the plasma proteome during exercise

Of 7289 proteins assayed, 47 plasma proteins were of differential abundance in the HFpEF cohort compared to controls following FDR adjustment. Of these, 41 were found in higher quantities in HFpEF and 6 were found to be lower. Following pathway analysis using the Reactome database, the key pathways found to be differentially regulated related to the extracellular matrix, lipid metabolism, growth factor signalling, mRNA processing and the complement system.

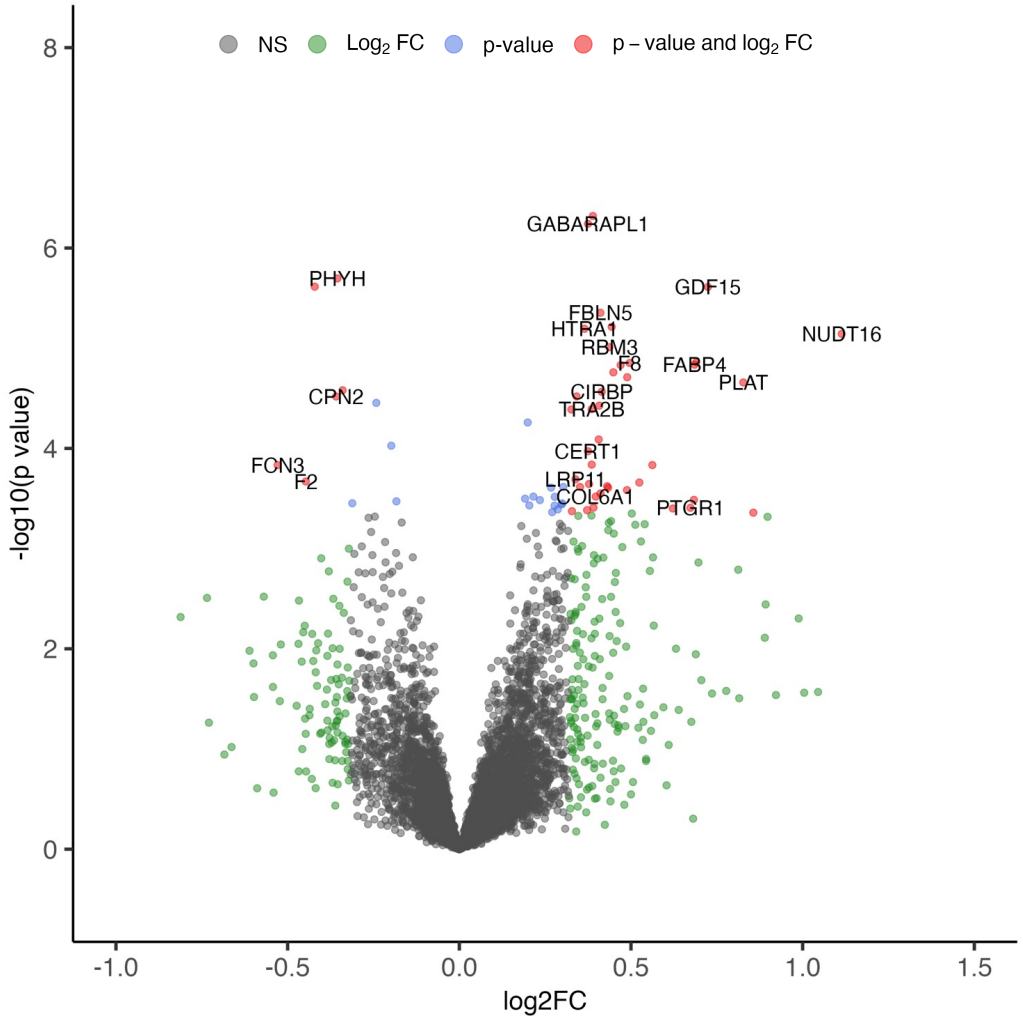

Figure 28: Volcano plot of relative protein abundance at exercise stress - HFpEF compared to control

This plot demonstrates relative protein abundance for the HFpEF cohort compared to the control cohort. The x-axis shows log2 fold change and the y-axis shows the log10 of the absolute p value for illustrative purposes. The Red dots represent proteins which have a relevant difference (25%) in abundance and is statistically significant following FDR correction. FC: Fold change

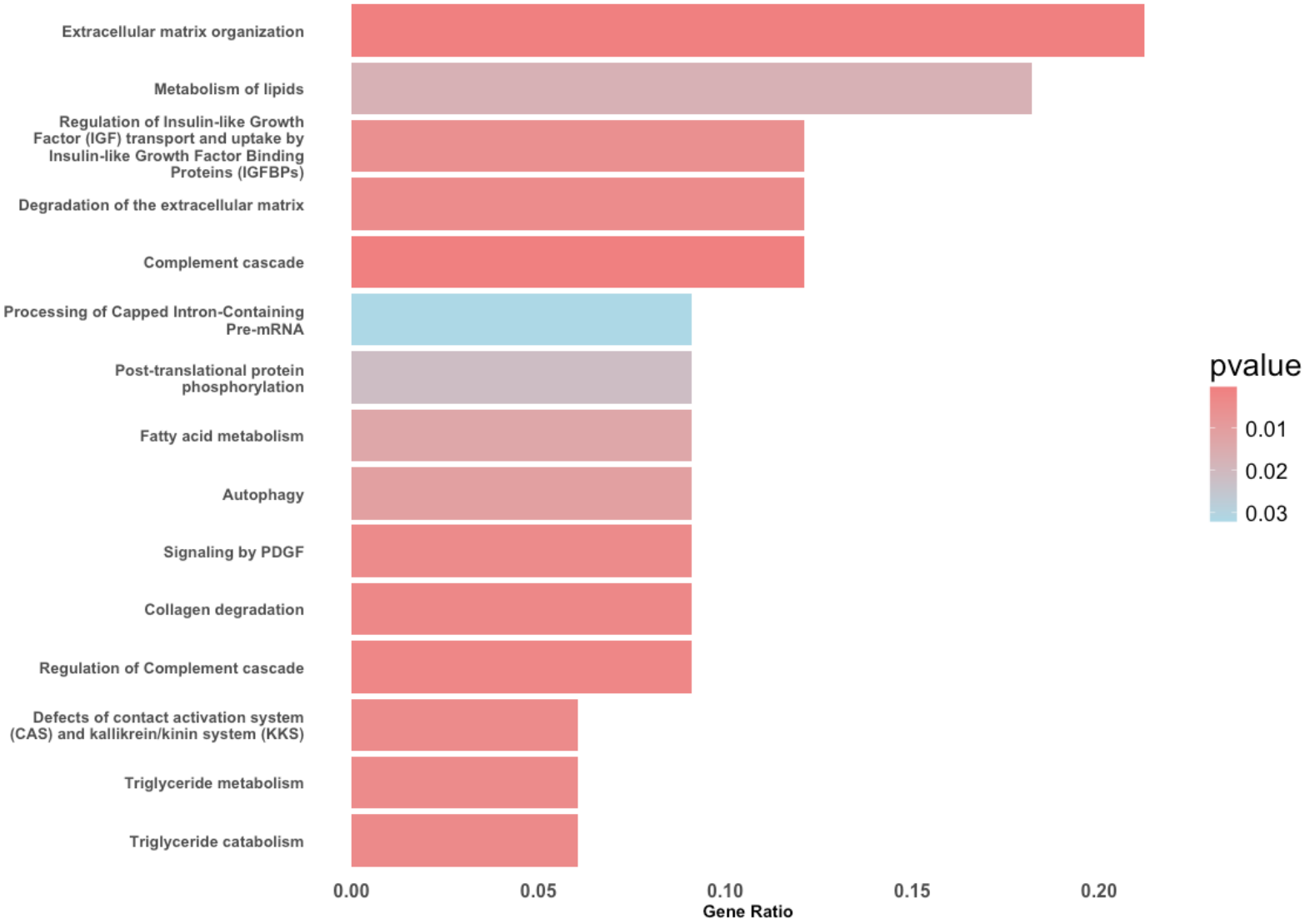

Figure 29: Pathway enrichment analysis - HFpEF vs Control

The top 15 pathways are shown. Gene ratio represents the proportion of genes within that pathway which have differential abundance

3.3.11 Heterogeneity using coefficient of variation

Despite the sample size of the HFpEF cohort being 4 times larger than the control cohort, the coefficient of variation is distinctly higher in the HFpEF cohort for a number of key variables. This includes ventricular volumes, stroke volume and cardiac index at rest with these differences becoming greater at stress, particularly in relation to the change in cardiac output.

To investigate the heterogeneity of exercise haemodynamic responses further, a model encompassing relevant features including rest biventricular morphology, systolic and diastolic function, the changes in these during exercise, key clinical parameters and functional capacity was produced. Only participants with HFpEF were included, with no controls in the model. Principal component analysis was performed and the 2 components explaining the greatest variability was used to create a 2-dimensional representation. Within this space, unsupervised k-means clustering was used to separate clusters different from each other while remaining similar within. Silhouette scoring indicated that 2 clusters were optimal.

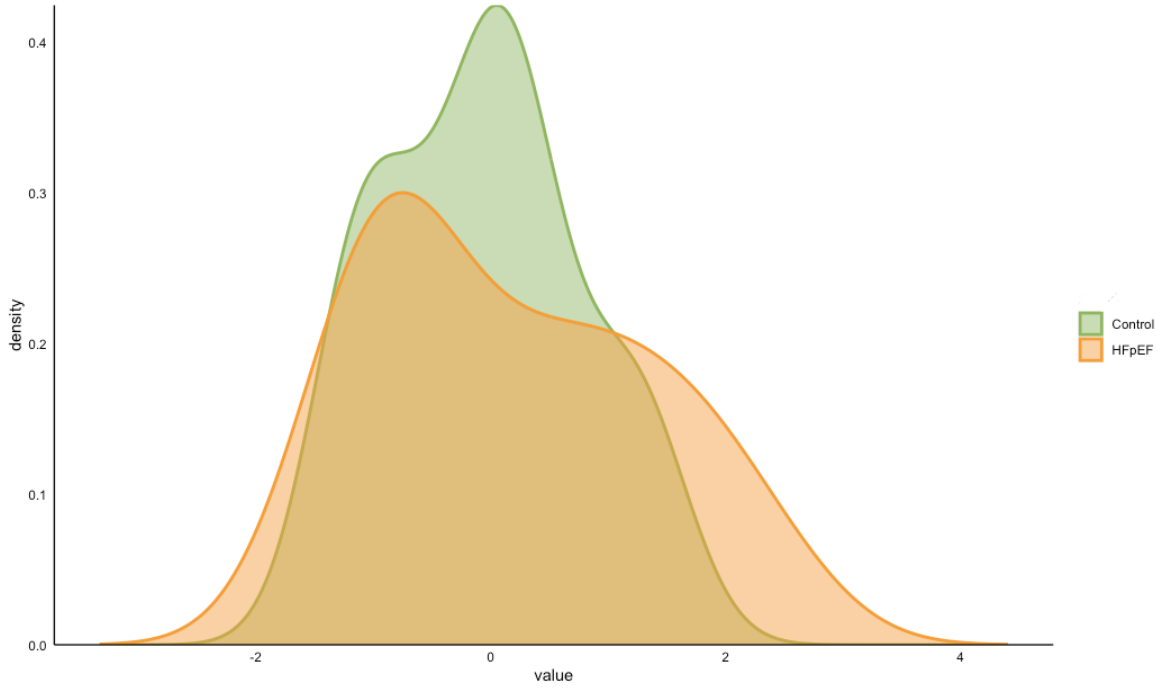

Figure 30: Kernel density distribution plot of Δ cardiac index during exercise stress

The figure has been shifted to have medians of both groups at 0 and show the greater, flatter spread of the HFpEF cohort indicative of heterogeneity in exercise response.

Table 17: Heterogeneity in key variables between control and HFpEF cohorts as measured by coefficient of variation

Coefficient of variation was calculated as:

$$\frac{Standard\ deviation}{Mean} \times 100$$

Coefficient of variation	***Control***	***HFpEF***
Rest LVEDVi	12.7	27.5
Rest LVEF	8.1	8.7
Rest LVSVi	13.6	23.2
Rest Cardiac Index	17.6	22.3
Stress LVSVi	11.5	21.8
Stress LVEF	7.9	9.4
Stress Cardiac Index	16.7	24.9
ΔCardiac Index rest→stress	26.2	50.2

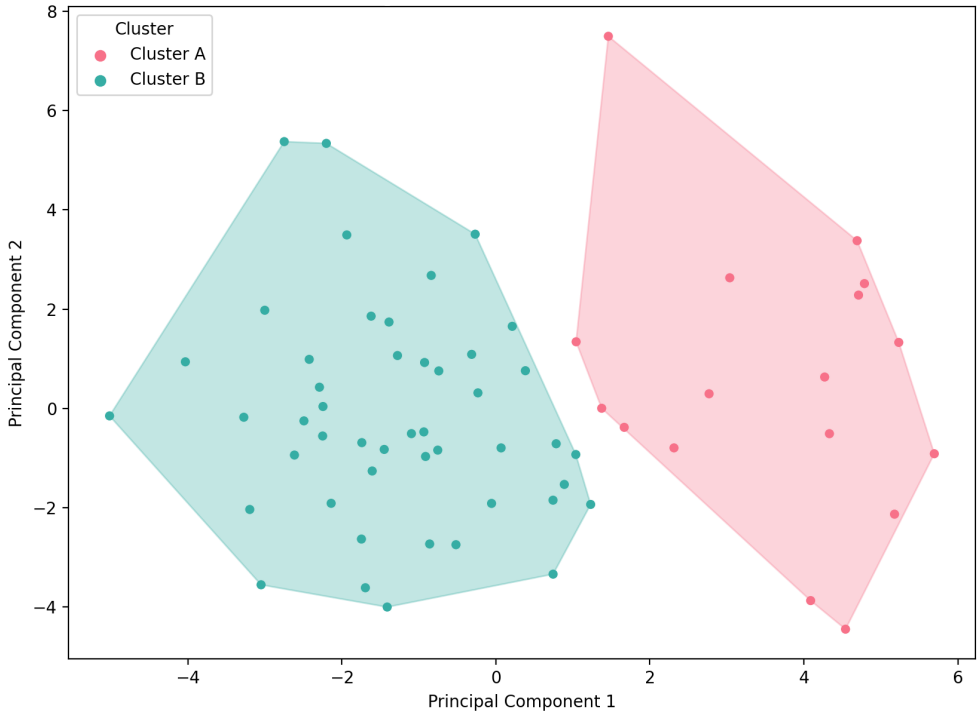

Figure 31: K-means clustering of the HFpEF cohort

Table 18: Salient features separating clusters within HFpEF

Parameters	***Cluster A***	***Cluster B***	***p-value***
Rest LVEDVi (ml/m²)	99.3 ± 12.5	63.7 ± 23.5	***<0.0001***
Rest LVESVi (ml/m²)	44.1 ± 7.4	23.5 ± 5.9	***<0.0001***
Rest LVEF (%)	55.5 ± 5.5	63.1 ± 5.5	***<0.0001***
Rest LVSVi (ml/m²)	55.2 ± 8.9	40.1 ± 7.6	***<0.0001***
ΔCardiac Index rest→stress (L/min/m²)	+2.14 ± 0.9	+1.62 ± 0.91	***0.049***
Male sex (not part of model)	88%	45%	***0.002***

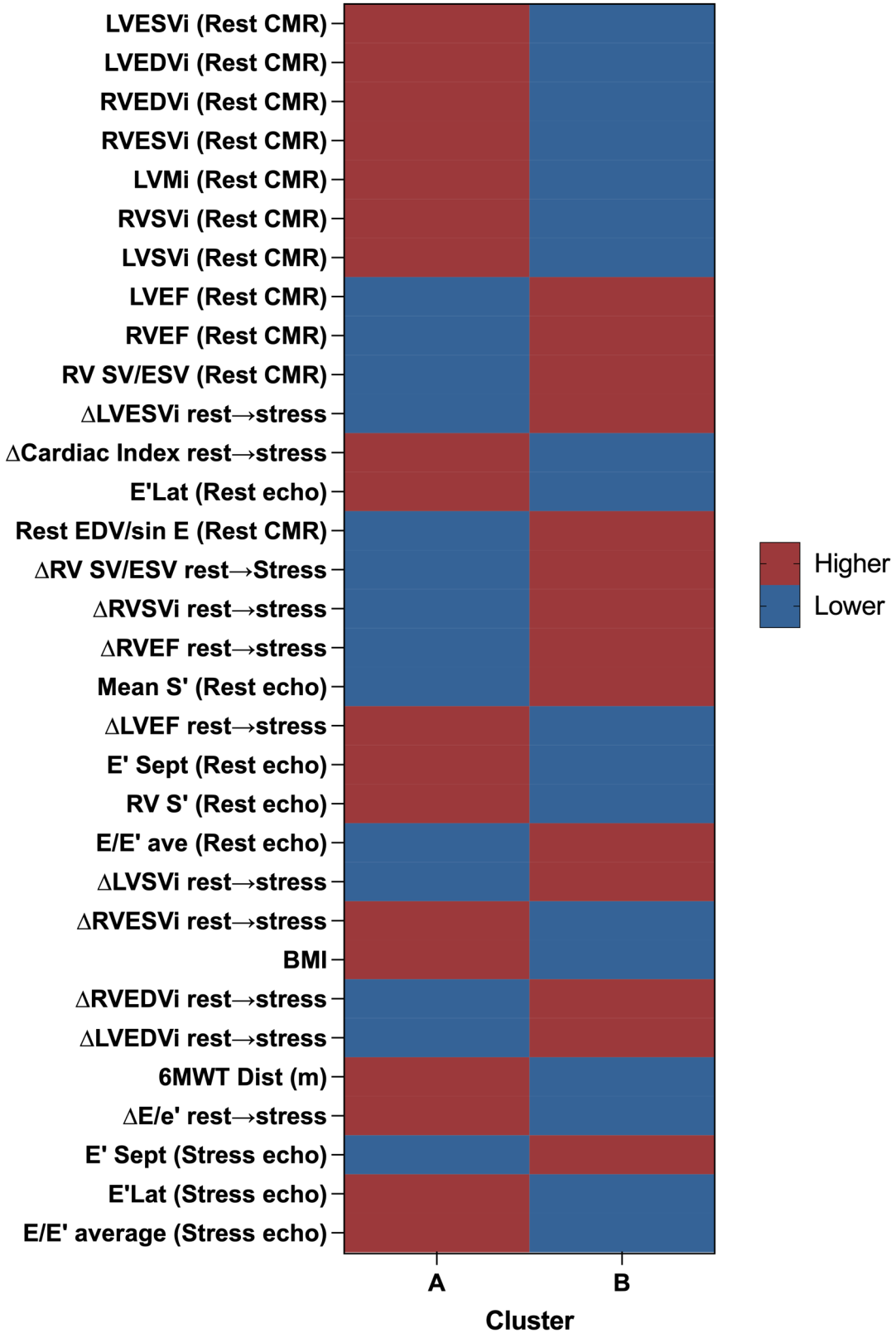

Figure 32: Heatmap representation of characteristics in the K-means clustering model

The clusters demonstrated significant differences in resting morphology and function as well as the ability to augment cardiac output in response to exercise stress. While not part of the model input, interestingly cluster A was predominantly composed of males whereas most females in the study were in cluster B. Given the results of the k-means clustering analysis, clinical trial data demonstrating differential treatment responses at an LVEF of approximately 57-60% and invasive studies showing variation in haemodynamic properties at 60%, a threshold was chosen close to this mark to investigate different haemodynamic endotypes of HFpEF. The final threshold for further analysis was set at 60% as this is a clinically relevant cut-off to use which can easily be applied in clinical practice.

3.4 Results Part B: Analysis of differences between endotypes of HFpEF

The groups were divided into HFpEF with LVEF 50-60% and LVEF > 60%. For ease of reading, these will be referred to as $HFpEF_{EF<60}$ and $HFpEF_{EF>60}$. Below, it can be seen that Cluster A is composed almost entirely of $HFpEF_{EF<60}$ while nearly all of the $HFpEF_{EF>60}$ cohort segregated to Cluster B.

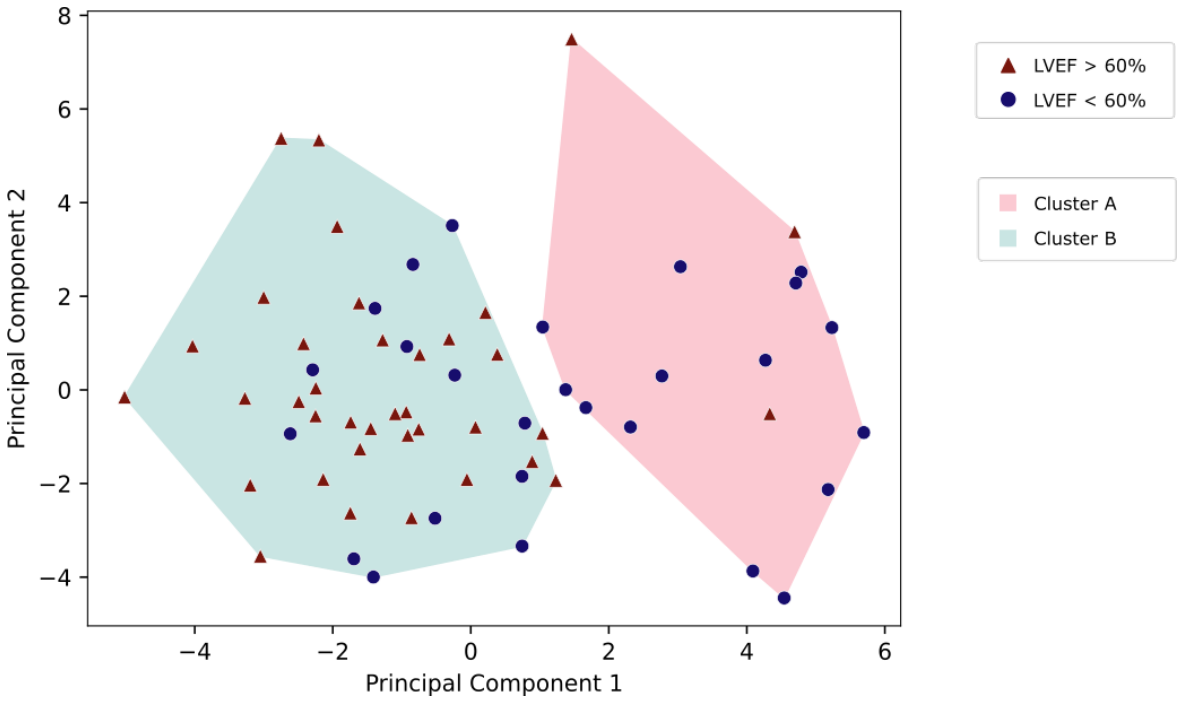

Figure 33: Allocation of clusters by LVEF group

Cluster A: 14 $HFpEF_{EF<60}$, 3 $HFpEF_{EF>60}$

Cluster B: 13 $HFpEF_{EF<60}$, 34 $HFpEF_{EF>60}$

3.4.1 Baseline characteristics

Both groups were of similar age with no differences in BMI and circulating NT-proBNP levels. The prevalence of AF, hypertension, diabetes and CKD were similar. The proportion of men in the $HFpEF_{EF<60}$ group was higher than the $HFpEF_{EF>60}$ group with a 46:54 ratio of male: female in the $HFpEF_{EF>60}$cohort (p=0.006). 25 of 28 women with HFpEF overall had an LVEF >60%. There were no significant differences in the use of key medication for hypertension or diabetes and diuretics. The vast majority of patients in both groups were in NYHA class 2 of

exercise intolerance. 2 commonly used scores to evaluate the probability of HFpEF (ESC HFA-PEFF, H2FPEF) scores were similar across both groups.

Table 19: Baseline characteristics - $HFpEF_{EF<60}$ vs $HFpEF_{EF>60}$

	$HFpEF_{EF<60}$ (n=18)	***$HFpEF_{EF>60}$ (n=46)***	***p-value***
Age (years)	75.3 ± 5.6	77.1 ± 5.4	0.24
Male	15 (83%)	21 (46%)	***0.006***
BMI (kg/m^2)	32.9 ± 7.5	31.7 ± 5.7	0.49
Waist circumference (cm)	116.1 ± 17.6	108.1 ± 15.7	0.10
Atrial fibrillation – no. (%)	13 (72%)	30 (65%)	0.59
Hypertension - no. (%)	13 (72%)	36 (78%)	0.61
Diabetes - no. (%)	5 (28%)	9 (20%)	0.47
Chronic kidney disease -no. (%)	6 (33%)	22 (48%)	0.29
Anaemia – no. (%)	6 (33%)	6 (13%)	0.06
NT-proBNP (ng/L)	1049 ± 666	1184 ± 1206	0.83
HFA-PEFF score	5 [5, 6]	5 [4, 6]	0.36
H2FPEF score	6.5 [4.0, 7.3]	6 [4.0, 8.0]	0.80
NYHA class	2 [2, 2]	2 [2, 2]	0.19

Table 20: Medication at enrolment - $HFpEF_{EF<60}$ vs $HFpEF_{EF>60}$

	$HFpEF_{EF<60}$	*$HFpEF_{EF>60}$*	*p-value*
ACE inhibitor - no. (%)	5 (28%)	13 (28%)	0.97
Angiotensin Receptor Blocker - no. (%)	5 (28%)	14 (30%)	0.83
Mineralocorticoid Receptor Antagonist - no. (%)	3 (17%)	16 (35%)	0.15
Beta blocker - no. (%)	13 (72%)	25 (54%)	0.19
Calcium Channel Blocker - no. (%)	10 (56%)	18 (39%)	0.23
Loop diuretic - no. (%)	10 (56%)	23 (50%)	0.69
Thiazide diuretic - no. (%)	3 (17%)	2 (4%)	0.10
Alpha-blocker - no. (%)	2 (11%)	3 (7%)	0.54
No of blood pressure lowering drugs	3 [2, 4]	2 [1, 3]	0.07
Metformin - no. (%)	3 (17%)	2 (4%)	0.10
Sulfonylurea - no. (%)	1 (6%)	1 (2%)	0.48
GLP-1 agonist - no. (%)	1 (6%)	0	0.11
DPP-4 inhibitor - no. (%)	1 (6%)	2 (4%)	0.84
Insulin - no. (%)	1 (6%)	3 (7%)	0.89

3.4.2 Ventricular volumes and function at rest

At rest, compared to $HFpEF_{EF<60}$, the $HFpEF_{EF>60}$ group had smaller LV volumes (LVEDVi 64.8 ± 14.7 vs 93.6 ± 17.1 ml/m², p<0.0001, LVESVi 22.7 ± 6.3 vs 41.8 ± 6.9 ml/m², p<0.0001), LVSVi (42.2 ± 9.1 vs 51.8 ± 10.7 ml/m², p=0.0006), better LV GLS (-15.5 ± 3.8 vs -13.5 ± 1.6 %, p=0.005) and higher LVEF (65.2 ± 3.2 vs 55.2 ± 2.6 %) on CMR. Diastolic function was similarly impaired at rest in both groups on echocardiography. Similarly, RV volumes were lower (RVEDVi 67.7 ± 16.6 vs 93.6 ± 21.5 ml/m², p<0.0001) with a higher RVEF (61.3 ± 6.6 vs 57.3 ± 6.5 %, p=0.03) and RV SV/ESV ratio (1.67 ± 0.49 vs 1.40 ± 0.44, p=0.01).

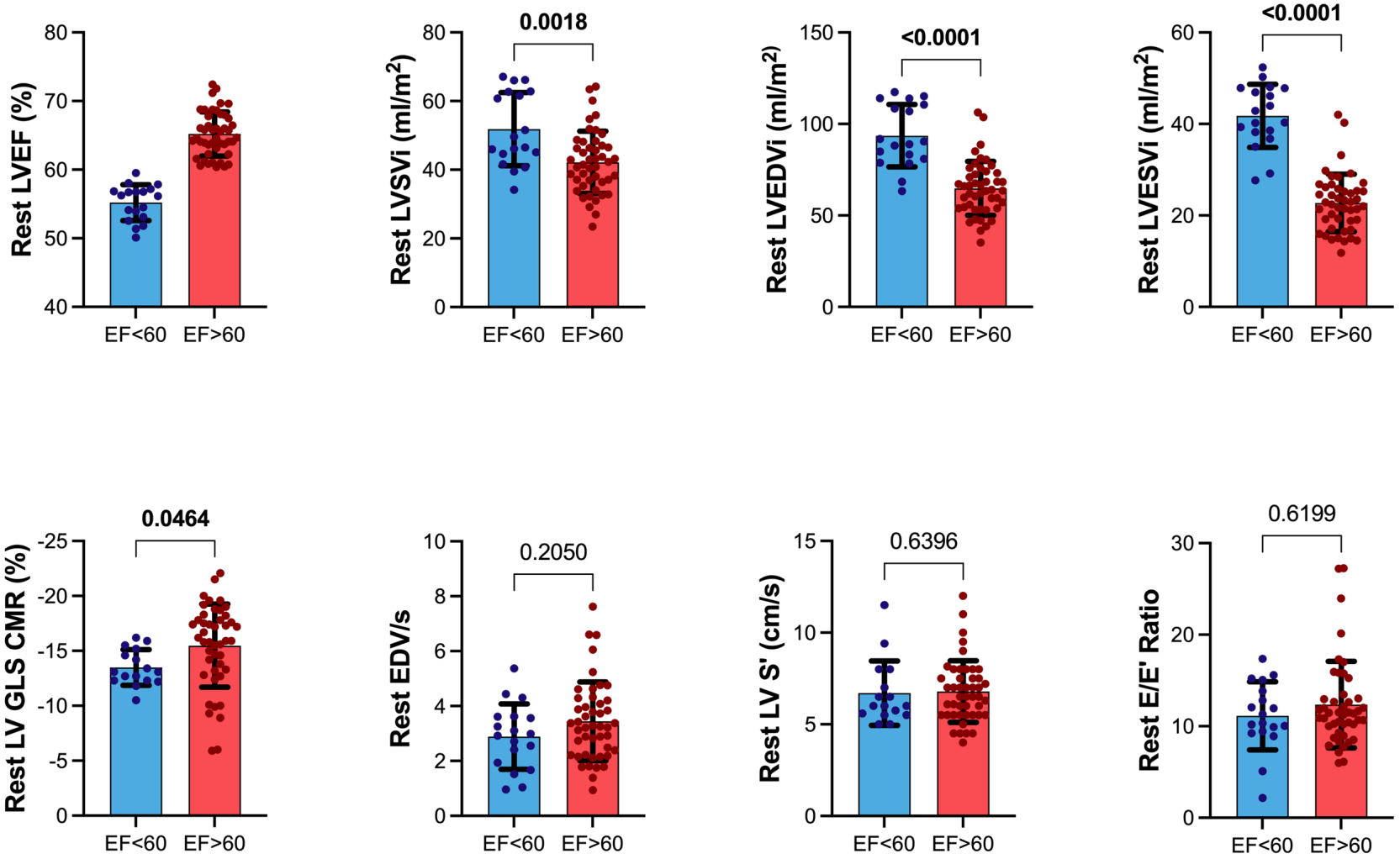

Figure 34: LV systolic and diastolic function at rest - $HFpEF_{EF<60}$ vs $HFpEF_{EF>60}$

LV S′ and E/E′ ratio on echocardiography. All other parameters measured on CMR.

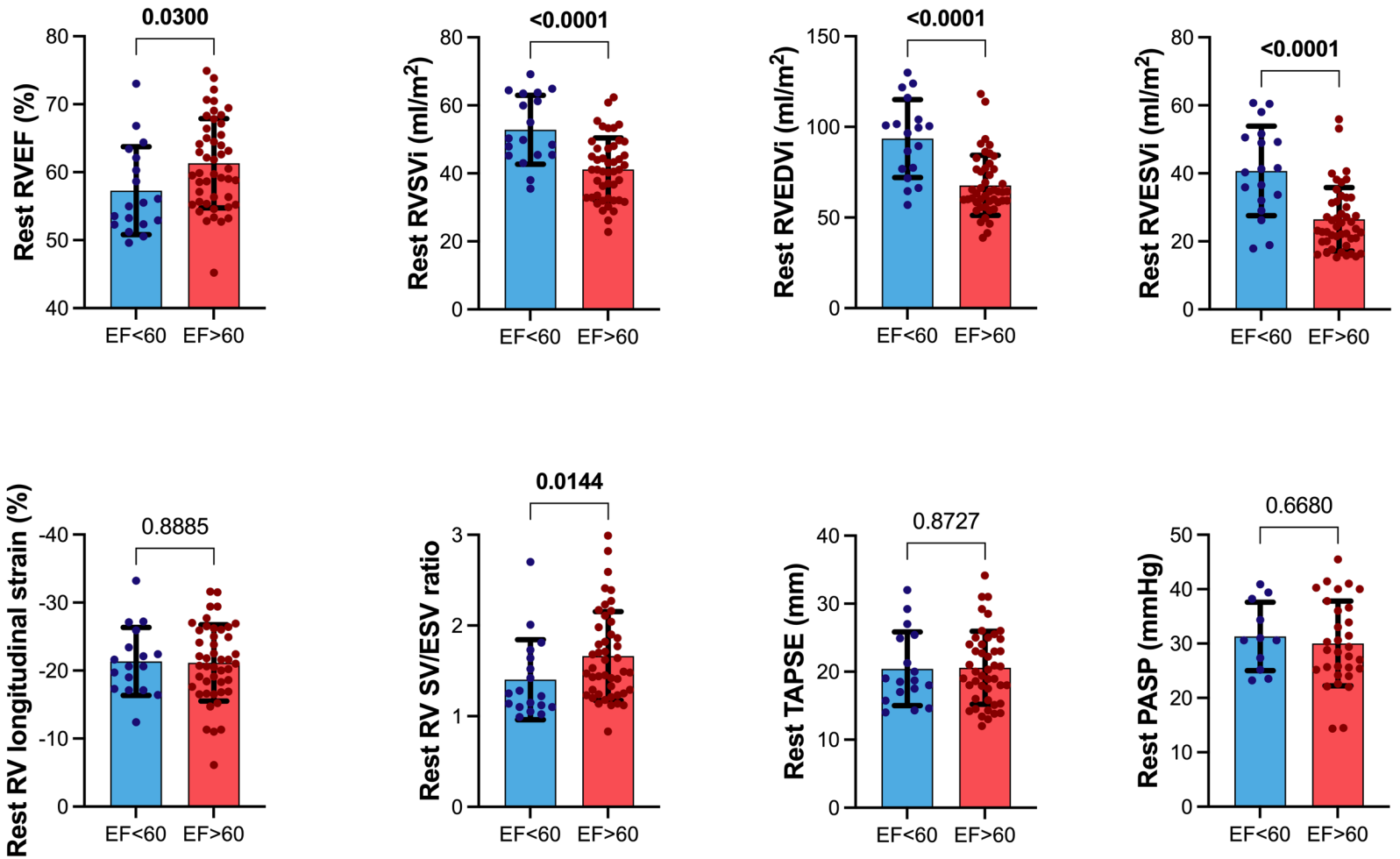

Figure 35: Rest RV systolic function - $HFpEF_{EF<60}$ vs $HFpEF_{EF>60}$

TAPSE and PASP measured on echocardiography. All other parameters are from CMR.

Table 21: Ventricular parameters on CMR at rest - $HFpEF_{EF<60}$ vs $HFpEF_{EF>60}$

	$HFpEF_{EF<60}$	$HFpEF_{EF>60}$	*p-value*
LVEDVi (ml/m²)	93.6 ± 17.1	64.8 ± 14.7	***<0.0001***
LVESVi (ml/m²)	41.8 ± 6.9	22.7 ± 6.3	***<0.0001***
LVEF (%)	55.2 ± 2.6	65.2 ± 3.2	N/A
LVSVi (ml/m²)	51.8 ± 10.7	42.2 ± 9.1	***0.0006***
LV GLS (%)	-13.5 ± 1.6	-15.5 ± 3.8	***0.005***
LVMi (g/m²)	64.6 ± 13.0	49.1 ± 12.7	***<0.0001***
LV mass: EDV ratio	0.70 ± 0.10	0.77 ± 0.19	0.10
LV peak early filling rate (EDV/s)	2.89 ± 1.19	3.45 ± 1.43	0.21
RVEDVi (ml/m²)	93.6 ± 21.5	67.7 ± 16.6	***<0.0001***
RVESVi (ml/m²)	40.7 ± 13.2	26.5 ± 9.3	***<0.0001***
RVEF (%)	57.3 ± 6.5	61.3 ± 6.6	***0.03***
RVSVi (ml/m²)	52.8 ± 10.1	41.2 ± 9.2	***<0.0001***
RV longitudinal strain (%)	-21.4 ± 5.0	-21.1 ± 5.6	0.89
RV SV/ESV ratio	1.40 ± 0.44	1.67 ± 0.49	***0.01***

Table 22: Echocardiography parameters at rest - $HFpEF_{EF<60}$ vs $HFpEF_{EF>60}$

	$HFpEF_{EF<60}$	*$HFpEF_{EF>60}$*	*p-value*
E/E′ average (ratio)	11.1 ± 3.7	12.4 ± 4.7	0.62
S′ LV (cm/s)	6.7 ± 1.8	6.8 ± 1.7	0.64
TAPSE (mm)	20.4 ± 5.4	20.6 ± 5.4	0.91
S′ RV (cm/s)	11.3 ± 3.3	12.2 ± 3.1	0.41
PASP (mmHg)	31.3 ± 6.3	30.0 ± 7.8	0.62
TAPSE / PASP ratio (mm/mmHg)	0.71 ± 0.34	1.09 ± 1.20	0.42
LA volume indexed biplane (ml/m^2)	61.2 ± 23.2	47.3 ± 19.1	***0.02***
LVMi (g/m^2)	106.4 ± 22.3	87.9 ± 29.2	***0.007***
Relative wall thickness	0.46 ± 0.09	0.50 ± 0.10	0.15

3.4.3 Atrial volumes and function at rest

Left atrial volume at ventricular end-systole was lower in the $HFpEF_{EF>60}$ cohort (71.7 ± 32.9 vs 82.7 ± 23.0 ml/m^2, p=0.046) with no significant differences in emptying fractions of either atrium or the right atrial volume.

Table 23: Atrial parameters at rest - $HFpEF_{EF<60}$ vs $HFpEF_{EF>60}$

	$HFpEF_{EF<60}$	*$HFpEF_{EF>60}$*	*p-value*
LAEDVi (ml/m^2)	63.1 ± 26.5	55.1 ± 31.8	0.20
LAESVi (ml/m^2)	82.7 ± 23.0	71.7 ± 32.9	***0.046***
LAEF (%)	26.6 ± 16.0	26.6 ± 14.1	0.90
RAEDVi (ml/m^2)	77.8 ± 41.0	64.4 ± 38.2	0.25
RAESVi (ml/m^2)	97.6 ± 37.8	80.6 ± 37.5	0.11
RAEF (%)	23.9 ± 15.4	25.0 ± 14.9	0.92

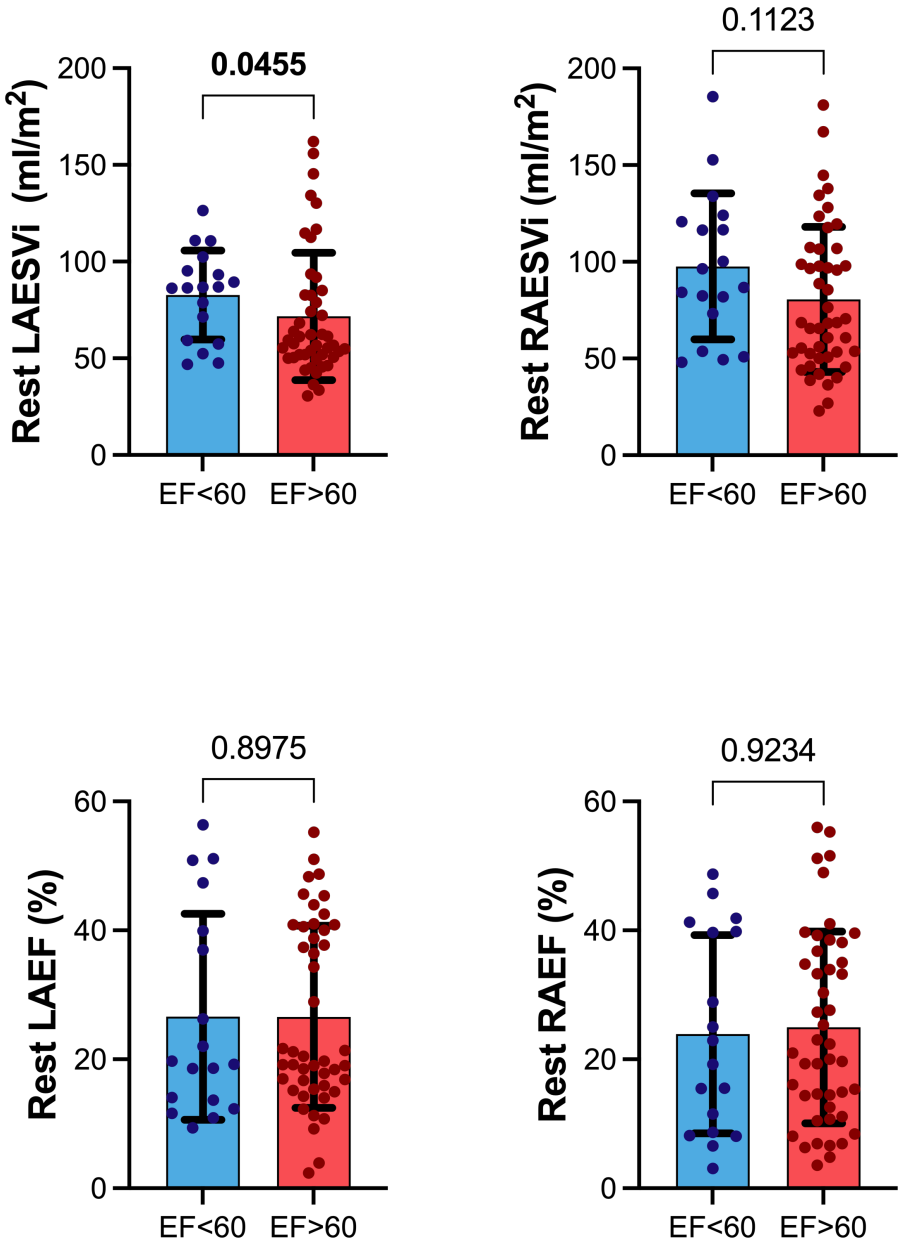

Figure 36: Rest atrial parameters on CMR - $HFpEF_{EF<60}$ vs $HFpEF_{EF>60}$

3.4.4 Ventricular volumes and function during exercise

Similar to rest, absolute volumes of the LV (LVEDVi 68.3 ± 13.7 vs 93.5 ± 16.4 ml/m^2, p<0.0001) and the stress LVSVi (46.5 ± 9.7 vs 56.7 ± 10.1 ml/m^2, p=0.0005) were lower in the $HFpEF_{EF>60}$ cohort despite similar increases in LVSVi during exercise. There was lower augmentation of LVEF in the $HFpEF_{EF>60}$ group (+3.1 ± 4.9 vs +5.4 ± 3.6 %, p=0.03) associated with diminished reduction in the end-systolic volume (-1.0 ± 4.2 vs -4.9 ± 5.5 ml/m^2, p=0.005). The early diastolic peak filling rate was higher in this group on CMR (EDV/s 3.90 ± 1.24 vs 3.14 ± 1.42, p=0.04). The $HFpEF_{EF<60}$ cohort had a greater change in E/E' (+2.2 ± 3.1 vs +0.2 ± 2.9, p=0.007) indicating a rise in LV filling pressures in this lower LVEF group and worsening diastolic function during exercise, consistent with the lower early diastolic filling rate on CMR. RV volumes were also lower in the $HFpEF_{EF>60}$ group (RVEDVi 75.2 ± 18.9 vs 99.6 ± 20.6 ml/m^2, p<0.0001) with a lower RVSVi (46.8 ± 9.8 vs 57.6 ± 9.6 ml/m^2, p=0.0002). Unlike the LV there was no difference in exercise-induced change in volume or function.

Table 24: Ventricular parameters during exercise - $HFpEF_{EF<60}$ vs $HFpEF_{EF>60}$

	$HFpEF_{EF<60}$	***$HFpEF_{EF>60}$***	***p-value***
LVEDVi (ml/m^2)	93.5 ± 16.4	68.3 ± 13.7	***<0.0001***
LVESVi (ml/m^2)	36.8 ± 8.0	21.7 ± 6.2	***<0.0001***
LVEF (%)	60.7 ± 4.1	68.3 ± 5.6	***<0.0001***
LVSVi (ml/m^2)	56.7 ± 10.1	46.5 ± 9.7	***0.0005***
LV peak early filling rate (EDV/s)	3.14 ± 1.42	3.90 ± 1.24	***0.04***
RVEDVi (ml/m^2)	99.6 ± 20.6	75.2 ± 18.9	***<0.0001***
RVESVi (ml/m^2)	42.0 ± 13.5	28.5 ± 11.9	***0.0002***
RVEF (%)	58.7 ± 7.5	63.2 ± 8.8	0.06
RVSVi (ml/m^2)	57.6 ± 9.6	46.8 ± 9.8	***0.0002***
RV SV/ESV ratio	1.52 ± 0.63	1.96 ± 1.14	0.06

Table 25: Change in ventricular parameters from rest to exercise - $HFpEF_{EF<60}$ vs $HFpEF_{EF>60}$

	$HFpEF_{EF<60}$	$HFpEF_{EF>60}$	*p-value*
ΔLVEDVi rest→stress (ml/m²)	-0.1 ± 8.3	3.4 ± 5.9	0.06
ΔLVESVi rest→stress (ml/m²)	-4.9 ± 5.5	-1.0 ± 4.2	***0.005***
ΔLVEF rest→stress (%)	5.4 ± 3.6	3.1 ± 4.9	***0.03***
ΔLVSVi rest→stress (ml/m²)	4.8 ± 4.7	4.3 ± 4.8	0.51
Δpeak early filling rate (EDV/s)	0.25 ± 1.45	0.36 ± 1.23	0.76
ΔRVEDVi rest→stress (ml/m²)	6.0 ± 8.7	7.5 ± 9.3	0.55
ΔRVESVi rest→stress (ml/m²)	1.2 ± 7.0	1.9 ± 6.6	0.71
ΔRVEF rest→stress (%)	1.4 ± 4.9	1.9 ± 6.7	0.78
ΔRVSVi rest→stress (ml/m²)	4.8 ± 5.1	5.6 ± 6.1	0.90
ΔRV SV/ESV ratio	0.12 ± 0.34	0.29 ± 0.96	0.78

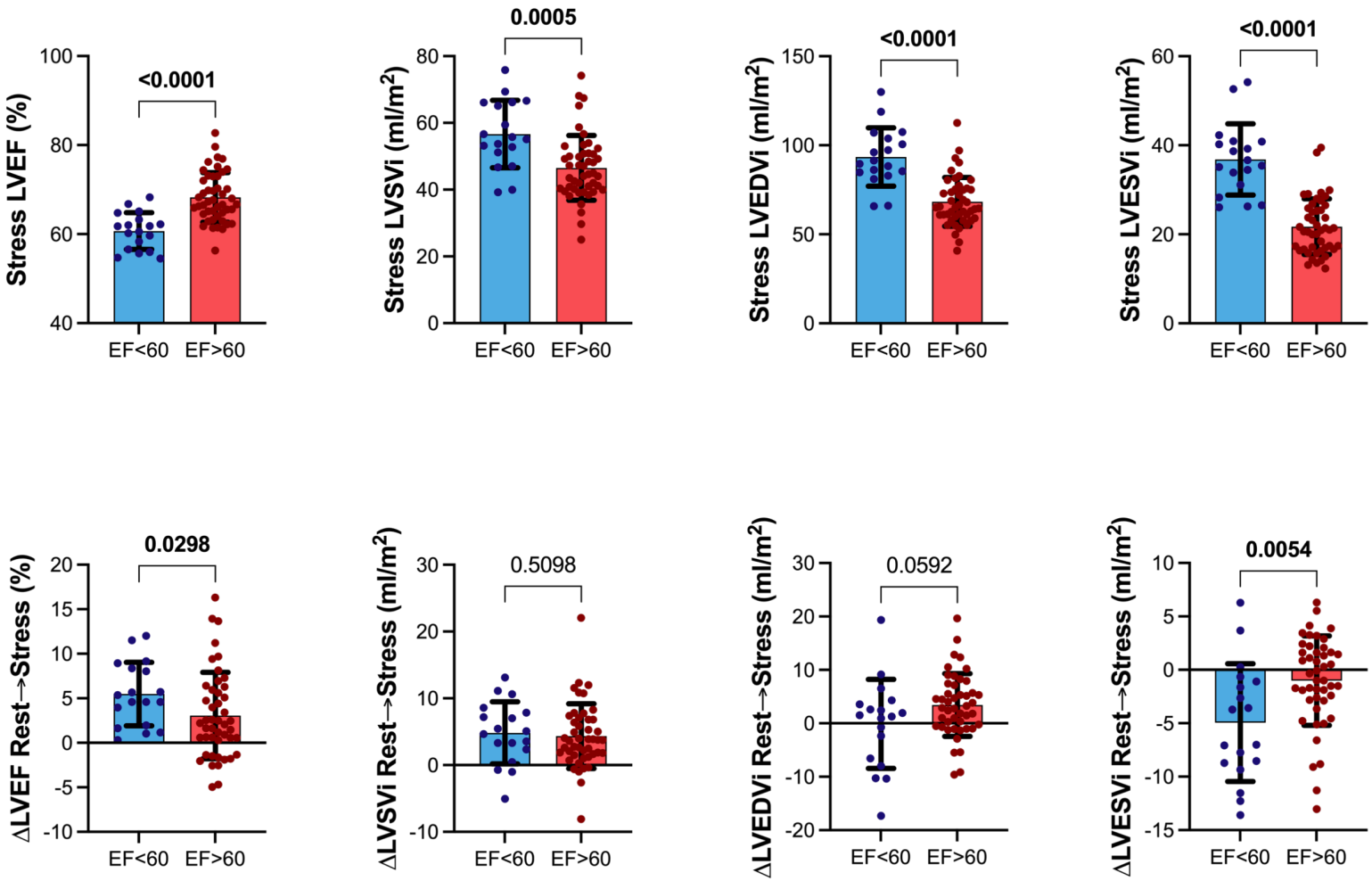

Figure 37: Stress LV systolic function on CMR - $HFpEF_{EF<60}$ vs $HFpEF_{EF>60}$

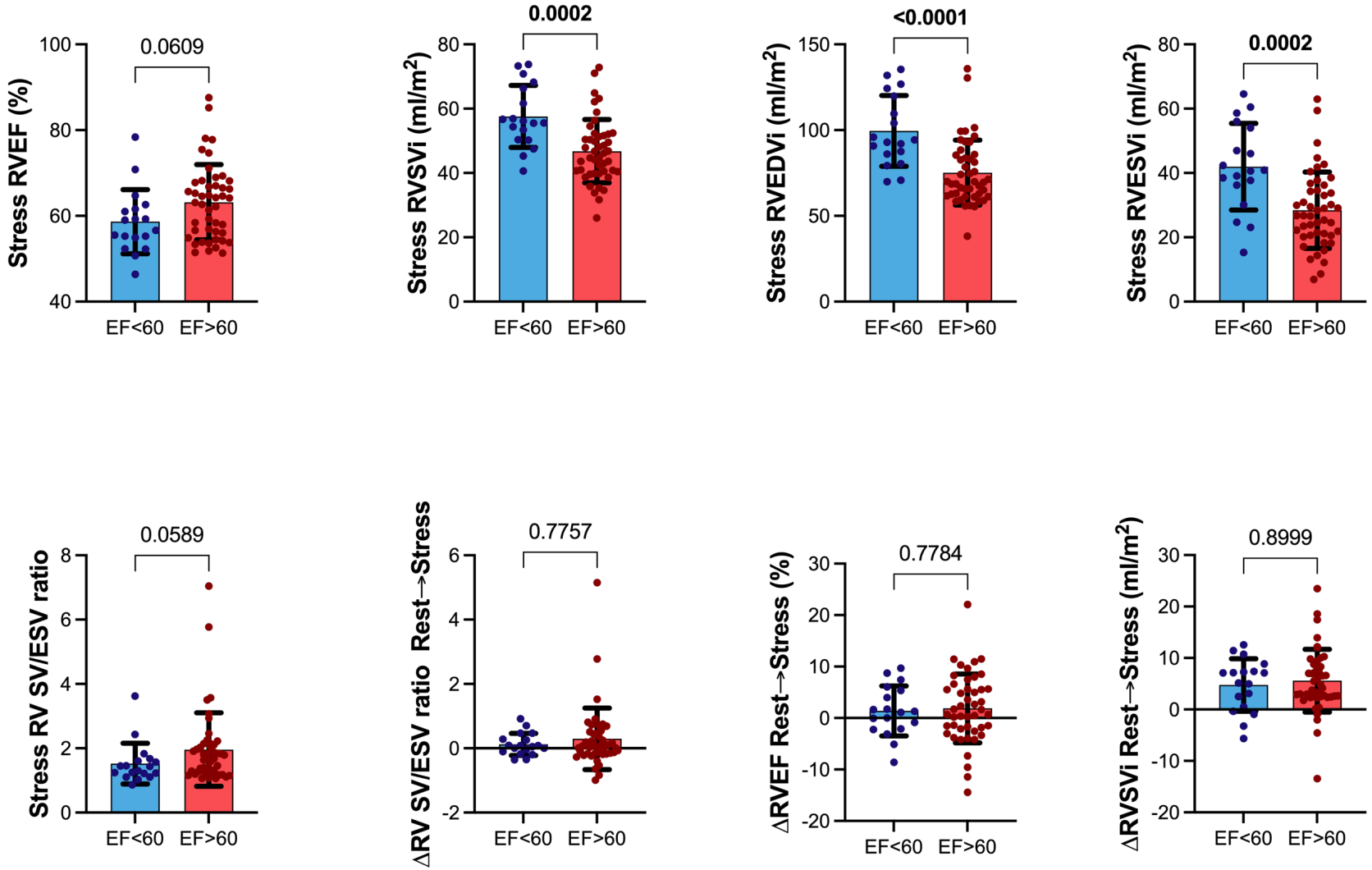

Figure 38: Stress RV systolic function on CMR - $HFpEF_{EF<60}$ vs $HFpEF_{EF>60}$

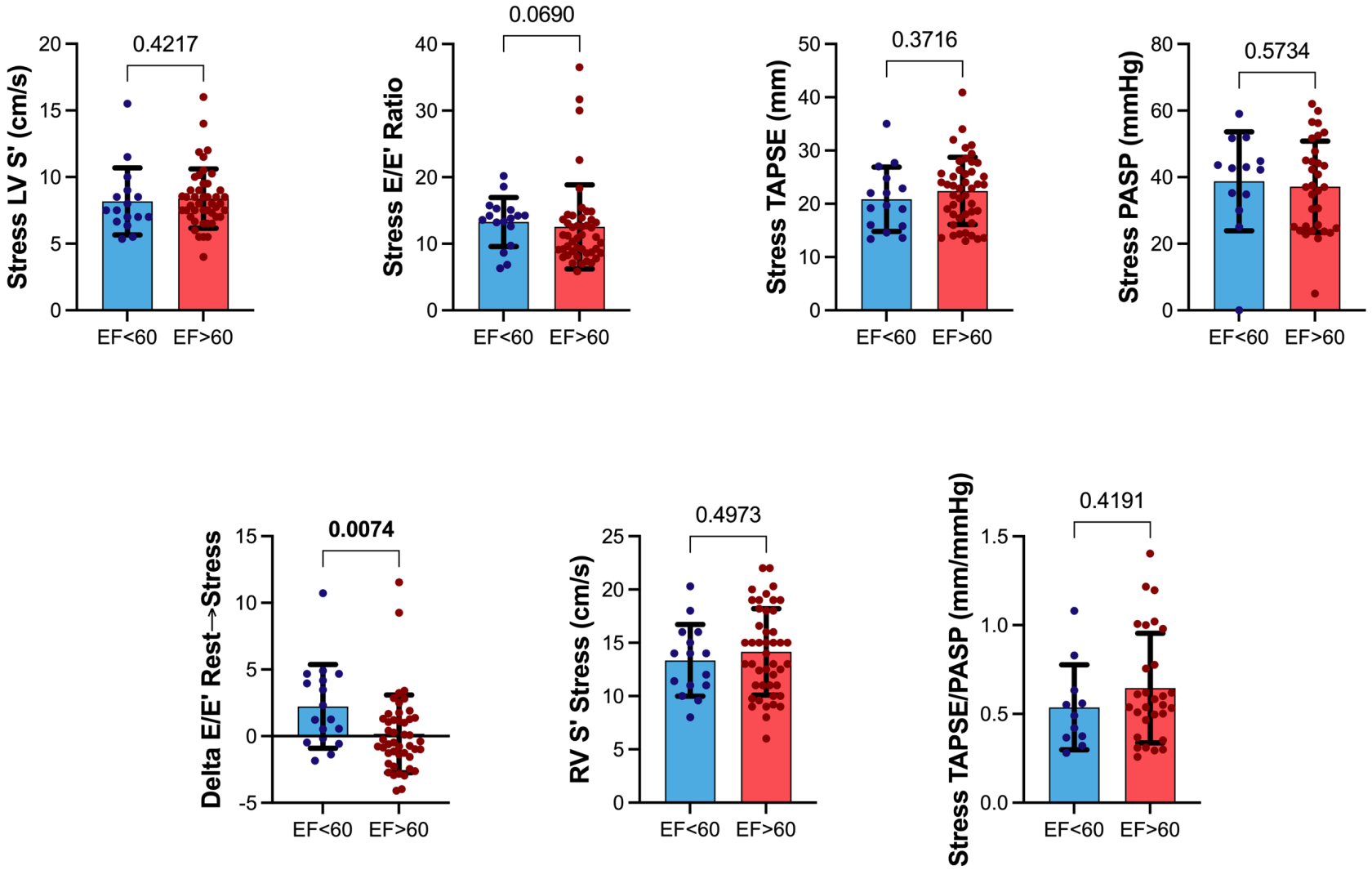

Figure 39: Stress echocardiography parameters - $HFpEF_{EF<60}$ vs $HFpEF_{EF>60}$

Table 26: Echocardiography parameters during exercise

	$HFpEF_{EF<60}$	$HFpEF_{EF>60}$	*p-value*
E/E′ average (ratio)	13.3 ± 3.7	12.5 ± 6.3	0.07
ΔE/E′ ratio rest→stress	2.2 ± 3.1	0.2 ± 2.9	**0.007**
S′ LV (cm/s)	8.2 ± 2.5	8.4 ± 2.2	0.42
TAPSE (mm)	20.9 ± 6.0	22.4 ± 6.3	0.41
S′ RV (cm/s)	13.4 ± 3.4	14.2 ± 4.1	0.50
PASP (mmHg)	38.8 ± 14.9	37.2 ± 13.7	0.73
TAPSE/PASP ratio (mm/mmHg)	0.54 ± 0.24	0.65 ± 0.31	0.42

3.4.5 Atrial volumes and function during exercise

As before, the LAESVi was lower in the $HFpEF_{EF>60}$ group (76.2 ± 33.7 vs 91.7 ± 27.2 ml/m², p=0.02). However, during exercise there was an attenuated increase in the LAESVi (+4.55 ± 8.83 vs +8.95 ± 8.11 ml/m², p=0.047) as well as the RAESVi in the $HFpEF_{EF>60}$ cohort (+9.3 ± 11.8 vs +19.0 ± 15.9 ml/m², p=0.01).

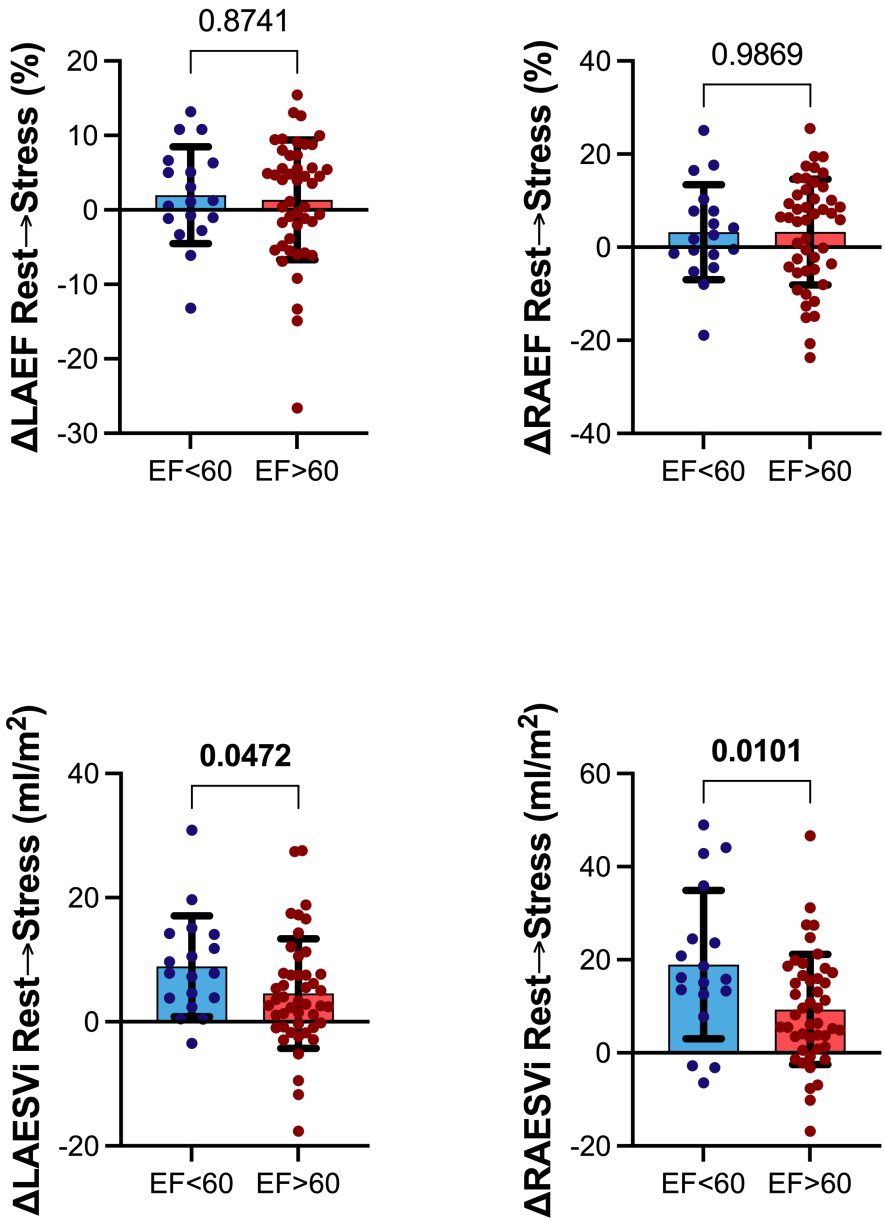

Figure 40: Stress atrial parameters on CMR - $HFpEF_{EF<60}$ vs $HFpEF_{EF>60}$

Table 27: Atrial parameters at stress and stress-induced change - $HFpEF_{EF<60}$ vs $HFpEF_{EF>60}$

	$HFpEF_{EF<60}$	$HFpEF_{EF>60}$	*p-value*
LAEDVi (ml/m²)	67.8 ± 27.3	57.2 ± 32.2	0.10
LAESVi (ml/m²)	91.7 ± 27.2	76.2 ± 33.7	***0.02***
LAEF (%)	28.6 ± 14.1	28.0 ± 14.3	0.96
RAEDVi (ml/m²)	88.4 ± 45.7	68.4 ± 40.1	0.13
RAESVi (ml/m²)	116.6 ± 47.2	89.9 ± 42.3	0.05
RAEF (%)	27.1 ± 13.0	28.2 ± 16.3	0.85
ΔLAESVi rest→stress (ml/m²)	+8.95 ± 8.11	+4.55 ± 8.83	***0.047***
ΔRAESVi rest→stress (ml/m²)	+19.0 ± 15.9	+9.3 ± 11.8	***0.01***
ΔLAEF rest→stress (%)	2.0 ± 6.5	1.3 ± 8.0	0.87
ΔRAEF rest→stress (%)	3.2 ± 10.2	3.3 ± 11.4	0.99

3.4.6 Cardiac output at rest and during exercise

There was a reduction in rest cardiac index in the $HFpEF_{EF>60}$ cohort as a result of the lower LVSVi (2.76 ± 0.58 vs 3.21 ± 0.69 L/min/m², p=0.02). Augmentation of cardiac index was similar in both cohorts (+1.79 ± 0.93 vs +1.99 ± 0.93 L/min/m², p=0.42) resulting a lower cardiac index during exercise in the $HFpEF_{EF>60}$ group (4.55 ± 1.10 vs 5.20 ± 1.28 L/min/m², p=0.048).

Table 28: Cardiac output at rest and stress - $HFpEF_{EF<60}$ vs $HFpEF_{EF>60}$

	$HFpEF_{EF<60}$	*$HFpEF_{EF>60}$*	*p-value*
Rest Cardiac Output (L/min)	6.78 ± 1.69	5.42 ± 1.43	***0.003***
Rest Cardiac Index (L/min/m²)	3.21 ± 0.69	2.76 ± 0.58	***0.02***
Stress Cardiac Output (L/min)	10.87 ± 2.56	8.94 ± 2.54	***0.008***
Stress Cardiac Index (L/min/m²)	5.20 ± 1.28	4.55 ± 1.10	***0.048***
ΔCardiac Index (L/min/m²)	1.99 ± 0.93	1.79 ± 0.93	0.42

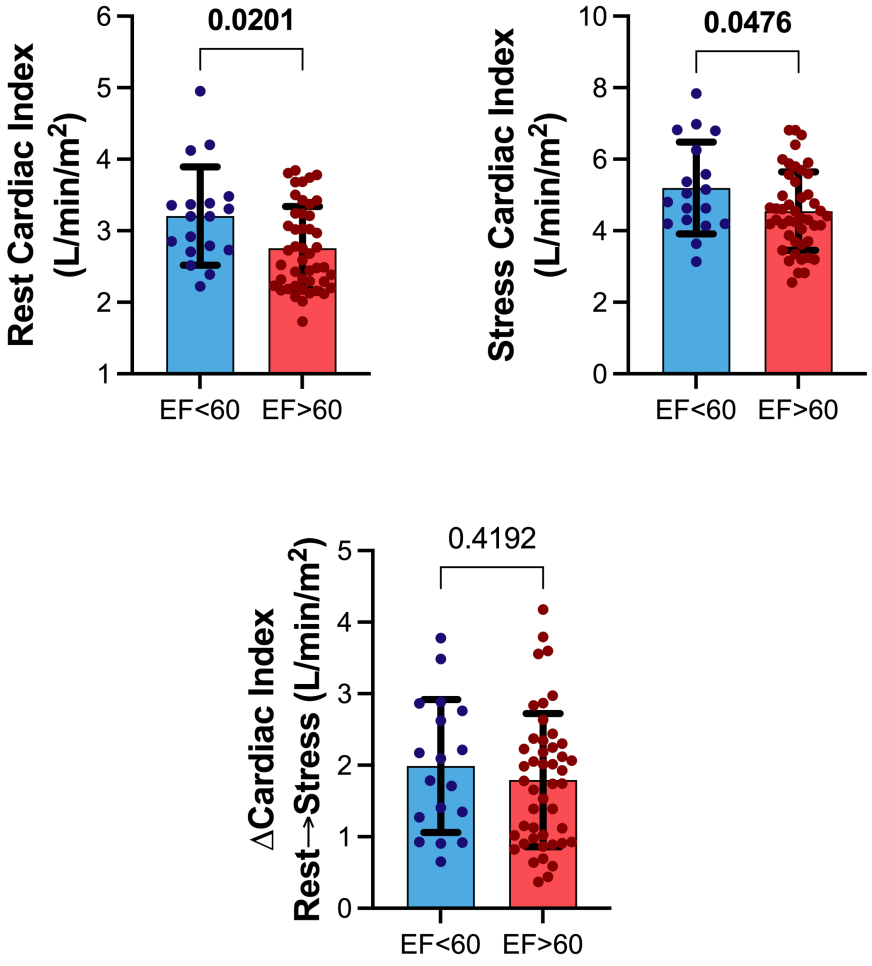

Figure 41: Cardiac index at rest and during exercise - $HFpEF_{EF<60}$ vs $HFpEF_{EF>60}$

Table 29: Blood pressure, heart rate and oxygen saturations at rest and stress - $HFpEF_{EF<60}$ vs $HFpEF_{EF>60}$

	$HFpEF_{EF<60}$	$HFpEF_{EF>60}$	*p-value*
REST			
SBP (mmHg)	146.2 ± 12.8	136.4 ± 18.5	***0.04***
DBP (mmHg)	80.3 ± 18.1	71.4 ± 11.1	0.05
MAP (mmHg)	102.3 ± 13.2	93.1 ± 9.9	***0.006***
Heart rate (bpm)	63.1 ± 12.3	67.0 ± 16.1	0.35
Peripheral oxygen saturation (%)	96.0 ± 1.7	96.4 ± 1.3	0.47
STRESS			
SBP (mmHg)	158.3 ± 20.5	159.1 ± 22.8	0.88
DBP (mmHg)	99.3 ± 20.9	92.0 ± 19.4	0.20
MAP (mmHg)	119.0 ± 15.8	114.4 ± 16.3	0.32
Heart rate (bpm)	92.1 ± 17.4	98.3 ± 16.4	0.18
Peripheral oxygen saturation (%)	95.3 ± 2.5	95.5 ± 2.9	0.57
ΔSBP rest→stress (mmHg)	+13.7 ± 18.8	+21.3 ± 18.9	0.08
ΔDBP rest→stress (mmHg)	+25.8 ± 24.4	+21.5 ± 21.0	0.49
ΔMAP rest→stress (mmHg)	+21.8 ± 15.9	+21.4 ± 16.0	0.94

3.4.7 Myocardial metabolism – energetics and triglyceride content

PCr / ATP ratio as measured on ^{31}P DRESS spectroscopy was similarly impaired in both cohorts. Myocardial triglyceride content was also not significantly different in the $HFpEF_{EF>60}$ group compared to $HFpEF_{EF<60}$ (1.74 ± 1.31 vs 2.08 ± 1.61 %, p=0.41).

Table 30: Myocardial energetics as assessed by PCr/ATP ratio and myocardial triglyceride content - $HFpEF_{EF<60}$ vs $HFpEF_{EF>60}$

	$HFpEF_{EF<60}$	*$HFpEF_{EF>60}$*	*p-value*
PCr/ATP ratio	1.48 ± 0.17	1.49 ± 0.34	0.97
Myocardial triglyceride content (%)	2.08 ± 1.61	1.74 ± 1.31	0.41

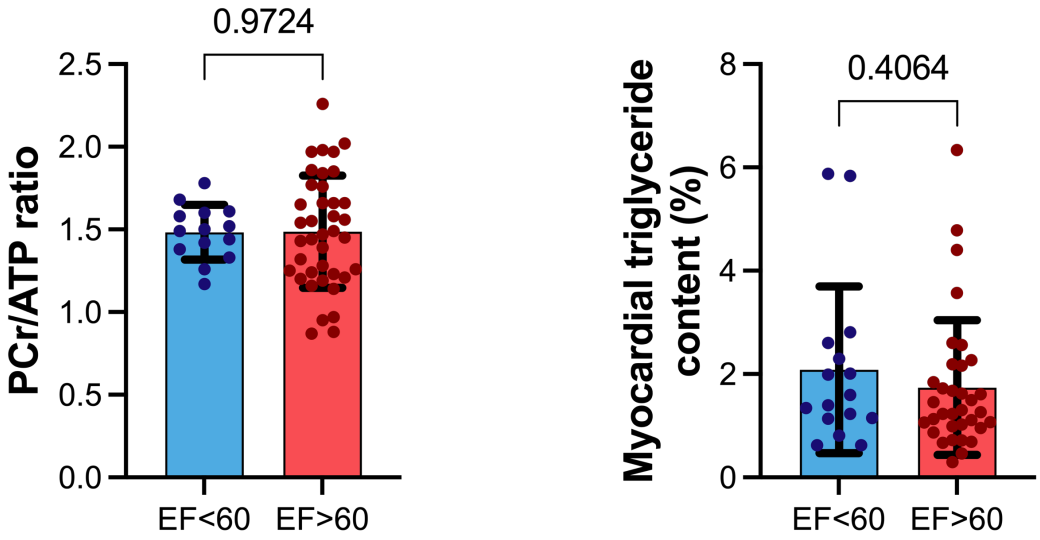

Figure 42: Myocardial energetics as assessed by PCr/ATP ratio and myocardial triglyceride content - $HFpEF_{EF<60}$ vs $HFpEF_{EF>60}$

3.4.8 Lung function tests at rest and exercise

There were no significant differences in FEV1, FVC, FEV1/FVC ratio or in DLCO, KCO and VA at rest. Similarly, there were no significant differences in these parameters during exercise, although VA was numerically lower following exercise in $HFpEF_{EF>60}$ (4.42 ± 1.14 vs 5.05 ± 0.83L, p=0.06).

Table 31: Lung function parameters at rest - $HFpEF_{EF<60}$ vs $HFpEF_{EF>60}$

	$HFpEF_{EF<60}$	*$HFpEF_{EF>60}$*	*p-value*
FEV1 (% predicted)	85.0 ± 14.3	85.3 ± 18.0	0.96
FVC (% predicted)	94.6 ± 15.0	92.7 ± 17.1	0.70
FEV1/FVC (% ratio)	68.4 ± 7.8	70.2 ± 7.6	0.40
DLCO (% predicted)	72.7 ± 14.2	78.7 ± 14.5	0.17
KCO (% predicted)	85.3 ± 17.8	92.3 ± 12.7	0.11
VA (L)	4.83 ± 0.90	4.27 ± 1.13	0.09

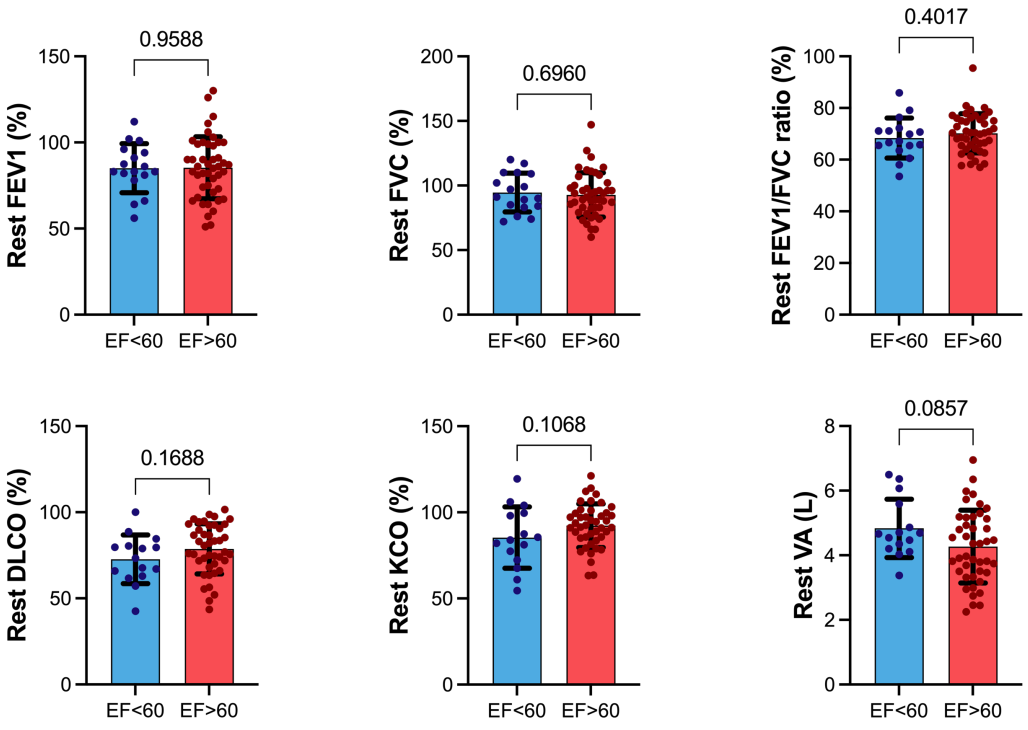

Figure 43: Rest Lung function parameters - $HFpEF_{EF<60}$ vs $HFpEF_{EF>60}$

Table 32: Lung function parameters following exercise - $HFpEF_{EF<60}$ vs $HFpEF_{EF>60}$

	$HFpEF_{EF<60}$	*$HFpEF_{EF>60}$*	*p-value*
FEV1 (% predicted)	87.8 ± 15.1	87.3 ± 18.8	0.92
FVC (% predicted)	98.5 ± 18.2	95.1 ± 16.2	0.50
FEV1/FVC (% ratio)	68.4 ± 7.9	69.4 ± 7.4	0.65
DLCO (% predicted)	82.4 ± 17.3	87.8 ± 18.5	0.35
KCO (% predicted)	93.3 ± 22.8	100.1 ± 15.1	0.20
VA (L)	5.05 ± 0.83	4.42 ± 1.14	0.06

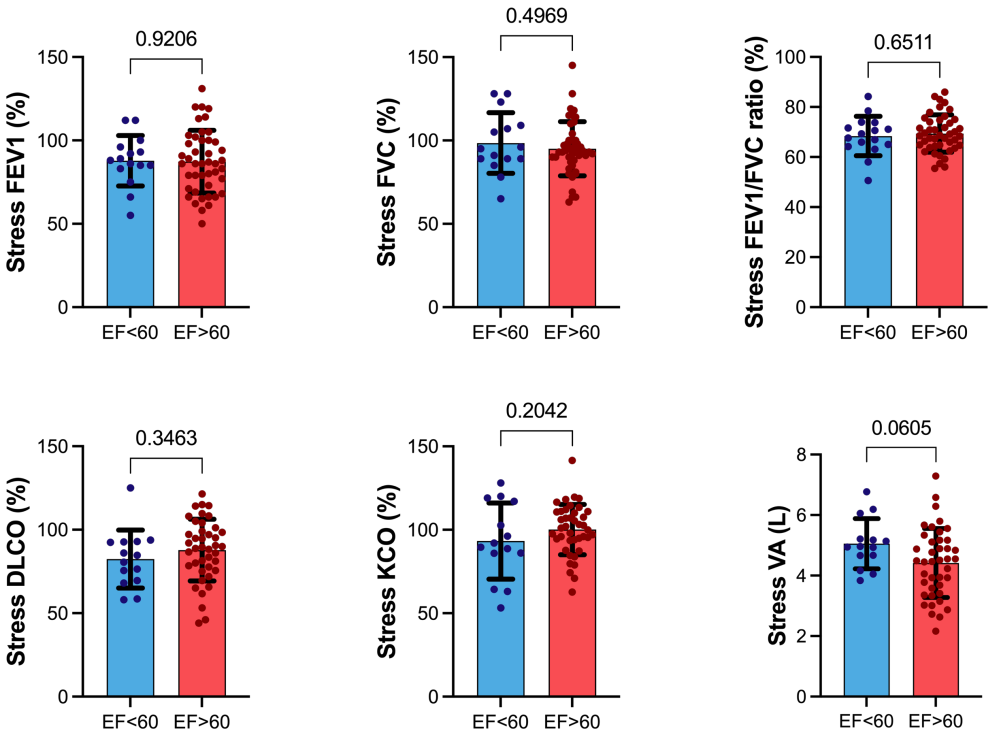

Figure 44: Lung function parameters at stress - $HFpEF_{EF<60}$ vs $HFpEF_{EF>60}$

3.4.9 Functional capacity and symptom burden

Functional capacity as assessed by 6-minute walk test distance was impaired to a greater degree in the $HFpEF_{EF>60}$ group (348.9 ± 94.7 vs 401.4 ± 75.7 m, p=0.04) with greater dyspnoea during the test (Modified Borg scale 3.2 ± 2.1 vs 2.0 ± 1.4, p=0.04). There was no significant difference in overall symptom burden as assessed by the KCCQ overall (66.4 ± 22.4 vs 74.9 ± 16.8, p=0.16) or clinical (67.8 ± 21.0 vs 74.6 ± 17.0, p=0.24) summary scores.

Table 33: Functional capacity and symptom burden - $HFpEF_{EF<60}$ vs $HFpEF_{EF>60}$

	$HFpEF_{EF<60}$	***$HFpEF_{EF>60}$***	***p-value***
6-minute walk test distance (m)	401.4 ± 75.7	348.9 ± 94.7	***0.04***
6MWT dyspnoea score (Modified Borg scale)	2.0 ± 1.4	3.2 ± 2.1	***0.04***
KCCQ overall summary score	74.9 ± 16.8	66.4 ± 22.4	0.16
Distribution - no (%)[221]	Of 17	Of 46	
75-100 (Good – excellent)	10 (58.8%)	19 (41.3%)	
50-74 (Fair – good)	5 (29.4%)	16 (34.8%)	
25-49 (Poor – fair)	2 (11.8%)	10 (21.7%)	
<25 (Very poor – poor)	0	1 (2.2%)	
KCCQ clinical summary score	74.6 ± 17.0	67.8 ± 21.0	0.24
Distribution - no (%)	Of 17	Of 46	
75-100 (Good – excellent)	10 (58.8%)	21 (45.6%)	
50-74 (Fair – good)	6 (35.3%)	16 (34.8%)	
25-49 (Poor – fair)	1 (5.9%)	8 (17.4%)	
<25 (Very poor – poor)	0	1 (2.2%)	

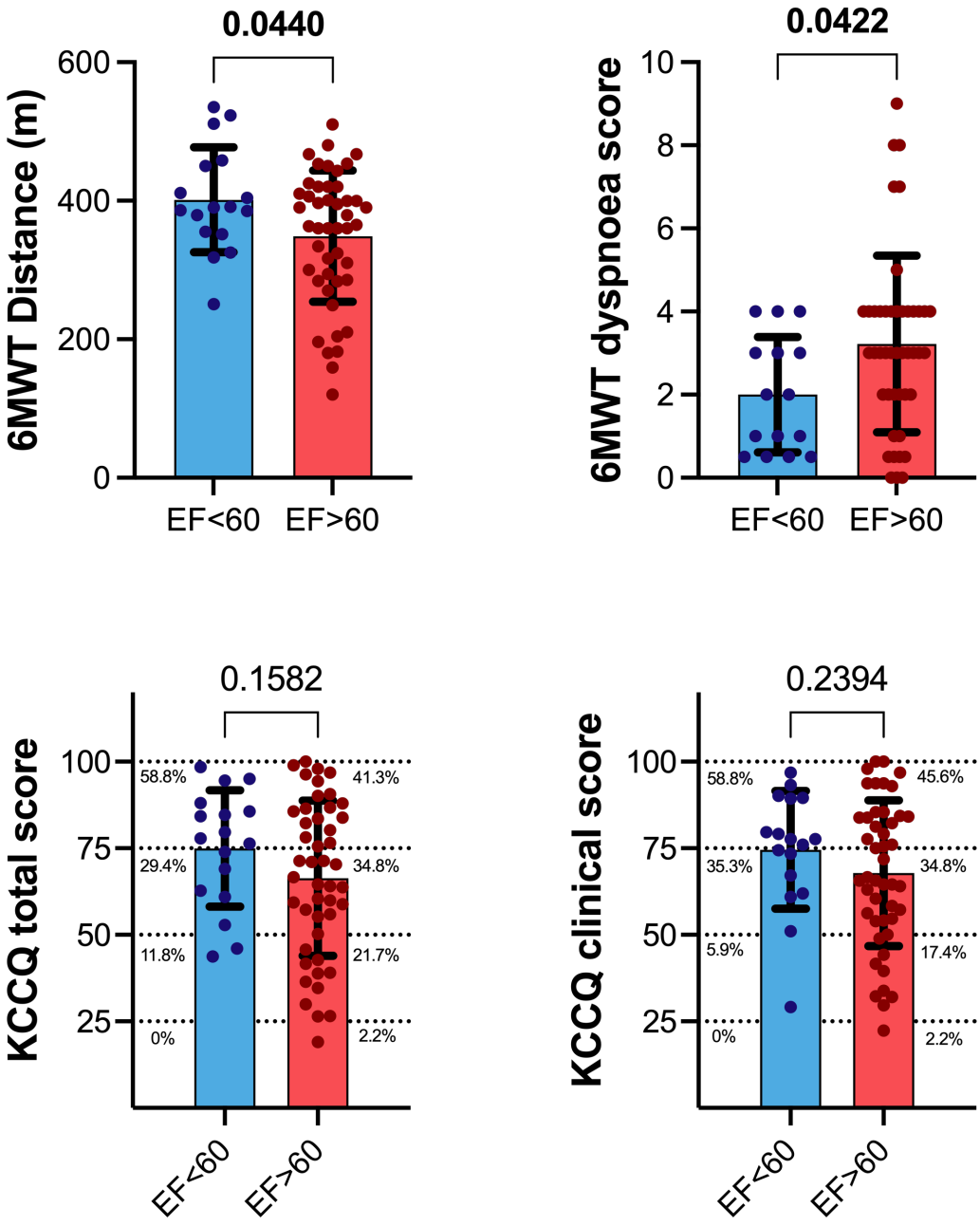

Figure 45: Functional capacity and symptom burden - $HFpEF_{EF<60}$ vs $HFpEF_{EF>60}$

The KCCQ total and clinical scores are divided into quartiles with increasing severity of symptoms with lower scores. The proportion of patients for each endotype of HFpEF within each quartile is shown as a percentage.

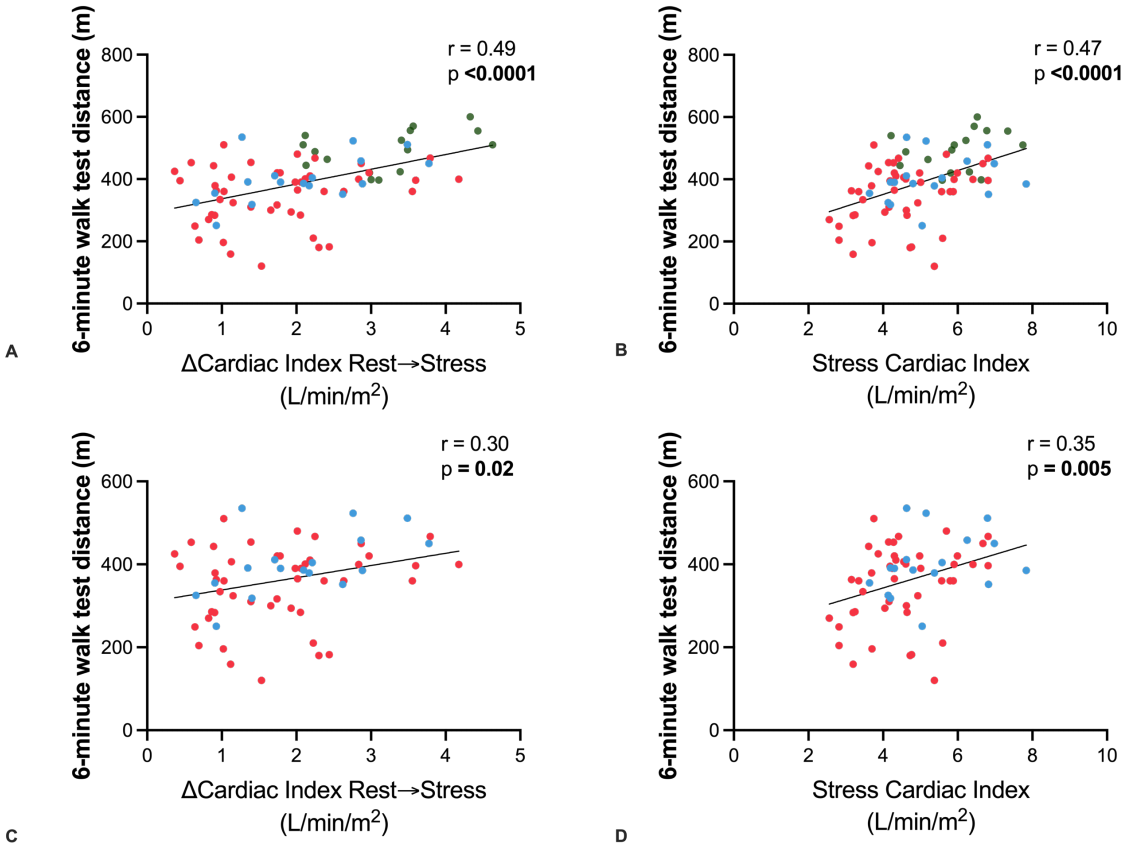

Figure 46: Correlation of 6MWT distance with stress-inducible change in cardiac index and final stress cardiac index across all 3 cohorts (A, B) and the 2 HFpEF endotypes only (C, D)

Green: Controls, Blue: $HFpEF_{EF<60}$, Red: $HFpEF_{EF>60}$

The key parameters which were correlated with 6MWT distance across all 3 cohorts including controls were the stress-inducible change in cardiac index ($r = 0.49$, $p<0.0001$) and the final stress cardiac index ($r = 0.47$, $p < 0.0001$). When looking at HFpEF alone, the correlations remained significant for both Δ cardiac index ($r = 0.30$, $p = 0.02$) and stress cardiac index ($r = 0.35$, $p = 0.005$).

3.4.10 Proteomics

When compared to controls, 20 proteins within the plasma proteome were of differential abundance in the $HFpEF_{EF>60}$ group (full list in the appendix). Of these, 17 were increased and 3 were detected in lower quantities. A greater proportion of the proteome was different in the $HFpEF_{EF<60}$ group with 80 proteins of distinct abundance – 67 with higher levels and 13 with lower levels.

On pathway analysis using the Reactome database, pathways involving metabolism of fatty acids and autophagy were primarily highlighted in the $HFpEF_{EF>60}$ group. In the $HFpEF_{EF<60}$ group, while mitochondrial fatty acid oxidation pathways were also overrepresented, a number of other pathways including extracellular matrix organisation, protein phosphorylation, mRNA processing, the complement cascade and insulin-like growth factor signalling were implicated.

Given that fatty acid metabolism represented a common perturbation in both cohorts, the proteins within the pathway 'Metabolism of lipids' were examined in greater detail particularly in relation to exercise response. In both HFpEF groups, the plasma levels of the proteins FABP-heart, FABP-adipocyte, ceramide transporter, phytanoyl-CoA dioxygenase and acyl-CoA binding protein were different from that of controls (p values for all <0.01). All of these protein levels were inversely related to cardiac stress responses with the exception of phytanyl-CoA dioxygenase which was positively correlated. All 5 proteins were related to augmentation of cardiac index during stress (p values for all ≤ 0.001) and stress cardiac index (p values for all ≤ 0.02). FABP-heart ($p=0.006$), FABP-adipocyte ($p=0.046$) and phytanyl-CoA dioxygenase ($p<0.0001$) were also associated with augmentation of LVEF during exercise, but acyl-CoA binding protein and ceramide transporter were not.

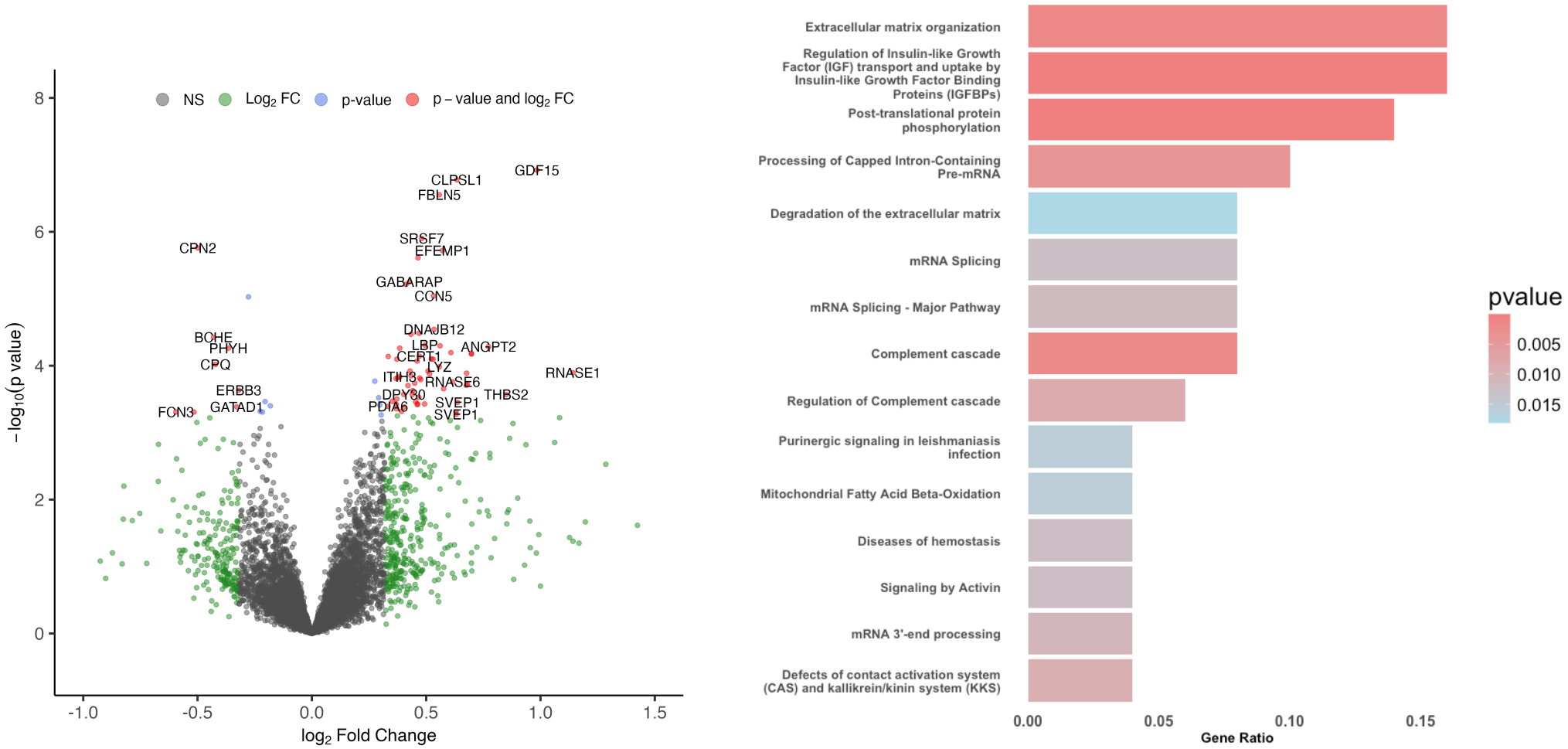

Figure 47: Volcano plot showing differential plasma protein abundance for the $HFpEF_{EF<60}$ group compared to controls and pathway overrepresentation analysis of these proteins

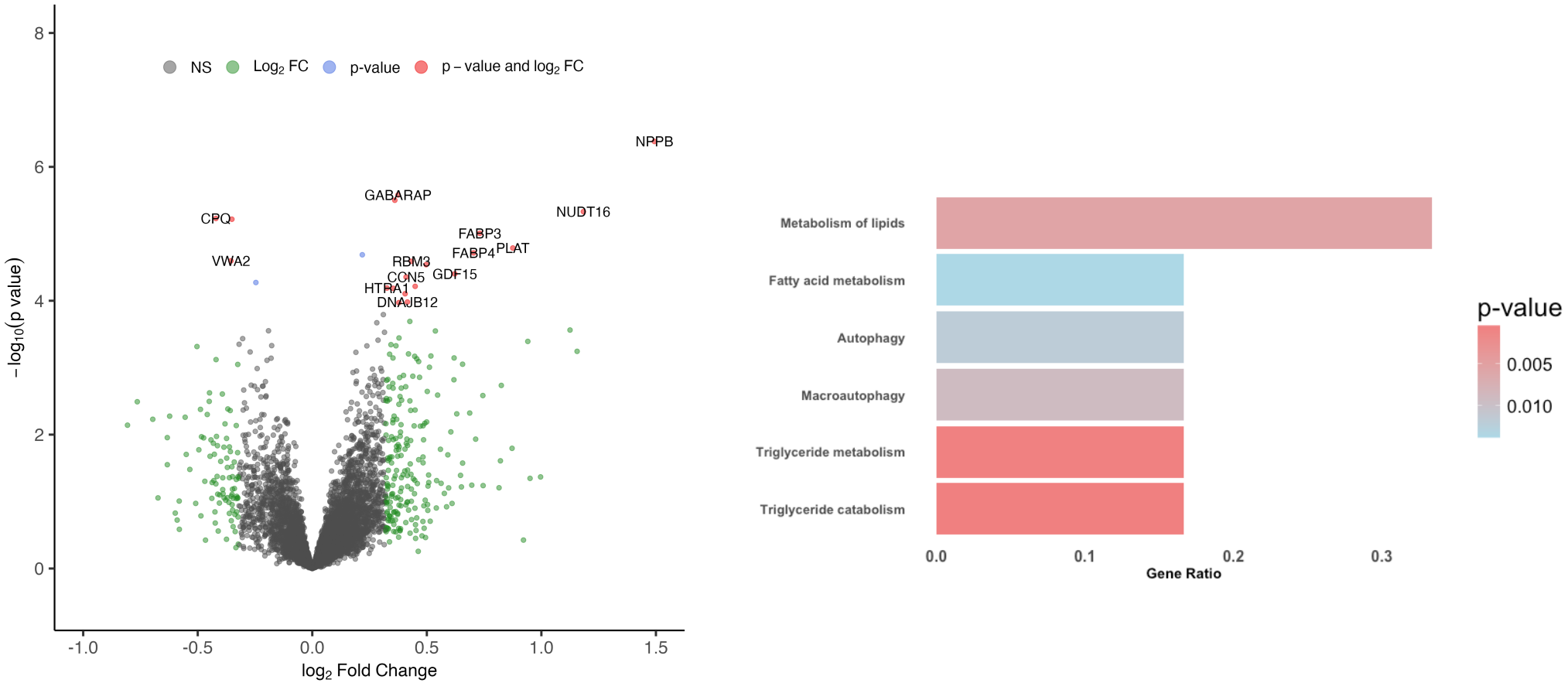

Figure 48: Volcano plot showing differential plasma protein abundance for the $HFpEF_{EF>60}$ group compared to controls and pathway overrepresentation analysis of these proteins

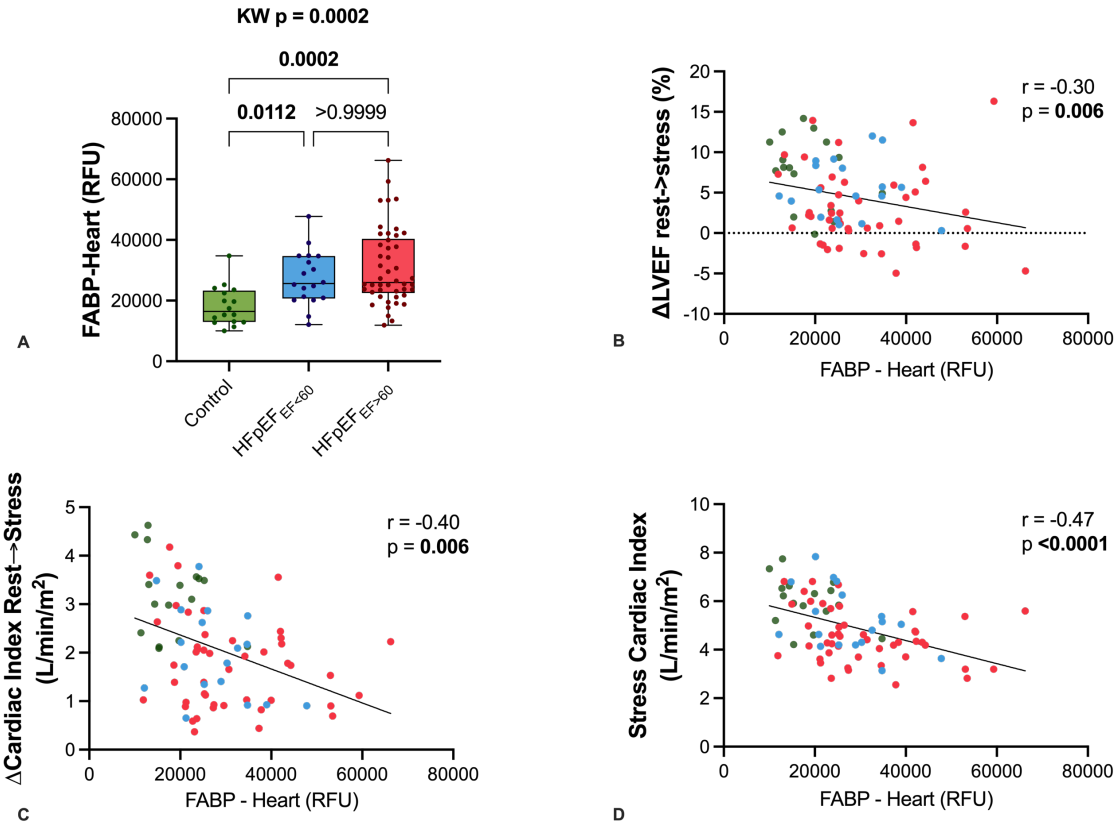

Figure 49: Relative abundance of FABP - Heart type in controls and endotypes of HFpEF and its correlation with key stress variables

RFU: Relative Fluorescence Units, KW: Kruskal-Wallis test

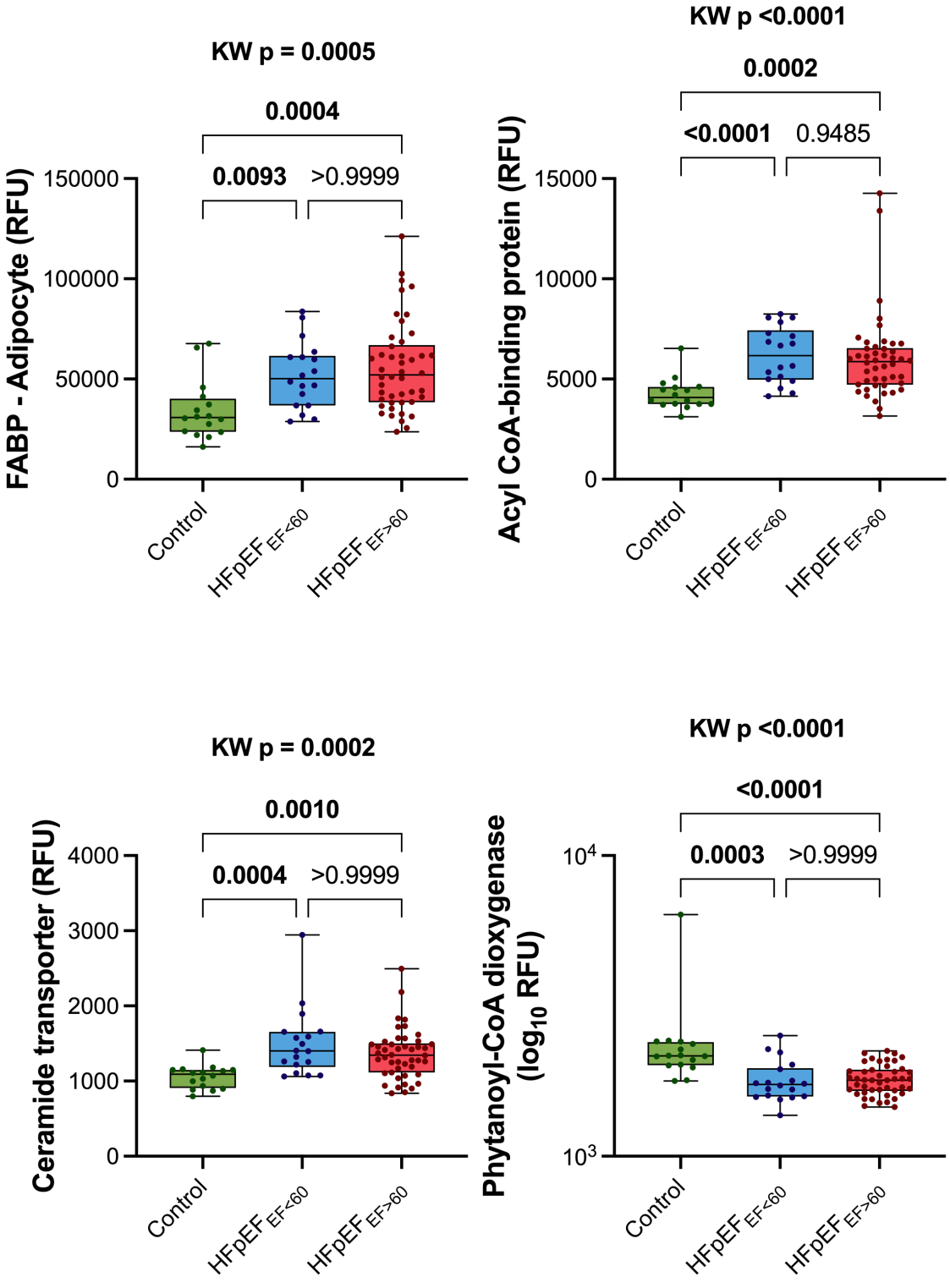

Figure 50: Key proteins with differential abundance involved in lipid metabolism

RFU: Relative Fluorescence Units, KW: Kruskal-Wallis test

Table 34: Correlation of exercise cardiac reserve and stress cardiac index with key proteins involved in lipid metabolism with differential abundance

	ΔLVEF rest→stress (%)		*ΔCardiac index rest→stress (L/min/m²)*		*Stress Cardiac Index (L/min/m²)*	
	r	**p-value**	**r**	**p-value**	**r**	**p-value**
FABP – heart	-0.30	***0.006***	-0.40	***0.0002***	-0.47	***<0.0001***
FABP – adipocyte	-0.22	**0.046**	-0.39	**0.0003**	-0.44	***<0.0001***
Phytanyl-CoA dioxygenase	0.44	***<0.0001***	0.39	***0.0003***	0.31	***0.005***
Acyl-CoA binding protein	-0.18	0.11	-0.33	***0.003***	-0.30	***0.007***
Ceramide transporter	-0.21	0.06	-0.35	***0.001***	-0.26	***0.02***

3.5 Discussion

The main findings of this chapter are:

1. There is impairment in LV contractile and stroke volume exercise reserve in HFpEF. Despite similar baseline properties compared to controls, exercise stress unmasks these resulting in impaired cardiac output during exercise. In addition, there are abnormalities seen in lung function tests. There is however significant heterogeneity in exercise responses.
2. Dichotomising 2 groups based on LVEF into those with a normal or supranormal LVEF (>60%) and those with low-normal LVEF (<60%) delineates differences in resting morphology, variation in systolic contractile reserve, diastolic reserve and cardiac output at rest and exercise. The $HFpEF_{EF>60}$ group demonstrates greater functional impairment linked to lower cardiac output during exercise.
3. Exercise stress proteomics reveals perturbations in fatty acid metabolism as common to both endotypes of HFpEF. This is linked to impairments in contractile and cardiac output reserve during exercise. However, there are

also additional abnormalities in proteins linked to the extracellular matrix, mRNA processing and inflammation within the $HFpEF_{EF<60}$ group.

4. The overall cardiac energetic state as indicated by the PCr/ATP ratio is potentially impaired in both HFpEF cohorts, but is similar to that of controls of similar age.

There is impairment in contractile, stroke volume and cardiac output exercise reserve in HFpEF but with a great deal of heterogeneity

An initial comparison between patients with HFpEF as a whole compared to controls suggests similar biventricular volumes, overall systolic function as indicated by LV ejection fraction and cardiac output at rest on CMR. Subtle abnormalities in systolic function are seen as indicated by a trend towards lower biventricular longitudinal strain on CMR as well as by a lower LV S' and TAPSE on echocardiography. There is a greater degree of diastolic dysfunction indicating raised LV pressures in the HFpEF cohort on echocardiography. As would be expected, atria are enlarged in the HFpEF cohort given the diastolic dysfunction and high prevalence of atrial fibrillation.

Interestingly, the LV mass as measured on CMR was not different between the control and HFpEF cohorts. When measured by CMR, LV mass only weakly correlates with maximal wall thickness[222]. However, an increased LV mass: EDV ratio indicated concentric remodelling as did the increased relative wall thickness on echocardiography. The LV mass as calculated on echocardiography was increased, although this relies on linear measurements at the basal ventricle without taking into account the geometry or change in wall thickness in the mid-ventricular or apical segments and is less accurate compared to CMR[223]. This becomes more important with increasing basal septal thickness often as a consequence of hypertension. Other possibilities for this disparity includes the presence of hypertension albeit well controlled in a significant proportion of the control population which could result in morphological changes without manifesting heart failure.

During exercise, there is impaired diastolic compliance within HFpEF with an inability to expand the diastolic volume. This results in blunted systolic contractile reserve with the LVEF and LVSVi falling behind those of controls. Ultimately, this

results in impaired cardiac output during exercise which is linked to exercise intolerance and reduced functional capacity.

Similar impairments are seen with the right heart, although here it appears to be an inability to contract down to a lower RVESVi which appears to drive a blunted contractile reserve as indicated by a lower RVEF and RVSVi. There is also impaired RV-PA coupling as suggested by the RV SV/ESV ratio on CMR. A potential reason for the differences between the RV and the LV is that there may be a greater degree of volume load placed on the RV due to tricuspid regurgitation either as a consequence of increased pulmonary pressures or an expanding atrial annulus and this is often exacerbated during exercise. This could drive an increase in diastolic volume which overcomes any intrinsic stiffness. Given that a significant component of HFpEF is likely to be driven by systemic factors, there is likely intrinsic impairment in RV contractility in a manner similar to the LV in addition to decompensation in response to high pulmonary pressures.

When characterising lung function, there is a reduction in both FEV1 and FVC in HFpEF at rest and during stress, but without a change in FEV1/FVC ratio. It is likely that both obstructive and restrictive spirometric abnormalities which have been associated with HFpEF in other studies are present in individuals within the HFpEF cohort[65]. Participants with HFpEF were found to have impaired lung diffusing capacity (DLCO) at rest and during exercise and in previous studies this has been thought to be due to a combination of lower alveolar-capillary membrane conductance and pulmonary capillary blood volume[66-68]. Despite this impairment in gas exchange at rest, none of the HFpEF cohort were symptomatic at rest with nearly all of them well compensated enough to be in NYHA 2 with a smaller number in class 3. However, during exercise, in combination with impaired cardiac output, this is likely to contribute to exercise intolerance, symptoms and reduced functional capacity.

However, there was a significant degree of heterogeneity within the HFpEF cohort compared to the control group, both in terms of resting morphology but also in terms of contractile and cardiac output reserve as indicated by high coefficients of variation, particularly at stress. Unsupervised k-means clustering identified 2 groups as optimal to differentiate phenotypes of HFpEF based on key rest and

stress CMR and echocardiography parameters as well as important features such as the presence of atrial fibrillation, BMI and 6-minute walk test distance. These clusters essentially differentiated a group with smaller biventricular volumes, higher LVEF yet lower stroke volumes at rest with greater impairment in cardiac output reserve in comparison to a group with larger ventricular volumes and a low-normal or borderline reduced LVEF at rest. Given a number of clinical trials demonstrating differential responses to inhibition of the renin-angiotensin system and SGLT-2 transporters converging around the 60% mark for resting LVEF, dichotomising the groups at this point was felt to provide a comparison of clinically relevant endotypes of HFpEF with potentially different underlying biology and therapeutic targets. This also provided an opportunity to identify pathway alterations common to both, which could provide targets to treat both endotypes.

Comparison of $HFpEF_{EF>60}$ to $HFpEF_{EF<60}$ demonstrates differences in resting morphology, variation in systolic contractile reserve, diastolic reserve and cardiac output at rest and exercise associated with greater functional impairment

When comparing the $HFpEF_{EF>60}$ group to $HFpEF_{EF<60}$, this cohort of patients exhibit smaller biventricular volumes, mass and stroke volumes at rest despite higher LVEF and RVEF at rest. This group also had a greater magnitude of global LV longitudinal strain on CMR suggesting elevated contractility. There were no significant differences in diastolic function on echocardiography at rest.

During exercise, there was less contractile reserve within $HFpEF_{EF>60}$ i.e., there was an inability to increase the LVEF further primarily as a result of being unable to contract to a lower LVESVi. This means that in order to increase the stroke volume, diastolic compliance is key and there is a trend towards an increase in LVEDVi in this group which was not present in the $HFpEF_{EF<60}$ cohort. However, despite no differences in the increase in LVSVi or cardiac output during exercise, the smaller LVSVi at rest means that without a proportionally greater increase in LVSVi this group had a lower LVSVi at stress. Whilst this may have been adequate during quiescence, during exertion it proved insufficient resulting in greater functional impairment as indicated by the lower 6-minute walk test distance.

In contrast, there was a greater increase in E/E' in response to exercise in the $HFpEF_{EF<60}$ group, indicating that they may develop greater LV filling pressures during exercise, leaving them vulnerable to development of greater pulmonary congestion. Consistent with this, there was a greater increase in left and right atrial volumes as a surrogate measure of pressure in this group which could predispose to development of pulmonary oedema. Interestingly, the rest SBP and MAP were higher in this group, although these differences disappeared during exercise. In fact, there was a trend towards a greater increase in SBP in the $HFpEF_{EF>60}$ cohort (21 vs 14 mmHg) and given that LVEF is also influenced by LV-Aorta coupling, this could also contribute to diminished LVEF augmentation in this group in addition to a lack of intrinsic contractile reserve.

The use of an absolute cutoff of LVEF 60% does result in reduced sensitivity to detect for example an inability to augment cardiac output in the manner unsupervised machine learning was able to. However, at present this represents a more clinically translatable approach as a simple measure readily obtainable in most echocardiography laboratories to identify patients who could be enrolled in clinical trials or derive benefit from targeted therapies.

Exercise stress proteomics demonstrated deranged whole body fatty acid metabolism linked to impairments in contractile and cardiac output reserve during exercise, but with additional abnormalities in other pathways within the $HFpEF_{EF<60}$ group.

In order to understand the underlying biology of these potential endotypes of HFpEF and given differential exercise responses, plasma proteomics was performed on blood samples derived during exercise. An initial comparison between HFpEF and controls was performed. This revealed significant changes in extracellular matrix pathways, lipid metabolism as well as changes in inflammatory pathways, RNA processing, protein phosphorylation and IGF signalling pathways.

A direct comparison between the two HFpEF endotypes did not reveal significant differences in protein abundance suggesting there are significant commonalities between the two. However, a comparison to controls allowed a more sensitive analysis of how they differed from a healthy control proteome. In the $HFpEF_{EF>60}$

group, the majority of alterations in pathways were related to fatty acid metabolism. In the $HFpEF_{EF<60}$ cohort, while this was also a key pathway which was affected, there were a wider variety of pathways involved including extracellular matrix, RNA processing, inflammatory and signalling pathways. In a previous study using myocardial biopsies, there was greater extracellular volume expansion in HFpEF patients with an LVEF of 50-60%. This is consistent with these alterations in plasma extracellular proteins indicating this may link directly to the myocardium[90].

Given that lipid metabolism pathways were noted to be altered in both groups, a more detailed analysis of key individual proteins as identified on the Reactome database was undertaken. This demonstrated that the abundance of these 5 proteins (FABP – heart and adipocyte subtypes, phytanyl-CoA dioxygenase, ACBP, Ceramide transporter) was significantly different from controls in both endotypes of HFpEF without significant differences between them. Moreover, all of these were significantly related to exercise cardiac output reserve and the stress cardiac output. FABP – heart and adipocyte as well as phytanyl-CoA dioxygenase were also linked to exercise contractile reserve (ΔLVEF). This suggests that perturbation in whole body fatty acid metabolism is common to both endotypes of HFpEF and is related to key factors underlying exercise intolerance. Given that fatty acid oxidation would be expected to be the key contributor to cardiac metabolism in the fasting state during which plasma was acquired, then this points towards a potentially significant contribution of altered myocardial energetics to the impairment of cardiac reserve in HFpEF which warrants further study. Given the fact that the ability to increase cardiac output during stress is key to overall functional capacity as demonstrated in this chapter, this presents a promising target in the pursuit of improving symptoms within HFpEF.

The overall cardiac energetic state as indicated by the PCr/ATP ratio is potentially impaired in both HFpEF cohorts, but is similar to that of controls of similar age with similarly increased myocardial triglyceride content

Compared to published normal values in literature of young adults of approximately 2, the PCr/ATP ratios of both HFpEF endotypes are low. But unexpectedly, it was also low in healthy controls with a mean age of 71.9. There

was no significant difference in myocardial triglyceride content between controls and HFpEF nor between the endotypes although this was increased compared to literature values in young healthy controls[224]. It has been demonstrated previously that in male hearts, there is a physiological increase in myocardial lipid content as measured by proton spectroscopy with ageing which in turn was associated with a decline in diastolic function[225]. This has been corroborated in mixed cohorts of males and females and this may provide an explanation for the similar values within the HFpEF and control cohorts[226].

3.6 Limitations

The participants with HFpEF were recruited on the basis of a clinical diagnosis. Whether they would meet strict invasive criteria for HFpEF is not known as right or left heart catheterisation was not performed. However, based on the ESC HFA-PEFF score, they all had scores of 4-6 indicating either high intermediate probability of or confirmed HFpEF status. The study also does not include patients with relatively low HFA-PEFF scores who may have met thresholds on invasive exercise testing such as might occur in some patients with obesity. Whilst strictly the control group was not age-matched, a mean difference of 5 years in the context of both groups having a mean age in the 70s allows for a valid comparison of cardiac structure and function with reference to healthy ageing.

All patients were able to complete the exercise protocol at a sub-maximal steady state workload of 35W. However, given the greater preponderance of women in the $HFpEF_{EF>60}$ group and the lower maximal power output for women compared to men, this may have represented a greater relative workload. This could result in greater stress on the cardiovascular reserve and influence the results[227].

Plasma samples may not represent pathophysiology within the heart as demonstrated in multiple proteomic studies. However, myocardial samples from patients with HFpEF are not easily available given limited indications for biopsy and is open to sampling bias as the most common indication for biopsy is to evaluate for cardiac amyloidosis[228]. Even when negative for amyloidosis, this could bias towards specific phenotypes of HFpEF. In addition, there are several advantages to using plasma samples for proteomics. Firstly, plasma proteomics

provides great advantages in non-invasiveness and reproducibility, thus providing opportunities to identify and characterise potential disease biomarkers for diagnosis and prognostication[229]. Even more so than HFrEF, HFpEF has a greater systemic component and peripheral factors both contribute to the development of myocardial dysfunction in the heart (inflammation and fibrosis), but also to impaired oxygen extraction and utilisation leading to exercise intolerance.

Proteomics at rest was not analysed within this study. Understanding the change from the baseline state will allow further characterisation of dynamic alterations in the proteome between HFpEF endotypes. Furthermore, part of the difference in proteome between the HFpEF endotypes and controls could be related to differences in comorbidities, the subtle difference in age and medication.

Another potential limitation is that the study cohort was composed of primarily Caucasian individuals of European descent. Proteomic signatures may vary with different ethnic origins and there may be differences in the plasma proteome of individuals of other ethnicities with HFpEF[230].

Quantification of the proteome only allows recognition of proteins and pathways which are altered in some way. How this differential abundance occurs cannot be directly inferred and is likely to represent either increased expression, secretion or release due to tissue damage, impaired clearance or a combination of these. However, they provide potential targets of interest to further interrogate.

3.7 Conclusions

Based on the data from this study, whilst CMR at rest was unable to differentiate between HFpEF and control physiology, exercise CMR revealed abnormalities in contractile, stroke volume and cardiac reserve in ambulatory HFpEF in conjunction with reproduction of symptoms. Exercise plasma proteomics demonstrated a markedly different systemic molecular milieu in HFpEF characterised by alterations in extracellular matrix, lipid metabolism, growth factor signalling, mRNA processing and inflammatory pathways.

However, marked heterogeneity was noted within the HFpEF cohort with 2 groups identified by unsupervised machine learning with differing morphology and LVEF. Based on this, further analysis was performed by dichotomising HFpEF groups into those with LVEF greater or less than 60% at rest. The $HFpEF_{EF>60}$ group demonstrated smaller biventricular volumes in addition to a higher LVEF. Despite this, stroke volume at rest and during exercise were lower with diminished exercise cardiac output. They experienced greater functional impairment as evidenced by a reduced 6MWT distance. Both groups demonstrated changes in lipid metabolism compared to controls on plasma proteomic analyses, yet this was the major change in the $HFpEF_{EF>60}$ cohort while the $HFpEF_{EF<60}$ group had additional changes relating to the extracellular matrix, inflammation and mRNA processing. This highlights the importance of understanding myocardial metabolism and energetics in HFpEF with both endotypes likely exhibiting alterations based on these results. Prior studies have only partially characterised cardiac energetics in HFpEF with no assessment of ATP delivery having been performed and I aim to rectify this in the next chapter.

CHAPTER 4: CREATINE KINASE FLUX AND MYOCARDIAL ENERGETICS IN HFpEF

ABSTRACT

Background

Multiple studies have demonstrated impaired overall cardiac energetics in HFpEF as assessed by phosphorus spectroscopy. But as demonstrated in chapter 3, the PCr/ATP ratio can be impaired in healthy ageing alone to a similar extent. However, dynamic cardiac energetics is incompletely characterised in HFpEF. Specifically, there have been no studies assessing creatine kinase kinetics or flux in HFpEF in comparison to a healthy ageing heart. Given that delivery of ATP is key to both diastolic and systolic function, here I aim to characterise this using phosphorus spectroscopy and saturation transfer techniques.

Methods

Twenty five participants with HFpEF and eight controls underwent a protocol encompassing magnetic resonance and echocardiography during rest and exercise. ^{31}P phosphorus spectroscopy was used to measure PCr/ATP ratio at rest and creatine kinase kinetics was measured using triple repetition saturation transfer. A similar protocol to that in chapter 3 was employed using real-time CMR imaging to assess whole-heart volumes and function at rest and during exercise in addition to echocardiography.

Results

Creatine kinase flux, but not the forward rate constant (k_f) was reduced in HFpEF in comparison to healthy controls despite a similar PCr/ATP ratio. Across the study population, CK flux was associated with LVEF, LV and RV longitudinal strain as well as LV S' and TAPSE on echocardiography at rest. CK k_f was associated with LVEF, biventricular longitudinal strain and LV S' at rest. In addition, resting CK flux was associated with LVEF, RVEF, LV S' and TAPSE during exercise and there was a relationship with exercise-induced change in cardiac index which was not statistically significant. CK k_f at rest was associated with cardiac index during exercise and LVEF.

Conclusions

Despite similar PCr/ATP ratios, dynamic cardiac energetics as assessed by CK flux is impaired in HFpEF compared to age-matched controls. CK flux and kinetics at rest are related to a number of parameters of overall systolic and longitudinal function at both rest and during exercise in addition to overall cardiac output during exercise. This raises the possibility of targeting cardiac metabolism in order to improve ATP delivery through the CK system as a means to improve systolic reserve and diastolic function in HFpEF.

4.1 Introduction

As demonstrated in chapter 3, there are whole-body level alterations in metabolism in HFpEF suggesting that cardiac energetics is also likely to be altered. In common with other myocardial diseases such as dilated cardiomyopathy, hypertrophic cardiomyopathy and ischaemic cardiomyopathy, myocardial energetics as measured by PCr/ATP has been shown to be impaired in HFpEF and has been linked to diastolic function[133]. Despite this, in chapter 3 I have demonstrated that when comparison is made to older healthy controls, the PCr/ATP ratio is not different between controls and HFpEF, but is equally low. This indicates an impaired energetic reserve despite the presence of a preserved LVEF overall in disease and healthy ageing - an unexpected finding. But this ratio only provides a snapshot assessment of the relative concentrations of the two metabolites.

Turnover of ATP through the CK system could give us a better understanding of myocardial energetic change in HFpEF including the balance between production, delivery and utilisation as it incorporates both metabolite concentrations and enzymatic activity. Given that diastole is susceptible to an energetic deficit and SERCA requires the greatest energy of hydrolysis, this requires further study to ascertain whether there is a deficit in ATP delivery by the CK system or whether there is inefficiency of use.

To date, no studies have addressed the measurement of CK flux within HFpEF. Comorbidities which contribute to the development have been studied in more detail, but do not provide a clear idea as to what may occur in HFpEF. In hypertensive LVH, flux through the CK system is impaired, particularly in the presence of heart failure[143]. In contrast, obesity results in an elevated k_f which in turn results in similar ATP delivery to controls at rest despite a lower PCr/ATP ratio[152].

In order to provide a more useful comparison, controls of similar age were recruited as it has been shown that healthy controls demonstrate lower PCr/ATP ratios with increasing age as seen in Chapter 3[231,232].

In this chapter, I aim to study the characteristics of flux within the creatine kinase system in HFpEF and to determine associations with systolic or diastolic

abnormalities at rest. If CK delivery is impaired at rest, then it stands to reason that it is also likely to remain impaired during exercise and therefore an exploratory analysis of associations of the rest CK characteristics with stress parameters are also performed.

4.2 Methods

Eight healthy volunteers and twenty-five participants with HFpEF were recruited and underwent ^{31}P MR spectroscopy, ^{1}H proton spectroscopy and rest and exercise stress CMR. These patients were generally also co-recruited to either the studies in Chapter 3 or 5. Inclusion and exclusion criteria for participants with HFpEF and controls were as described in Chapter 3. PCr/ATP ratio was measured using a 3D CSI technique while CK kinetics was assessed using TRiST. CK flux was calculated as k_f x [PCr]. [PCr] values are derived from the PCr/ATP ratio as biopsy derived values for [ATP] are available. In order to maintain consistency with previously published assessments of CK flux, literature values for [ATP] were taken to be 5.7 μmol/g/wet weight for controls and 5.2 μmol/g/wet weight for heart failure patients[125]. While the heart failure value was originally derived from patients with HFrEF, a study of direct measurement has demonstrated [ATP] in diastolic dysfunction with preserved ejection fraction to be at least as low as DCM[141] and NMR measurement of [ATP] to be ~5.0 μmol/g in patients with LVH and heart failure, regardless of preserved or low ejection fraction.

^{1}H proton spectroscopy was performed using water-suppression cycling. Real-time rest short axis imaging was performed and repeated during ergometer exercise stress at 35W after 5 minutes. Volumes were indexed to take into account differences in body surface area. They also underwent rest and stress echocardiography to assess diastolic function.

Due to the non-parametric nature of the k_f and CK flux data, correlation was performed using the Spearman rank correlation test. Graphs have been plotted with linear regression lines to show the direction of effect.

4.3 Results

4.3.1 Baseline characteristics

Both HFpEF and control cohorts were age-matched with no significant differences in sex distribution. BMI and waist circumference were elevated in the HFpEF cohort as was the prevalence of AF, hypertension and diabetes. NT-proBNP was higher in the HFpEF cohort whereas there was no difference in blood pressure at rest.

The full spectrum of measured CMR and echocardiographic parameters will not be described further within the body of the chapter as this has been characterised in larger cohorts in Chapter 3 and broadly replicate the results presented there. Detailed tables are presented in the appendix.

Table 35: Baseline characteristics

	Control (n=8)	*HFpEF (n=25)*	*p-value*
Age (years)	73.8 ± 6.6	76.5 ± 5.3	0.23
Male – no. (%)	4 (50%)	18 (72%)	0.25
BMI (kg/m^2)	25.0 ± 3.3	31.1 ± 6.4	***0.01***
Waist circumference (cm)	90.9 ± 13.1	111.4 ± 14.8	***0.002***
SBP (mmHg)	139.3 ± 21.0	141.0 ± 20.8	0.84
DBP (mmHg)	74.8 ± 8.5	77.3 ± 18.9	0.72
MAP (mmHg)	96.2 ± 10.9	98.5 ± 16.2	0.71
Atrial fibrillation – no. (%)	0 (0%)	19 (76%)	***0.0002***
Hypertension - no. (%)	3 (37.5)	20 (80%)	***0.03***
Diabetes - no. (%)	0 (0%)	6 (24%)	0.13
NT-proBNP (ng/L)	200 ± 121	1159 ± 1193	***0.0002***

4.3.2 Myocardial energetics

As in Chapter 3, the PCr/ATP ratio was not different between the HFpEF cohort and the age-matched controls. Similarly, the CK forward rate constant was not different between the groups. However, there was a reduction in CK flux in the HFpEF cohort relative to controls despite this (1.99 ± 1.34 vs 3.40 ± 2.13 μmol/g/s, p=0.047). This correlated with increasing NT-proBNP levels (ϱ= -0.39, p=0.046).

Within the HFpEF cohort only, there was a significant inverse relationship of age with k_f (ϱ= -0.41, p=0.047) and CK flux (ϱ= -0.50, p=0.03). Whilst there was a numerical trend towards increasing CK flux with increasing BMI (ϱ=0.40, p = 0.07), there was no relationship with k_f.

Table 36: Myocardial energetics and creatine kinase kinetics at rest - Control vs HFpEF

	Control	*HFpEF*	*p-value*
PCr/ATP ratio	1.47 ± 0.35	1.41 ± 0.25	0.60
k_f (s^{-1})	0.40 ± 0.21	0.37 ± 0.29	0.45
CK flux (μmol/g/s)	3.40 ± 2.13	1.99 ± 1.34	***0.047***

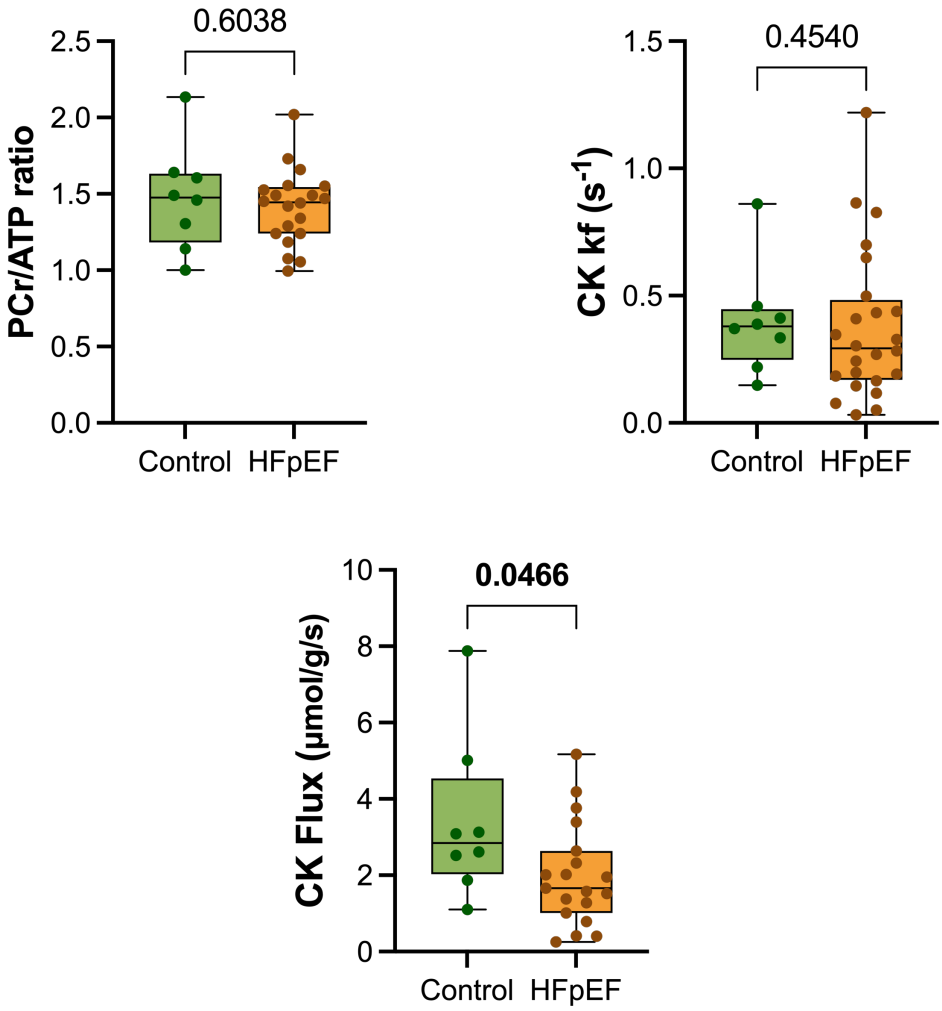

Figure 51: Myocardial energetics, CK kinetics and flux at rest

Table 37: Correlation of k_f and CK flux with key baseline variables within HFpEF only

	k_f		*CK flux*	
	ϱ	**p-value**	**ϱ**	**p-value**
Age	-0.41	***0.047***	-0.50	***0.03***
BMI	0.15	0.49	0.40	0.07

4.3.3 Correlation of CK flux and k_f with LV and RV function at rest

Across HFpEF and control cohorts, there was a significant relationship of CK flux with LVEF at rest (ϱ=0.40, p=0.04) driven by a correlation with k_f (ϱ=0.42, p=0.02). There was also a positive correlation between CK flux and longitudinal LV GLS (ϱ=0.49, p=0.009) again due to a relationship with k_f (ϱ=0.48, p=0.005). This was corroborated on echocardiography (LV S' vs CK flux ϱ=0.49, p=0.01). There was no significant correlation with diastolic function on echocardiography (E/E' vs CK flux, p=0.25).

In a similar manner to LV longitudinal function, RV longitudinal strain was related to CK flux (ϱ=0.44, p=0.02). Again, this was corroborated on echocardiography (TAPSE vs CK flux ϱ=0.40, p=0.04). There was no significant relationship with RVEF at rest however.

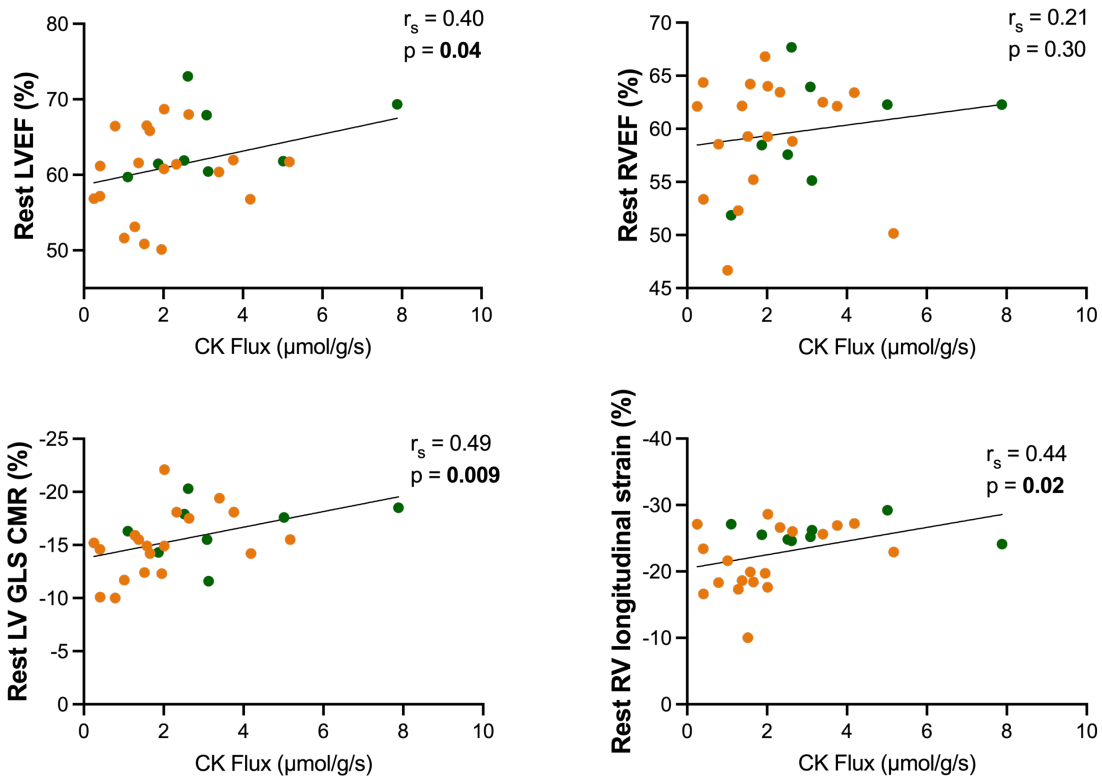

Figure 52: Correlation of creatine kinase flux at rest with resting systolic function parameters on CMR

Green dots indicate controls and orange dots indicate patients with HFpEF

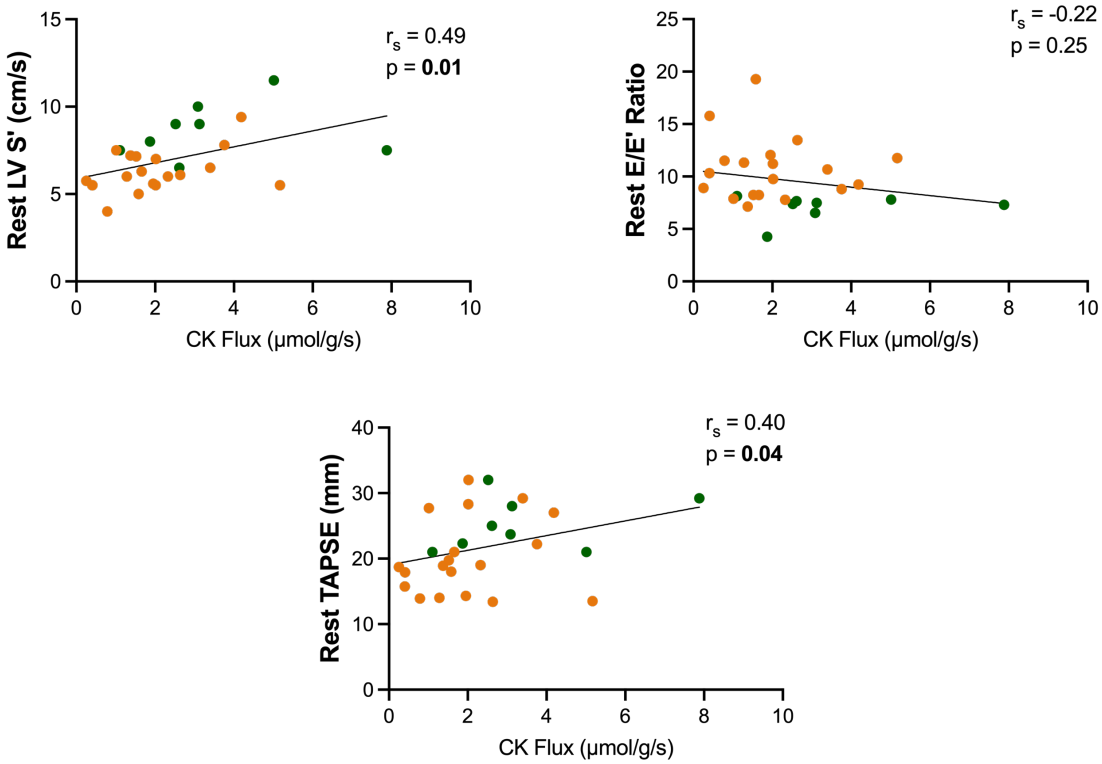

Figure 53: Correlation of CK flux at rest with resting biventricular longitudinal systolic and LV diastolic function on echocardiography

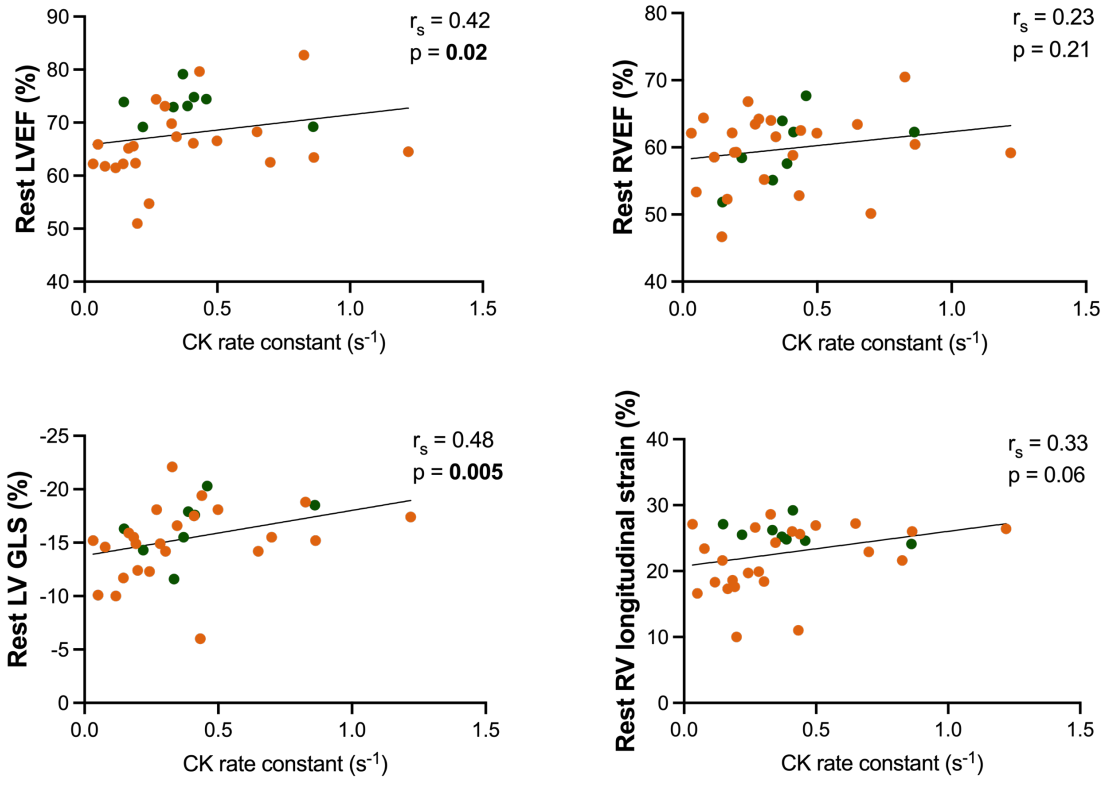

Figure 54: Correlation of creatine kinase forward rate constant at rest with resting systolic function parameters on CMR

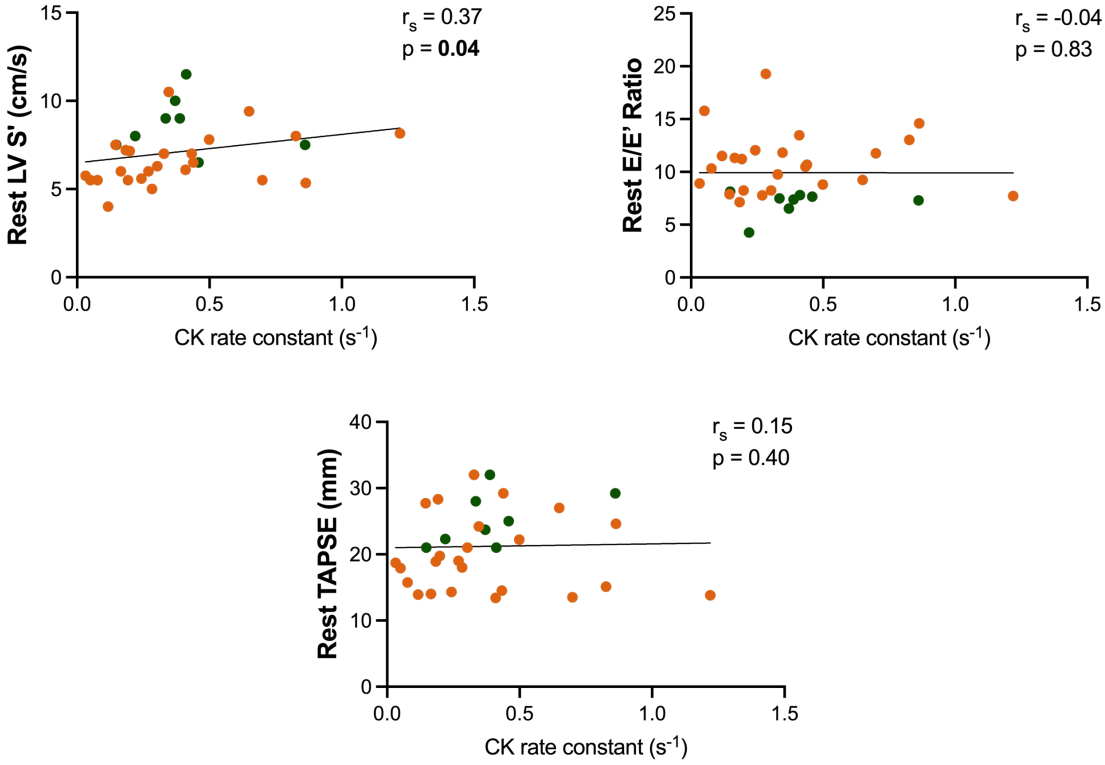

Figure 55: Correlation of creatine kinase forward rate constant at rest with resting biventricular longitudinal systolic and LV diastolic function on echocardiography

Table 38: Associations of k_f and flux at rest with biventricular systolic and diastolic function at rest on CMR and echocardiography – HFpEF and control

	k_f		*CK flux*	
	ϱ	**p-value**	ϱ	**p-value**
LVEF - CMR	0.42	***0.02***	0.40	***0.04***
LV GLS - CMR *(-%)*	0.48	***0.005***	0.49	***0.009***
LV S' – Echo	0.37	***0.04***	0.49	***0.01***
LV E/E' – Echo	-0.04	0.83	-0.23	0.25
RVEF – CMR	0.23	0.21	0.21	0.30
RV Longitudinal strain - CMR (-%)	0.33	0.06	0.44	***0.02***
TAPSE – Echo	0.15	0.40	0.40	***0.04***
Cardiac index - CMR	0.08	0.67	-0.17	0.40
NT-pro BNP	-0.20	0.28	-0.39	***0.046***

4.3.4 Association of CK flux and forward rate constant at rest with LV and RV function during exercise

Similarly to the above, stress LVEF was related to k_f (ϱ=0.43, p=0.02) and CK flux (ϱ=0.51, p=0.009) acquired at rest. On echocardiography, there was a significant correlation of LV S' with CK flux (ϱ=0.41, p=0.03) but not with k_f. There was no relationship of either with LV E/E'. Stress RVEF (ϱ=0.46, p=0.02) and TAPSE (ϱ=0.40, p=0.04) were also related to CK flux but not k_f.

Whilst CK flux was not related to cardiac output during exercise, k_f was (ϱ=0.38, p=0.04). There was a statistically non-significant relationship of both k_f (ϱ=0.38, p=0.05) and CK flux (ϱ=0.40, p=0.05) with exercise-related augmentation of cardiac output. This may partly be related to a relationship with the peak heart rate achieved. CK flux was also related to exercise-related increase in RVSVi (ϱ=0.42, p=0.04).

Table 39: Associations of CK forward rate constant and flux at rest with biventricular systolic and diastolic function during exercise on CMR and echocardiography – HFpEF and control

	k_f		*CK flux*	
	ϱ	p-value	ϱ	p-value
LVEF - CMR	0.43	***0.02***	0.51	***0.009***
LV S′ – Echo	0.22	0.23	0.41	***0.03***
LV E/E′ – Echo	-0.09	0.62	-0.15	0.47
RVEF – CMR	0.29	0.12	0.46	***0.02***
TAPSE – Echo	0.14	0.46	0.40	***0.04***
Cardiac index - CMR	0.38	***0.04***	0.32	0.12
ΔCardiac index	0.38	0.05	0.40	0.05
Peak heart rate	0.36	0.05	0.37	0.07
Stress LVSVi	0.18	0.34	0.08	0.70
ΔLVSVi	0.13	0.48	0.27	0.19
ΔRVSVi	0.24	0.21	0.42	***0.04***

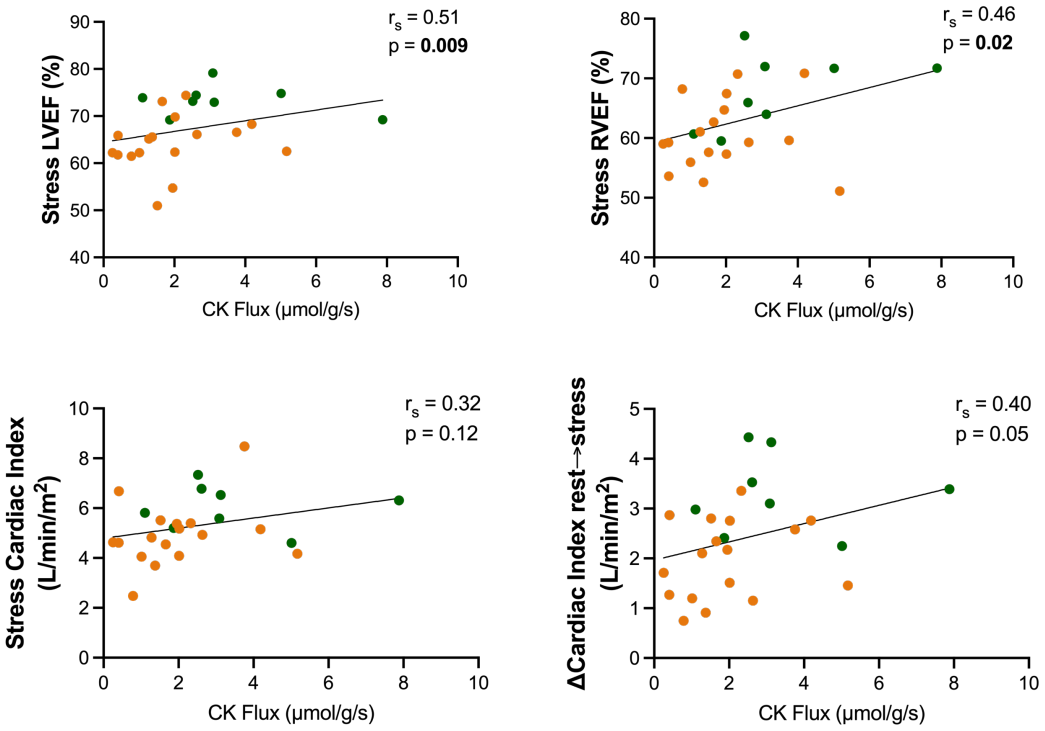

Figure 56: Correlation of creatine kinase flux at rest with systolic function parameters during exercise on CMR

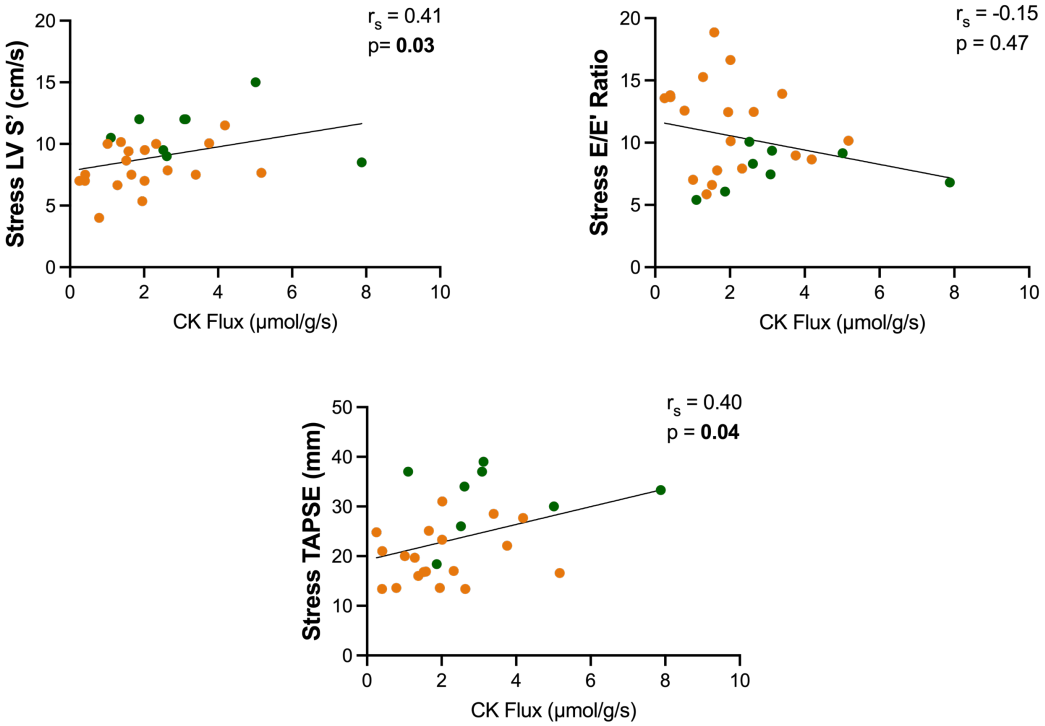

Figure 57: Correlation of CK flux at rest with longitudinal systolic and diastolic function during exercise on echocardiography

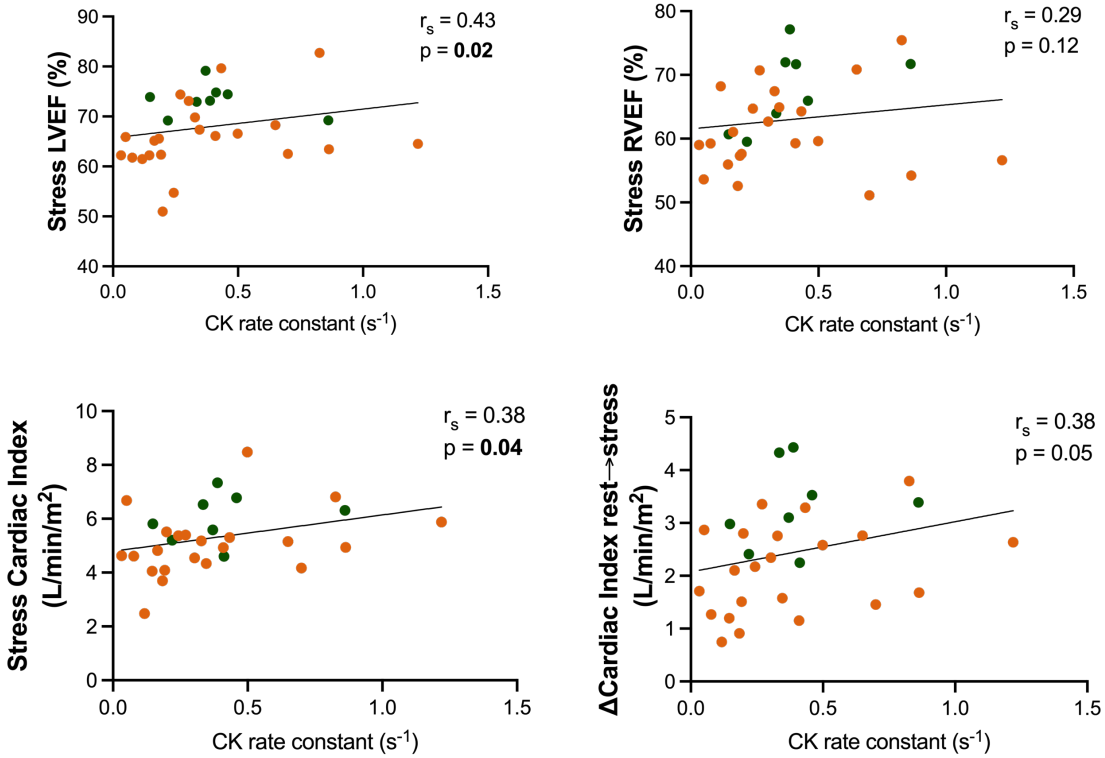

Figure 58: Correlation of CK forward rate constant at rest with systolic function parameters during exercise on CMR

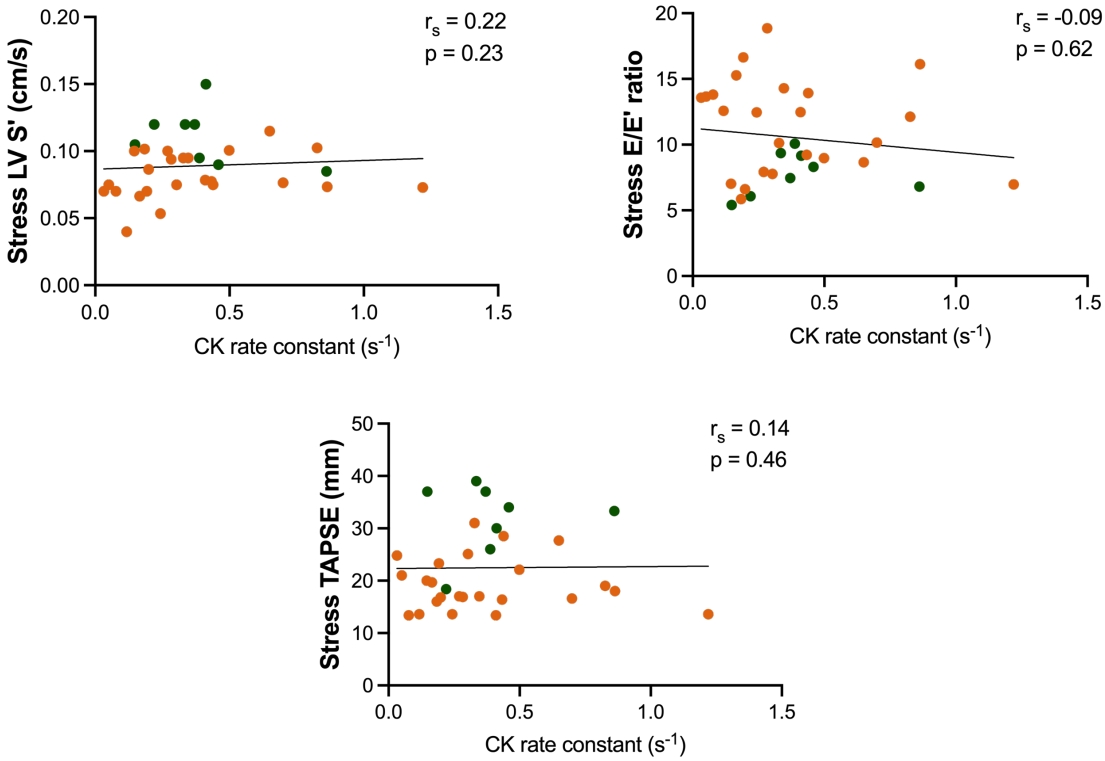

Figure 59: Correlation of CK forward rate constant at rest with systolic and diastolic function during exercise on echocardiography

4.3.5 Association of CK flux and k_f at rest with changes in atrial volumes during exercise within the HFpEF cohort only

Both CK flux (ϱ =-0.65, p=0.005) and k_f (ϱ =-0.65, p=0.001) exhibited significant negative correlations with absolute change in left atrial volumes (measured in ml/m^2) within the HFpEF cohort. This extended to proportional change (measured in %) relative to baseline left atrial volume (CK flux ϱ =-0.52, p=0.04, k_f ϱ =-0.52, p=0.01). There were no statistically significant correlations with changes in right atrial volume, although there was a notable trend in the relationship of CK flux with absolute change in right atrial volumes (ϱ =-0.46, p=0.07).

Table 40: Correlation of creatine kinase flux and k_f at rest with changes in atrial volumes during exercise within the HFpEF cohort only

	k_f		***CK flux***	
	ϱ	**p-value**	**ϱ**	**p-value**
Absolute change in indexed LA volume rest→stress	-0.65	***0.001***	-0.65	***0.005***
Proportional change in LA volume rest→stress	-0.52	***0.01***	-0.52	***0.04***
Absolute change in indexed RA volume rest→stress	-0.19	0.39	-0.46	0.07
Proportional change in RA volume rest→stress	-0.22	0.32	-0.31	0.23

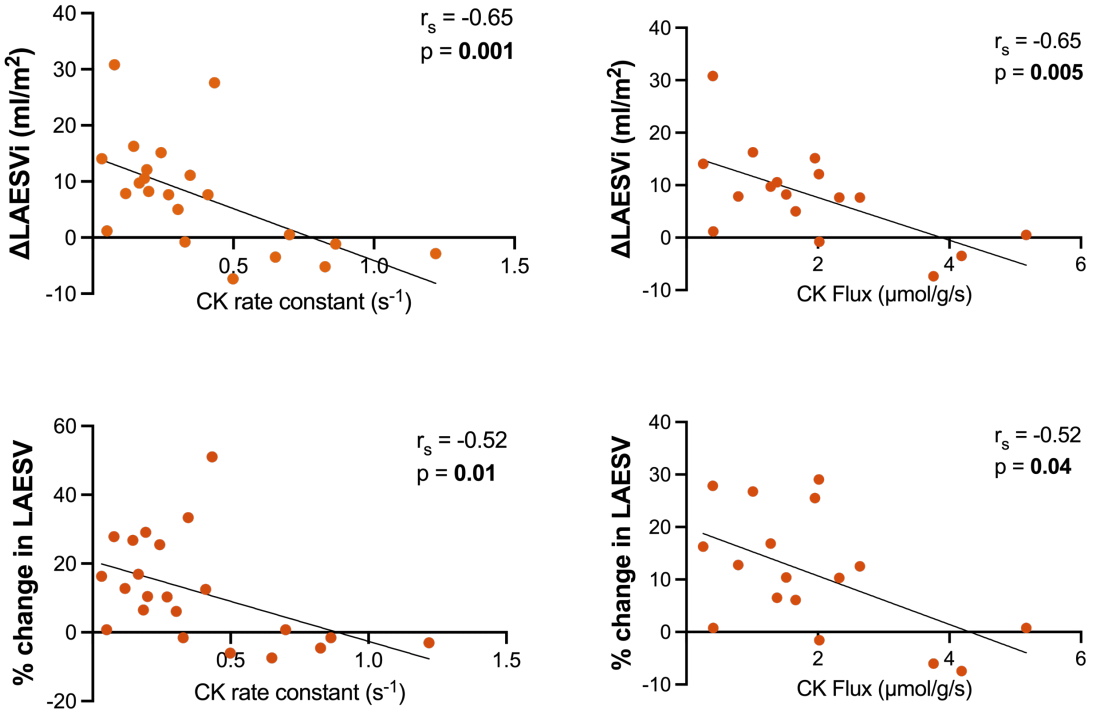

Figure 60: Correlation of creatine kinase flux and k_f at rest with changes in left atrial volumes during exercise within the HFpEF cohort only

4.4 Discussion

The findings of this chapter can be summarised as follows:

1. Despite similar PCr/ATP ratios to age-matched controls, there is an impairment in ATP delivery as measured by CK flux in HFpEF.
2. The CK flux and CK forward rate constant at rest is related to overall LV function at rest and biventricular longitudinal function as well as NT-pro BNP, but not conventional diastolic function measures on echocardiography.
3. CK flux at rest is linked to biventricular systolic function during stress and may influence the ability to augment cardiac output during exercise.
4. Within HFpEF, the CK forward rate constant and CK flux fell with increasing age whilst a reduction in these parameters was associated with an increase in left atrial volumes during exercise.
5. There is a trend towards an increase in CK flux as the BMI increases within HFpEF

ATP delivery is impaired in HFpEF

The first key finding was that CK flux was lower in HFpEF compared to age-matched controls. That neither PCr/ATP nor k_f was significantly different between the groups suggests that on an individual level one or the other is likely contributory to diminished CK flux within HFpEF. This may reflect the heterogeneity of the patient cohort as well as HFpEF in general. But the final common pathway of development of heart failure even with preserved ejection fraction seems to relate to a deficiency in overall ATP delivery to key enzymes consistent with the energetic hypothesis of heart failure[233].

CK flux and CK forward rate constant at rest is linked to systolic function at rest

Across the HFpEF and control cohorts, both overall and longitudinal LV systolic function were strongly linked to the CK forward rate constant and CK flux. A fall in CK k_f or flux correlated with a decrease in LVEF. This is consistent with prior studies in HFrEF, suggesting this link is maintained even in HFpEF where some patients exhibit borderline low LVEF[153]. Additionally, a reduction in these parameters were also linked to a decrease in both LV and RV longitudinal function on CMR and echocardiography. Longitudinal LV dysfunction is a well-recognised feature of HFpEF and reflects subtle systolic dysfunction not captured by measuring LVEF[14]. Thus, if the impairment in the ATP delivery pathway were to be potentially contributory to these defects, this could reflect either insufficient substrate delivery, utilisation or impaired oxygenation. The longitudinally oriented subendocardial fibres are most susceptible to early ischaemia. Microvascular dysfunction in HFpEF has been linked to impaired global longitudinal strain and could be contributory to the reduction in overall ATP delivery[56].

CK parameters were not linked to diastolic function on echocardiography, but were linked to left atrial volume expansion during exercise

Whilst longitudinal function was associated with ATP delivery, this was not the case for conventional diastolic echocardiography parameters at rest. This may be partly explained by the relatively insensitive techniques used to measure diastolic function non-invasively, particularly with comparatively small numbers of participants. Whilst E/E' is the most readily available non-invasive measure of LV filling pressures, it has poor sensitivity in detecting high LV pressures when

comparing different individuals although it has been demonstrated to be more effective in detecting intra-individual changes following intervention[234-236]. Despite this, it is likely that ATP delivery affects diastolic function. LV GLS determined using the same feature-tracking technique on CMR is strongly correlated with the invasively derived measure of LV relaxation Tau[237]. Given the impairment in GLS, it remains possible that diastolic function is impaired in a manner linked to CK flux, but not captured in this study.

In support of this, within HFpEF a reduction in CK k_f or flux was strongly linked to a rise in left atrial volumes during exercise which in turn may reflect a rise in LA pressures. While the measured CK flux relates primarily to the ventricular myocardium, pressures in the ventricle will necessarily influence that in the atria to provide a forward gradient across the atrio-ventricular valve. In addition, CK flux is inversely related to NT-proBNP which is secreted in increasing quantities with rising myocardial wall stress and LV filling pressures[238].

CK flux at rest remains linked to systolic function during stress and may influence the ability to augment cardiac output during exercise

If ATP delivery is impaired at rest, it appears likely that it remains impaired during exercise with a depleted reserve. Whilst this study did not directly assess CK kinetics during exercise, rest CK flux remained highly correlated with biventricular EF and longitudinal function during exercise. In the case of the CK k_f, exercise LVEF and overall stress cardiac output were strongly correlated. Both CK k_f and CK flux demonstrated correlations with the ability to increase cardiac output but narrowly did not meet statistical significance (both $p=0.05$). Intriguingly, there were also correlations with peak heart rate. This suggests that ATP delivery and CK kinetics is likely to play a significant overall role in systolic cardiac reserve as well as chronotropic reserve within HFpEF.

Creatine kinase kinetics is progressively impaired with increasing age within HFpEF

Despite a relatively narrow age range within the HFpEF cohort (65-89, 21/25 participants within the age range 71-82), there is a significant negative correlation of age with both the CK forward rate constant and CK flux. This is likely to

represent a contribution of ageing towards changing metabolism and an impaired energetic state which predisposes to heart failure.

There is a trend towards an increase in CK flux as the BMI increases within HFpEF

As noted in previous studies of HFrEF, there was a trend towards an increase in CK flux with BMI within HFpEF which could reflect a change in the relative efficiency of ATP use, but requires further evaluation[153]. Whether a change in adiposity through weight-loss measures results in a change in CK kinetics within HFpEF warrants further study.

4.5 Limitations

All energetic assessments were performed at rest. Due to the lengthy nature of the MR protocol lasting approximately 150 minutes, it was not feasible to perform additional stress assessments of CK flux whilst in the scanner on this relatively frail cohort within a study visit. However, given that many abnormalities in HFpEF physiology are unmasked during exercise, assessments of CK kinetics during stress may reveal additional abnormalities and could support an argument for causality in exercise related impairments in cardiac reserve. At present however, such assessment can only be performed during pharmacological stress using dobutamine with additional sequences such as StreST. Given that this does not accurately replicate the afterload and preload abnormalities in HFpEF, this may not accurately represent the work done by the HFpEF heart during exercise.

The primary measure of diastolic function in this study was the conventional echocardiographic measure of E/E'. Given the limited utility of E/E' in distinguishing diastolic function in a relatively small cohort, invasive measurements of PCWP or the end-diastolic pressure volume relationship through right and left heart catheterisation is likely to be beneficial in investigating the effects of CK flux on LV relaxation.

While a correlation between CK flux and a number of metrics have been demonstrated here, causality cannot be demonstrated. A number of pre-clinical

studies as described in Chapter 1 have demonstrated that altering CK flux directly affects systolic and diastolic properties of the heart. To demonstrate this in a clinical setting, studies using agents capable of altering CK flux without directly affecting cardiovascular haemodynamics would be beneficial.

In this study, the conventional literature values for ATP content have been used for heart failure and control populations. There are a few considerations to be taken into account here as there is limited data on ATP content specifically in older healthy individuals or in heart failure with preserved ejection fraction. ATP content of hearts has been demonstrated to be slightly lower with increasing age[239]. However, disease states result in progressive decline in myocardial ATP content with restrictive cardiomyopathy measured to have levels almost half of that of DCM[141]. Even if one were to assume that ATP content was similar in both cohorts, there is a strong trend towards the product of PCr/ATP x k_f being lower in those with HFpEF (p=0.08, see appendix).

4.6 Conclusions

This study demonstrates that despite a similar PCr/ATP ratio at rest, myocardial energetics in HFpEF is impaired compared to healthy age-matched controls as evidenced by reduced CK flux. CK k_f and flux at rest were linked to impairment of cardiac function at rest and during exercise, stress cardiac output and wall stress as indicated by NT-proBNP. This suggests that energetic deficits are likely to be intrinsically linked to the pathophysiology of HFpEF. Manipulation of substrate metabolism to mitigate this therefore represents a potential therapeutic target.

CHAPTER 5: SUBSTRATE SELECTION IN HEART FAILURE WITH PRESERVED EJECTION FRACTION

ABSTRACT

Background

Despite impairments in cardiac metabolism having been demonstrated in HFpEF, overall substrate utilisation is poorly characterised. Given the metabolic co-morbidity burden within HFpEF it is likely that there are alterations in both fatty acid metabolism and glucose utilisation. Whether increasing supply and potentially metabolism of substrates such as glucose, long chain fatty acids or ketone bodies impacts cardiac energetics and function has not been previously studied.

Methods

Twenty four participants with HFpEF were randomised to receive either intralipid infusion, a hyperinsulinaemic-euglycaemic clamp or oral ketone ester. They underwent an identical CMR protocol to chapter 4 with cardiac energetics being assessed by phosphorus spectroscopy with whole-heart function and volumes measured during rest and stress by exercise CMR and echocardiography. 7 participants within the insulin-glucose group and 4 within the intralipid group took part in an additional visit where they underwent administration of the index infusion in addition to oral ketone ester to study the effects of mixed substrate augmentation.

Results

Infusion of intralipid did not lead to any appreciable change in systolic function or cardiac output during rest or exercise despite increasing cardiac work. However, it resulted in impairment of CK flux and the PCr/ATP ratio. Insulin-glucose infusion did not result in any change to LV function or energetics. Ketone ester administration resulted in an increase in LVSV, heart rate and cardiac output at rest whilst reducing MAP and right atrial volume. Similar trends of an increase in LVSV and cardiac index during exercise were seen during ketonaemia with a reduction in both RAEDV and LAEDV as well as an improvement in E/E'. There was a trend towards increased CK flux, but with no change in PCr/ATP at rest. In the mixed

ketone ester administration experiments, the overall pattern of improvement in cardiac index was maintained, although as the study was underpowered, few of the endpoints met statistical significance.

Conclusions

There is a difference in cardiac energetics, CK flux as well as systolic and diastolic function depending on provision of the different primary cardiac substrates to stimulate uptake and utilisation. Lipid administration results in an impairment in cardiac energetics without great change in systolic or diastolic function and insulin-glucose has limited effects overall. Administration of ketone ester resulted in improvement in contractility, cardiac output, systolic and diastolic function along with a potential reduction in preload and afterload. However, despite this increased cardiac work, myocardial energetics and ATP delivery was preserved. Similar functional effects were seen during co-administration of the other substrates with ketone. The mechanism by which they exert their effects warrant further study. The results overall demonstrate a fundamental difference in the cardiac energetic state and potentially function within HFpEF depending on the dominance of substrate supply.

5.1 Introduction

Given that deficits in cardiac energy status have been demonstrated in HFpEF as well as the key aetiological contributors including diabetes, obesity, hypertensive LVH and advanced age, it stands to reason that addressing this could provide a new therapeutic avenue. Chapter 4 also demonstrates a novel finding of impaired creatine kinase flux in HFpEF and ATP delivery is therefore a potential therapeutic target in HFpEF. Moreover, the changes in whole-body lipid metabolism within HFpEF seen in Chapter 3 suggests that substrate utilisation merits further study, particularly given the potential link to functional capacity.

There are numerous unanswered questions regarding the heart's ability to flexibly use substrate commensurate with availability or the optimal substrate in HFpEF which improves cardiac energetics and function. In addition, given symptoms only occur during exercise in a significant proportion of patients and the high prevalence of microvascular dysfunction, this may vary at rest and stress. If the heart is oxygen starved, particularly during exercise this may favour glucose oxidation. However, if this were not the case and the heart is starved of substrate and not oxygen, given the greater ATP production per mole fatty acid oxidation is well placed to provide supply to the ATPases responsible for contraction and relaxation. In a scenario where ATP production and delivery is already at maximal capacity and insulin resistance poses a limit to glucose uptake and oxidation, then bypassing this through ketone bodies which retain a favourable P:O ratio could be beneficial.

It has previously been shown in HFrEF that altering supply of different substrates in the form of either an intralipid infusion or a hyperinsulinaemic euglycaemic clamp leads to preferential usage of the given substrate to generate ATP and could influence both cardiac energetic status and contractility[186]. In this chapter I will aim to assess the effects of such substrate switching through the provision of lipid, glucose as well as ketones on systolic and diastolic function at rest and stress as well as the resting myocardial energetic status.

Ketone bodies are taken up by cardiomyocytes in a circulating concentration-dependent manner[155]. Therefore, it would be pertinent to assess if providing ketone bodies in addition to a supply of glucose or lipid could alter cardiac function or energetics in a manner these substrates cannot do alone.

5.2 Methods

Inclusion and exclusion criteria for patients with HFpEF were identical to that described in Chapter 3 with an additional exclusion criterion: egg or soy allergy (for intralipid administration).

Participants were randomised to one of three groups: intralipid, ketone or insulin-glucose. All participants attended a minimum of 2 visits – a baseline visit as well as a visit with a single substrate. A number of participants who were randomised to the intralipid or insulin-glucose arms attended an optional third visit where they were given ketone simultaneous to the original substrate.

Participants were fasted for a minimum of 9 hours – usually overnight for a morning study visit. Following the baseline visit with no substrate, participants received either 20% intralipid (Fresenius Kabi), a hyper-insulinaemic euglycaemic clamp or 0.6ml/kg of oral ketone ester (TdeltaS) as outlined in Chapter 2 as part of their second visit. Those who received ketone ester received 0.9% sodium chloride intravenously in addition to balance intravascular fluid load across substrates.

Baseline blood samples were drawn before substrates were provided. Blood samples following commencement of substrates were taken 1 hour following intralipid or insulin/dextrose infusions to establish equilibrium and 30 minutes after ketone ester ingestion to coincide with peak blood levels from literature[240]. Participants underwent MRI scanning immediately after the blood tests. This was followed by echocardiography. Those who had ingested ketone ester also had additional ketone levels measured opportunistically during the MRI and immediately prior to echocardiography with no further ketone ester provided. Those in the lipid or glucose groups had continuous infusions for the duration of the study visit until all imaging aspects of the protocol were completed. In the text, the substrates will primarily be referred to as glucose, (intra-)lipid or ketone.

The Homeostatic Model assessment for Insulin Resistance (HOMA-IR) was calculated to estimate insulin resistance from fasting venous samples at baseline using the HOMA-2 calculator[241].

From CMR and clinical measurements the following calculations were performed:

Stroke work was calculated as:

$$Stroke\ work = Stroke\ volume \times Mean\ arterial\ pressure$$

Cardiac work, i.e. the total work done in a minute was calculated as:

$$Cardiac\ work = Stroke\ work \times Heart\ rate$$

Rate pressure product as:

$$Rate\ Pressure\ Product = Systolic\ Blood\ Pressure \times Heart\ rate$$

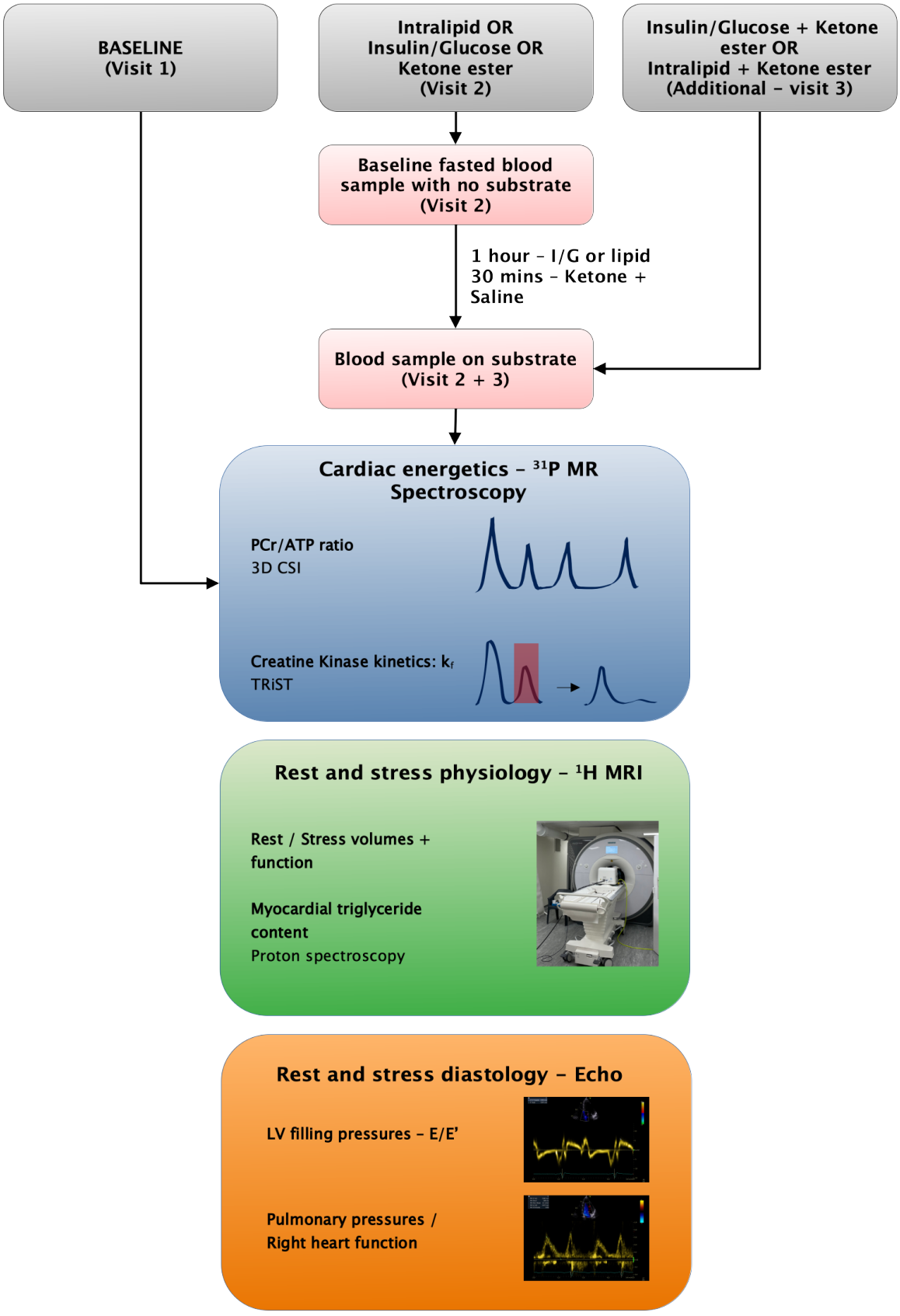

Figure 61: Substrate selection study protocol

5.3 Results part A: Single substrate study (Baseline and single substate only)

5.3.1 Baseline demographics and clinical characteristics

Twenty-four participants were recruited and randomised to one of three groups with eight in each group. All participants undertook at least two visits – the first for a baseline scan, fasted for at least 9 hours and the second, where they received the primary substrate in the allocated group in a similar fasting state. 7 participants from the insulin-glucose group had a 3rd visit where they received ketone ester in addition to insulin-glucose. 4 participants from the intralipid group had a 3rd visit where they also received ketone ester in addition to lipid.

All 3 groups were of mean age over 70 in keeping with the higher prevalence of HFpEF in this cohort, although the ketone ester group were slightly older with a mean age of 80.0 ± 4.7 (ANOVA p=0.04). There were no significant differences in BMI, waist circumference or blood pressure at rest. The prevalence of key comorbidities including AF, hypertension, diabetes and obesity were not different between groups. There were no significant differences in insulin resistance as measured by HOMA or in NT-proBNP levels indicative of cardiac wall stress.

There were no significant differences in the prescription of loop diuretics, mineralocorticoid receptor antagonists or SGLT-2 inhibitors among the groups. A majority of participants in the insulin-glucose and intralipid groups were on calcium channel blockers compared to none in the ketone ester group. Rates of other hypertension and diabetes medicines were similar.

Table 41: Baseline characteristics by substrate allocation

	Insulin+glucose (n=8)	*Intralipid (n=8)*	*Ketone ester (n=8)*	*p-value*
Age (years)	76.3 ± 4.6	73.3 ± 5.2	80.0 ± 4.7	**0.04**
Male – no. (%)	6 (75%)	5 (63%)	6 (75%)	0.81
BMI (kg/m²)	31.0 ± 4.8	32.9 ± 7.4	28.9 ± 7.0	0.48
Waist circumference (cm)	110.8 ± 13.9	114.0 ± 14.7	107.4 ± 17.0	0.69
SBP (mmHg)	135.1 ± 7.4	144.8 ± 19.3	142.0 ± 31.5	0.67
DBP (mmHg)	72.8 ± 12.1	80.1 ± 28.0	79.8 ± 14.9	0.67
MAP (mmHg)	93.5 ± 8.5	102.2 ± 22.1	100.5 ± 17.0	0.56
Atrial fibrillation – no. (%)	5 (62.5%)	7 (87.5%)	6 (62.5%)	0.51
Hypertension - no. (%)	7 (87.5%)	6 (75%)	6 (75%)	0.78
Diabetes - no. (%)	0 (0%)	3 (37.5%)	2 (25%)	0.17
Obesity (BMI>30) - no. (%)	5 (62.5%)	5 (62.5%)	3 (37.5%)	0.51
NT-proBNP (ng/L)	776 ± 600	1674 ± 1886	918 ± 563	0.47
HOMA-IR	0.93 ± 0.44	1.16 ± 0.82	0.75 ± 0.34	0.38

Table 42: Medication on enrolment by substrate allocation

	Insulin + glucose	*Intralipid*	*Ketone ester*	*p-value*
ACE inhibitor - no. (%)	4 (50%)	3 (37.5%)	3 (37.5%)	0.84
Angiotensin Receptor Blocker - no. (%)	0 (0%)	2 (25%)	1 (12.5%)	0.32
Mineralocorticoid receptor antagonist - no. (%)	2 (25%)	2 (25%)	4 (50%)	0.47
Beta-blocker - no. (%)	6 (75%)	5 (62.5%)	6 (75%)	0.82
Loop diuretic - no. (%)	3 (37.5%)	4 (50%)	5 (62.5%)	0.61
Calcium channel blocker - no. (%)	6 (75%)	5 (62.5%)	0	***0.006***
Sodium-glucose cotransporter 2 inhibitor - no. (%)	0 (0%)	1 (12.5%)	3 (37.5%)	0.13
Metformin - no. (%)	0 (0%)	2 (25%)	0	0.11
Sulfonylurea - no. (%)	0 (0%)	1 (12.5%)	0	0.35
Dipeptidyl Peptidase IV inhibitors - no. (%)	0 (0%)	0 (0%)	1 (12.5%)	0.35

5.3.2 Infusion volumes and serum metabolite levels

There was no significant difference in the intravenous volumes administered between any of the substrates with saline infusion being used in the ketone group.

In the insulin-dextrose group, the desired hyper-insulinaemia was achieved (48.8 ± 22.6 → 258.5 ± 62.6 pmol/L, p<0.0001) while maintaining a stable glucose level. This also resulted in a reduction in venous free fatty acid levels (0.66 ± 0.18 → 0.30 ± 0.13 mmol/L, p<0.0001). There were no differences in lactate or βOHB levels. In addition, there was also a drop in NT-proBNP levels by 5% (775 ± 600 → 736 ± 584 ng/L, p=0.04). In the intralipid group, there was an elevation in the NEFA (0.48 ± 0.10 → 1.08 ± 0.73 mmol/L, p=0.008) and βOHB (0.078 ± 0.060 → 0.230 ± 0.111 mmol/L, p=0.008) levels. There was no change in insulin, glucose, lactate or NT-proBNP levels. At 30 minutes following ketone ester ingestion there was a large increase in serum βOHB levels (0.061 ± 0.032 → 2.46 ± 0.63 mmol/L, p<0.0001) and a more modest increase in insulin concentration (39.1 ± 18.5 → 89.3 ± 44.4 pmol/L, p=0.008). There was a numerical reduction in NT-proBNP in addition to this (918 ± 563 → 871 ± 516 ng/L, p=0.06).

Table 43: Infused intravenous volumes in each substrate group

	Insulin + glucose	*Intralipid*	*Ketone ester*	*p-value*
Infused volume (ml)	288.9 ± 107.1	245.6 ± 30.2	230.0 ± 31.88	0.21

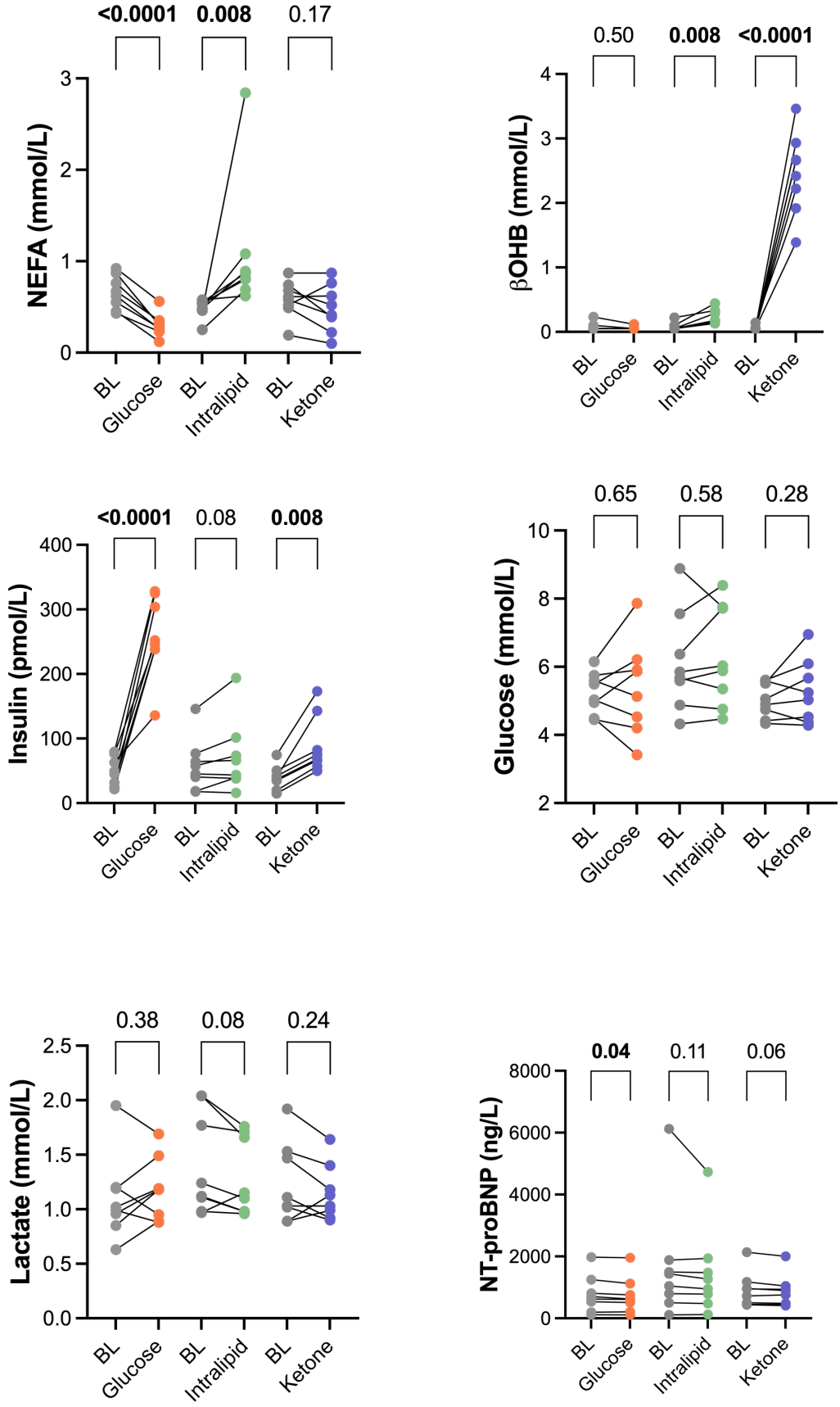

Figure 62: Serum metabolite and NT-proBNP levels on substrate switching

Table 44: Circulating metabolites on a single substrate in each group

	Insulin+glucose			*Intralipid*			*Ketone ester*		
	Baseline	**I + G**	**p-value**	**Baseline**	**Intralipid**	**p-value**	**Baseline**	**KE**	**p-value**
NEFA (mmol/L)	0.66 ± 0.18	0.30 ± 0.13	<**0.0001**	0.48 ± 0.10	1.08 ± 0.73	**0.008**	0.59 ± 0.20	0.49 ± 0.26	0.17
Glucose (mmol/L)	5.24 ± 0.62	5.39 ± 1.38	0.65	6.1 ± 1.5	6.3 ± 1.5	0.58	5.02 ± 0.51	5.27 ± 0.93	0.28
Insulin (pmol/L)	48.8 ± 22.6	258.5 ± 62.6	**<0.0001**	58.4 ± 40.1	71.5 ± 56.0	0.08	39.1 ± 18.5	89.3 ± 44.4	**0.008**
Lactate (mmol/L)	1.10 ± 0.39	1.18 ± 0.29	0.38	1.4 ± 0.5	1.3 ± 0.4	0.08	1.23 ± 0.37	1.15 ± 0.26	0.24
βOHB (mmol/L) ^	0.079 ± 0.064	0.059 ± 0.025	0.50	0.078±0.060	0.230 ± 0.111	**0.008**	0.061±0.032	2.46 ± 0.63	**<0.0001**
NT-proBNP (ng/L)	775 ± 600	736 ± 584	**0.04**	1674 ± 1886	1468 ± 1437	0.11	918 ± 563	871 ± 516	0.06

^ where values were below the laboratory limit of detection i.e. <0.1, a constant of 0.05, the limit of detection/2 has been used for statistical analysis.

5.3.3 Ventricular volumes and function at rest

In both the glucose and intralipid groups, there were no changes in stroke volume or ejection fraction at rest. There was an increase in LVEDV with glucose (150.2 ± 46.4 → 158.5 ± 49.2 ml, p=0.04), but no changes in ventricular volumes on intralipid. There was a trend towards an improvement in LV diastolic function as measured by E/E' on the intralipid infusion (11.4 ± 2.7 → 9.9 ± 2.7, p=0.07), but no change with glucose.

At rest, administration of ketone resulted in an increase in LVEF (60.6 ± 5.1 → 66.7 ± 6.2%, p=0.003), LV stroke volume (94.4 ± 22.2 → 105.6 ± 17.4 ml, p=0.005) and improved global longitudinal strain on CMR (-13.8 ± 3.5 → -17.2 ± 3.8%, p=0.001) with a trend towards improved LV longitudinal function as measured by tissue doppler (S') on echocardiography (6.5 ± 1.2 → 7.3 ± 1.5 cm/s, p=0.07). The increase in LV stroke volume was potentially driven by a reduction in end-systolic volume (64.5 ± 25.2 → 55.2 ± 19.0 ml, p=0.08) rather than an increase in end-diastolic volume. There was no change to E/E' at rest.

Glucose infusion increased RV stroke volume (90.0 ± 25.4 → 97.6 ± 26.8 ml, p=0.02), RV SV/ESV ratio (1.60 ± 0.48 → 1.68 ± 0.51, p=0.04) and improved RV longitudinal strain on CMR (-20.3 ± 5.9 → -24.6 ± 4.1%, p=0.006) without changing RVEF on CMR or echo measures of RV function. Intralipid had no effect on RV volumes or systolic function, although there was a trend towards a subtle reduction in echocardiography-derived PASP (28.4 ± 5.9 → 26.0 ± 4.6 mmHg, p=0.07).

There was a trend towards an increase in RVSV in the ketone group (92.5 ± 24.1 → 102.6 ± 18.0 ml, p=0.06) with no change to RV systolic function metrics on CMR or echocardiography.

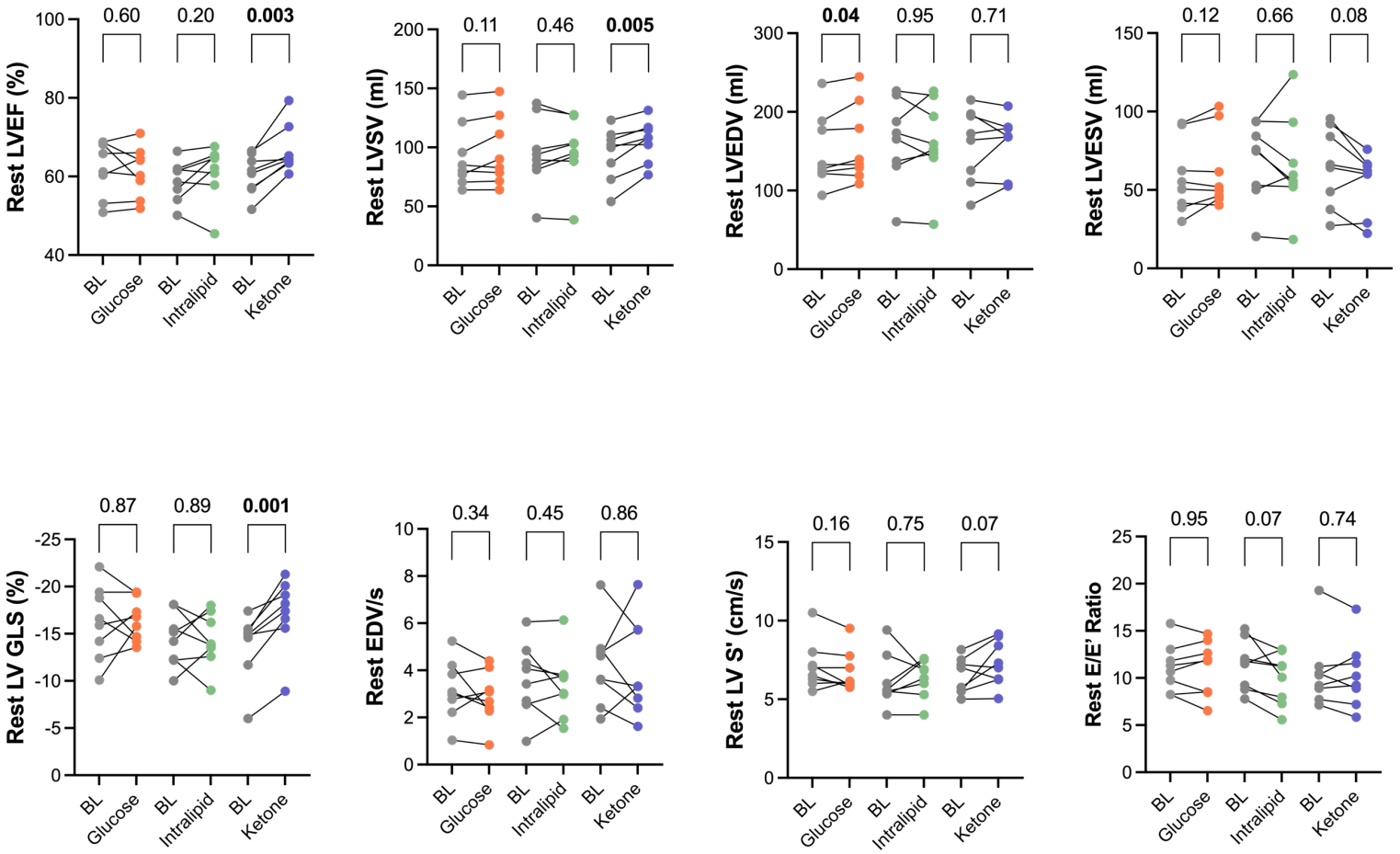

Figure 63: LV systolic and diastolic function at rest on substrate switching as measured on CMR and echocardiography

BL: Baseline, EF: LV Ejection Fraction, SV: LV Stroke Volume, EDV: LV End Diastolic Volume, ESV: LV End Systolic Volume, GLS: Global Longitudinal Strain, EDV/s: Peak filling rate in early diastole normalised to the EDV, S': Mean S' doppler measure of longitudinal function, E/E' Ratio: Mean doppler measure of diastolic function

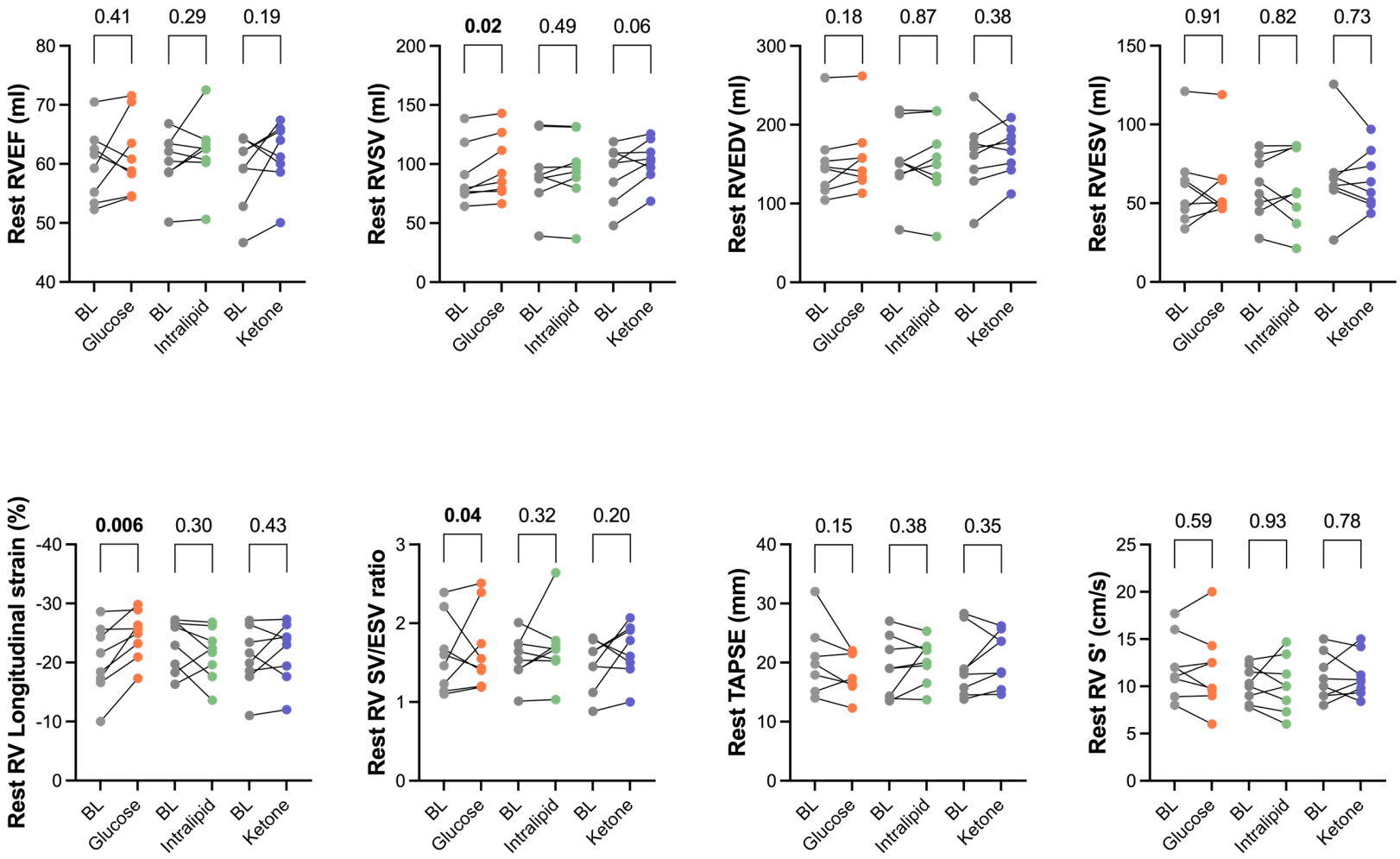

Figure 64: RV systolic function at rest on substrate switching as measured on CMR and echocardiography

BL: Baseline, RVEF: RV Ejection Fraction, RVSV: RV Stroke Volume, RVEDV: RV End Diastolic Volume, ESV: RV End Systolic Volume, TAPSE: Tricuspid Annular Plane Systolic Excursion, S': Mean S' doppler measure of longitudinal function

Table 45: Ventricular parameters at rest on substrate switching compared to baseline – CMR

	Insulin + glucose			*Intralipid*			*Ketone ester*		
	Baseline	**Glucose**	**p-value**	**Baseline**	**Intralipid**	**p-value**	**Baseline**	**Ketone**	**p-value**
LVEDV (ml)	150.2 ± 46.4	158.5 ± 49.2	***0.04***	162.9 ± 54.0	162.4 ± 53.9	0.95	157.7 ± 47.2	160.7 ± 35.6	0.71
LVESV (ml)	57.8 ± 23.4	61.9 ± 24.6	0.12	68.2 ± 25.4	65.4 ± 31.2	0.66	64.5 ± 25.2	55.2 ± 19.0	0.08
LVEF (%)	62.1 ± 7.1	61.3 ± 6.4	0.60	58.9 ± 5.1	61.1 ± 7.0	0.20	60.6 ± 5.1	66.7 ± 6.2	***0.003***
LVSV (ml)	92.3 ± 27.5	96.6 ± 29.2	0.11	94.7 ± 30.7	97.0 ± 27.8	0.46	94.4 ± 22.2	105.6 ± 17.4	***0.005***
LV GLS (%)	-16.2 ± 3.9	-16.4 ± 2.2	0.87	-14.5 ± 2.9	-14.3 ± 2.9	0.89	-13.8 ± 3.5	-17.2 ± 3.8	***0.001***
LV peak early filling rate (EDV/s)	3.2 ± 1.3	2.9 ± 1.1	0.34	3.6 ± 1.6	3.4 ± 1.4	0.45	4.18 ± 1.76	4.07 ± 2.06	0.86
RVEDV (ml)	152.0 ± 48.2	159.1 ± 46.1	0.18	153.8 ± 47.8	154.9 ± 51.8	0.87	159.3 ± 46.7	167.4 ± 31.2	0.38
RVESV (ml)	60.1 ± 27.3	61.5 ± 24.4	0.91	60.7 ± 19.9	59.7 ± 24.6	0.82	66.8 ± 27.3	64.9 ± 18.5	0.73
RVEF (%)	59.8 ± 6.1	61.6 ± 6.6	0.41	60.5 ± 5.0	62.1 ± 6.0	0.29	58.9 ± 6.2	61.6 ± 5.6	0.19
RVSV (ml)	90.0 ± 25.4	97.6 ± 26.8	***0.02***	93.1 ± 30.2	95.1 ± 30.2	0.49	92.5 ± 24.1	102.6 ± 18.0	0.06
RV longitudinal strain (%)	-20.3 ± 5.9	-24.6 ± 4.1	***0.006***	-23.0 ± 4.4	-21.4 ± 4.4	0.30	-20.7 ± 5.2	-21.8 ± 5.1	0.43
RV SV/ESV ratio	1.60 ± 0.48	1.68 ± 0.51	***0.04***	1.56 ± 0.30	1.70 ± 0.45	0.32	1.47 ± 0.33	1.65 ± 0.35	0.20

Table 46: Rest echocardiography parameters on substrate switching

	Insulin + glucose			*Intralipid*			*Ketone ester*		
	Baseline	**Glucose**	**p-value**	**Baseline**	**Intralipid**	**p-value**	**Baseline**	**Ketone**	**p-value**
E/E′ average (ratio)	11.1 ± 2.5	11.1 ± 2.9	0.95	11.4 ± 2.7	9.9 ± 2.7	0.07	10.5 ± 3.8	10.3 ± 3.5	0.74
S′ LV (cm/s)	7.1 ± 1.6	6.8 ± 1.3	0.16	6.1 ± 1.7	6.3 ± 1.2	0.75	6.5 ± 1.2	7.3 ± 1.5	0.07
TAPSE (mm)	20.6 ± 6.1	18.2 ± 3.7	0.15	19.2 ± 5.1	20.3 ± 3.8	0.38	19.5 ± 5.6	20.7 ± 4.6	0.35
S′ RV (cm/s)	12.1 ± 3.3	11.7 ± 4.2	0.59	10.2 ± 1.9	10.2 ± 2.9	0.93	11.0 ± 2.5	11.1 ± 2.3	0.78
Estimated PASP (mmHg)	31.1 ± 11.3	32.9 ± 8.6	0.52	28.4 ± 5.9	26.0 ± 4.6	0.07	35.3 ± 7.8	32.3 ± 5.6	0.30

5.3.4 Atrial volumes and function at rest

Neither glucose or intralipid infusions altered left or right atrial volumes or emptying fraction at rest. In the ketone group, there was a reduction in right atrial volumes (RAEDV 177.0 ± 79.9 → 163.7 ± 73.7 ml, p=0.03, RAESV 217.4 ± 69.9 → 199.6 ± 66.7 ml, p=0.06), but not left atrial volumes or emptying fractions.

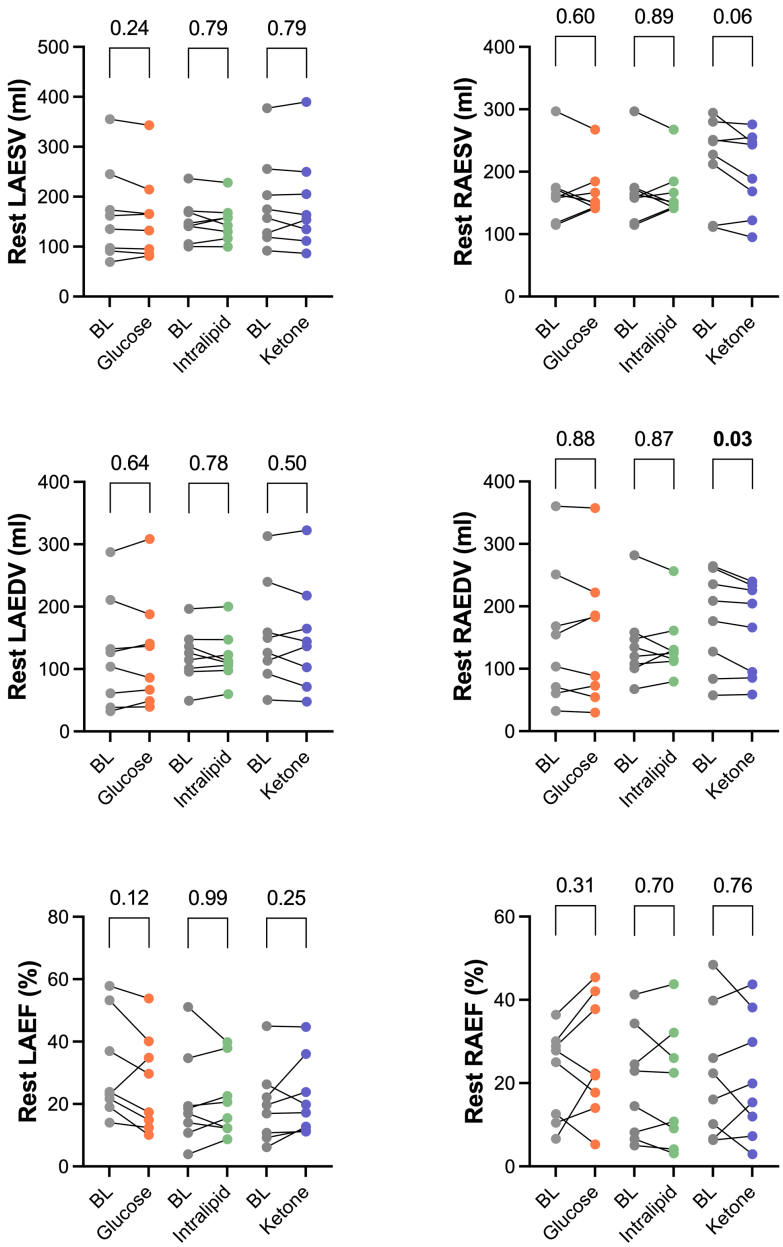

Figure 65: Resting atrial parameters on substrate switching on CMR

BL: Baseline, LA: Left atrium, RA: Right atrium, ESV: Atrial volume at ventricular end-systole, EDV: Atrial volume at ventricular end-diastole, EF: Emptying Fraction

Table 47: Atrial parameters at rest on substrate switching

	Insulin + glucose			*Intralipid*			*Ketone ester*		
	Baseline	**Glucose**	**p-value**	**Baseline**	**Intralipid**	**p-value**	**Baseline**	**Ketone**	**p-value**
LAEDV (ml)	124.2 ± 88.1	126.9 ± 89.4	0.64	120.9 ± 42.9	119.6 ± 40.7	0.78	155.6 ± 84.2	151.0 ± 87.5	0.50
LAESV (ml)	166.1 ± 94.6	160.4 ± 87.2	0.24	151.4 ± 42.9	150.0 ± 39.0	0.79	188.3 ± 92.1	186.9 ± 96.7	0.79
LAEF (%)	31.2 ± 16.4	26.7 ± 15.6	0.12	21.2 ± 15.0	21.2 ± 11.8	0.99	19.5 ± 12.4	22.2 ± 12.3	0.25
RAEDV (ml)	150.3 ± 110.2	149.3 ± 109.5	0.88	139.7 ± 64.2	138.4 ± 52.8	0.87	177.0 ± 79.9	163.7 ± 73.7	***0.03***
RAESV (ml)	182.9 ± 117.6	186.7 ± 111.5	0.60	169.6 ± 56.3	168.3 ± 42.7	0.89	217.4 ± 69.9	199.6 ± 66.7	0.06
RAEF (%)	22.2 ± 10.8	25.8 ± 14.4	0.31	19.7 ± 13.4	19.0 ± 14.6	0.70	22.0 ± 15.6	21.2 ± 14.7	0.76

5.3.5 Cardiac output and haemodynamics at rest

Glucose infusion did not result in a change in cardiac output, blood pressure, heart rate, work or the rate pressure product. Intralipid infusion resulted in increased cardiac work (584.8 ± 289.1 → 675.4 ± 279.7 mmHg.ml/min x 10^3, p=0.03) and rate pressure product (8959 ± 1703 → 10110 ± 2128 mmHg.bpm, p=0.02) despite no individual differences being detected in heart rate or any of the blood pressure indices. However, there was no increase in cardiac output.

Ketone ingestion resulted in an increase in heart rate at rest (59.9 ± 9.0 → 66.6 ± 8.6 bpm, p=0.03) which together with the increase in LVSV produced an increase in cardiac output (cardiac index 2.77 ± 0.44 → 3.51 ± 0.58 L/min/m^2, p=0.0004). This heart rate effect resulted in an increase in cardiac work (549.4 ± 107.3 → 626.4 ± 114.3 mmHg.ml/min x 10^3, p=0.04), but not stroke work. The levels of work were attenuated by a drop in blood pressure (MAP 100.5 ± 17.0 → 91.2 ± 19.3 mmHg, p=0.002).

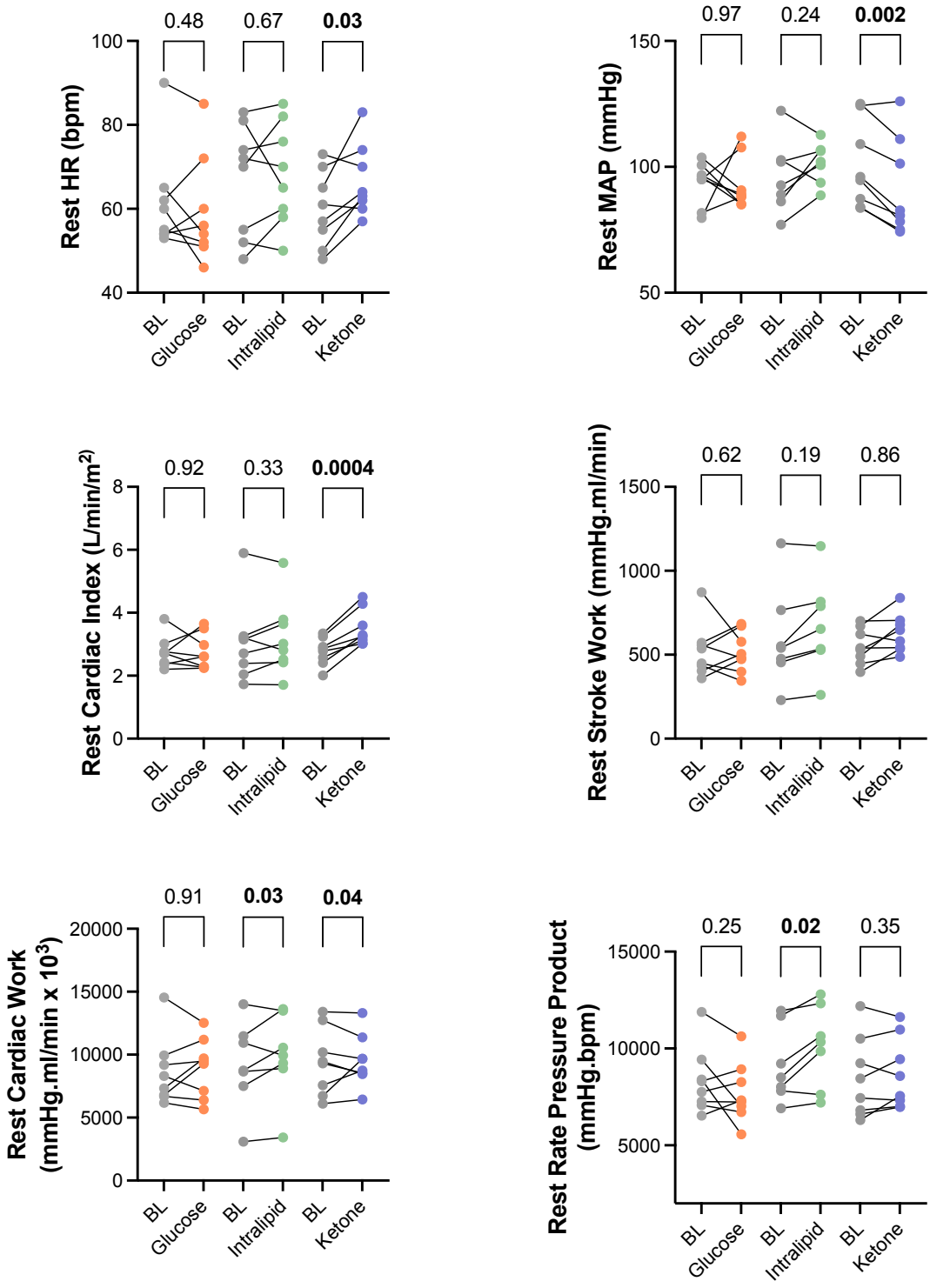

Figure 66: Resting haemodynamic parameters on substrate switching

BL: Baseline, HR: Heart rate, MAP: Mean arterial pressure

Table 48: Cardiac output and work parameters at rest on substrate switching

	Insulin + glucose			*Intralipid*			*Ketone ester*		
	Baseline	**Glucose**	**p-value**	**Baseline**	**Intralipid**	**p-value**	**Baseline**	**Ketone**	**p-value**
Cardiac Output (L/min)	5.57 ± 1.52	5.63 ± 1.63	0.90	6.29 ± 2.48	6.55 ± 2.23	0.36	5.50 ± 0.83	6.95 ± 0.92	***0.0004***
Cardiac Index ($L/min/m^2$)	2.75 ± 0.50	2.77 ± 0.56	0.92	3.05 ± 1.28	3.18 ± 1.18	0.33	2.77 ± 0.44	3.51 ± 0.58	***0.0004***
Stroke Work (mmHg.ml/min)	8621 ± 2723	8918 ± 2377	0.62	9009 ± 3386	9896 ± 3427	0.06	9436 ± 2653	9527 ± 2071	0.86
Cardiac Work (mmHg.ml/min x 10^3)	522.7 ± 160.3	516.6 ± 120.8	0.91	584.8 ± 289.1	675.4 ± 279.7	***0.03***	549.4 ± 107.3	626.4 ± 114.3	***0.04***
Rate Pressure Product (mmHg.bpm)	8330 ± 1694	7711 ± 1545	0.25	8959 ± 1703	10110 ± 2128	***0.02***	8445 ± 2088	8686 ± 1825	0.35

Table 49: Rest blood pressure and heart rate on substrate switching

	Insulin + glucose			*Intralipid*			*Ketone ester*		
	Baseline	**Glucose**	**p-value**	**Baseline**	**Intralipid**	**p-value**	**Baseline**	**Ketone**	**p-value**
HR (bpm)	61.6 ± 12.3	59.5 ± 12.9	0.48	66.9 ± 13.4	68.3 ± 12.2	0.67	59.9 ± 9.0	66.6 ± 8.6	***0.03***
SBP (mmHg)	135.1 ± 7.4	130.4 ± 13.6	0.30	142.3 ± 19.4	147.1 ± 14.0	0.42	142.0 ± 31.5	131.8 ± 29.6	***0.007***
DBP (mmHg)	72.8 ± 12.1	74.8 ± 10.4	0.66	72.9 ± 17.7	78.7 ± 8.6	0.28	79.8 ± 14.9	70.9 ± 16.7	***0.03***
MAP (mmHg)	93.5 ± 8.5	93.3 ± 10.5	0.97	96.0 ± 14.7	101.5 ± 8.2	0.24	100.5 ± 17.0	91.2 ± 19.3	***0.002***

5.3.6 Ventricular volumes and function during exercise stress

Neither glucose nor intralipid infusion resulted in a change to either LV volumes, systolic or diastolic function parameters during exercise. In the ketone group, there was an increase in LV stroke volume (112.5 ± 9.2 → 124.9 ± 15.9 ml, p=0.047) driven primarily by a numerical increase in end-diastolic volume (172.5 ± 15.0 → 185.6 ± 26.0 ml, p=0.08). There was no change in LVEF or peak filling rate on CMR. Diastolic function improved during exercise as measured by E/E' on echocardiography (11.5 ± 4.9 → 8.4 ± 3.4, p=0.006).

There was no change to RV volumes or function during exercise with glucose or lipid infusions. In the presence of ketonaemia, there was an increase in RV stroke volume (110.1 ± 8.5 → 125.3 ± 13.7 ml, p=0.02), RV SV/ESV ratio (1.39 ± 0.22 → 1.75 ± 0.45, p=0.0495) and a numerical increase in longitudinal function on echocardiography (TAPSE 18.1 ± 4.3 → 22.1 ± 7.8 mm, p=0.05) and overall function on CMR (RVEF 57.9 ± 3.6 → 62.7 ± 6.3 %, p=0.07).

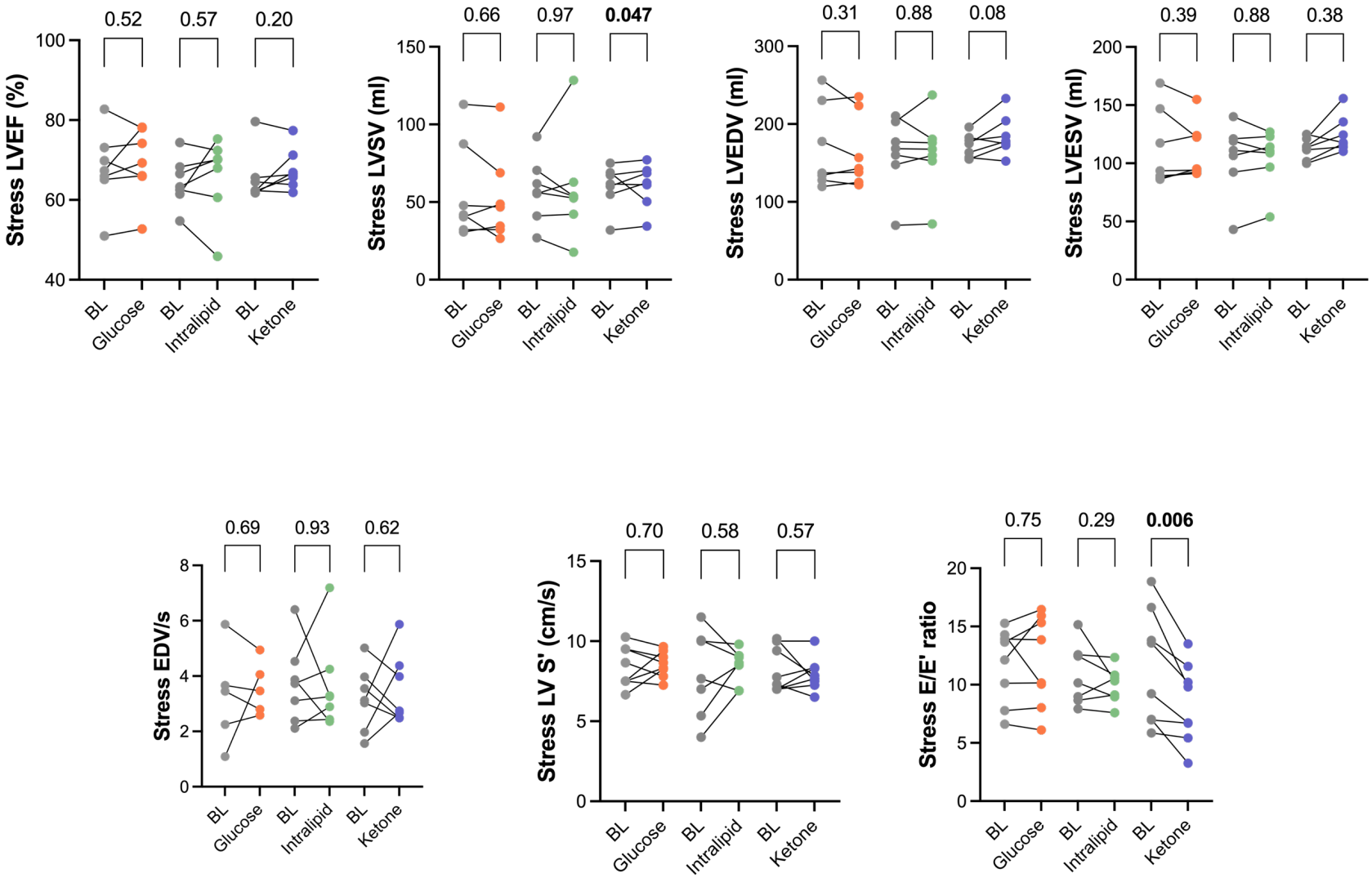

Figure 67: LV systolic and diastolic function at stress on substrate switching on CMR and echocardiography

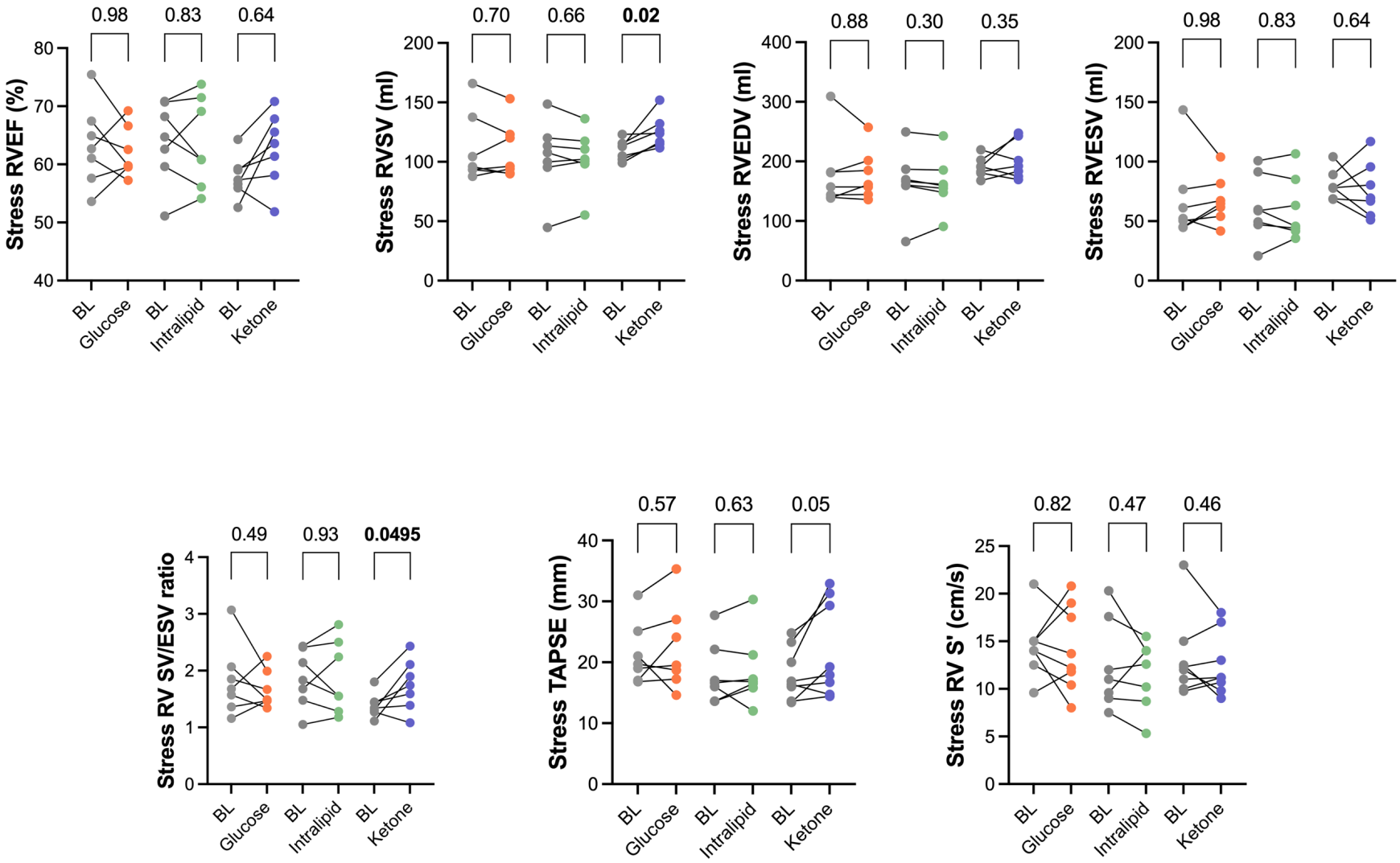

Figure 68: RV systolic function at stress on substrate switching on CMR and echocardiography

Table 50: Ventricular parameters during exercise on substrate switching

	Insulin + glucose			*Intralipid*			*Ketone ester*		
	Baseline	**Glucose**	**p-value**	**Baseline**	**Intralipid**	**p-value**	**Baseline**	**Ketone**	**p-value**
LVEDV (ml)	169.0 ± 54.5	163.4 ± 46.7	0.37	162.5 ± 46.5	163.6 ± 49.2	0.88	172.5 ± 15.0	185.6 ± 26.0	0.08
LVESV (ml)	56.2 ± 31.5	52.7 ± 29.3	0.39	57.7 ± 20.8	58.8 ± 34.0	0.88	60.0 ± 14.0	60.6 ± 14.3	0.38
LVEF (%)	67.9 ± 9.6	69.2 ± 8.9	0.52	64.5 ± 6.1	66.1 ± 10.0	0.57	65.5 ± 6.4	67.6 ± 5.2	0.20
LVSV (ml)	112.8 ± 33.2	110.7 ± 24.1	0.66	104.8 ± 30.9	104.9 ± 24.6	0.97	112.5 ± 9.2	124.9 ± 15.9	***0.047***
LV peak early filling rate (EDV/s)	3.3 ± 1.8	3.6 ± 1.0	0.69	3.73 ± 1.45	3.70 ± 1.68	0.93	3.17 ± 1.17	3.52 ± 1.29	0.62
RVEDV (ml)	178.9 ± 60.4	177.4 ± 41.8	0.88	165.4 ± 54.1	163.2 ± 45.5	0.30	190.7 ± 16.6	201.8 ± 31.5	0.35
RVESV (ml)	67.7 ± 35.2	67.9 ± 20.0	0.98	61.1 ± 27.2	60.3 ± 26.5	0.83	80.6 ± 12.5	76.4 ± 23.4	0.64
RVEF (%)	63.3 ± 7.1	62.1 ± 4.3	0.63	64.0 ± 7.0	63.8 ± 7.7	0.91	57.9 ± 3.6	62.7 ± 6.3	0.07
RVSV (ml)	111.2 ± 29.3	109.6 ± 23.7	0.70	104.3 ± 31.5	102.9 ± 24.8	0.66	110.1 ± 8.5	125.3 ± 13.7	***0.02***
RV SV/ESV ratio	1.82 ± 0.63	1.67 ± 0.33	0.49	1.86 ± 0.51	1.88 ± 0.64	0.93	1.39 ± 0.22	1.75 ± 0.45	***0.0495***

Table 51: Stress echocardiography parameters on substrate switching

	Insulin + glucose			*Intralipid*			*Ketone ester*		
	Baseline	**Glucose**	**p-value**	**Baseline**	**Intralipid**	**p-value**	**Baseline**	**Ketone**	**p-value**
E/E′ average (ratio)	11.7 ± 3.2	12.0 ± 3.9	0.75	10.8 ± 2.6	10.0 ± 1.5	0.29	11.5 ± 4.9	8.4 ± 3.4	***0.006***
S′ LV (cm/s)	8.4 ± 1.3	8.5 ± 0.1	0.70	7.9 ± 2.7	8.4 ± 1.1	0.58	8.2 ± 1.4	7.9 ± 1.0	0.57
TAPSE (mm)	21.4 ± 5.1	22.4 ± 7.1	0.57	18.1 ± 5.1	18.6 ± 5.8	0.63	18.1 ± 4.3	22.1 ± 7.8	0.05
S′ RV (cm/s)	14.5 ± 3.2	14.2 ± 4.5	0.82	12.4 ± 4.7	11.5 ± 3.6	0.47	13.2 ± 4.3	12.5 ± 3.3	0.46
Estimated PASP (mmHg)	42 ± 13.7	47.6 ± 7.4	0.13	38.9 ± 7.4	46.3 ± 3.5	0.20	45.0 ± 13.5	35.8 ± 5.2	0.21

5.3.7 Atrial volumes and function during exercise

In the intralipid and glucose groups, there were no changes in atrial volumes or emptying fraction. In the ketone group, there was a reduction in left (162.8 ± 78.9 → 147.4 ± 70.6 ml, p=0.04) and right atrial volumes at ventricular end-diastole (208.4 ± 90.2 → 187.7 ± 88.6 ml, p=0.03) and a numerical decrease in right atrial volume at ventricular end-systole (267.6 ± 81.3 → 247.9 ± 93.9 ml, p=0.05). There was no change to emptying fractions.

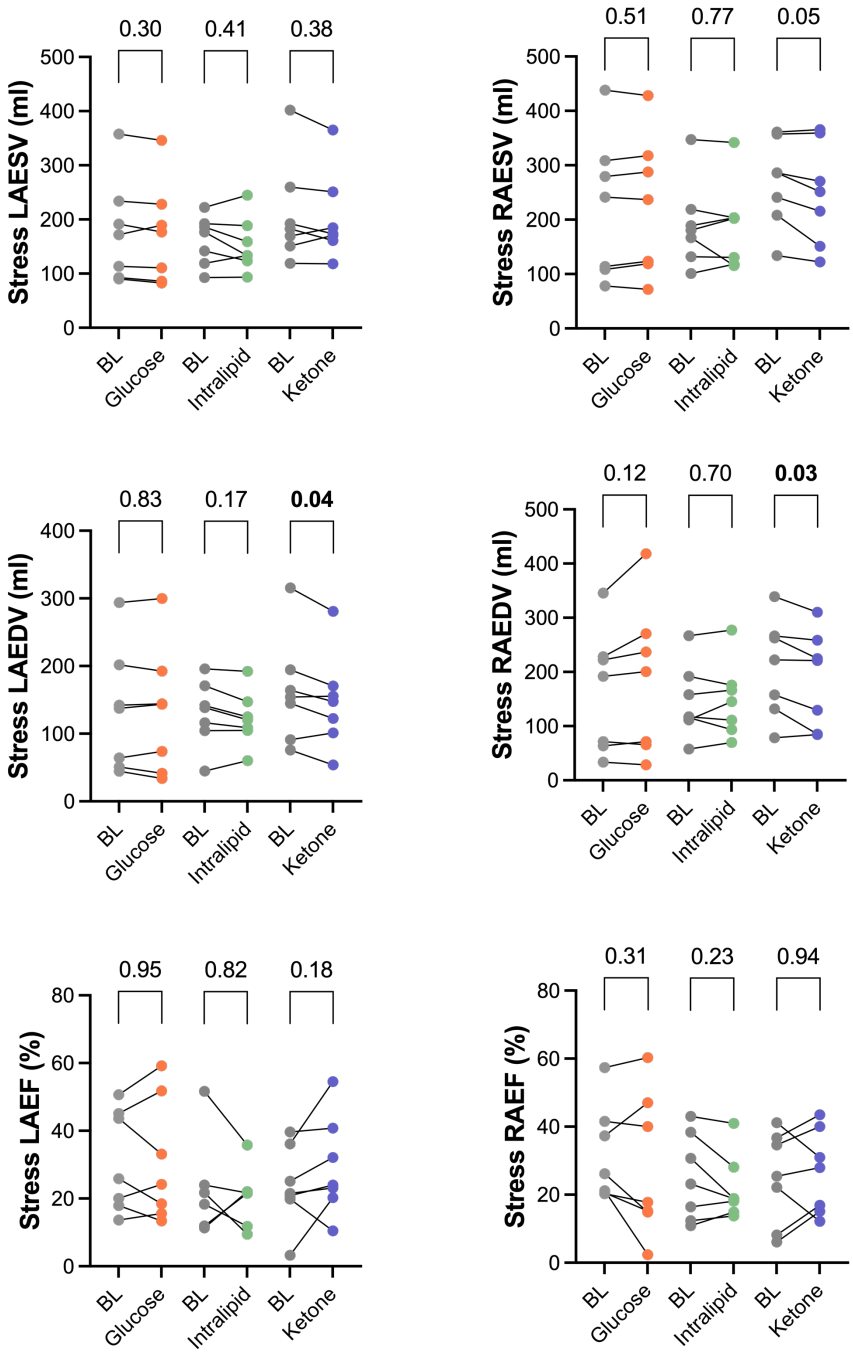

Figure 69: Stress atrial parameters on substrate switching on CMR

Table 52: Atrial parameters during exercise on substrate switching

	Insulin + glucose			*Intralipid*			*Ketone ester*		
	Baseline	**Glucose**	**p-value**	**Baseline**	**Intralipid**	**p-value**	**Baseline**	**Ketone**	**p-value**
LAEDV (ml)	133.5 ± 91.3	132.8 ± 94.2	0.83	130.3 ± 48.8	122.6 ± 40.6	0.17	162.8 ± 78.9	147.4 ± 70.6	***0.04***
LAESV (ml)	178.7 ± 95.6	174.2 ± 93.8	0.30	161.7 ± 45.5	153.8 ± 49.9	0.41	210.9 ± 94.7	203.5 ± 81.4	0.38
LAEF (%)	31.0 ± 15.1	30.8 ± 18.2	0.95	21.5 ± 14.2	20.5 ± 8.5	0.82	23.8 ± 11.9	29.3 ± 14.6	0.18
RAEDV (ml)	165.2 ± 113.2	184.5 ± 139.2	0.12	145.6 ± 67.8	148.5 ± 68.7	0.70	208.4 ± 90.2	187.7 ± 88.6	***0.03***
RAESV (ml)	224.1 ± 131.0	226.4 ± 128.4	0.51	190.9 ± 79.1	187.9 ± 79.4	0.77	267.6 ± 81.3	247.9 ± 93.9	0.05
RAEF (%)	32.1 ± 14.0	28.2 ± 21.0	0.31	25.0 ± 12.7	21.9 ± 9.6	0.23	24.9 ± 13.8	26.7 ± 12.4	0.94

5.3.8 Cardiac output and haemodynamics during exercise

There were no changes to cardiac output, work or rate pressure product on glucose or intralipid infusions. In the ketone group, there was a trend towards an increase in cardiac output (cardiac index 4.61 ± 0.76 → 5.48 ± 0.92 L/min/m², p=0.08) despite no significant change in heart rate and was therefore driven by an increase in LVSV as described earlier. There were no changes to blood pressure, cardiac work or rate pressure product.

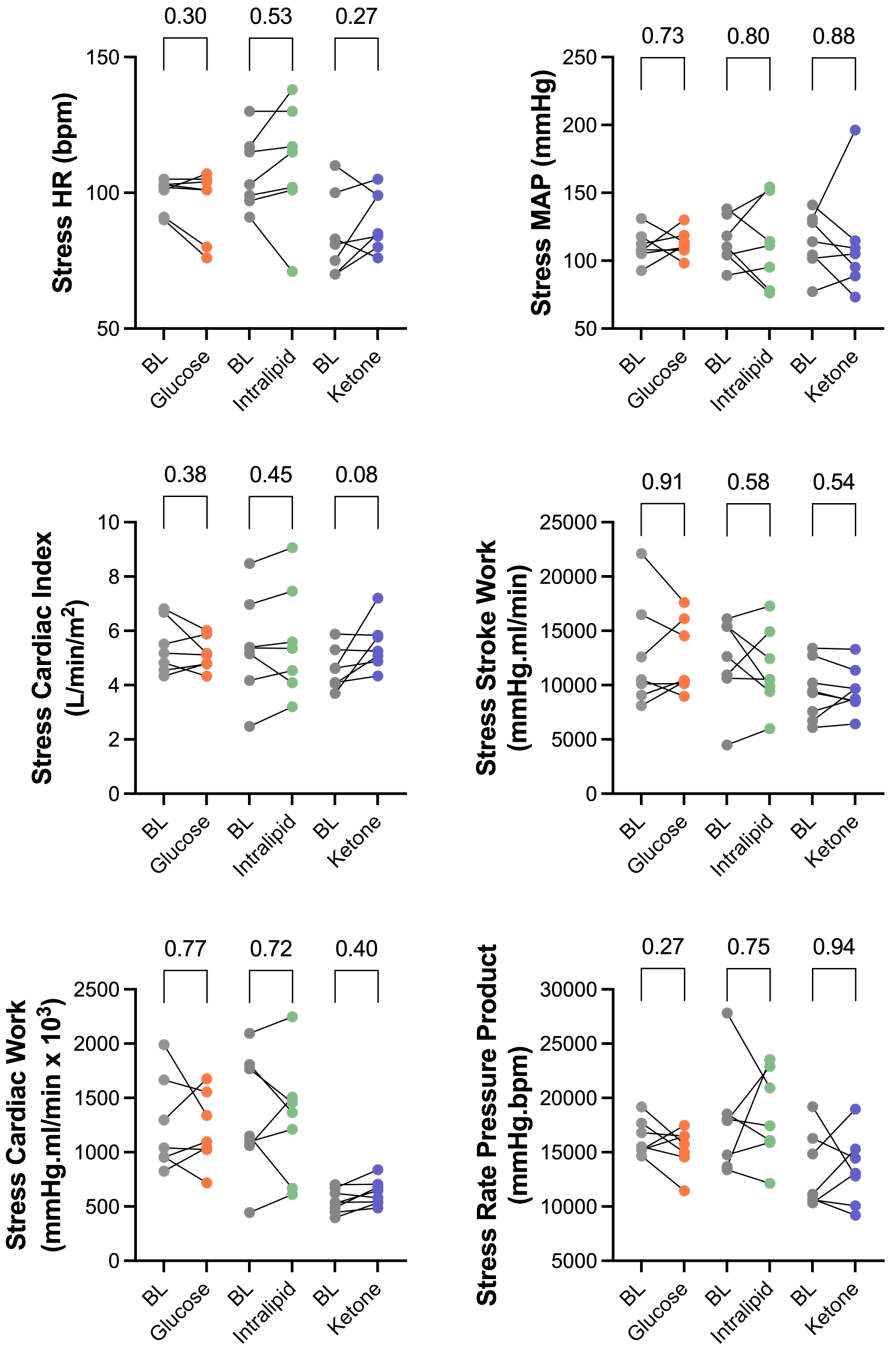

Figure 70: Stress haemodynamic parameters on substrate switching

Table 53: Cardiac output and work parameters during exercise on substrate switching

	Insulin + glucose			*Intralipid*			*Ketone ester*		
	Baseline	**Glucose**	**p-value**	**Baseline**	**Intralipid**	**p-value**	**Baseline**	**Ketone**	**p-value**
Cardiac Output (L/min)	11.12 ± 2.93	10.56 ± 2.11	0.39	11.36 ± 3.89	11.69 ± 4.01	0.38	9.43 ± 1.67	11.19 ± 1.83	0.08
Cardiac Index ($L/min/m^2$)	5.41 ± 0.99	5.15 ± 0.61	0.38	5.43 ± 1.92	5.62 ± 2.03	0.45	4.61 ± 0.76	5.48 ± 0.92	0.08
Stroke Work (mmHg.ml/min)	12718 ± 4982	12592 ± 3419	0.91	12235 ± 4077	11501 ± 3750	0.58	12875 ± 3097	14030 ± 5377	0.54
Cardiac Work (mmHg.ml/min x 10^3)	1248 ± 432	1207 ± 334	0.77	1346 ± 570	1296 ± 556	0.72	1079 ± 304	1238 ± 403.6	0.40
Rate Pressure Product (mmHg.bpm)	16327 ± 1631	15302 ± 1968	0.27	17732 ± 4947	18422 ± 4176	0.75	13303 ± 3498	13410 ± 3286	0.94

Table 54: Exercise blood pressure and heart rate on substrate switching

	Insulin + glucose			*Intralipid*			*Ketone ester*		
	Baseline	**Glucose**	**p-value**	**Baseline**	**Intralipid**	**p-value**	**Baseline**	**Ketone**	**p-value**
HR (bpm)	99.3 ± 6.1	96.3 ± 12.7	0.30	107.4 ± 13.7	110.6 ± 22.1	0.53	84.1 ± 15.4	89.7 ± 11.1	0.27
SBP (mmHg)	165.3 ± 23.1	160.3 ± 23.2	0.51	163.0 ± 25.7	168.0 ± 30.5	0.79	158.4 ± 32.0	151.1 ± 43.5	0.56
DBP (mmHg)	83.3 ± 10.7	89.0 ± 16.5	0.53	93.4 ± 28.5	83.4 ± 42.4	0.50	91.6 ± 24.8	92.1 ± 40.2	0.97
MAP (mmHg)	110.6 ± 11.8	112.8 ± 9.8	0.73	116.6 ± 21.5	111.6 ± 31.8	0.61	113.9 ± 21.6	111.8 ± 39.8	0.88

5.3.9 Myocardial energetics and triglyceride content during substrate switching

Intralipid resulted in a fall in the PCr/ATP ratio ($1.80 \pm 0.33 \rightarrow 1.26 \pm 0.42$, $p=0.04$) and therefore a fall in CK flux ($4.23 \pm 1.66 \rightarrow 2.10 \pm 1.05$ μmol/g/s, $p=0.02$). Whilst there was a numerical increase in triglyceride content this was not statistically significant. In the presence of insulin-glucose infusion there was no change in measured myocardial energetics parameters although there was an increase in myocardial triglyceride content ($1.38 \pm 1.06 \rightarrow 1.94 \pm 1.10\%$, $p=0.006$). Ketone ester ingestion did not result in a significant change in PCr/ATP ratio, k_f or triglyceride content. There was however a numerical increase in CK flux ($1.28 \pm 0.74 \rightarrow 4.25 \pm 4.32$ μmol/g/s, $p=0.06$).

Table 55: Myocardial energetics and triglyceride content during substrate switching

	Insulin + glucose			*Intralipid*			*Ketone ester*		
	Baseline	**Glucose**	**p-value**	**Baseline**	**Intralipid**	**p-value**	**Baseline**	**Ketone**	**p-value**
PCr/ATP ratio	1.32 ± 0.46	1.51 ± 0.23	0.33	1.80 ± 0.33	1.26 ± 0.42	***0.04***	1.57 ± 0.39	1.31 ± 0.22	0.15
CK forward pseudo first order rate constant (s^{-1})	0.37 ± 0.22	0.51 ± 0.46	0.94	0.48 ± 0.28	0.33 ± 0.17	0.27	0.32 ± 0.38	0.56 ± 0.63	0.40
Creatine kinase flux (μmol/g/s)	1.50 ± 0.65	5.00 ± 5.00	0.25	4.23 ± 1.66	2.10 ± 1.05	***0.02***	1.28 ± 0.74	4.25 ± 4.32	0.06
Myocardial triglyceride content (%)	1.38 ± 1.06	1.94 ± 1.10	***0.006***	2.25 ± 1.45	3.09 ± 2.02	0.20	3.04 ± 2.03	2.83 ± 1.84	0.82

5.3.10 Comparison of effects of substrate switching on energetics

A direct comparison of the effects of substrate switching illustrates that their effects on PCr/ATP are different (Kruskal Wallis p=0.03) with a statistically significant difference (p=0.03) noted between intralipid (-0.54 ± 0.50) and glucose (+0.19 ± 0.38). There were more marked differences in the effects of different substrates on CK flux (KW p=0.007). In particular, the effect of intralipid (-2.13 ± 1.33 μmol/g/s) was again different to that of glucose (+3.50 ± 4.88 μmol/g/s, p=0.03), but also ketone (+2.25 ± 4.18 μmol/g/s, p=0.04). There was no significant difference in their effects on k_f.

Table 56: Comparison of effects of substrates on cardiac energetic parameters

	Insulin + glucose	*Intralipid*	*Ketone ester*	*p-value*
PCr/ATP ratio	+0.19 ± 0.38¥	-0.54 ± 0.50¥	-0.26 ± 0.41	***0.03***
CK forward pseudo first order rate constant (s^{-1})	+0.14 ± 0.55	-0.15 ± 0.33	+0.26 ± 0.83	0.42
Creatine kinase flux (μmol/g/s)	+3.50 ± 4.88¥	-2.13 ± 1.33¥¥	+2.25 ± 4.18¥	***0.007***

Φ: Pairs of data significantly different at p<0.001, ‡: Pairs of data significantly different at p<0.01, ¥: Pairs of data significantly different at p<0.05

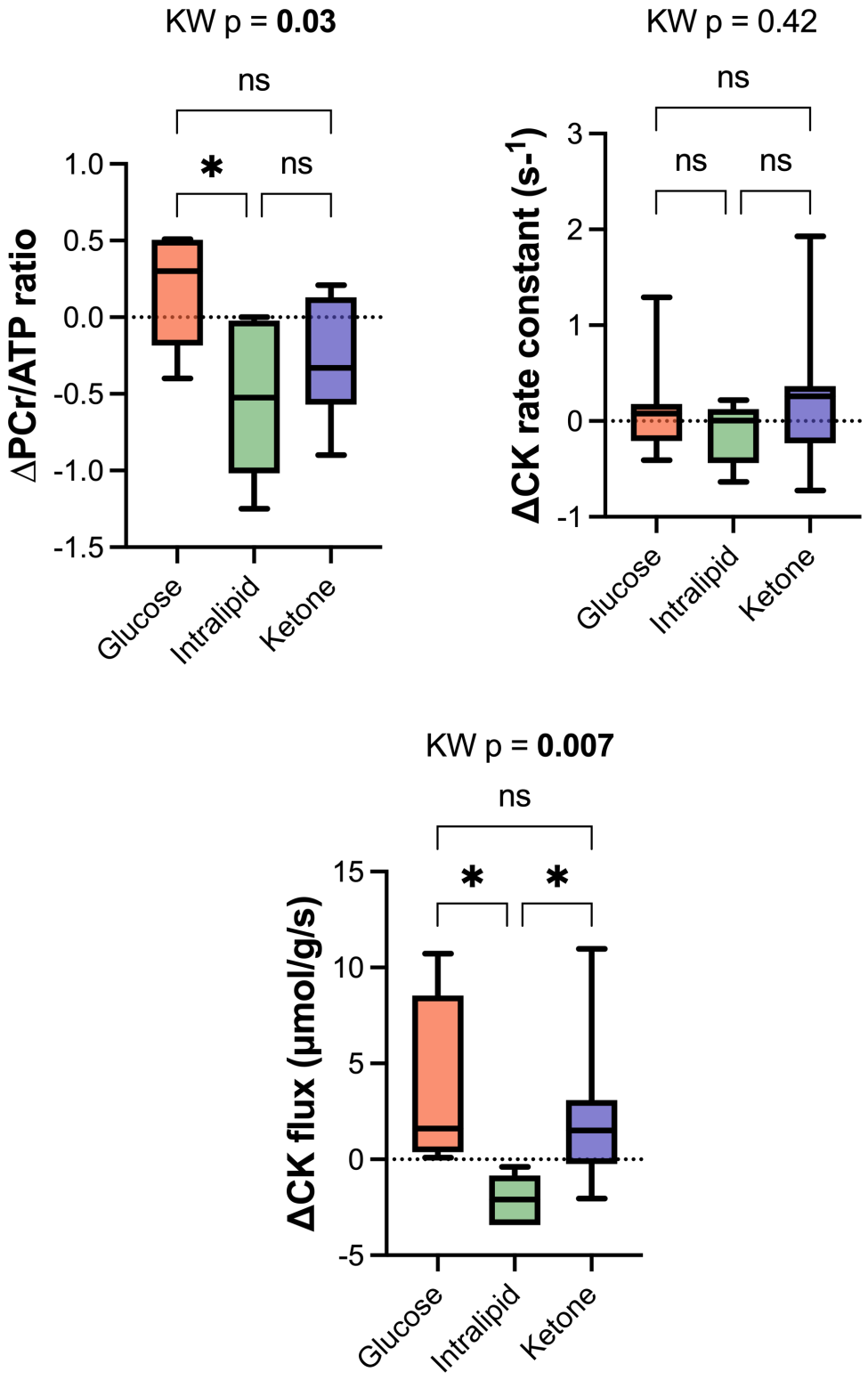

Figure 71: Changes in myocardial energetics on substrate switching

Data presented as medians and interquartile range.

KW: Kruskal Wallis, *p<0.05

5.3.11 Comparison of effects of substrate switching on cardiac function and output

At rest, there was a significant difference between the effects of different substrates on LVEF (ANOVA p=0.01), most marked between glucose (-0.8 ± 4.2%) and ketone (+6.2 ± 3.9%, p=0.01). Similarly, there was a notable difference in augmentation of cardiac index (ANOVA p=0.006) with the effect of ketone (+0.74 ± 0.33 L/min/m^2) being different to both glucose (+0.02 ± 0.55 L/min/m^2, p=0.007) and lipid (+0.13 ± 0.36L/min/m^2, p=0.02). There was a trend towards increased stroke volume augmentation in the ketone group (+5.8 ± 4.6 ml/m^2) compared to the others which did not meet statistical significance (ANOVA p=0.05). There was no difference in LVEDVi, LVESVi or diastolic function as measured on echocardiography by the E/E' ratio.

Table 57: Comparison of substrate effects on LV volumes and function at rest

	Insulin + glucose	***Intralipid***	***Ketone ester***	***p-value***
ΔLVEDVi (ml/m^2)	+4.0 ± 4.4	-0.9 ± 10.5	+1.8 ± 12.1	0.60
ΔLVESVi (ml/m^2)	+1.9 ± 3.1	-1.7 ± 7.9	-4.6 ± 6.7	0.14
ΔLVEF (%)	-0.8 ± 4.2‡	+2.2 ± 4.5	+6.2 ± 3.9‡	***0.01***
ΔLVSVi (ml/m^2)	+2.1 ± 3.3	+0.8 ± 3.8	+5.8 ± 4.6	0.05
ΔCardiac Index (L/min/m^2)	+0.02 ± 0.55‡	+0.13 ± 0.36¥	+0.74 ± 0.33‡¥	***0.006***
ΔE/E' (ratio)	-0.03 ± 1.2	-1.4 ± 1.9	-0.04 ± 1.6	0.14

Φ: Pairs of data significantly different at p<0.001, ‡: Pairs of data significantly different at p<0.01, ¥: Pairs of data significantly different at p<0.05

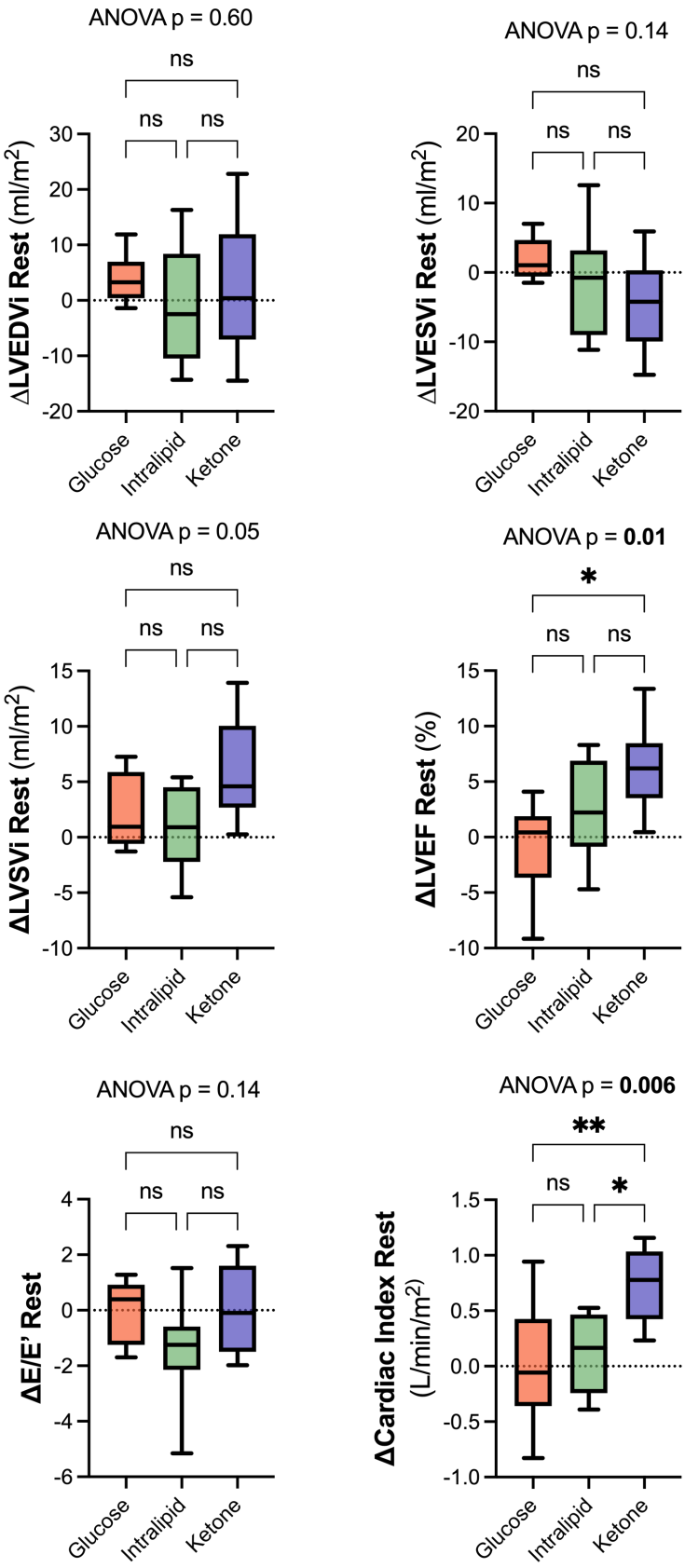

Figure 72: Comparison of substrate effects on LV volumes and function at rest

*p<0.05, **p<0.01

During exercise, there was a trend towards increased stroke volume augmentation by ketone (+0.87 ± 1.07 L/min/m², ANOVA p=0.06) but no differences in LVEDVi, LVESVi, LVEF or LVSVi. However, there was a relative improvement in diastolic function induced by ketosis (E/E' ratio -3.1 ± 2.3, ANOVA p=0.02), particularly compared to glucose (0.3 ± 2.3, p=0.02).

Table 58: Comparison of effects of substrates on LV function during exercise

	Insulin + glucose	***Intralipid***	***Ketone ester***	***p-value***
ΔLVEDVi (ml/m²)	-2.4 ± 7.1	+0.2 ± 9.0	+6.7 ± 8.5	0.13
ΔLVESVi (ml/m²)	-1.5 ± 4.6	-0.1 ± 7.8	+0.2 ± 4.6	0.62
ΔLVEF (%)	-5.8 ± 7.5	-0.7 ± 6.9	-2.7 ± 5.2	0.37
ΔLVSVi (ml/m²)	-0.8 ± 5.7	+0.2 ± 4.5	+6.5 ± 6.9	0.06
ΔCardiac Index (L/min/m²)	-0.26 ± 0.72	-0.46 ± 1.89	+0.87 ± 1.07	0.19
ΔE/E' (ratio)	0.3 ± 2.3¥	-0.9 ± 2.0	-3.1 ± 2.3¥	***0.02***

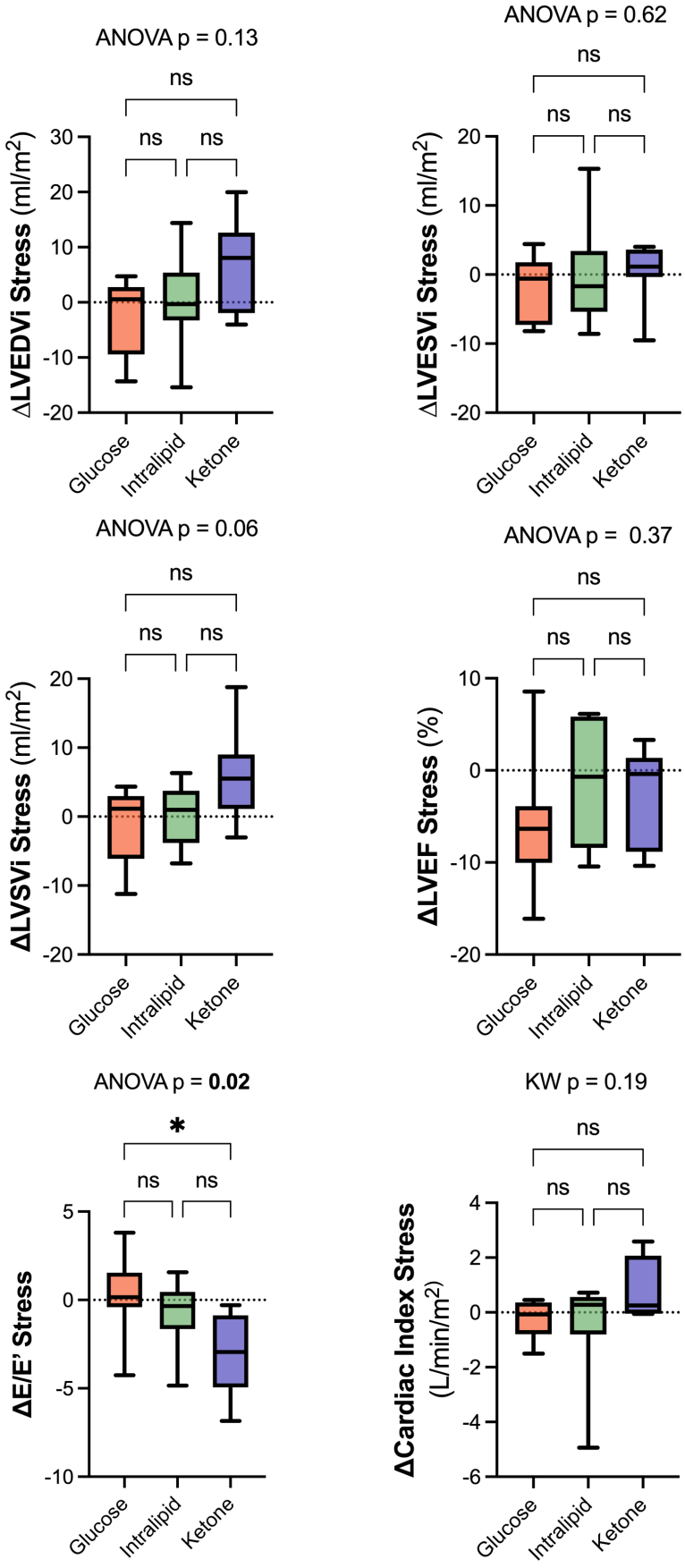

Figure 73: Comparison of effects of substrates on LV function during exercise

5.4 Results Part B: Mixed substrate augmentation

5.4.1 Circulating metabolites

In the glucose + ketone group, there was a significant difference in the levels of NEFA between baseline and substrates with progressively decreasing concentrations on addition of glucose followed by simultaneous ketone. As expected, addition of ketone ester results in an increase in βOHB ($p=0.001$) while insulin levels ($p<0.0001$) were higher with the euglycaemic clamp. There were no significant changes in the levels of lactate or NT-proBNP and glucose levels were held steady in the presence of the clamp.

In the small ($n=4$) intralipid + ketone group, the difference in NEFA levels were not significant nor were the levels of glucose, lactate or NT-proBNP. Insulin ($p=0.03$) and βOHB ($p=0.002$) levels were higher with co-administration of ketone ester.

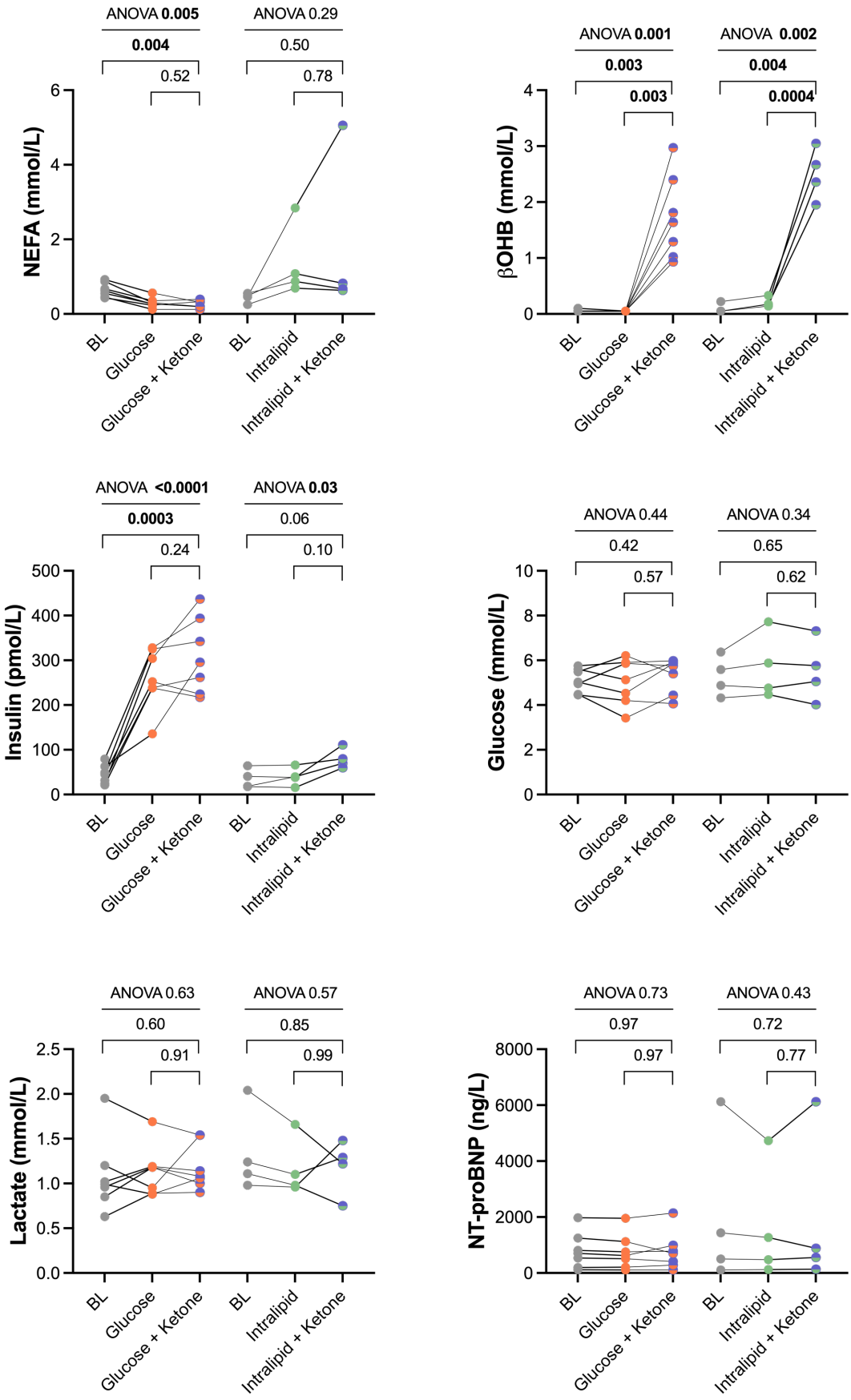

Figure 74: Change in metabolites with mixed substrate augmentation

Table 59: Change in metabolites with mixed substrate augmentation

	Insulin + glucose group				*Intralipid*			
	Baseline	**Glucose**	**Glucose + Ketone**	**p-value (ANOVA)**	**Baseline**	**Intralipid**	**Intralipid + Ketone**	**p-value (ANOVA)**
NEFA (mmol/L)	0.64 ± 0.19Φ‡	0.30 ± 0.14Φ	0.25 ± 0.10‡	***0.005***	0.44 ± 0.13	1.37 ± 0.99	1.80 ± 2.18	0.29
Glucose (mmol/L)	5.11 ± 0.53	5.04 ± 1.03	5.34 ± 0.78	0.44	5.29 ± 0.89	5.71 ± 1.47	5.54 ± 1.38	0.34
Insulin (pmol/L)	44.8 ± 21.2	260.3 ± 67.4	310.3 ± 84.2	***<0.0001***	35.3 ± 22.0	39.9 ± 20.7	80.1 ± 22.2	***0.03***
Lactate (mmol/L)	1.09 ± 0.42	1.14 ± 0.28	1.18 ± 0.26	0.63	1.34 ± 0.48	1.18 ± 0.33	1.19 ± 0.31	0.57
βOHB (mmol/L)	0.06 ± 0.02‡	0.05 ± 0.00‡	1.72 ± 0.75‡‡	***0.001***	0.09 ± 0.09‡‡	0.21 ± 0.09‡‡	2.51 ± 0.47‡‡	***0.002***
NT-proBNP (ng/L)	798 ± 645	755 ± 628	775 ± 677	0.73	2043 ± 2776	1650 ± 2110	1925 ± 2817	0.43

Φ: Pairs of data significantly different at p<0.001, ‡: Pairs of data significantly different at p<0.01, ¥: Pairs of data significantly different at p<0.05

5.4.2 Ventricular volumes and function at rest during mixed substrate augmentation

There was an increase in LVEF (p=0.0008) and LVSV (p=0.02) on CMR and LV S' on echocardiography (p=0.0001) when ketone was administered in addition to glucose relative to baseline state or glucose infusion alone. This was driven primarily by a decrease in LV end-systolic volume (p=0.003). In the intralipid group, similar trends were seen overall with an increase in LVSV (p=0.07) and LVEF (p=0.01). Unlike where ketone was administered alone, there was no change to LV GLS. No changes were seen in diastolic function.

Again, similar increases in RVEF (p=0.002) and RVSV (p=0.04) were seen in the glucose group when ketone ester was added. There was also an increase in RV SV/ESV (p=0.005). Similar trends persisted in the lipid group (p values for RVEF = 0.04, RVSV = 0.0004, RV SV/ESV = 0.05).

5.4.3 Atrial volumes and function at rest

There was no significant change to atrial volumes or emptying fraction with additional ketone in the glucose or lipid groups. The decrease in right atrial volumes seen on isolated ketone administration was not replicated in the presence of an additional substrate.

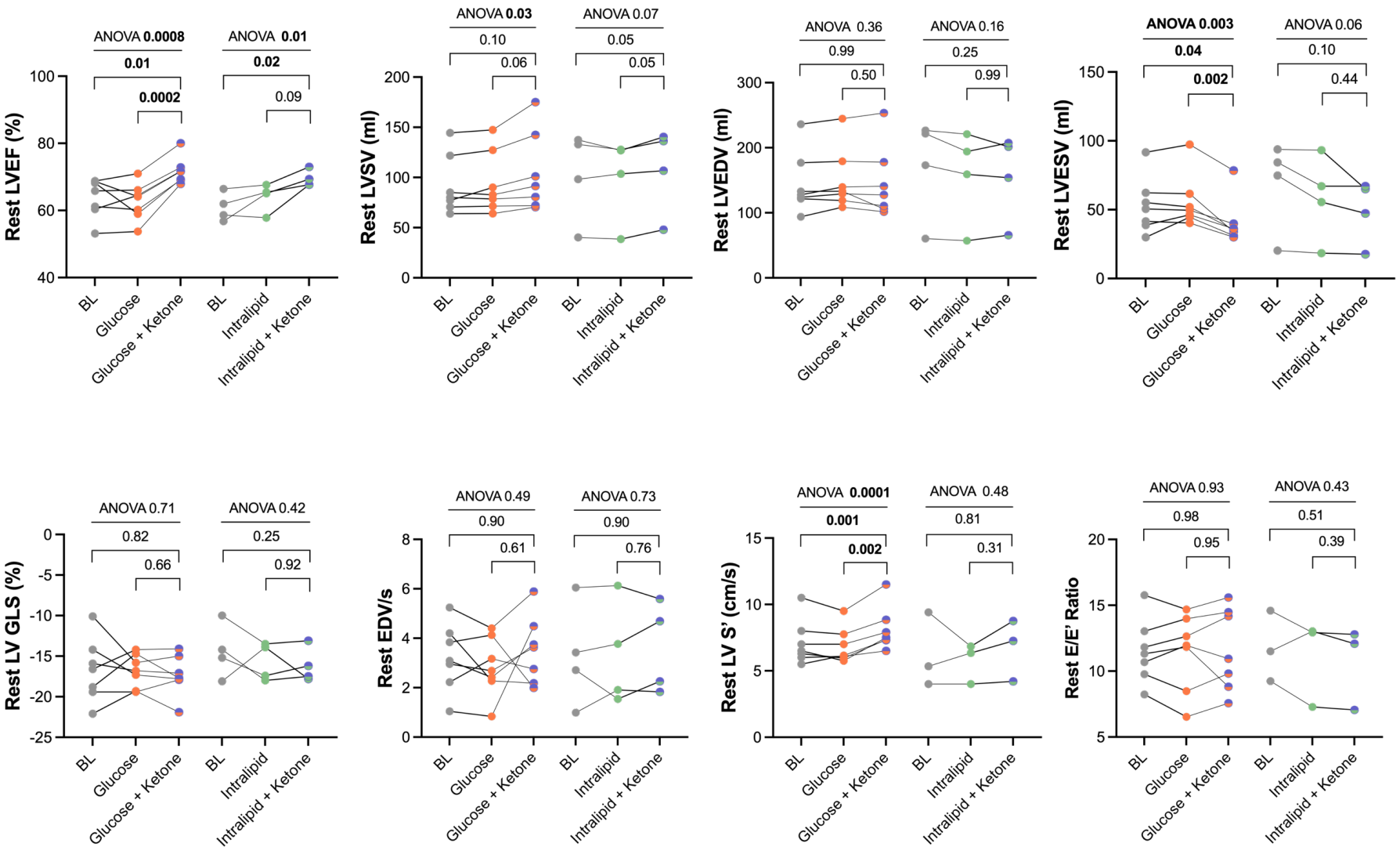

Figure 75: LV systolic and diastolic function at rest on mixed substrate augmentation

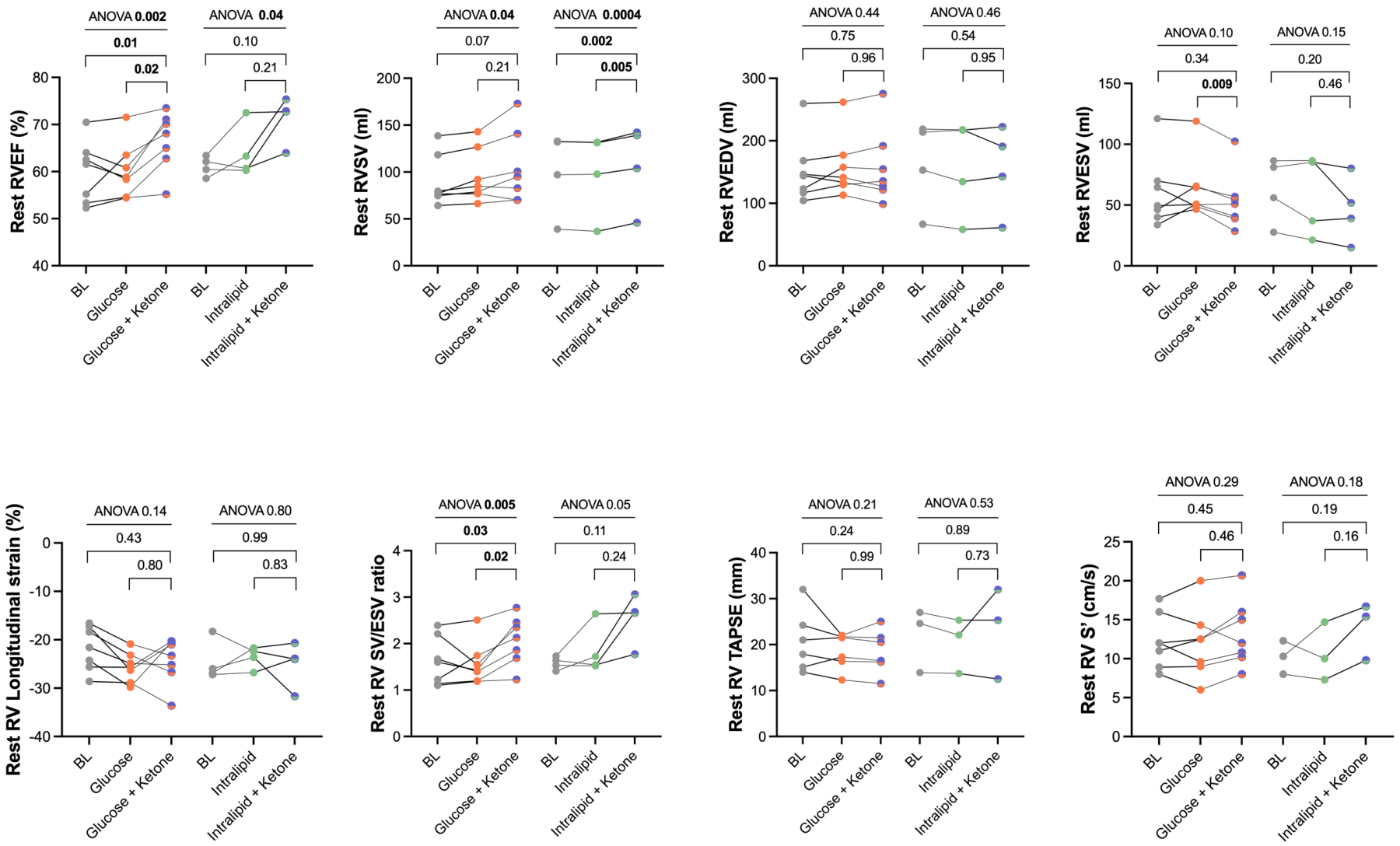

Figure 76: RV systolic function at rest on mixed substrate augmentation

Table 60: Ventricular parameters at rest on single and mixed substrates

	Insulin + glucose group (n=7)				*Intralipid (n=4)*			
	Baseline	**Glucose**	**Glucose + Ketone**	**p-value (ANOVA)**	**Baseline**	**Intralipid**	**Intralipid + Ketone**	**p-value (ANOVA)**
LVEDV (ml)	144.7 ± 47.2	150.4 ± 47.2	145.4 ± 54.4	***<0.0001***	170.5 ± 77.2	157.7 ± 71.7	157.1 ± 65.5	0.16
LVESV (ml)	52.9 ± 20.3¥	56.0 ± 19.4‡	40.7 ± 16.9¥‡	***0.003***	68.3 ± 32.9	58.6 ± 31.0	49.3 ± 22.9	0.05
LVEF (%)	63.7 ± 62.7¥	62.7 ± 5.6Φ	71.8 ± 4.0¥Φ	***0.0008***	61.0 ± 4.2¥	64.0 ± 4.3	69.4 ± 2.5¥	***0.01***
LVSV (ml)	91.9 ± 29.7	94.5 ± 30.9	104.7 ± 39.6	***0.02***	102.2 ± 44.9	99.2 ± 41.9	107.8 ± 42.7	0.07
LV GLS (%)	-16.7 ± 3.9	-16.8 ± 2.1	-17.4 ± 2.5	0.71	-14.4 ± 3.4	-15.7 ± 2.3	-16.2 ± 2.1	0.42
LV peak early filling rate (EDV/s)	3.23 ± 1.37	2.8 ± 1.2	3.5 ± 1.4	0.49	3.29 ± 2.10	3.33 ± 2.10	3.59 ± 1.83	0.72
RVEDV (ml)	151.8 ± 52.0	159.2 ± 49.8	157.9 ± 59.5	0.44	163.1 ± 70.8	156.9 ± 76.5	154.3 ± 70.3	0.46
RVESV (ml)	60.7 ± 29.5	63.7 ± 25.6‡	53.2 ± 23.9‡	0.10	62.8 ± 26.9	57.6 ± 33.4	46.5 ± 27.1	0.15
RVEF (%)	59.9 ± 6.6¥	60.3 ± 5.9¥	66.5 ± 6.2¥¥	***0.002***	61.1 ± 2.1	64.2 ± 5.7	71.2 ± 5.0	***0.04***
RVSV (ml)	89.9 ± 27.4	95.6 ± 28.3	104.7 ± 38.6	***0.04***	100.3 ± 44.1‡	99.3 ± 44.7‡	107.8 ± 44.7‡‡	***0.0004***
RV longitudinal strain (%)	-21.8 ± 4.6	-25.7 ± 3.1	-24.4 ± 4.8	0.14	-24.6 ± 4.2	-23.6 ± 2.3	-25.1 ± 4.7	0.80
RV SV/ESV ratio	1.62 ± 0.52¥	1.57 ± 0.46¥	2.07 ± 0.52¥¥	***0.005***	1.58 ± 0.14	1.85 ± 0.53	2.54 ± 0.55	0.05

Φ: Pairs of data significantly different at p<0.001, ‡: Pairs of data significantly different at p<0.01, ¥: Pairs of data significantly different at p<0.05

Table 61: Echocardiography at rest on single and mixed substrates

	Insulin + glucose group				*Intralipid*			
	Baseline	**Glucose**	**Glucose + Ketone**	**p-value (ANOVA)**	**Baseline**	**Intralipid**	**Intralipid + Ketone**	**p-value (ANOVA)**
E/E' average (ratio)	11.5 ± 2.4	11.4 ± 2.9	11.6 ± 3.1	0.93	11.8 ± 2.7	11.1 ± 3.3	10.6 ± 3.1	0.43
S' LV (cm/s)	7.1 ± 1.7‡	6.9 ±1.3‡	8.1 ±1.6‡‡	***0.0001***	6.3 ± 2.8	5.7 ± 1.5	6.7 ± 2.3	0.48
TAPSE (mm)	20.7 ± 6.7	18.5 ± 3.9	18.5 ± 4.8	0.21	21.8 ± 7.0	20.4 ± 6.0	23.3 ± 9.9	0.53
S' RV (cm/s)	12.2 ± 3.5	12.0 ± 4.5	13.2 ± 4.3	0.32	10.2 ± 2.2	10.7 ± 3.7	14.0 ± 3.7	0.18
Estimated PASP (mmHg)	31.1 ± 11.3	32.9 ± 8.6	31.7 ± 10.4	0.59	22.0	20.4	17.1	N/A (1 dataset)

Table 62: Atrial parameters at rest on single and mixed substrates

	Insulin + glucose group				*Intralipid group*			
	Baseline	**Glucose**	**Glucose + Ketone**	**p-value (ANOVA)**	**Baseline**	**Intralipid**	**Intralipid + Ketone**	**p-value (ANOVA)**
LAEDV (ml)	123.0 ± 95.1	125.5 ± 96.4	120.6 ± 91.5	0.73	110.7 ± 61.8	116.1 ± 59.5	99.7 ± 57.3	0.12
LAESV (ml)	165.0 ± 102.1	159.7 ± 94.1	156.1 ± 93.5	0.40	147.3 ± 63.0	150.5 ± 57.2	130.1 ± 51.2	0.15
LAEF (%)	32.3 ± 17.4	28.0 ± 16.3	30.1 ± 17.8	0.31	26.7 ± 20.6	24.7 ± 16.5	26.5 ± 21.0	0.65
RAEDV (ml)	149.7 ± 119.1	144.1 ± 117.2	151.2 ± 112.1	0.53	139.4 ± 96.7	144.7 ± 77.5	124.3 ± 88.3	0.20
RAESV (ml)	178.4 ± 126.3	179.5 ± 118.4	196.6 ± 130.9	0.10	173.3 ± 85.4	176.1 ± 61.1	166.7 ± 83.7	0.71
RAEF (%)	21.4 ± 11.4	26.4 ± 15.4	27.6 ± 11.0	0.12	23.8 ± 16.9	20.8 ± 18.0	29.3 ± 19.2	0.08

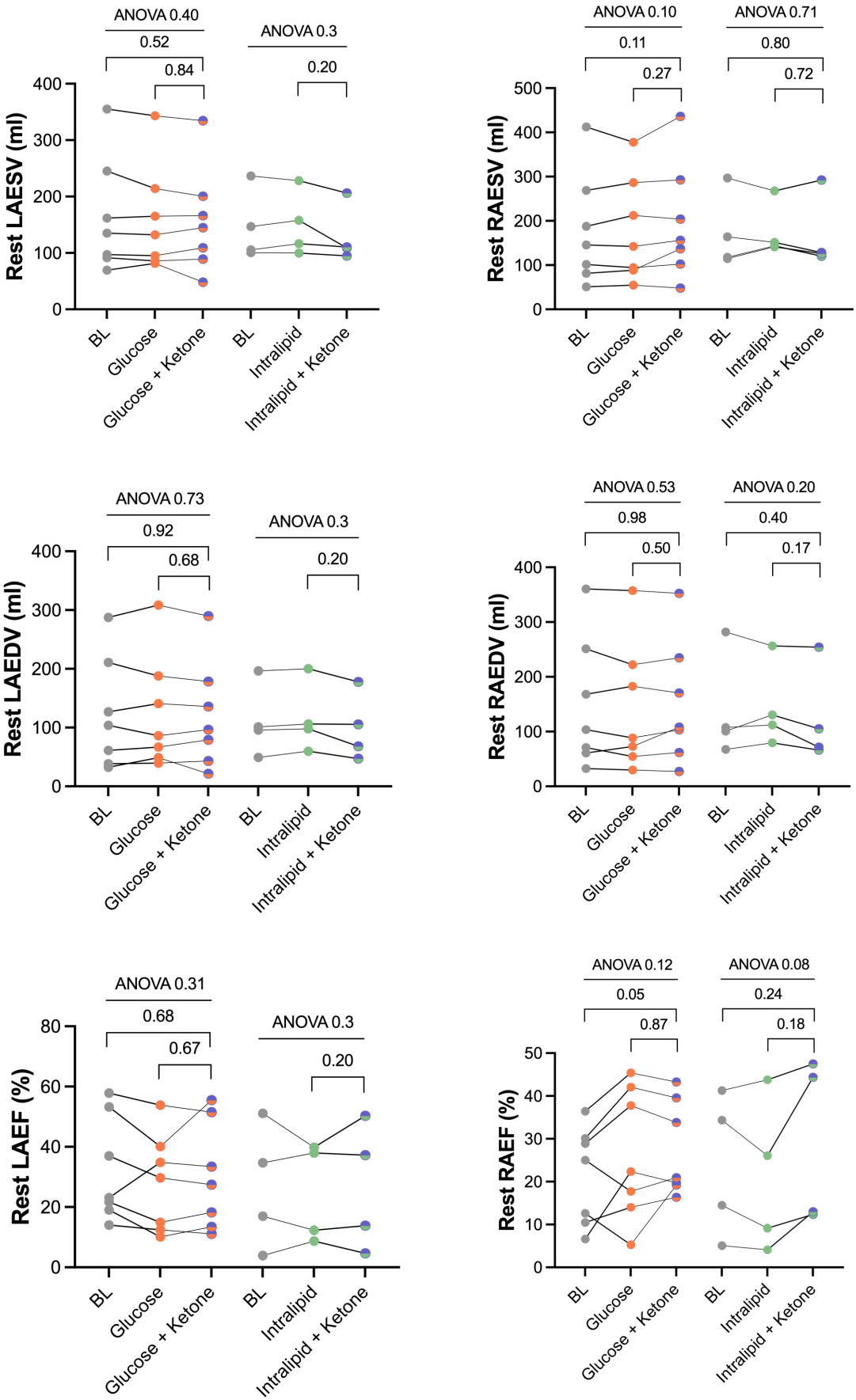

Figure 77: Atrial parameters at rest on single and mixed substrates

5.4.4 Cardiac output and haemodynamics at rest

There was an increase in cardiac output when ketone was added to glucose (p=0.005) or lipid (p=0.03), driven by an increase in LVSV and heart rate (p=0.04 for both groups). While there were numerical reductions in blood pressure in the presence of ketone compared to either glucose or intralipid alone, this did not meet statistical significance in either group.

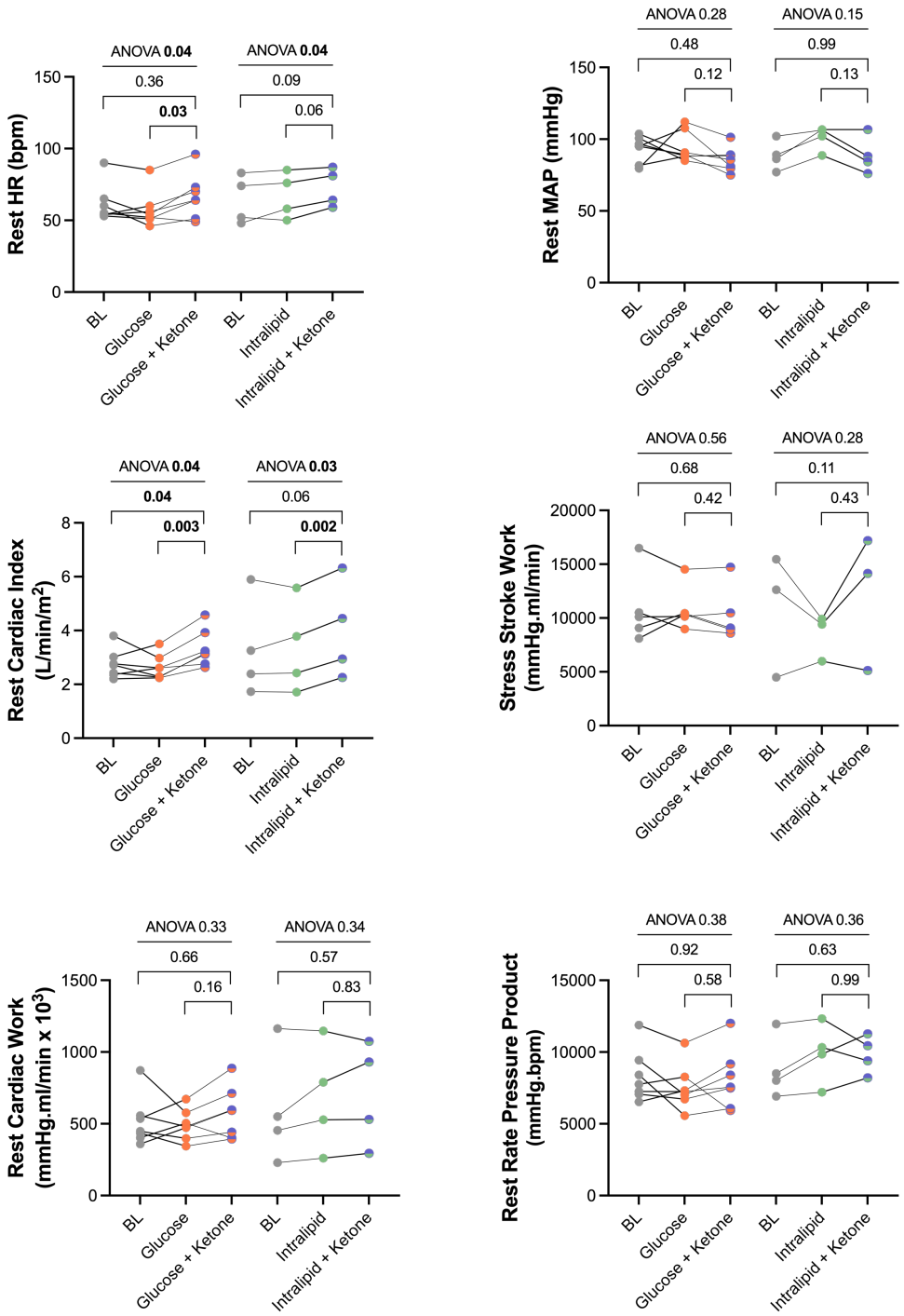

Figure 78: Cardiac output and work at rest on single and mixed substrate

Table 63: Cardiac output and work at rest on single and mixed substrate

	Insulin + glucose group				*Intralipid*			
	Baseline	**Glucose**	**Glucose + Ketone**	**p-value (ANOVA)**	**Baseline**	**Intralipid**	**Intralipid + Ketone**	**p-value (ANOVA)**
Cardiac Output (L/min)	5.52 ± 1.63	5.29 ± 1.42‡	6.70 ± 2.00‡	***0.005***	6.47 ± 3.58	6.58 ± 3.35‡	7.78 ± 3.56‡	***0.03***
Cardiac Index (L/min/m^2)	2.76 ± 0.54¥	2.64 ± 0.46‡	3.34 ±0.69¥‡	***0.003***	3.32 ± 1.83	3.37 ± 1.71‡	4.00 ± 1.80‡	***0.03***
Stroke Work (mmHg.ml/min)	8538 ± 2930	8836 ± 2555	8941 ± 3261	0.74	9331 ± 4679	10274 ± 4781	9882 ± 4744	0.46
Cardiac Work (mmHg.ml/min x 10^3)	515.9 ± 171.9	492.8 ± 108.3	575.0 ± 181.5	0.33	599.3 ± 399.1	681.2 ± 378.4	707.7 ± 358.7	0.34
Rate Pressure Product (mmHg.bpm)	8333 ± 1830	7537 ± 1582	8086 ± 2080	0.38	8849 ± 2174	9930 ± 2110	9825 ± 1325	0.36

Table 64: Heart rate and blood pressure at rest on single and mixed substrate

	Insulin + glucose group				*Intralipid*			
	Baseline	**Glucose**	**Glucose + Ketone**	**p-value (ANOVA)**	**Baseline**	**Intralipid**	**Intralipid + Ketone**	**p-value (ANOVA)**
HR (bpm)	61.6 ± 13.3	57.7 ± 12.8¥	66.7 ± 15.7¥	***0.04***	64.3 ± 16.9	67.3 ± 16.1	72.8 ± 13.4	**0.04**
SBP (mmHg)	135.3 ± 8.0	131.3 ± 14.4	120.9 ± 4.5	0.06	139.8 ± 21.8	148.8 ± 14.7	137.8 ± 27.4	0.28
DBP (mmHg)	72.1 ± 12.9	76.0 ± 10.6	68.1 ± 12.4	0.47	63.0 ± 14.8	77.0 ± 9.4	64.3 ± 9.0	0.17
MAP (mmHg)	93.2 ± 9.1	94.4 ± 10.7	85.7 ± 8.5	0.28	88.6 ± 10.3	100.9 ± 8.4	88.8 ± 13.0	0.15

5.4.5 Cardiac energetics at rest

There were no significant differences in PCr/ATP ratio, CK k_f, CK flux or myocardial triglyceride content across groups when ketone was added to either glucose or lipid. Numbers of acceptable data points were however low, particularly in the intralipid group.

Table 65: Myocardial energetics and CK flux at rest on single and mixed substrate

	Insulin + glucose group			
	Baseline	**Glucose**	**Glucose + Ketone**	**p-value**
PCr/ATP ratio	1.26 ± 0.50	1.49 ± 0.26	1.33 ± 0.43	0.65
k_f (s^{-1})	0.45 ± 1.22	0.35 ± 0.18	0.59 ± 0.30	0.39
CK flux (μmol/g/s)	1.69 ± 0.96	2.34 ± 1.75	3.97 ± 4.12	N/A
Myocardial triglyceride (%)	1.41 ± 1.16	1.99 ± 1.20	1.26 ± 0.73	0.33

	Intralipid group			
	Baseline	**Intralipid**	**Intralipid + Ketone**	**p-value**
PCr/ATP ratio	1.98 ± 0.40	1.34 ± 0.46	1.38 ± 0.04	N/A (2 datasets)
k_f (s^{-1})	0.68 ± 0.15	0.37 ± 0.23	0.27 ± 0.17	0.12
CK flux (μmol/g/s)	5.78 ± 0.11	3.02 ± 1.05	1.28 ± 0.06	N/A (2 datasets)
Myocardial triglyceride (%)	1.49 ± 0.78	2.78 ± 1.37	1.78 ± 0.83	0.23

5.4.6 Ventricular volumes and function during exercise

The number of participants who underwent exercise stress in each group were small and results are exploratory and to provide comparison to effects of isolated ketone administration. There is insufficient statistical power to perform direct comparisons with the effect sizes in most cases.

The trends of an increase in LVEF and LVSV driven by a reduction in LVESV were seen in both glucose and intralipid groups when ketone was added. This is consistent with the results of isolated ketone administration and from mixed substrate augmentation at rest. Similar trends of improvement in LV diastolic function and an increase in RVEF and RVSV were seen. There was also a reduction in estimated pulmonary artery systolic pressure with ketone administered in addition to glucose infusion ($p=0.002$).

5.4.7 Atrial volumes and function during exercise

In both groups, there were trends toward a decrease in left and right atrial volumes at ventricular end-diastole, but less pronounced at ventricular end-systole. There were no significant changes to emptying fractions.

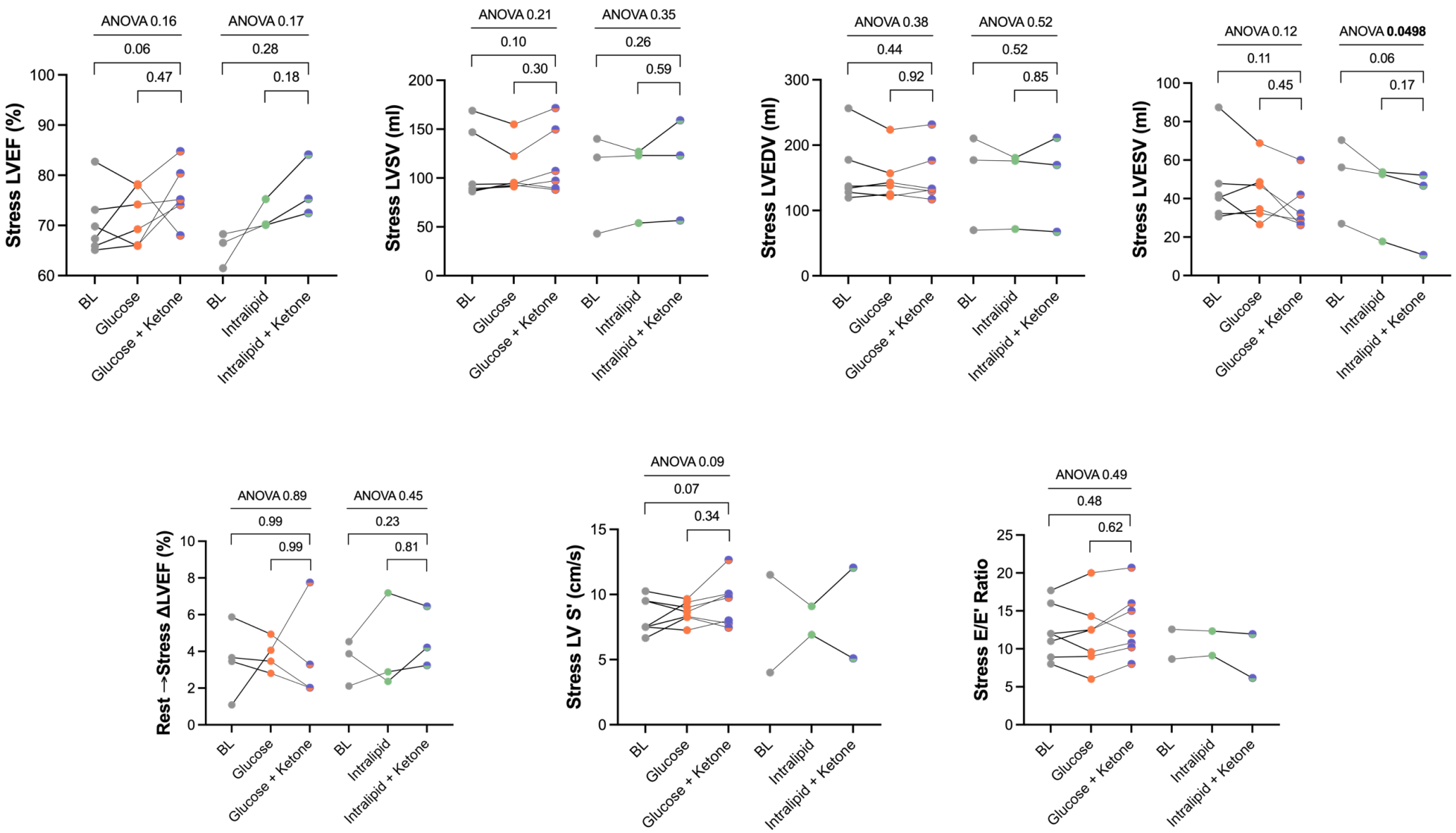

Figure 79: LV systolic and diastolic function during exercise on mixed substrate augmentation

Table 66: Ventricular parameters at stress on single and mixed substrates

	Insulin + glucose group				*Intralipid*			
	Baseline	**Glucose**	**Glucose + Ketone**	**p-value (ANOVA)**	**Baseline**	**Intralipid**	**Intralipid + Ketone**	**p-value (ANOVA)**
LVEDV (ml)	158.8 ± 51.8	151.4 ± 37.6	153.3 ± 43.4	0.38	152.5 ± 73.4	142.7 ± 61.6	149.4 ± 74.1	0.52
LVESV (ml)	46.7 ± 20.9	42.9 ± 15.2	36.1 ± 13.1	0.12	51.2 ± 22.1	41.4 ± 20.5	36.5 ± 22.5	***0.0498***
LVEF (%)	70.7 ± 6.6	71.9 ± 5.6	76.3 ± 5.7	0.16	65.4 ± 3.5	71.9 ± 2.9	77.3 ± 6.1	0.17
LVSV (ml)	112.1 ± 36.3	108.5 ± 25.6	117.2 ± 35.0	0.21	101.4 ± 51.4	101.3 ± 41.1	112.9 ± 52.0	0.35
LV peak early filling rate (EDV/s)	3.5 ± 1.95	3.8 ± 0.9	3.8 ± 2.7	0.89	3.5 ± 1.3	4.15 ± 2.65	4.63 ± 1.65	0.45
RVEDV (ml)	178.5 ± 66.1	173.4 ± 44.3	171.6 ± 63.0	0.74	161.4 ± 92.2	164.3 ± 76.2	169.6 ± 101.6	0.79
RVESV (ml)	66.2 ± 38.3	65.6 ± 20.9	55.5 ± 28.6	0.28	57.0 ± 40.5	61.3 ± 39.4	55.6 ± 54.9	0.77
RVEF (%)	64.2 ± 7.2	62.5 ± 4.6	68.4 ± 7.2	0.09	66.2 ± 5.9	63.6 ± 9.1	71.8 ± 12.5	0.26
RVSV (ml)	112.3 ± 31.9	107.8 ± 25.4	116.1 ± 39.1	0.28	104.5 ± 53.7	103.0 ± 42.4	114.0 ± 50.8	0.23
RV SV/ESV ratio	1.90 ± 0.65	1.70 ± 0.35	2.33 ± 0.85	0.12	2.02 ± 0.49	1.89 ± 0.82	2.95 ± 1.40	0.21

Φ Pairs of data significantly different at p<0.001, ‡ :significantly different at p<0.01, ¥ : significantly different at p<0.05

Table 67: Atrial parameters at stress on single and mixed substrates

	Insulin + glucose group				*Intralipid group*			
	Baseline	**Glucose**	**Glucose + Ketone**	**p-value (ANOVA)**	**Baseline**	**Intralipid**	**Intralipid + Ketone**	**p-value (ANOVA)**
LAEDV (ml)	132.1 ± 100.0	130.9 ± 103.1	131.5 ± 106.4	0.91	115.2 ± 76.0	119.1 ± 67.2	100.2 ± 61.6	0.13
LAESV (ml)	176.6 ± 104.5	173.8 ± 102.8	179.2 ± 108.7	0.59	144.6 ± 68.4	157.4 ± 78.4	145.1 ± 68.6	0.28
LAEF (%)	35.5 ± 15.3	36.3 ± 19.0	38.4 ± 20.2	0.60	25.1 ± 22.9	26.3 ± 8.2	33.4 ± 21.1	0.46
RAEDV (ml)	155.6 ± 120.9	175.8 ± 150.4	159.8 ± 122.2	0.25	147.3 ± 107.7	152.8 ± 110.0	117.9 ± 77.43	0.21
RAESV (ml)	214.9 ± 141.0	216.2 ± 137.5	216.6 ± 144.2	0.90	193.4 ± 134.2	196.8 ± 125.7	185.3 ± 116.4	0.52
RAEF (%)	34.0 ± 14.3	30.0 ± 22.5	32.5 ± 14.9	0.59	25.7 ± 16.2¥	24.9 ± 14.1	36.2 ± 17.4¥	0.08

Table 68: Echocardiography at stress on single and mixed substrates

	Insulin + glucose group				*Intralipid group*			
	Baseline	**Glucose**	**Glucose + Ketone**	**p-value (ANOVA)**	**Baseline**	**Intralipid**	**Intralipid + Ketone**	**p-value (ANOVA)**
E/E' average (ratio)	12.5 ± 2.7	12.8 ± 3.4	12.0 ± 2.5	0.49	10.6 ± 2.8	10.7 ± 2.3	9.1 ± 4.1	N/A
S' LV (cm/s)	8.3 ± 1.4	8.6 ± 0.8	9.4 ± 1.8	0.09	7.8 ± 5.3	8.0 ± 1.6	8.6 ± 4.9	N/A
TAPSE (mm)	22.1 ± 5.1	23.2 ± 7.3	21.3 ± 4.9	0.57	20.7 ± 10.0	23.1 ± 10.3	21.2 ± 7.4	N/A
S' RV (cm/s)	14.4 ± 4.2	13.7 ± 5.3	12.8 ± 2.3	0.47	14.7 ± 8.0	11.4 ± 3.7	15.0 ± 3.7	N/A
Estimated PASP (mmHg)	42.0 ± 13.7	47.6 ± 7.4¥	31.0 ±9.4¥	***0.002***	No data*	No data*	No data*	N/A

***Only 2 stress datasets for intralipid**

5.4.8 Cardiac output and haemodynamics during exercise

As before, the numerical cardiac output was highest in the presence of ketonaemia in both groups with no clear patterns to changes in cardiac work. However, these trends were not statistically significant.

There were no significant changes to heart rate during exercise across groups. However, SBP was significantly lower with the addition of ketone in the intralipid + ketone group ($p=0.04$), although MAP was not. Numerically all BP metrics were lower with addition of ketone in the glucose + ketone group, but none met statistical significance.

Table 69: Cardiac output and work at stress on single and mixed substrate

	Insulin + glucose group				*Intralipid group*			
	Baseline	**Glucose**	**Glucose + Ketone**	**p-value (ANOVA)**	**Baseline**	**Intralipid**	**Intralipid + Ketone**	**p-value (ANOVA)**
Cardiac Output (L/min)	10.96 ± 3.18	10.18 ± 2.02	11.11 ± 2.25	0.23	10.55 ± 6.08	10.59 ± 6.22	11.76 ± 6.75	0.43
Cardiac Index ($L/min/m^2$)	5.40 ± 1.08	5.03 ± 0.57	5.51 ± 0.75	0.20	5.37 ± 3.01	5.45 ± 3.16	6.06 ± 3.43	0.40
Stroke Work (mmHg.ml/min)	10860 ± 3287	10883 ± 2119	10364 ± 2544	0.56	10856 ± 5694	8433 ± 2124	12156 ± 6272	0.29
Cardiac Work (mmHg.ml/min x 10^3)	1089 ± 331.7	1087 ± 300	1026 ± 200	0.59	1134 ± 682	881.8 ± 420.5	1257 ± 768.1	0.27
Rate Pressure Product (mmHg.bpm)	15975 ± 1233	14782 ± 2061	14131 ± 1724	0.11	16606 ± 2815	17050 ± 5446	14390 ± 2791	0.66

Table 70: Heart rate and blood pressure at stress on single and mixed substrate

	Insulin + glucose group				*Intralipid group*			
	Baseline	**Glucose**	**Glucose + Ketone**	**p-value (ANOVA)**	**Baseline**	**Intralipid**	**Intralipid + Ketone**	**p-value (ANOVA)**
HR (bpm)	98.7 ± 6.5	95.0 ± 13.4	96.8 ± 8.9	0.51	102.3 ± 13.3	103.7 ± 33.5	103.3 ± 21.0	0.96
SBP (mmHg)	159.2 ± 10.4	149.4 ± 10.0	141.6 ± 15.5	0.17	149.7 ± 3.1	164.3 ± 7.6Φ	139.7 ± 6.8Φ	***0.04***
DBP (mmHg)	81.2 ± 12.3	89.0 ± 12.8	75.4 ± 5.1	0.29	84.7 ± 3.8	50.7 ± 33.2	87.0 ± 15.4	0.30
MAP (mmHg)	107.2 ± 9.4	109.1 ± 7.3¥	97.5 ± 5.4¥	0.16	106.3 ± 3.5	88.6 ± 19.7	104.6 ± 12.5	0.41

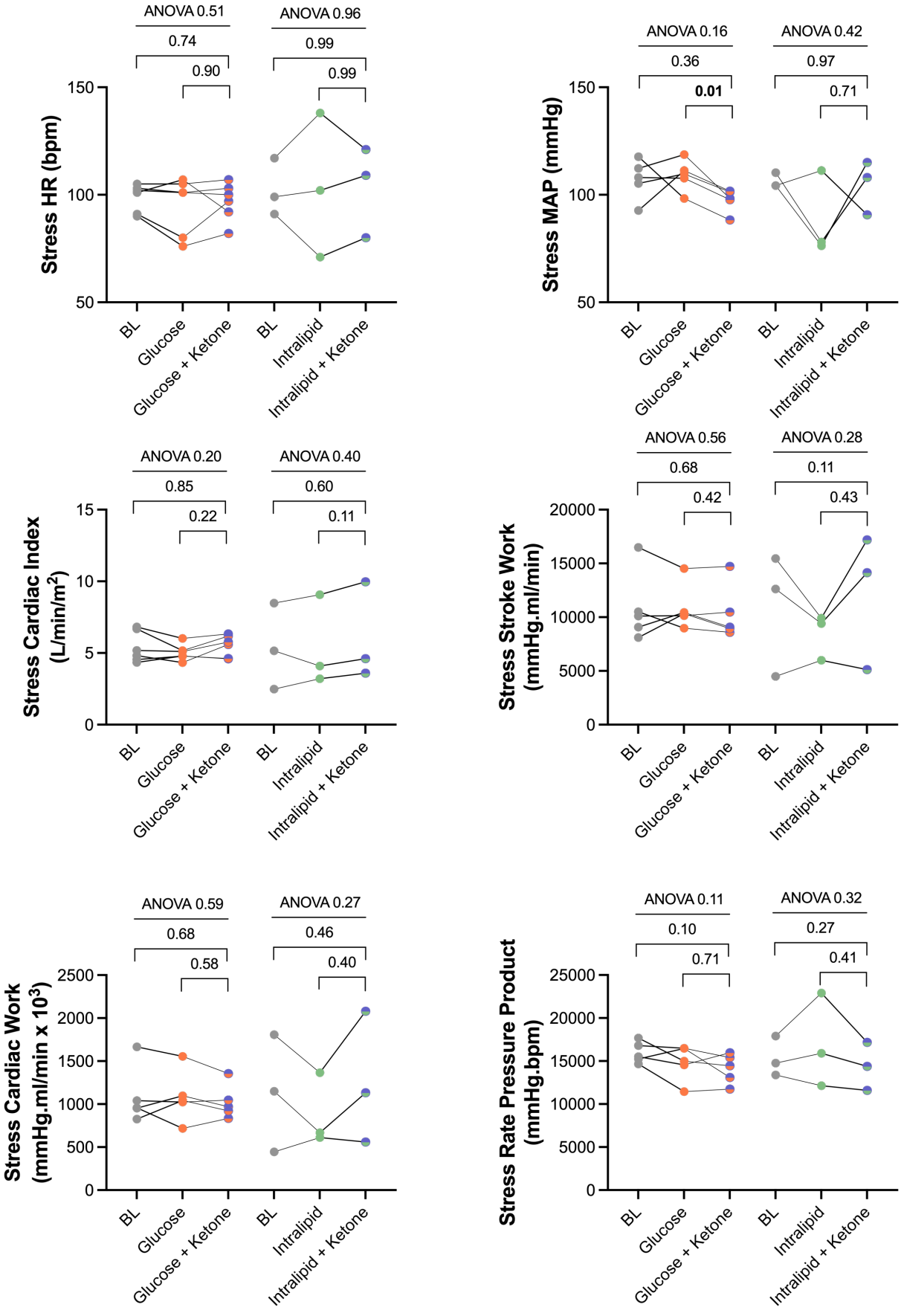

Figure 80: Cardiac output and work at stress on single and mixed substrate

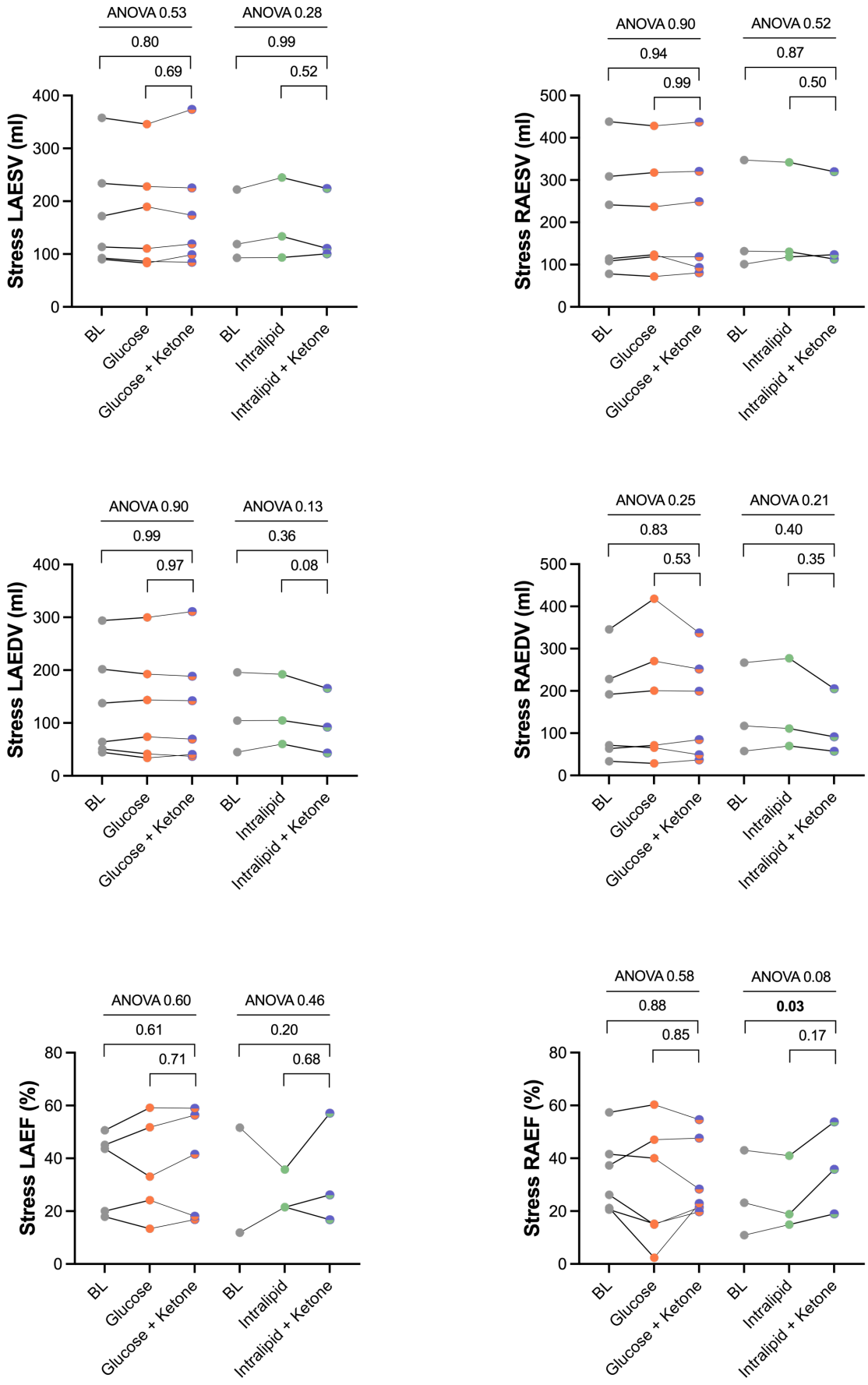

Figure 81: Heart rate and blood pressure at stress on single and mixed substrate

5.5 Results Part C: Invasive paired blood sampling for trans-cardiac extraction

One of the patients who took part in the MRI study and was randomised to the ketone group was invited for a pilot trans-cardiac extraction study. There was trans-cardiac extraction of NEFA and ketones at all 4 sampling points in this individual. There was also an increase in coronary sinus flow rate in the presence of ketonaemia resulting in increased oxygen extraction at both rest and during exercise. Lactate consumption increased following exercise as expected. Right atrial pressure at rest was lower following ketone administration although arterial pressures were not.

Table 71: Trans-cardiac extraction of metabolites at baseline and on provision of ketone

	Baseline - Rest		**Baseline - Exercise**		**Ketone - Rest**		**Ketone - Exercise**	
	Art	**CS**	**Art**	**CS**	**Art**	**CS**	**Art**	**CS**
NEFA (mmol/L)	1.85	1.34	1.67	1.37	1.43	1.18	0.99	0.78
Glucose (mmol/L)	5.76	5.75	5.79	5.81	5.68	5.60	5.62	5.65
Insulin (pmol/L)	58.3	46.2	91.1	87.7	153.5	163.3	141.3	142.7
Lactate (mmol/L)	1.43	1.28	3.92	2.80	2.01	2.03	4.35	3.46
βOHB (mmol/L)	0.46	0.25	0.59	0.35	2.56	1.66	2.11	1.44
Coronary sinus flow rate (ml/min)	220		430		330		710	

Oxygen content difference (ml/dl)	15.7	15	16.4	15.8
Oxygen extraction (MVO_2, ml/min)	34.5	64.5	54.1	112.2
Right atrial pressure (mmHg)	23	20	14	16
Radial blood pressure (mmHg)	120/68	156/90	161/89	186/88

Green indicates potential extraction. Haemoglobin was 162 g/L in this individual. Oxygen content was calculated as (Haemoglobin x 1.36) x (Oxygen saturation / 100) + partial pressure of oxygen x 0.003). Oxygen extraction was calculated as coronary sinus flow x Oxygen content.

5.6 Discussion

The key findings of this chapter are:

1. There are fundamental differences in the cardiac energetic state, left ventricular function and cardiac output on substrate switching.
2. Provision of long chain fatty acids results in impairment of the overall cardiac energetic state (PCr/ATP ratio) and ATP delivery (CK flux) but without discernible effects on cardiac function or cardiac output despite an increase in cardiac work and rate pressure product.
3. Ketonaemia results in improved systolic function and cardiac output at rest and potentially during exercise. It also improved diastolic function during exercise. This does not appear to impair PCr/ATP at rest and may result in an increase in ATP delivery (CK flux) along with increased cardiac work at rest.
4. Ketonaemia results in systemic effects including vasodilatation and increase in heart rate.
5. The effects of ketones on cardiac function and output generally appear preserved even when co-administered with insulin-glucose or intralipid.
6. Insulin-glucose infusion has no significant effects on overall myocardial energetics, LV function or cardiac output but alters RV metrics at rest.

There is impairment of the cardiac energetic state and ATP delivery with provision of free fatty acids

Compared to the baseline state, there is a significant reduction in PCr/ATP indicative of deterioration in the overall cardiac energetic state. This appears to drive a decline in ATP delivery as measured by CK flux. This occurred despite relatively modest increases in circulating free fatty acid, likely due to heparin not being co-administered. There are a few potential ways in which this could occur.

If the ability to utilise fatty acids in oxidative phosphorylation is exhausted and any additional fatty acids are stored as indicated by raised myocardial triglyceride storage at baseline, then provision of fatty acids is unlikely to enable greater production of ATP. Simultaneously, elevation of FFA levels in the plasma result in a reduction in cardiac glucose uptake further depriving the myocardium of an alternative fuel source[160]. Interestingly, there was no statistically significant increase in myocardial

triglyceride content. This could potentially reflect sufficiently fast utilisation of fatty acids.

In such a scenario where fatty acids are oxidised, then inhibition of glycolysis and glucose oxidation may result in an unfavourable energetic state. Microvascular dysfunction may limit blood supply relative to demand particularly during exercise and can starve the heart of oxygen, thus favouring use of a substrate with a higher P:O ratio[242]. If the heart were to switch to using free fatty acids, then ATP production may fall resulting in a lower PCr/ATP ratio and reduced ATP delivery via the CK shuttle.

These results indicate that metabolism in HFpEF is fundamentally different to that of healthy myocardium and HFrEF. In healthy myocardium, administration of intralipid compared to insulin-glucose increases LVEF while PCr/ATP remains the same, but there is an increase in the CK k_f and potentially CK flux[186]. In HFrEF, intralipid resulted in an increase in PCr/ATP ratio and LVEF without change in k_f and a numerical but not statistically significant increase in CK flux.

It is worth noting that these changes occur against a backdrop of increased cardiac work and rate pressure product likely mediated by the sympathetic stimulation seen with intralipid[243]. Intralipid has been shown to have vasoconstrictive properties which lead to an increase in blood pressure including in obesity[244]. If provision of LCFA is unable to augment ATP supply, a fall in PCr/ATP could also occur as a result of increased work in a manner analogous to adrenergic stress such as when using dobutamine[242,245]. In studies of HFrEF with dobutamine stress this either leads to static ATP delivery in those of normal weight or a fall in ATP delivery in those with obesity[153]. Given high levels of obesity in this cohort, the increase in cardiac work and RPP induced by intralipid may be contributory. However, unlike these scenarios or indeed in non-ischaemic cardiomyopathy there was no notable increase in contractility in this study as measured by LVEF on an intralipid infusion suggesting that this is unlikely to wholly account for energetic deterioration.

Ketonaemia results in improved systolic and diastolic function with preserved PCr/ATP and potentially increased ATP delivery

Provision of ketone ester resulted in improvement of LV systolic function at rest with an increase in LVEF and LV GLS on CMR. The ensuing increase in stroke volume in combination with a rise in heart rate increased cardiac output at rest. In addition, there was a trend towards similar changes during exercise stress. Whilst diastolic function was not noted to be improved at rest, this appeared to improve during exercise and there was also a trend towards an increase in LVEDV during exercise indicating greater diastolic compliance. This is consistent with studies in HFrEF where an intravenous 3-OHB infusion has been shown to reduce resting PCWP and CVP indicating potential to change diastolic function[246]. Similar reductions have been seen in patients in cardiogenic shock provided with enteral ketone ester[247]. GLS as measured using speckle-tracking echocardiography has been noted to improve with ketone provision in both scenarios.

There are a number of potential ways in which ketonaemia could result in this beneficial response.

Firstly, ketone bodies can directly act as a substrate to an energy-starved heart. Particularly if the ability to utilise fat or glucose is exhausted, then this provides an alternative fuel able to bypass these and enter the TCA cycle. Despite an increase in cardiac contractility and work at rest, there is no significant drop in PCr/ATP and there is a trend towards an increase in CK flux suggesting that myocardial ATP production is not depleted and delivery is maintained commensurate to need. Whilst invasive paired trans-cardiac sampling was performed only in a single individual and would need replicate measurements in a larger number of patients with HFpEF, βOHB appeared to be extracted at baseline and following ketone ester administration at both rest and during exercise. This would be in line with previous studies in healthy hearts and HFrEF[168]. If this is truly the case, ketone bodies must be used as a substrate as it is not stored within cardiomyocytes unlike lipid or glucose[248].

In addition, ketone bodies are capable of increasing glucose oxidation in animal studies of HFrEF although whether this is the case in HFpEF is unknown[249]. It is intriguing that insulin levels are almost doubled following ketone administration and

this could provide a further potential mechanism. In any case, if microvascular dysfunction were to limit oxygen supply, oxidation of ketone bodies (either alone or in addition to glucose) provides a more favourable P:O ratio to produce ATP compared to lipid. In addition to such energetic enhancement, ketone bodies may also produce systemic effects which affect cardiac function.

Ketone administration results in decreased afterload and potentially preload

In the presence of ketonaemia, there is a drop in blood pressure at rest associated with a rise in heart rate. Therefore, there is a reduction in the afterload faced by the LV which could mediate an increase in LVEF. Acute vasodilatation can result in improvements in stroke volume and cardiac output while reducing the LVEDP and pulmonary pressures in HFpEF[250]. Despite this, there is an increase in cardiac work with ketonaemia noted in this study.

A systemic vasodilatory effect of ketone bodies has been confirmed on isolated arteries and veins in animal models[251]. However, there is some variation in effect within different human populations. In prior studies of ketone provision in healthy controls, the diastolic pressure has been shown to drop due to a vasodilatory effect[252]. Yet, in another study ketone ester supplementation has been shown to increase heart rate and systolic blood pressure whilst increasing LVEF in healthy volunteers[253]. A study in cardiogenic shock demonstrated an increase in cardiac output while reducing right and left ventricular filling pressures without changing heart rate, MAP and pulmonary arterial pressures[247].

There is a reduction in right atrial volumes at rest and potentially bi-atrial volumes during exercise. This could indicate a lower preload. Although in a proportion of patients with HFpEF, stroke volume can in fact decrease in this scenario driven by preload sensitivity, this was not seen in this cohort.

Reduced preload and afterload results in a rise in heart rate mediated by the baroreceptor reflex system which is present in the atria and carotid sinus/aortic arch. It could also maintain and possibly augment contractility in the form of stroke volume and ejection fraction. This could partly explain changes in LVEF, LV GLS and cardiac output.

Vasodilatation may also impact cardiac energetics. In one study studying acute effects of vasodilator therapy such as glyceryl trinitrate on cardiac work and energetics in healthy volunteers, stroke work and rate pressure product fell with an increase in LVEF. In this particular instance, PCr/ATP fell although this is attributed to the direct inhibition of the electron transport chain rather than a direct consequence of the effects of vasodilatation. There was however an increase in CK flux seen which is similar to that seen in this study.

The effects of ketones on cardiac function may not be limited to energetics and vasodilatation. Whilst not directly assessed in this study, potential additional effects include augmentation of myocardial blood flow or signalling properties. Increasing myocardial blood flow particularly during exercise could ameliorate microvascular dysfunction and improve oxygen supply. In support of this, studies using positron emission tomography have indicated that ketonaemia results in increased myocardial blood flow[170].

In addition, ketone bodies appear to have a role in epigenetic modulation. For instance, beta hydroxybutyrate was able to preserve PGC1α (PPAR gamma coactivator 1 alpha) expression, preventing mitochondrial dysfunction and onward development of heart failure[254]. Given their ability to modulate histone deacetylases and that the inhibition of these enzymes results in improved myofilament relaxation properties and LVEDP, this could represent an additional mechanism of interest[255,256].

The effects of ketone ester administration on cardiac function appear to be preserved during concomitant glucose or lipid provision

The increase in stroke volume, heart rate and cardiac output at rest persisted when ketone ester was administered simultaneously to either insulin-glucose or intralipid. This part of the study was underpowered to detect such changes during exercise or in blood pressure or changes in atrial volume. Insulin can also induce subtle increases in blood pressure and exert inotropic effects through calcium dependent and independent mechanisms which in addition to the sympathomimetic properties of intralipid could attenuate some of the vasodilatory effects of ketone bodies[257-259].

That the effects of ketone ester appeared preserved regardless of additional substrate could be a result of multiple factors which require further exploration. Firstly, given ketone bodies can continue to provide substrate for oxidative phosphorylation even in the presence of glucose or lipid, this means that it could continue to provide ATP supply to support improved systolic function. Secondly, sufficient effects on afterload and preload may persist despite antagonistic effects from insulin or intralipid.

Insulin-glucose appears to have effects on the RV at rest, but not the LV

Administration of insulin-glucose increases RVSV and RV longitudinal strain, but there was no concomitant increase in LVSV. The exact reasons for this are not clear. Quantification of valvular regurgitation or changes were not performed and it is plausible that an increase in tricuspid regurgitation may account for this as part of the additional RVSV would simply reflect backwards flow into the RA.

Intriguingly, insulin-glucose infusion resulted in an increase in myocardial triglyceride content. Insulin is known to increase fatty acid uptake in cardiomyocytes by promoting the translocation of CD36/FAT, mediated by phosphatidylinositol-3 kinase activation and this could provide a mechanism to achieve this[260,261]. This is unlikely to result in increased fatty acid use however given competition through the Randle cycle. Of note, circulating free fatty acids were not suppressed to the levels seen in some other studies in the presence of a euglycaemic clamp despite a 55% reduction[262]. The baseline fasting FFA level of 0.66 mmol/L was higher than what is considered to be the upper limit of normal in most reference laboratories (0.60 mmol/L)[263]. This could reflect the prevailing insulin resistant state within HFpEF as well as the associated comorbidities.

There are fundamental differences in the cardiac energetic state, left ventricular function and cardiac output on substrate switching

Overall, the results point towards the key role that substrate delivery and utilisation is likely to have in altering myocardial energetics and perhaps haemodynamics in HFpEF. Furthermore, they contrast with prior studies in HFrEF with intralipid proving potentially deleterious to the cardiac energetic state in HFpEF. However, despite the association between CK flux and a number of metrics of systolic function in chapter 4, this did not result in an impairment in cardiac function. The effects of

ketone ester captured in this study add to recent literature highlighting their positive effects on cardiac function and output in a number of cardiovascular disease states, but their ability to do so without compromising cardiac energetics will be key to exploiting this as a potential therapeutic target for chronic therapy in HFpEF.

5.7 Limitations

As an observational study in relatively small numbers of patients, all relevant effects of substrate switching may not be captured particularly during exercise where one would expect greater noise in observations. Despite this, the study was able to demonstrate key effects of substrate switching on energetics and cardiac function.

Secondly, the mechanism by which changes in energetics or function occurs with provision of substrate cannot be ascertained by MR studies alone. There are additional pressing questions which require trans-cardiac fuel utilisation studies. The first is that of flexibility in utilisation of the presented substrates. For example, this would be necessary to establish whether increased LCFA use is indeed the culprit for the fall in energetic state with intralipid. Secondly, given that ketone bodies have systemic effects which could then affect cardiac function, its ability to contribute to ATP production needs to be scrutinised.

Despite randomisation, there were differences in age and medication in the ketone group with none receiving calcium channel blockers and numerically more participants receiving SGLT-2 inhibitors. This could potentially have influenced the results.

Finally, the effects seen here are produced following a short-term increase in supply of substrates. Adaptation may occur in response to these in the long-term and the effects of this in the chronic phase requires further study.

5.8 Conclusions

The findings of this chapter demonstrate that substrate delivery and utilisation has a key role to play in determining the energetic status of the heart and function within HFpEF. Substrate switching to lipids results in an impairment in overall energetics as evidenced by reduced PCr/ATP and ATP delivery. Ketonaemia results in improved systolic and diastolic function. However, the mechanism is potentially multifactorial with contributions from vasodilatory properties and direct effects on energy provision given the preservation of overall energetic status with a possible commensurate increase in ATP delivery. The effects of ketone were generally maintained despite co-administration with glucose or lipid. While further study of substrate utilisation and in particular, ketone metabolism in the HFpEF heart is warranted, manipulation of fuel delivery and metabolism holds promise in delivering therapeutic targets.

SUMMARY AND FUTURE DIRECTIONS

This thesis aims to characterise heart failure with preserved ejection fraction in greater detail, particularly during exercise stress when symptoms manifest in the majority of patients. Incomplete understanding of the pathophysiology of this particularly heterogenous cardiovascular condition has hampered efforts to develop effective medicines. Understanding the biology behind exercise responses to HFpEF as well as alterations in the myocardial energetic state could identify new therapeutic targets and biomarkers.

Chapter 1 set out an overview of the multi-faceted pathophysiology of heart failure with preserved ejection fraction combining both myocardial and systemic elements. This included the current understanding of cardiac energetics and substrate metabolism in HFpEF compared to the normal state. It discussed contemporary approaches to phenotyping HFpEF including the expanding interest in haemodynamic characterisation. An overview of proteomics approaches in cardiovascular disease and current application to HFpEF is also provided.

Chapter 2 lays out an overview of the experimental methods utilised within this thesis. Exercise provides a physiological way to assess stress responses of the heart in contrast to pharmacological stress. The ability to assess these using precise cardiac magnetic resonance techniques is a recent development. A description of an ergometer based supine exercise method used throughout this thesis is provided in conjunction with both real-time and conventional CMR techniques for quantification of volume and function. ^{31}P phosphorus spectroscopy was used to gain greater understanding of both overall cardiac energetic state and ATP delivery. This included techniques such as DRESS and 3D CSI to measure the PCr/ATP ratio and saturation transfer to measure the forward rate constant of the creatine kinase reaction, together allowing quantification of ATP delivery to key cardiac enzymes. While PCr/ATP ratios have been shown to be lower in HFpEF, this has not been compared to healthy ageing nor have CK shuttle kinetics been explored leaving our understanding of energetics incomplete. Proton spectroscopy techniques were used to measure myocardial triglyceride content to supplement understanding of myocardial metabolism. Additional imaging using echocardiography was performed to measure well-validated biomarkers of systolic and diastolic function in routine clinical use.

Such multi-parametric characterisation of HFpEF using a combination of these techniques has not previously been performed.

Chapter 3 aimed to characterise the exercise responses in HFpEF as a whole in comparison to controls of similar age both at organ-level physiology and at a whole-body molecular level using multi-modality exercise cardiac imaging and aptamer-based proteomics. Given marked heterogeneity in exercise reserve within the HFpEF cohort and a clear difference in response to modern therapeutic options in clinical trials based on LVEF, the exercise responses of those with HFpEF and LVEF >60% were contrasted to those with an LVEF <60%. There was greater impairment in contractile reserve in $HFpEF_{EF>60}$ with an associated reduction in stress cardiac output and greater functional impairment. This suggests that therapies tailored to this group should be considered to provide treatment benefit. Exercise proteomics demonstrated differences between the two groups with a greater number of pathways potentially affected in the $HFpEF_{EF<60}$ cohort including RNA processing, inflammation and the extracellular matrix. Intriguingly, there were impairments in metabolism and particularly lipid pathways common to both groups of HFpEF indicating a potential way to target therapeutics of benefit to both cohorts.

In chapter 4, characterisation of myocardial energetics in HFpEF was performed and its relationship to cardiac function explored. PCr/ATP ratio whilst low was similar to that related to an age-induced decline in controls in a comparison not previously performed in the literature. However, despite this creatine kinase flux at rest was impaired in HFpEF demonstrating an energetic deficit. CK flux was related to biventricular longitudinal systolic function, LVEF and NT-proBNP at rest. Similarly, CK flux at rest remained related to biventricular systolic function during exercise likely reflecting a depleted energetic reserve. In addition, there was potentially a relationship with the ability to augment cardiac output in response to exercise. Within HFpEF, there was greater increase in LA volumes in response to exercise as CK flux declined. These results indicate that ATP delivery is impaired in HFpEF and that this is potentially implicated in systolic and diastolic dysfunction. As such, in concert with the results of chapter 3, manipulation of myocardial metabolism in order to augment ATP delivery represents a potential therapeutic avenue.

To pursue this further, substrate manipulation was performed in Chapter 5 with patients randomised to receive either long chain fatty acids in the form of intralipid, glucose in a hyperinsulinaemic state using a euglycaemic clamp or oral ketone ester. Provision of lipid resulted in a fall in PCr/ATP and CK flux with no improvement in cardiac output whereas there were no major changes with insulin-glucose. In contrast, induction of ketonaemia by ingestion of ketone ester resulted in improvements in LV systolic function and cardiac output at rest. There was an indication of this being the case during stress whilst improving exercise diastolic function. There may potentially be increased ATP delivery in this state without exhausting ATP production as indicated by a trend towards increased CK flux with a preserved PCr/ATP ratio. In addition to this, there was also a drop in blood pressure and atrial volumes indicative of vasodilatation and this may also have influenced cardiac function with diminished preload and afterload.

The contribution of ketone bodies to ATP production requires further study and an n=1 illustrative case provides a hypothesis that ketone bodies are taken up by the heart during rest and exercise states. Moreover, the flexibility of substrate use requires additional investigation using trans-cardiac extraction studies in a larger group of patients under similar conditions to this experiment. While the change in energetics suggests modification of substrates utilised in oxidation, the manner in which this is achieved cannot be inferred with certainty, i.e. if there is a true increase in use of the substrate provided compared to alterations in the use of other substrates through means of the complex feedback loops in play. In particular, this would also help understand the mechanism of an impaired energetic state created by intralipid infusion. If indeed such studies were to indicate that bypassing exhausted long chain fatty acid and glucose oxidative machinery with ketone bodies is a viable metabolic approach, there are additional candidates which could achieve this including short or medium chain fatty acids. Their uptake is independent of carnitine and they may possess some of the advantages of ketone bodies as an anaplerotic fuel[264].

In conclusion, this thesis highlights an impairment in cardiac reserve during exercise in HFpEF which is marked by significant heterogeneity. Different haemodynamic endotypes exist with varied exercise responses, most easily identified by their LV ejection fraction with both differences and commonalities in their plasma proteomic signature. There is impairment of cardiac energetics in HFpEF and both energetics

and function are amenable to modification by substrate switching suggesting a viable therapeutic target.

Future directions

While chapter 3 addressed the whole-body level proteome, there is a need to understand the myocardial biology particularly during stress. This could be performed through trans-cardiac extraction studies with serial blood sampling at rest, during exercise and recovery. Multi-omic profiling in this context using transcriptomics, proteomics and metabolomics would allow greater understanding of interaction between different pathways. Doing this simultaneously with substrate switching or other forms of metabolic modulation will inform as to which pathways are druggable. Combining this with study of different endotypes of HFpEF whether they be haemodynamic in nature or related to a specific dominant comorbidity such as obesity or diabetes will allow personalised, precision medicine.

The data presented here illustrates the utility of exercise CMR and cardiac energetics to better understand the phenotypes within HFpEF. This could have particular diagnostic utility. While chapter 3 pragmatically dichotomised HFpEF subgroups based on resting LVEF, using exercise metrics in conjunction with resting morphology is more likely to clearly identify different endotypes of HFpEF as shown with unsupervised clustering. Leveraging machine learning techniques with radiomic and plasma multi-omic profiling will help identify biologically distinct groups beyond conventional imaging measures and these CMR techniques can be of great diagnostic value within this framework in the future.

This thesis also demonstrates the ability of exercise CMR and phosphorus spectroscopy to be viable biomarkers in future phase 2 clinical trials or as part of a larger phase 3 study in HFpEF. With direct manipulation of myocardial mechanics now possible with the advent of myosin modulators, the effects of these on diastolic compliance, contractility and stroke volume reserve can be assessed for safety and as surrogate endpoints using the techniques outlined here. This could allow for optimal patient selection, by identifying the endotypes with the best response. Similarly, the effects of more chronic metabolic modulation with ketone or other similar interventions can be interrogated in terms of energetics, rest and exercise cardiac

function and output in phase 2 or 3 clinical trials using these techniques, serving as surrogate biomarkers.

APPENDICES

Chapter 3:

Table 72: Plasma proteins of differential abundance in the HFpEF cohort as a whole compared to controls

Target ID	Full target name	Log_2 Fold change	FDR adjusted p-value
N-terminal pro-BNP	N-terminal pro-BNP	1.52630338	0.00064121
GBRAP	Gamma-aminobutyric acid receptor-associated protein	0.38919964	0.00139239
GBRL1	Gamma-aminobutyric acid receptor-associated protein-like 1	0.37484762	0.00139239
PAHX	Phytanoyl-CoA dioxygenase, peroxisomal	-0.3550495	0.00297069
Aminopeptidase	Carboxypeptidase Q	-0.4210103	0.00297069
MIC-1	Growth/differentiation factor 15	0.72394459	0.00297069
fibulin 5	Fibulin-5	0.41099422	0.00460919
WISP-2	WNT1-inducible-signaling pathway protein 2	0.44383596	0.00518288
HTRA1	Serine protease HTRA1	0.36481681	0.00518288
NUD16	U8 snoRNA-decapping enzyme	1.11379828	0.00524104
RBM3	RNA-binding protein 3	0.43719145	0.00647284
FABP	Fatty acid-binding protein, heart	0.69015036	0.00716012
Coagulation Factor VIII	Coagulation Factor VIII	0.49585657	0.00716012
FABPA	Fatty acid-binding protein, adipocyte	0.68526572	0.00716012
ACBP	Acyl-CoA-binding protein	0.46973581	0.00716012
DJB12	DnaJ homolog subfamily B member 12	0.44867806	0.00793156
Inhibin bB chain	Inhibin beta B chain	0.48906109	0.00834991
tPA	Tissue-type plasminogen activator	0.82716433	0.008888
VWA2	von Willebrand factor A domain-containing protein 2	-0.3400081	0.00992652
CIRBP	Cold-inducible RNA-binding protein	0.41483091	0.00992652
SRSF7	Serine/arginine-rich splicing factor 7	0.34152925	0.01004463
CPN2	Carboxypeptidase N subunit 2	-0.3588073	0.01004463
FBLN3	EGF-containing fibulin-like extracellular matrix protein 1	0.40748484	0.01137007
TRA2B	Transformer-2 protein homolog beta	0.38546156	0.01145797
CPSF5	Cleavage and polyadenylation specificity factor subunit 5	0.32647525	0.01145797

iC3b	Complement C3b, inactivated	0.40598618	0.02119229
C43BP:START domain	Collagen type IV alpha-3-binding protein:StAR-related lipid-transfer domain, isoform 2	0.37476255	0.02589069
Cystatin C	Cystatin-C	0.38563469	0.03241821
HCC-1	C-C motif chemokine 14	0.56221005	0.03241821
Ficolin-3	Ficolin-3	-0.5291188	0.03241821
LRP11	Low-density lipoprotein receptor-related protein 11	0.33839256	0.04287445
Thrombin	Thrombin	-0.4470689	0.04287445
BNP	Natriuretic peptides B	0.52433821	0.04287445
COLL1	Colipase-like protein 1	0.37792799	0.04287445
Lysozyme	Lysozyme C	0.43082737	0.04287445
Tenascin	Tenascin	0.35160825	0.04287445
RL12	60S ribosomal protein L12	0.43311649	0.04287445
RNAS6	Ribonuclease K6	0.48842219	0.04419596
MMP19	Matrix metalloproteinase-19	0.41123161	0.04667525
Collagen a1(VI)	Collagen alpha-1(VI) chain	0.39727632	0.04717101
TSP2	Thrombospondin-2	0.68327249	0.0478135
FABPA	Fatty acid-binding protein, adipocyte	0.39079276	0.04917134
LTB4DH	Prostaglandin reductase 1	0.67311135	0.04917134
MMP-8	Neutrophil collagenase	0.6219654	0.04917134
p130	Retinoblastoma-like protein 2	0.3722377	0.04943682
Lamin-B2	Lamin-B2	0.32807127	0.04975365
RNase 1	Ribonuclease pancreatic	0.85633368	0.04986316

Table 73: Plasma proteins of differential abundance in the $HFpEF_{EF>60}$group compared to controls

Ordered by FDR corrected p-value. +ve values indicate greater abundance and -ve values indicate reduced levels.

Target ID	Full target name	Log_2 Fold change	FDR adjusted p-value
N-terminal pro-BNP	N-terminal pro-BNP	1.4934361	0.00304113
GBRAP	Gamma-aminobutyric acid receptor-associated protein	0.37457628	0.00735523
GBRL1	Gamma-aminobutyric acid receptor-associated protein-like 1	0.3602443	0.00735523
NUD16	U8 snoRNA-decapping enzyme	1.18324842	0.00735523
Aminopeptidase	Carboxypeptidase Q	-0.420766	0.00735523
PAHX	Phytanoyl-CoA dioxygenase, peroxisomal	-0.3509858	0.00735523
FABP	Fatty acid-binding protein, heart	0.7311525	0.01024058
tPA	Tissue-type plasminogen activator	0.87524792	0.01484782
FABPA	Fatty acid-binding protein, adipocyte	0.70423783	0.01498625

VWA2	von Willebrand factor A domain-containing protein 2	-0.3551839	0.01565291
RBM3	RNA-binding protein 3	0.43229712	0.01565291
Coagulation Factor VIII	Coagulation Factor VIII	0.49701405	0.01620186
MIC-1	Growth/differentiation factor 15	0.62209265	0.02065725
WISP-2	WNT1-inducible-signaling pathway protein 2	0.40939043	0.02149195
ACBP	Acyl-CoA-binding protein	0.44907423	0.02504303
HTRA1	Serine protease HTRA1	0.32584044	0.02504303
fibulin 5	Fibulin-5	0.35368948	0.02504303
CIRBP	Cold-inducible RNA-binding protein	0.40523543	0.02864293
DJB12	DnaJ homolog subfamily B member 12	0.41519984	0.03533107
TRA2B	Transformer-2 protein homolog beta	0.37803412	0.03533107

Table 74: Plasma proteins of differential abundance in the $HFpEF_{EF<60}$ group compared to controls

Target ID	Full target name	Log_2 Fold change	FDR adjusted p-value
MIC-1	Growth/differentiation factor 15	0.98423288	0.00040655
COLL1	Colipase-like protein 1	0.63423011	0.00040655
fibulin 5	Fibulin-5	0.55743968	0.00051
SRSF7	Serine/arginine-rich splicing factor 7	0.48091957	0.0018314
CPN2	Carboxypeptidase N subunit 2	-0.4991984	0.00198428
FBLN3	EGF-containing fibulin-like extracellular matrix protein 1	0.57118767	0.00198428
HTRA1	Serine protease HTRA1	0.46442308	0.00222715
N-terminal pro-BNP	N-terminal pro-BNP	1.61029753	0.00246127
GBRAP	Gamma-aminobutyric acid receptor-associated protein	0.42657044	0.00403658
GBRL1	Gamma-aminobutyric acid receptor-associated protein-like 1	0.41216723	0.00403658
WISP-2	WNT1-inducible-signaling pathway protein 2	0.53186342	0.00525307
Kallistatin	Kallistatin	-0.2770344	0.00525307
DJB12	DnaJ homolog subfamily B member 12	0.53423354	0.01494429
C3d	Complement C3d fragment	0.46905653	0.01545359
TXN4A	Thioredoxin-like protein 4A	0.43372738	0.01545359
Pseudocholinesterase	Cholinesterase	-0.4299566	0.01613066
LBP	Lipopolysaccharide-binding protein	0.49427497	0.01815142
MMP19	Matrix metalloproteinase-19	0.56071561	0.01815142
Angiopoietin-2	Angiopoietin-2	0.77294256	0.01815142
EWS	RNA-binding protein EWS	0.38424626	0.01815142

PAHX	Phytanoyl-CoA dioxygenase, peroxisomal	-0.3654344	0.01815142
Cadherin-11:ECD	Cadherin-11:Extracellular domain	0.60811167	0.01945214
Angiopoietin-2	Angiopoietin-2	0.69748505	0.01945214
GPR37	Prosaposin receptor GPR37	0.69831404	0.01945214
C43BP:START domain	Collagen type IV alpha-3-binding protein:StAR-related lipid-transfer domain, isoform 2	0.46998633	0.01945214
QSCN6	Sulfhydryl oxidase 1	0.33418735	0.01945214
ACBP	Acyl-CoA-binding protein	0.52253764	0.01945214
UBL5	Ubiquitin-like protein 5	0.37153479	0.01945214
COSA1	Collagen alpha-1(XXVIII) chain	0.53026999	0.01945214
Tenascin	Internal Use Only: Tenascin	0.46064248	0.02011823
Aminopeptidase	Carboxypeptidase Q	-0.4216344	0.02178283
Lysozyme	Lysozyme C	0.55721158	0.02300091
LRP11	Low-density lipoprotein receptor-related protein 11	0.42918732	0.0250095
sTREM-1	Triggering receptor expressed on myeloid cells 1	0.50777928	0.0250095
RNase 1	Ribonuclease pancreatic	1.14217649	0.02528894
VSIG4	V-set and immunoglobulin domain-containing protein 4	0.67649869	0.02528894
Collagen a1(VI)	Collagen alpha-1(VI) chain	0.51491249	0.02528894
Lamin-B2	Lamin-B2	0.43371638	0.02635896
ITIH3	Inter-alpha-trypsin inhibitor heavy chain H3	0.38409454	0.02635896
ASC	Apoptosis-associated speck-like protein containing a CARD	0.37609044	0.02635896
Cystatin C	Cystatin-C	0.47109005	0.02635896
CPSF5	Cleavage and polyadenylation specificity factor subunit 5	0.36812811	0.02635896
iC3b	Complement C3b, inactivated	0.47618381	0.02670101
CRIM1:ECD	Cysteine-rich motor neuron 1 protein:Extracellular domain	0.27530029	0.02757305
RNAS6	Ribonuclease K6	0.61542973	0.02760668
RBM3	RNA-binding protein 3	0.44969919	0.02826568
Apo F	Apolipoprotein F	0.68079274	0.02876128
HCC-1	C-C motif chemokine 14	0.67578313	0.02876128
SPD2B	SH3 and PX domain-containing protein 2B	0.42019675	0.02876128
GFRP	GTP cyclohydrolase I feedback regulatory protein	0.57622183	0.03152948
ERBB3	Receptor tyrosine-protein kinase erbB-3	-0.3201918	0.03238999
TXND5	Thioredoxin domain-containing protein 5	0.4408597	0.03238999
DPY30	Protein dpy-30 homolog	0.40215266	0.03513602
CIRBP	Cold-inducible RNA-binding protein	0.43935267	0.03513602
TSP2	Thrombospondin-2	0.84938717	0.03513602

p130	Retinoblastoma-like protein 2	0.46797929	0.03773828
HSP 70	Internal Use Only: Heat shock 70 kDa protein 1A	0.29180599	0.03773828
ACBD6	Acyl-CoA-binding domain-containing protein 6	0.37128812	0.0388743
VP26A	Vacuolar protein sorting-associated protein 26A	0.35158471	0.04052312
Apo C-I	Apolipoprotein C-I	-0.2045916	0.04052312
FSTL3	Follistatin-related protein 3	0.4538973	0.04052312
SVEP1:Sushi 15-18	Sushi, von Willebrand factor type A, EGF and pentraxin domain-containing protein 1:Sushi 15-18	0.6370855	0.04091155
LRP11	Low-density lipoprotein receptor-related protein 11	0.46240638	0.04142704
Coagulation Factor VIII	Coagulation Factor VIII	0.49289859	0.04142704
DPYS	Dihydropyrimidinase	0.37000755	0.04142704
Epithelial cell kinase	Ephrin type-A receptor 2	0.46118967	0.04142704
fibulin 5	Fibulin-5	0.29710543	0.04145954
Carbonic Anhydrase IV	Carbonic anhydrase 4	-0.1817596	0.04191885
PDIA6	Protein disulfide-isomerase A6	0.3334539	0.04191885
GATD1	GATA zinc finger domain-containing protein 1	-0.3286724	0.04191885
TRA2B	Transformer-2 protein homolog beta	0.4044428	0.04191885
TIMP-1	Metalloproteinase inhibitor 1	0.37020091	0.04395805
Kallistatin	Kallistatin	-0.2262402	0.04545806
LRP11	Low-density lipoprotein receptor-related protein 11	0.39184328	0.04545806
MP2K2	Dual specificity mitogen-activated protein kinase kinase 2	0.63055878	0.04545806
Ficolin-3	Ficolin-3	-0.5950011	0.04545806
Thrombin	Thrombin	-0.5159339	0.04545806
ERBB1	Epidermal growth factor receptor	-0.2163319	0.04545806
SVEP1:EGF-like domains 4-6	Sushi, von Willebrand factor type A, EGF and pentraxin domain-containing protein 1:EGF-like domains 4-6	0.63191147	0.0485422
MLP3A	Microtubule-associated proteins 1A/1B light chain 3A	0.3030133	0.04897718

Table 75: Indexed volumes and function of ventricles at rest – Control vs HFpEF

	Control	*HFpEF*	*p-value*
REST			
Left ventricular end diastolic volume indexed (LVEDVi, ml/m²)	74.1 ± 6.5	77.7 ± 22.6	0.66
LV end systolic volume indexed (LVESVi, ml/m²)	26.2 ± 3.5	31.2 ± 11.6	0.25
LV ejection fraction (LVEF, %)	64.5 ± 4.9	60.8 ± 5.8	0.12
LV stroke volume indexed (LVSVi, ml/m²)	47.9 ± 6.8	46.7 ± 12.3	0.80
LV Global Longitudinal Strain (GLS, %)	-16.5 ± 2.7	-14.9 ± 3.4	0.24
LV Mass indexed (g/m²)	49.9 ± 8.6	56.7 ± 12.1	0.16
LV peak early filling rate (EDV/s)	2.88 ± 0.98	3.58 ± 1.55	0.24
RV end diastolic volume indexed (RVEDVi, ml/m²)	79.1 ± 10.4	77.3 ± 22.0	0.82
RV end systolic volume indexed (RVESVi, ml/m²)	32.1 ± 6.2	31.3 ± 11.6	0.87
RV ejection fraction (RVEF, %)	59.9 ± 5.1	59.7 ± 5.4	0.92
RV stroke volume indexed (RVSVi, ml/m²)	47.1 ± 7.2	45.8 ± 12.3	0.78
RV longitudinal strain (%)	-25.8 ± 1.7	-21.5 ± 5.1	***0.03***
RV SV/ESV ratio	1.51 ± 0.32	1.54 ± 0.36	0.81

Table 76: Indexed volumes and function of atria at rest - Control vs HFpEF

	Control	*HFpEF*	*p-value*
REST			
LA end diastolic volume indexed (LAEDVi, ml/m^2)	32.8 ± 11.6	65.5 ± 34.6	***0.01***
LA end systolic volume indexed (LAESVi, ml/m^2)	56.1 ± 11.4	82.5 ± 35.9	***0.02***
LA emptying fraction (LAEF, %)	42.8 ± 8.9	23.8 ± 14.7	***0.002***
Right atrial end diastolic volume indexed (RAEDVi, ml/m^2)	38.9 ± 16.7	77.7 ± 41.9	***0.005***
RA end systolic volume indexed (RAESVi, ml/m^2)	61.4 ± 13.8	94.5 ± 41.3	***0.03***
RA emptying fraction (RAEF, %)	38.6 ± 12.4	21..0 ± 12.7	***0.002***

Table 77: Echocardiography parameters at rest - Control vs HFpEF

	Control	*HFpEF*	*p-value*
REST			
E/E' average (ratio)	7.1 ± 1.2	11.1 ± 3.0	***<0.0001***
S' Left ventricle (cm/s)	8.6 ± 1.6	6.6 ± 1.4	***0.002***
Tricuspid annular plane systolic excursion (TAPSE, mm)	25.2 ± 4.1	19.8 ± 5.6	***0.01***
S' Right ventricle (cm/s)	14.3 ± 3.1	11.1 ± 2.6	***0.007***
Estimated pulmonary artery systolic pressure (PASP, mmHg)	23.7 ± 4.3	30.6 ± 9.4	0.13
Left atrial volume indexed biplane (ml/m^2)	26.1 ± 7.6	54.7 ± 21.1	***<0.0001***
Left ventricular mass indexed (g/m^2)	68.5 ± 10.7	104.8 ± 30.4	***0.003***

Table 78: Indexed volumes and function of ventricles during exercise stress - Control vs HFpEF

	Control	*HFpEF*	*p-value*
EXERCISE STRESS			
LVEDVi (ml/m^2)	84.9 ± 7.6	82.8 ± 17.8	0.75
LVESVi (ml/m^2)	22.7 ± 3.7	28.7 ± 9.9	0.11
LVEF (%)	73.4 ± 3.2	65.8 ± 7.0	***0.007***
LVSVi (ml/m^2)	62.3 ± 5.7	54.1 ± 10.9	0.06
LV peak early filling rate (EDV/s)	3.03± 0.59	3.32 ± 1.36	0.57
RVEDVi (ml/m^2)	92.5 ± 8.7	88.5 ± 21.1	0.61
RVESVi (ml/m^2)	30.1 ± 7.8	35.0 ± 24.7	0.30
RVEF (%)	67.8 ± 6.2	61.3 ± 6.4	***0.02***
RVSVi (ml/m^2)	62.5 ± 5.3	53.5 ± 10.5	***0.03***
RV SV/ESV ratio	2.80 ± 0.49	2.08 ± 0.83	***0.002***

Table 79: Change in ventricular parameters from rest to exercise - Control vs HFpEF

	Control	*HFpEF*	*p-value*
ΔLVEF rest→stress (%)	8.9 ± 5.5	5.2 ± 5.4	0.11
ΔLVSVi rest→stress (ml/m²)	14.4 ± 6.7	6.6 ± 5.8	***0.004***
Δpeak early filling rate (EDV/s)	0.15 ± 1.08	-0.23 ± 1.27	0.45
ΔRVEF rest→stress (%)	13.5 ± 5.3	6.5 ± 8.4	***0.04***
ΔRVSVi rest→stress (ml/m²)	15.4 ± 8.9	6.8 ± 6.4	***0.006***
ΔRV SV/ESV ratio	1.30 ± 0.50	0.56 ± 0.81	***0.003***

Table 80: Atrial volumes and function at stress and exercise-induced change in these parameters - Control vs HFpEF

	Control	*HFpEF*	*p-value*
LAEDVi (ml/m²)	34.4 ± 9.4	66.6 ± 31.8	***0.009***
LAESVi (ml/m²)	66.9 ± 11.2	87.3 ± 33.7	***0.06***
LAEF (%)	49.2 ± 6.9	26.4 ± 13.6	***0.0003***
RAEDVi (ml/m²)	36.4 ± 11.7	82.9 ± 43.2	***0.006***
RAESVi (ml/m²)	70.7 ± 19.6	109.2 ± 45.6	***0.03***
RAEF (%)	49.1 ± 6.5	27.4 ± 12.8	***<0.0001***
ΔLAESVi rest→stress (ml/m²)	10.8 ± 6.4	7.6 ± 9.6	0.39
ΔRAESVi rest→stress (ml/m²)	9.3 ± 9.8	17.8 ± 14.7	0.14

Table 81: Rest and stress cardiac output - Control vs HFpEF

	Control	*HFpEF*	*p-value*
Rest Cardiac Output (L/min)	4.91 ± 0.80	5.89 ± 1.76	0.10
Rest Cardiac Index (L/min/m^2)	2.72 ± 0.35	2.89 ± 0.81	0.82
Stress Cardiac Output (L/min)	10.85 ± 1.79	10.61 ± 2.83	0.83
Stress Cardiac Index (L/min/m^2)	6.02 ± 0.89	5.13 ± 1.25	0.08
ΔCardiac Index (L/min/m^2)	3.30 ± 0.80	2.19 ± 0.90	***0.005***

Table 82: Echocardiography parameters during stress - Control vs HFpEF

	Control	*HFpEF*	*p-value*
E/E′ average (ratio)	7.8 ± 1.7	11.6 ± 3.6	***0.007***
ΔE/E′ rest→stress	0.8 ± 1.7	0.6 ± 2.1	0.42
S′ Left ventricle (cm/s)	11.1 ± 2.1	8.1 ± 1.7	***0.0004***
TAPSE (mm)	31.8 ± 6.9	19.2 ± 5.1	***<0.0001***
S′ Right ventricle (cm/s)	19.1 ± 3.4	13.5 ± 4.1	***0.002***
Estimated PASP (mmHg)	33.7 ± 10.7	39.9 ± 13.0	0.45

Table 83: Calculation of CK flux - Control vs HFpEF

	Control	*HFpEF*	*p-value*
PCr/ATP ratio	1.47 ± 0.35	1.41 ± 0.25	0.60
K_f (s^{-1})	0.40 ± 0.21	0.37 ± 0.29	0.45
Product of PCr/ATP * K_f	1.11 ± 0.97	0.63 ± 0.81	0.075
CK flux (μmol/g/s)	3.40 ± 2.13	1.99 ± 1.34	***0.047***

Table 84: Peak recorded ketone levels for all cohorts receiving ketone ester

	Ketone only	*Insulin-glucose + Ketone*	*Intralipid + Ketone*
βOHB (mmol/L)	3.4 ± 0.8	4.0 ± 1.1	4.7 ± 0.6

REFERENCES

1. Dunlay, S.M., Roger, V.L. & Redfield, M.M. Epidemiology of heart failure with preserved ejection fraction. *Nat Rev Cardiol* **14**, 591-602 (2017).
2. Tribouilloy, C., *et al.* Prognosis of heart failure with preserved ejection fraction: a 5 year prospective population-based study. *Eur Heart J* **29**, 339-347 (2008).
3. Borlaug, B.A. The pathophysiology of heart failure with preserved ejection fraction. *Nature Reviews Cardiology* **11**, 507-515 (2014).
4. Borlaug, B.A., Nishimura, R.A., Sorajja, P., Lam, C.S.P. & Redfield, M.M. Exercise Hemodynamics Enhance Diagnosis of Early Heart Failure With Preserved Ejection Fraction. *Circulation: Heart Failure* **3**, 588-595 (2010).
5. Mcdonagh, T.A., *et al.* 2021 ESC Guidelines for the diagnosis and treatment of acute and chronic heart failure. *European Heart Journal* **42**, 3599-3726 (2021).
6. Reddy, Y.N.V., *et al.* Diagnosis of Heart Failure With Preserved Ejection Fraction Among Patients With Unexplained Dyspnea. *Jama Cardiology* (2022).
7. Sorimachi, H., Omote, K. & Borlaug, B.A. Clinical Phenogroups in Heart Failure with Preserved Ejection Fraction. *Heart Failure Clinics* **17**, 483-498 (2021).
8. Starling, E.H. On the Absorption of Fluids from the Connective Tissue Spaces. *The Journal of Physiology* **19**, 312-326 (1896).
9. Kaye, D.M., *et al.* Comprehensive Physiological Modeling Provides Novel Insights Into Heart Failure With Preserved Ejection Fraction Physiology. *J Am Heart Assoc* **10**, e021584 (2021).
10. Guyton, A.C., Lindsey, A.W., Johnnie O., H., John W., W. & Malcolm A., F. Effect of Elevated Left Atrial Pressure and Decreased Plasma Protein Concentration on the Development of Pulmonary Edema. *Circulation Research* **7**, 649-657 (1959).
11. Davies, S.W., *et al.* Reduced pulmonary microvascular permeability in severe chronic left heart failure. *Am Heart J* **124**, 137-142 (1992).
12. Witte, M.H., *et al.* Lymph Circulation in Congestive Heart Failure. *Circulation* **39**, 723-733 (1969).
13. GA, L., SJ, A., J, K., JC, G. & RE, D. Effect of systemic venous pressure elevation on lymph flow and lung edema formation. *Journal of applied physiology (Bethesda, Md. : 1985)* **61**(1986).
14. Morris, D.A., *et al.* Left ventricular longitudinal systolic function analysed by 2D speckle-tracking echocardiography in heart failure with preserved ejection fraction: a meta-analysis. *Open Heart* **4**, e000630 (2017).
15. Shin, H.W., *et al.* Tissue Doppler Imaging as a Prognostic Marker for Cardiovascular Events in Heart Failure with Preserved Ejection Fraction and Atrial Fibrillation. *J Am Soc Echocardiog* **23**, 755-761 (2010).
16. Ennezat, P.V., *et al.* Left ventricular abnormal response during dynamic exercise in patients with heart failure and preserved left ventricular ejection fraction at rest. *Journal of Cardiac Failure* **14**, 475-480 (2008).
17. Abudiab, M.M., *et al.* Cardiac output response to exercise in relation to metabolic demand in heart failure with preserved ejection fraction. *Eur J Heart Fail* **15**, 776-785 (2013).
18. Takizawa, D., *et al.* Pathophysiologic and Prognostic Importance of Cardiac Power Output Reserve in Heart Failure with Preserved Ejection Fraction. *Eur Heart J Cardiovasc Imaging* (2023).

19. Opdahl, A., Remme, E.W., Helle-Valle, T., Edvardsen, T. & Smiseth, O.A. Myocardial Relaxation, Restoring Forces, and Early-Diastolic Load Are Independent Determinants of Left Ventricular Untwisting Rate. *Circulation* **126**, 1441-1451 (2012).
20. Udelson, J.E., Bacharach, S.L., Cannon, R.O. & Bonow, R.O. Minimum Left-Ventricular Pressure during Beta-Adrenergic Stimulation in Human-Subjects - Evidence for Elastic Recoil and Diastolic Suction in the Normal Heart. *Circulation* **82**, 1174-1182 (1990).
21. Tan, Y.T., *et al.* Abnormal left ventricular function occurs on exercise in well-treated hypertensive subjects with normal resting echocardiography. *Heart* **96**, 948-955 (2010).
22. Wachter, R., *et al.* Blunted frequency-dependent upregulation of cardiac output is related to impaired relaxation in diastolic heart failure. *European Heart Journal* **30**, 3027-3036 (2009).
23. Westermann, D., *et al.* Role of left ventricular stiffness in heart failure with normal ejection fraction. *Circulation* **117**, 2051-2060 (2008).
24. Zile, M.R., *et al.* Myocardial Stiffness in Patients With Heart Failure and a Preserved Ejection Fraction Contributions of Collagen and Titin. *Circulation* **131**, 1247-1259 (2015).
25. Phan, T.T., *et al.* Increased atrial contribution to left ventricular filling compensates for impaired early filling during exercise in heart failure with preserved ejection fraction. *J Card Fail* **15**, 890-897 (2009).
26. Tan, Y.T., *et al.* Reduced left atrial function on exercise in patients with heart failure and normal ejection fraction. *Heart* **96**, 1017-1023 (2010).
27. Kurt, M., Wang, J., Torre-Amione, G. & Nagueh, S.F. Left atrial function in diastolic heart failure. *Circ Cardiovasc Imaging* **2**, 10-15 (2009).
28. Omote, K., *et al.* Biatrial myopathy in heart failure with preserved ejection fraction. *Eur J Heart Fail* (2023).
29. Reddy, Y.N.V., Obokata, M., Verbrugge, F.H., Lin, G. & Borlaug, B.A. Atrial Dysfunction in Patients With Heart Failure With Preserved Ejection Fraction and Atrial Fibrillation. *J Am Coll Cardiol* **76**, 1051-1064 (2020).
30. Zakeri, R., *et al.* Impact of Atrial Fibrillation on Exercise Capacity in Heart Failure With Preserved Ejection Fraction A RELAX Trial Ancillary Study. *Circ-Heart Fail* **7**, 123-130 (2014).
31. Gorter, T.M., *et al.* Right Heart Dysfunction in Heart Failure With Preserved Ejection Fraction: The Impact of Atrial Fibrillation. *Journal of Cardiac Failure* **24**, 177-185 (2018).
32. Kanagala, P., *et al.* Prevalence of right ventricular dysfunction and prognostic significance in heart failure with preserved ejection fraction. *Int J Cardiovasc Imaging* **37**, 255-266 (2021).
33. Lam, C.S.P., *et al.* Pulmonary Hypertension in Heart Failure With Preserved Ejection Fraction A Community-Based Study. *Journal of the American College of Cardiology* **53**, 1119-1126 (2009).
34. Fayyaz, A.U., *et al.* Global Pulmonary Vascular Remodeling in Pulmonary Hypertension Associated With Heart Failure and Preserved or Reduced Ejection Fraction. *Circulation* **137**, 1796-1810 (2018).
35. Gorter, T.M., Obokata, M., Reddy, Y.N.V., Melenovsky, V. & Borlaug, B.A. Exercise unmasks distinct pathophysiologic features in heart failure with preserved ejection fraction and pulmonary vascular disease. *European Heart Journal* **39**, 2825-2835 (2018).

36. Borlaug, B.A., Kane, G.C., Melenovsky, V. & Olson, T.P. Abnormal right ventricular-pulmonary artery coupling with exercise in heart failure with preserved ejection fraction. *European Heart Journal* **37**, 3293.3292-3302 (2016).
37. Reddy, Y.N.V., *et al.* The haemodynamic basis of lung congestion during exercise in heart failure with preserved ejection fraction. *European Heart Journal* **40**, 3721-3730 (2019).
38. Melenovsky, V., Hwang, S.-J., Lin, G., Redfield, M.M. & Borlaug, B.A. Right heart dysfunction in heart failure with preserved ejection fraction. *European Heart Journal* **35**, 3452-3462 (2014).
39. Rommel, K.P., *et al.* Load-Independent Systolic and Diastolic Right Ventricular Function in Heart Failure With Preserved Ejection Fraction as Assessed by Resting and Handgrip Exercise Pressure-Volume Loops. *Circ Heart Fail* **11**, e004121 (2018).
40. Cornwell, W.K., *et al.* New insights into resting and exertional right ventricular performance in the healthy heart through real-time pressure-volume analysis. *J Physiol* **598**, 2575-2587 (2020).
41. Chen, Z.W., *et al.* Right Ventricular-Vascular Uncoupling Predicts Pulmonary Hypertension in Clinically Diagnosed Heart Failure With Preserved Ejection Fraction. *J Am Heart Assoc* **13**, e030025 (2024).
42. Esmaeeli, A., *et al.* Reduced Rv Longitudinal Strain Predicts Exercise Pvr Response In Hfpef: Invasive Cpet And Cardiac Mri Study. *Journal of Cardiac Failure* **30**, 212 (2024).
43. Vanderpool, R.R., *et al.* RV-pulmonary arterial coupling predicts outcome in patients referred for pulmonary hypertension. *Heart* **101**, 37-43 (2015).
44. von Roeder, M., *et al.* Right atrial-right ventricular coupling in heart failure with preserved ejection fraction. *Clin Res Cardiol* **109**, 54-66 (2020).
45. van Wezenbeek, J., *et al.* Right Ventricular and Right Atrial Function Are Less Compromised in Pulmonary Hypertension Secondary to Heart Failure With Preserved Ejection Fraction: A Comparison With Pulmonary Arterial Hypertension With Similar Pressure Overload. *Circ Heart Fail* **15**, e008726 (2022).
46. Hahn, R.T., *et al.* Tricuspid Regurgitation in Patients With Heart Failure and Preserved Ejection Fraction: JACC State-of-the-Art Review. *J Am Coll Cardiol* **84**, 195-212 (2024).
47. Obokata, M., Reddy, Y.N.V., Pislaru, S.V., Melenovsky, V. & Borlaug, B.A. Evidence Supporting the Existence of a Distinct Obese Phenotype of Heart Failure With Preserved Ejection Fraction. *Circulation* **136**, 6-19 (2017).
48. Koepp, K.E., Obokata, M., Reddy, Y.N.V., Olson, T.P. & Borlaug, B.A. Hemodynamic and Functional Impact of Epicardial Adipose Tissue in Heart Failure With Preserved Ejection Fraction. *Jacc-Heart Fail* **8**, 657-666 (2020).
49. Dauterman, K., *et al.* Contribution of External Forces to Left-Ventricular Diastolic Pressure - Implications for the Clinical Use of the Starling Law. *Ann Intern Med* **122**, 737-742 (1995).
50. Borlaug, B.A. & Reddy, Y.N.V. The Role of the Pericardium in Heart Failure Implications for Pathophysiology and Treatment. *Jacc-Heart Fail* **7**, 574-585 (2019).
51. Borlaug, B.A., *et al.* Surgical pericardiotomy to treat heart failure with preserved ejection fraction: a first clinical study. *Eur Heart J* (2023).
52. Chirinos, J.A., Segers, P., Hughes, T. & Townsend, R. Large-Artery Stiffness in Health and Disease JACC State-of-the-Art Review. *Journal of the American College of Cardiology* **74**, 1237-1263 (2019).

53. Zamani, P., *et al.* Resistive and Pulsatile Arterial Load as Predictors of Left Ventricular Mass and Geometry The Multi-Ethnic Study of Atherosclerosis. *Hypertension* **65**, 85-+ (2015).
54. Borlaug, B.A., *et al.* Global Cardiovascular Reserve Dysfunction in Heart Failure With Preserved Ejection Fraction. *Journal of the American College of Cardiology* **56**, 845-854 (2010).
55. Hwang, S.J., Melenovsky, V. & Borlaug, B.A. Implications of Coronary Artery Disease in Heart Failure With Preserved Ejection Fraction. *Journal of the American College of Cardiology* **63**, 2817-2827 (2014).
56. Shah, S.J., *et al.* Prevalence and correlates of coronary microvascular dysfunction in heart failure with preserved ejection fraction: PROMIS-HFpEF. *European Heart Journal* **39**, 3439-3450 (2018).
57. Paulus, W.J. & Tschope, C. A Novel Paradigm for Heart Failure With Preserved Ejection Fraction Comorbidities Drive Myocardial Dysfunction and Remodeling Through Coronary Microvascular Endothelial Inflammation. *Journal of the American College of Cardiology* **62**, 263-271 (2013).
58. Mohammed, S.F., *et al.* Coronary Microvascular Rarefaction and Myocardial Fibrosis in Heart Failure With Preserved Ejection Fraction. *Circulation* **131**, 550-559 (2015).
59. Bhella, P.S., *et al.* Abnormal haemodynamic response to exercise in heart failure with preserved ejection fraction. *European Journal of Heart Failure* **13**, 1296-1304 (2011).
60. Haykowsky, M.J., *et al.* Determinants of Exercise Intolerance in Elderly Heart Failure Patients With Preserved Ejection Fraction. *Journal of the American College of Cardiology* **58**, 265-274 (2011).
61. Zamani, P., *et al.* Multimodality assessment of heart failure with preserved ejection fraction skeletal muscle reveals differences in the machinery of energy fuel metabolism. *Esc Heart Failure* **8**, 2698-2712 (2021).
62. Bekfani, T., *et al.* Skeletal Muscle Function, Structure, and Metabolism in Patients With Heart Failure With Reduced Ejection Fraction and Heart Failure With Preserved Ejection Fraction. *Circ-Heart Fail* **13**(2020).
63. Beale, A.L., *et al.* Iron deficiency in heart failure with preserved ejection fraction: a systematic review and meta-analysis. *Open Heart* **6**(2019).
64. von Haehling, S., *et al.* Anaemia among patients with heart failure and preserved or reduced ejection fraction: results from the SENIORS study. *European Journal of Heart Failure* **13**, 656-663 (2011).
65. Eckhardt, C.M., *et al.* Lung function impairment and risk of incident heart failure: the NHLBI Pooled Cohorts Study. *Eur Heart J* **43**, 2196-2208 (2022).
66. Fermoyle, C.C., Stewart, G.M., Borlaug, B.A. & Johnson, B.D. Simultaneous Measurement of Lung Diffusing Capacity and Pulmonary Hemodynamics Reveals Exertional Alveolar-Capillary Dysfunction in Heart Failure With Preserved Ejection Fraction. *Journal of the American Heart Association* **10**, e019950 (2021).
67. Olson, T.P., Johnson, B.D. & Borlaug, B.A. Impaired Pulmonary Diffusion in Heart Failure With Preserved Ejection Fraction. *JACC: Heart Failure* **4**, 490-498 (2016).
68. Guazzi, M., Reina, G., Tumminello, G. & Guazzi, M.D. Alveolar-capillary membrane conductance is the best pulmonary function correlate of exercise ventilation efficiency in heart failure patients. *European Journal of Heart Failure* **7**, 1017-1022 (2005).

69. Paulus, W.J. & Zile, M.R. From Systemic Inflammation to Myocardial Fibrosis: The Heart Failure With Preserved Ejection Fraction Paradigm Revisited. *Circ Res* **128**, 1451-1467 (2021).
70. Sanders-van Wijk, S., *et al.* Proteomic Evaluation of the Comorbidity-Inflammation Paradigm in Heart Failure With Preserved Ejection Fraction: Results From the PROMIS-HFpEF Study. *Circulation* **142**, 2029-2044 (2020).
71. Petrie, M., *et al.* HERMES: Effects Of Ziltivekimab Versus Placebo On Morbidity And Mortality In Patients With Heart Failure With Mildly Reduced Or Preserved Ejection Fraction And Systemic Inflammation. *Journal of Cardiac Failure* **30**, 126-126 (2024).
72. Schiattarella, G.G., Rodolico, D. & Hill, J.A. Metabolic inflammation in heart failure with preserved ejection fraction. *Cardiovasc Res* **117**, 423-434 (2021).
73. Budde, H., Hassoun, R., Mugge, A., Kovacs, A. & Hamdani, N. Current Understanding of Molecular Pathophysiology of Heart Failure With Preserved Ejection Fraction. *Front Physiol* **13**, 928232 (2022).
74. Aslam, M.I., *et al.* Reduced Right Ventricular Sarcomere Contractility in Heart Failure With Preserved Ejection Fraction and Severe Obesity. *Circulation* **143**, 965-967 (2021).
75. Samson, R., Jaiswal, A., Ennezat, P.V., Cassidy, M. & Le Jemtel, T.H. Clinical Phenotypes in Heart Failure With Preserved Ejection Fraction. *J Am Heart Assoc* **5**(2016).
76. Berlot, B., Bucciarelli-Ducci, C., Palazzuoli, A. & Marino, P. Myocardial phenotypes and dysfunction in HFpEF and HFrEF assessed by echocardiography and cardiac magnetic resonance. *Heart Fail Rev* **25**, 75-84 (2020).
77. Harada, T., Kagami, K., Kato, T. & Obokata, M. Echocardiography in the diagnostic evaluation and phenotyping of heart failure with preserved ejection fraction. *J Cardiol* **79**, 679-690 (2022).
78. Chamsi-Pasha, M.A., Zhan, Y., Debs, D. & Shah, D.J. CMR in the Evaluation of Diastolic Dysfunction and Phenotyping of HFpEF: Current Role and Future Perspectives. *JACC Cardiovasc Imaging* **13**, 283-296 (2020).
79. Eltelbany, M., Shah, P. & deFilippi, C. Biomarkers in HFpEF for Diagnosis, Prognosis, and Biological Phenotyping. *Curr Heart Fail Rep* **19**, 412-424 (2022).
80. Peters, A.E., *et al.* Phenomapping in heart failure with preserved ejection fraction - insights, limitations, and future directions. *Cardiovasc Res* (2022).
81. Shah, S.J., *et al.* Phenomapping for novel classification of heart failure with preserved ejection fraction. *Circulation* **131**, 269-279 (2015).
82. Cohen, J.B., *et al.* Clinical Phenogroups in Heart Failure With Preserved Ejection Fraction: Detailed Phenotypes, Prognosis, and Response to Spironolactone. *JACC Heart Fail* **8**, 172-184 (2020).
83. Segar, M.W., *et al.* Phenomapping of patients with heart failure with preserved ejection fraction using machine learning-based unsupervised cluster analysis. *Eur J Heart Fail* **22**, 148-158 (2020).
84. Sotomi, Y., *et al.* Phenotyping of acute decompensated heart failure with preserved ejection fraction. *Heart* **108**, 1553-1561 (2022).
85. Sotomi, Y., *et al.* Pathophysiological insights into machine learning-based subphenotypes of acute heart failure with preserved ejection fraction. *Heart* (2023).
86. Sotomi, Y., *et al.* Medications for specific phenotypes of heart failure with preserved ejection fraction classified by a machine learning-based clustering model. *Heart* **109**, 1231-1240 (2023).

87. Solomon, S.D., *et al.* Angiotensin-Neprilysin Inhibition in Heart Failure with Preserved Ejection Fraction. *N Engl J Med* **381**, 1609-1620 (2019).
88. Solomon, S.D., *et al.* Influence of ejection fraction on outcomes and efficacy of spironolactone in patients with heart failure with preserved ejection fraction. *Eur Heart J* **37**, 455-462 (2016).
89. Anker, S.D., *et al.* Empagliflozin in Heart Failure with a Preserved Ejection Fraction. *N Engl J Med* **385**, 1451-1461 (2021).
90. Rosch, S., *et al.* Characteristics of Heart Failure With Preserved Ejection Fraction Across the Range of Left Ventricular Ejection Fraction. *Circulation* **146**, 506-518 (2022).
91. Popovic, D., *et al.* Ventricular Stiffening and Chamber Contracture in Heart Failure with Higher Ejection Fraction. *Eur J Heart Fail* (2023).
92. Forrest, I.S., *et al.* Genetic and phenotypic profiling of supranormal ejection fraction reveals decreased survival and underdiagnosed heart failure. *Eur J Heart Fail* **24**, 2118-2127 (2022).
93. Wu, P., *et al.* Impaired coronary flow reserve in patients with supra-normal left ventricular ejection fraction at rest. *Eur J Nucl Med Mol Imaging* **49**, 2189-2198 (2022).
94. Maredziak, M., *et al.* Microvascular dysfunction and sympathetic hyperactivity in women with supra-normal left ventricular ejection fraction (snLVEF). *Eur J Nucl Med Mol Imaging* **47**, 3094-3106 (2020).
95. Imamura, T., *et al.* Clinical Implication of Supra-Normal Left Ventricular Ejection Fraction in Patients Undergoing Transcatheter Aortic Valve Replacement. *J Clin Med* **12**(2023).
96. Ohte, N., *et al.* Unfavourable outcomes in patients with heart failure with higher preserved left ventricular ejection fraction. *Eur Heart J Cardiovasc Imaging* **24**, 293-300 (2023).
97. van Essen, B.J., *et al.* Characteristics and clinical outcomes of patients with acute heart failure with a supranormal left ventricular ejection fraction. *Eur J Heart Fail* **25**, 35-42 (2023).
98. Foa, A., *et al.* Sacubitril/Valsartan-Related Hypotension in Patients With Heart Failure and Preserved or Mildly Reduced Ejection Fraction. *J Am Coll Cardiol* **83**, 1731-1739 (2024).
99. Aebersold, R., *et al.* How many human proteoforms are there? *Nat Chem Biol* **14**, 206-214 (2018).
100. Smith, J.G. & Gerszten, R.E. Emerging Affinity-Based Proteomic Technologies for Large-Scale Plasma Profiling in Cardiovascular Disease. *Circulation* **135**, 1651-1664 (2017).
101. Sinha, A. & Mann, M. A beginner's guide to mass spectrometry–based proteomics. *The Biochemist* **42**, 64-69 (2020).
102. Lundberg, M., Eriksson, A., Tran, B., Assarsson, E. & Fredriksson, S. Homogeneous antibody-based proximity extension assays provide sensitive and specific detection of low-abundant proteins in human blood. *Nucleic Acids Res* **39**, e102 (2011).
103. Assarsson, E., *et al.* Homogenous 96-plex PEA immunoassay exhibiting high sensitivity, specificity, and excellent scalability. *PLoS One* **9**, e95192 (2014).
104. Gold, L., *et al.* Aptamer-based multiplexed proteomic technology for biomarker discovery. *PLoS One* **5**, e15004 (2010).
105. Candia, J., Daya, G.N., Tanaka, T., Ferrucci, L. & Walker, K.A. Assessment of variability in the plasma 7k SomaScan proteomics assay. *Sci Rep* **12**, 17147 (2022).

106. Joshi, A. & Mayr, M. In Aptamers They Trust: The Caveats of the SOMAscan Biomarker Discovery Platform from SomaLogic. *Circulation* **138**, 2482-2485 (2018).
107. Sun, B.B., *et al.* Genomic atlas of the human plasma proteome. *Nature* **558**, 73-79 (2018).
108. Adamo, L., *et al.* Proteomic Signatures of Heart Failure in Relation to Left Ventricular Ejection Fraction. *Journal of the American College of Cardiology* **76**, 1982-1994 (2020).
109. Kresoja, K.P., *et al.* Proteomics to improve phenotyping in obese patients with heart failure with preserved ejection fraction. *Eur J Heart Fail* **23**, 1633-1644 (2021).
110. Hanff, T.C., *et al.* Quantitative Proteomic Analysis of Diabetes Mellitus in Heart Failure With Preserved Ejection Fraction. *Jacc-Basic Transl Sc* **6**, 89-99 (2021).
111. Chandramouli, C., *et al.* Sex differences in proteomic correlates of coronary microvascular dysfunction among patients with heart failure and preserved ejection fraction. *Eur J Heart Fail* **24**, 681-684 (2022).
112. Shah, R.V., *et al.* Proteomics and Precise Exercise Phenotypes in Heart Failure With Preserved Ejection Fraction: A Pilot Study. *J Am Heart Assoc* **12**, e029980 (2023).
113. Emilsson, V., *et al.* Proteomic prediction of incident heart failure and its main subtypes. *Eur J Heart Fail* **26**, 87-102 (2024).
114. Shah, A.M., *et al.* Large scale plasma proteomics identifies novel proteins and protein networks associated with heart failure development. *Nat Commun* **15**, 528 (2024).
115. Ramonfaur, D., *et al.* High Throughput Plasma Proteomics and Risk of Heart Failure and Frailty in Late Life. *JAMA Cardiol* (2024).
116. Patel-Murray, N.L., *et al.* Aptamer Proteomics for Biomarker Discovery in Heart Failure With Preserved Ejection Fraction: The PARAGON-HF Proteomic Substudy. *J Am Heart Assoc* **13**, e033544 (2024).
117. Chirinos, J.A., *et al.* Multiple Plasma Biomarkers for Risk Stratification in Patients With Heart Failure and Preserved Ejection Fraction. *Journal of the American College of Cardiology* **75**, 1281-1295 (2020).
118. Michaelsson, E., *et al.* Myeloperoxidase Inhibition Reverses Biomarker Profiles Associated With Clinical Outcomes in HFpEF. *JACC Heart Fail* **11**, 775-787 (2023).
119. Hage, C., *et al.* Metabolomic Profile in HFpEF vs HFrEF Patients. *Journal of Cardiac Failure* **26**, 1050-1059 (2020).
120. Zordoky, B.N., *et al.* Metabolomic Fingerprint of Heart Failure with Preserved Ejection Fraction. *PLOS ONE* **10**, e0124844 (2015).
121. Javaheri, A., Allegood, J.C., Cowart, L.A. & Chirinos, J.A. Circulating Ceramide 16:0 in Heart Failure With Preserved Ejection Fraction. *Journal of the American College of Cardiology* **75**, 2273-2275 (2020).
122. Januzzi, J.L. & Murphy, S.P. Proteomics as a Path to More Refined Heart Failure Therapeutics. *JACC: Heart Failure* **9**, 278-280 (2021).
123. Wallimann, T., Wyss, M., Brdiczka, D., Nicolay, K. & Eppenberger, H.M. Intracellular compartmentation, structure and function of creatine kinase isoenzymes in tissues with high and fluctuating energy demands: the 'phosphocreatine circuit' for cellular energy homeostasis. *Biochem J* **281 (Pt 1)**, 21-40 (1992).
124. Ingwall, J.S. & Shen, W. The chemistry of ATP in the failing heart the fundamentals. *Heart failure reviews* **4**, 221-228 (1999).

125. Weiss, R.G., Gerstenblith, G. & Bottomley, P.A. ATP flux through creatine kinase in the normal, stressed, and failing human heart. *P Natl Acad Sci USA* **102**, 808-813 (2005).
126. Lygate, C.A. Maintaining energy provision in the heart: the creatine kinase system in ischaemia-reperfusion injury and chronic heart failure. *Clin Sci (Lond)* **138**, 491-514 (2024).
127. O'Gorman, E., Beutner, G., Wallimann, T. & Brdiczka, D. Differential effects of creatine depletion on the regulation of enzyme activities and on creatine-stimulated mitochondrial respiration in skeletal muscle, heart, and brain. *Biochim Biophys Acta* **1276**, 161-170 (1996).
128. Zervou, S., Whittington, H.J., Russell, A.J. & Lygate, C.A. Augmentation of Creatine in the Heart. *Mini Rev Med Chem* **16**, 19-28 (2016).
129. Pucar, D., *et al.* Adenylate kinase AK1 knockout heart: energetics and functional performance under ischemia-reperfusion. *Am J Physiol Heart Circ Physiol* **283**, H776-782 (2002).
130. Pucar, D., *et al.* Cellular energetics in the preconditioned state: protective role for phosphotransfer reactions captured by 18O-assisted 31P NMR. *J Biol Chem* **276**, 44812-44819 (2001).
131. Simson, P., *et al.* Restricted ADP movement in cardiomyocytes: Cytosolic diffusion obstacles are complemented with a small number of open mitochondrial voltage-dependent anion channels. *J Mol Cell Cardiol* **97**, 197-203 (2016).
132. Neubauer, S., *et al.* Myocardial phosphocreatine-to-ATP ratio is a predictor of mortality in patients with dilated cardiomyopathy. *Circulation* **96**, 2190-2196 (1997).
133. Mahmod, M., *et al.* The interplay between metabolic alterations, diastolic strain rate and exercise capacity in mild heart failure with preserved ejection fraction: a cardiovascular magnetic resonance study. *J Cardiovasc Magn Reson* **20**, 88 (2018).
134. Phan, T.T., *et al.* Heart failure with preserved ejection fraction is characterized by dynamic impairment of active relaxation and contraction of the left ventricle on exercise and associated with myocardial energy deficiency. *J Am Coll Cardiol* **54**, 402-409 (2009).
135. Burrage, M.K., *et al.* Energetic Basis for Exercise-Induced PulmonaryCongestion in Heart Failure With PreservedEjection Fraction. *Circulation*, CIRCULATIONAHA.121.054858 (2021).
136. Lamb, H.J., *et al.* Diastolic Dysfunction in Hypertensive Heart Disease Is Associated With Altered Myocardial Metabolism. *Circulation* **99**, 2261-2267 (1999).
137. Diamant, M., *et al.* Diastolic dysfunction is associated with altered myocardial metabolism in asymptomatic normotensive patients with well-controlled type 2 diabetes mellitus. *Journal of the American College of Cardiology* **42**, 328-335 (2003).
138. Valkovic, L., *et al.* Increased cardiac Pi/PCr in the diabetic heart observed using phosphorus magnetic resonance spectroscopy at 7T. *PLoS One* **17**, e0269957 (2022).
139. Diamant, M., *et al.* Diastolic dysfunction is associatedwith altered myocardial metabolism inasymptomatic normotensive patientswith well-controlled type 2 diabetes mellitus. *Journal of the American College of Cardiology* **42**, 328-335 (2003).

140. Rayner, J.J., *et al.* The relative contribution of metabolic and structural abnormalities to diastolic dysfunction in obesity. *Int J Obes (Lond)* **42**, 441-447 (2018).
141. Starling, R.C., Hammer, D.F. & Altschuld, R.A. Human myocardial ATP content and in vivo contractile function. *Mol Cell Biochem* **180**, 171-177 (1998).
142. Beer, M., *et al.* Absolute concentrations of high-energy phosphate metabolites in normal, hypertrophied, and failing human myocardium measured noninvasively with (31)P-SLOOP magnetic resonance spectroscopy. *J Am Coll Cardiol* **40**, 1267-1274 (2002).
143. Smith, C.S., Bottomley, P.A., Schulman, S.P., Gerstenblith, G. & Weiss, R.G. Altered creatine kinase adenosine triphosphate kinetics in failing hypertrophied human myocardium. *Circulation* **114**, 1151-1158 (2006).
144. Gabr, R.E., *et al.* Cardiac work is related to creatine kinase energy supply in human heart failure: a cardiovascular magnetic resonance spectroscopy study. *Journal of Cardiovascular Magnetic Resonance* **20**(2018).
145. Bottomley, P.A., *et al.* Metabolic Rates of ATP Transfer Through Creatine Kinase (CK Flux) Predict Clinical Heart Failure Events and Death. *Science Translational Medicine* **5**(2013).
146. O'Sullivan, J.F., *et al.* Cardiac Substrate Utilization and Relationship to Invasive Exercise Hemodynamic Parameters in HFpEF. *JACC: Basic to Translational Science* (2024).
147. Tian, R. & Ingwall, J.S. Energetic basis for reduced contractile reserve in isolated rat hearts. *Am J Physiol* **270**, H1207-1216 (1996).
148. Hamman, B.L., *et al.* Inhibition of the creatine kinase reaction decreases the contractile reserve of isolated rat hearts. *Am J Physiol* **269**, H1030-1036 (1995).
149. Keceli, G., *et al.* Mitochondrial Creatine Kinase Attenuates Pathologic Remodeling in Heart Failure. *Circ Res* **130**, 741-759 (2022).
150. Gupta, A., *et al.* Creatine kinase-mediated improvement of function in failing mouse hearts provides causal evidence the failing heart is energy starved. *Journal of Clinical Investigation* **122**, 291-302 (2012).
151. Tian, R., Nascimben, L., Ingwall, J.S. & Lorell, B.H. Failure to maintain a low ADP concentration impairs diastolic function in hypertrophied rat hearts. *Circulation* **96**, 1313-1319 (1997).
152. Rayner, J.J., *et al.* Myocardial Energetics in Obesity: Enhanced ATP Delivery Through Creatine Kinase With Blunted Stress Response. *Circulation* **141**, 1152-1163 (2020).
153. Rayner, J.J., *et al.* Obesity modifies the energetic phenotype of dilated cardiomyopathy. *Eur Heart J* (2021).
154. Peterzan, M.A., *et al.* Cardiac Energetics in Patients With Aortic Stenosis and Preserved Versus Reduced Ejection Fraction. *Circulation* **141**, 1971-1985 (2020).
155. Murashige, D., *et al.* Comprehensive quantification of fuel use by the failing and nonfailing human heart. *Science* **370**, 364-368 (2020).
156. Gertz, E.W., Wisneski, J.A., Stanley, W.C. & Neese, R.A. Myocardial substrate utilization during exercise in humans. Dual carbon-labeled carbohydrate isotope experiments. *J Clin Invest* **82**, 2017-2025 (1988).
157. Paulson, D.J., Ward, K.M. & Shug, A.L. Malonyl CoA inhibition of carnitine palmityltransferase in rat heart mitochondria. *FEBS Lett* **176**, 381-384 (1984).
158. Young, L.H., Coven, D.L. & Russell, R.R., 3rd. Cellular and molecular regulation of cardiac glucose transport. *J Nucl Cardiol* **7**, 267-276 (2000).
159. Slot, J.W., Geuze, H.J., Gigengack, S., James, D.E. & Lienhard, G.E. Translocation of the glucose transporter GLUT4 in cardiac myocytes of the rat. *Proc Natl Acad Sci U S A* **88**, 7815-7819 (1991).

160. Nuutila, P., *et al.* Glucose-free fatty acid cycle operates in human heart and skeletal muscle in vivo. *J Clin Invest* **89**, 1767-1774 (1992).
161. Russell, R.R., 3rd, Mrus, J.M., Mommessin, J.I. & Taegtmeyer, H. Compartmentation of hexokinase in rat heart. A critical factor for tracer kinetic analysis of myocardial glucose metabolism. *J Clin Invest* **90**, 1972-1977 (1992).
162. Papandreou, I., Cairns, R.A., Fontana, L., Lim, A.L. & Denko, N.C. HIF-1 mediates adaptation to hypoxia by actively downregulating mitochondrial oxygen consumption. *Cell Metab* **3**, 187-197 (2006).
163. Simonsen, S. & Kjekshus, J.K. The effect of free fatty acids on myocardial oxygen consumption during atrial pacing and catecholamine infusion in man. *Circulation* **58**, 484-491 (1978).
164. Puchalska, P. & Crawford, P.A. Metabolic and Signaling Roles of Ketone Bodies in Health and Disease. *Annu Rev Nutr* **41**, 49-77 (2021).
165. Williamson, D.H., Lund, P. & Krebs, H.A. The redox state of free nicotinamide-adenine dinucleotide in the cytoplasm and mitochondria of rat liver. *Biochem J* **103**, 514-527 (1967).
166. Ho, K.L., *et al.* Ketones can become the major fuel source for the heart but do not increase cardiac efficiency. *Cardiovasc Res* **117**, 1178-1187 (2021).
167. Grundler, F., Mesnage, R., Ruppert, P.M.M., Kouretas, D. & Wilhelmi de Toledo, F. Long-Term Fasting-Induced Ketosis in 1610 Subjects: Metabolic Regulation and Safety. *Nutrients* **16**(2024).
168. Monzo, L., *et al.* Myocardial ketone body utilization in patients with heart failure: The impact of oral ketone ester. *Metabolism* **115**, 154452 (2021).
169. Stanley, W.C., Meadows, S.R., Kivilo, K.M., Roth, B.A. & Lopaschuk, G.D. beta-Hydroxybutyrate inhibits myocardial fatty acid oxidation in vivo independent of changes in malonyl-CoA content. *Am J Physiol Heart Circ Physiol* **285**, H1626-1631 (2003).
170. Gormsen, L.C., *et al.* Ketone Body Infusion With 3-Hydroxybutyrate Reduces Myocardial Glucose Uptake and Increases Blood Flow in Humans: A Positron Emission Tomography Study. *J Am Heart Assoc* **6**(2017).
171. Sweatt, A.J., *et al.* Branched-chain amino acid catabolism: unique segregation of pathway enzymes in organ systems and peripheral nerves. *Am J Physiol Endocrinol Metab* **286**, E64-76 (2004).
172. Gao, S., *et al.* Animal models of heart failure with preserved ejection fraction (HFpEF): from metabolic pathobiology to drug discovery. *Acta Pharmacol Sin* **45**, 23-35 (2024).
173. Deng, Y., *et al.* Targeting Mitochondria-Inflammation Circuit by beta-Hydroxybutyrate Mitigates HFpEF. *Circ Res* **128**, 232-245 (2021).
174. Withaar, C., *et al.* The effects of liraglutide and dapagliflozin on cardiac function and structure in a multi-hit mouse model of heart failure with preserved ejection fraction. *Cardiovasc Res* **117**, 2108-2124 (2021).
175. From, A.M., Scott, C.G. & Chen, H.H. The development of heart failure in patients with diabetes mellitus and pre-clinical diastolic dysfunction a population-based study. *J Am Coll Cardiol* **55**, 300-305 (2010).
176. Ernande, L., *et al.* Diastolic Dysfunction in Patients with Type 2 Diabetes Mellitus: Is It Really the First Marker of Diabetic Cardiomyopathy? *J Am Soc Echocardiog* **24**, 1268-U1147 (2011).
177. Hu, L.J., *et al.* The association between diabetes mellitus and reduction in myocardial glucose uptake: a population-based F-18-FDG PET/CT study. *Bmc Cardiovasc Disor* **18**(2018).

178. Labbe, S.M., *et al.* Increased myocardial uptake of dietary fatty acids linked to cardiac dysfunction in glucose-intolerant humans. *Diabetes* **61**, 2701-2710 (2012).
179. Peterson, L.R., *et al.* Effect of obesity and insulin resistance on myocardial substrate metabolism and efficiency in young women. *Circulation* **109**, 2191-2196 (2004).
180. Rijzewijk, L.J., *et al.* Altered myocardial substrate metabolism and decreased diastolic function in nonischemic human diabetic cardiomyopathy: studies with cardiac positron emission tomography and magnetic resonance imaging. *J Am Coll Cardiol* **54**, 1524-1532 (2009).
181. Green, P.G. Cardiac Resynchronisation Therapy and Myocardial Metabolism: Acute and Chronic Effects in Heart Failure. *Doctoral Thesis, University of Oxford* (2021).
182. Hahn, V.S., *et al.* Myocardial Gene Expression Signatures in Human Heart Failure With Preserved Ejection Fraction. *Circulation* **143**, 120-134 (2021).
183. de las Fuentes, L., *et al.* Hypertensive left ventricular hypertrophy is associated with abnormal myocardial fatty acid metabolism and myocardial efficiency. *Journal of Nuclear Cardiology* **13**, 369-377 (2006).
184. Kolwicz, S.C., Jr. & Tian, R. Glucose metabolism and cardiac hypertrophy. *Cardiovasc Res* **90**, 194-201 (2011).
185. Marchandise, S., *et al.* Left Atrial Glucose Metabolism Evaluation by (18)F-FDG-PET in Persistent Atrial Fibrillation and in Sinus Rhythm. *JACC Basic Transl Sci* **9**, 459-471 (2024).
186. Watson, W.D., *et al.* Retained Metabolic Flexibility of the Failing Human Heart. *Circulation* **148**, 109-123 (2023).
187. Green, P.G., *et al.* Metabolic flexibility and reverse remodelling of the failing human heart. *Eur Heart J* **46**, 2422-2433 (2025).
188. Sun, Q., *et al.* Mitochondrial fatty acid oxidation is the major source of cardiac ATP production in heart failure with preserved ejection fraction. *Cardiovasc Res* (2024).
189. Hahn, V.S., *et al.* Myocardial Metabolomics of Human Heart Failure With Preserved Ejection Fraction. *Circulation* (2023).
190. Yoshihisa, A., *et al.* Associations between acylcarnitine to free carnitine ratio and adverse prognosis in heart failure patients with reduced or preserved ejection fraction. *ESC Heart Fail* **4**, 360-364 (2017).
191. Lopaschuk, G.D., Ussher, J.R., Folmes, C.D., Jaswal, J.S. & Stanley, W.C. Myocardial fatty acid metabolism in health and disease. *Physiol Rev* **90**, 207-258 (2010).
192. Leggat, J., Bidault, G. & Vidal-Puig, A. Lipotoxicity: a driver of heart failure with preserved ejection fraction? *Clin Sci (Lond)* **135**, 2265-2283 (2021).
193. Wu, C.K., *et al.* Myocardial adipose deposition and the development of heart failure with preserved ejection fraction. *Eur J Heart Fail* **22**, 445-454 (2020).
194. Wei, J., *et al.* Myocardial steatosis as a possible mechanistic link between diastolic dysfunction and coronary microvascular dysfunction in women. *Am J Physiol Heart Circ Physiol* **310**, H14-19 (2016).
195. Allard, M.F., Schonekess, B.O., Henning, S.L., English, D.R. & Lopaschuk, G.D. Contribution of oxidative metabolism and glycolysis to ATP production in hypertrophied hearts. *Am J Physiol* **267**, H742-750 (1994).
196. Fillmore, N., *et al.* Uncoupling of glycolysis from glucose oxidation accompanies the development of heart failure with preserved ejection fraction. *Mol Med* **24**, 3 (2018).

197. Koleini, N., *et al.* Landscape of glycolytic metabolites and their regulating proteins in myocardium from human heart failure with preserved ejection fraction. *Eur J Heart Fail* (2024).
198. Ritterhoff, J., *et al.* Metabolic Remodeling Promotes Cardiac Hypertrophy by Directing Glucose to Aspartate Biosynthesis. *Circ Res* **126**, 182-196 (2020).
199. Umbarawan, Y., *et al.* Glucose is preferentially utilized for biomass synthesis in pressure-overloaded hearts: evidence from fatty acid-binding protein-4 and -5 knockout mice. *Cardiovasc Res* **114**, 1132-1144 (2018).
200. Voros, G., *et al.* Increased Cardiac Uptake of Ketone Bodies and Free Fatty Acids in Human Heart Failure and Hypertrophic Left Ventricular Remodeling. *Circ Heart Fail* **11**, e004953 (2018).
201. Mizuno, Y., *et al.* The diabetic heart utilizes ketone bodies as an energy source. *Metabolism* **77**, 65-72 (2017).
202. Liao, S., *et al.* beta-Hydroxybutyrate Mitigated Heart Failure with Preserved Ejection Fraction by Increasing Treg Cells via Nox2/GSK-3beta. *J Inflamm Res* **14**, 4697-4706 (2021).
203. Yurista, S.R., *et al.* Exploring The Therapeutic Potential Of Empagliflozin And Oral Ketone Ester In HFpEF: A Study On Cardiac Function, Structure, And Metabolism. *Journal of Cardiac Failure* **30**, 279 (2024).
204. Gopalasingam, N., *et al.* Randomized Crossover Trial of 2-Week Ketone Ester Treatment in Patients With Type 2 Diabetes and Heart Failure With Preserved Ejection Fraction. *Circulation* (2024).
205. Cameron, D., *et al.* Evaluation of Acute Supplementation With the Ketone Ester (R)-3-Hydroxybutyl-(R)-3-Hydroxybutyrate (deltaG) in Healthy Volunteers by Cardiac and Skeletal Muscle (31)P Magnetic Resonance Spectroscopy. *Front Physiol* **13**, 793987 (2022).
206. van de Bovenkamp, A.A., *et al.* Trimetazidine in heart failure with preserved ejection fraction: a randomized controlled cross-over trial. *ESC Heart Fail* (2023).
207. Maier, L.S., *et al.* RAnoLazIne for the treatment of diastolic heart failure in patients with preserved ejection fraction: the RALI-DHF proof-of-concept study. *JACC Heart Fail* **1**, 115-122 (2013).
208. Serati, A.R., Motamedi, M.R., Emami, S., Varedi, P. & Movahed, M.R. L-carnitine treatment in patients with mild diastolic heart failure is associated with improvement in diastolic function and symptoms. *Cardiology* **116**, 178-182 (2010).
209. Bottomley, P.A., Foster, T.B. & Darrow, R.D. Depth-resolved surface-coil spectroscopy (DRESS) for in Vivo 1H, 31P, and 13C NMR. *Journal of Magnetic Resonance (1969)* **59**, 338-342 (1984).
210. Tyler, D.J., *et al.* Reproducibility of 31P cardiac magnetic resonance spectroscopy at 3 T. *NMR Biomed* **22**, 405-413 (2009).
211. Purvis, L.A.B., *et al.* OXSA: An open-source magnetic resonance spectroscopy analysis toolbox in MATLAB. *PLOS ONE* **12**, e0185356 (2017).
212. Vanhamme, L., van den Boogaart, A. & Van Huffel, S. Improved method for accurate and efficient quantification of MRS data with use of prior knowledge. *J Magn Reson* **129**, 35-43 (1997).
213. Tyler, A., *et al.* Compartment-based reconstruction of 3D acquisition-weighted (31) P cardiac magnetic resonance spectroscopic imaging at 7 T: A reproducibility study. *NMR Biomed*, e4950 (2023).
214. Tyler, A., *et al.* Compartment-based reconstruction of acquisition-weighted (31)P cardiac MRSI reduces sensitivity to cardiac motion and scan planning. *Front Physiol* **14**, 1325458 (2023).

215. Schar, M., El-Sharkawy, A.M., Weiss, R.G. & Bottomley, P.A. Triple repetition time saturation transfer (TRiST) 31P spectroscopy for measuring human creatine kinase reaction kinetics. *Magn Reson Med* **63**, 1493-1501 (2010).
216. El-Sharkawy, A.M., Schar, M., Ouwerkerk, R., Weiss, R.G. & Bottomley, P.A. Quantitative cardiac 31P spectroscopy at 3 Tesla using adiabatic pulses. *Magn Reson Med* **61**, 785-795 (2009).
217. Ding, B., *et al.* Water-suppression cycling 3-T cardiac
1
H-MRS detects altered creatine and choline in patients with aortic or mitral stenosis. *NMR in Biomedicine* **34**(2021).
218. Poliner, L.R., *et al.* Left ventricular performance in normal subjects: a comparison of the responses to exercise in the upright and supine positions. *Circulation* **62**, 528-534 (1980).
219. Lee, R., *et al.* Artifactual elevation of plasma sCD40L by residual platelets in patients with coronary artery disease. *Int J Cardiol* **168**, 1648-1650 (2013).
220. DeFronzo, R.A., Tobin, J.D. & Andres, R. Glucose clamp technique: a method for quantifying insulin secretion and resistance. *Am J Physiol* **237**, E214-223 (1979).
221. Spertus, J.A., Jones, P.G., Sandhu, A.T. & Arnold, S.V. Interpreting the Kansas City Cardiomyopathy Questionnaire in Clinical Trials and Clinical Care: JACC State-of-the-Art Review. *J Am Coll Cardiol* **76**, 2379-2390 (2020).
222. Olivotto, I., *et al.* Assessment and significance of left ventricular mass by cardiovascular magnetic resonance in hypertrophic cardiomyopathy. *J Am Coll Cardiol* **52**, 559-566 (2008).
223. Perdrix, L., *et al.* How to calculate left ventricular mass in routine practice? An echocardiographic versus cardiac magnetic resonance study. *Arch Cardiovasc Dis* **104**, 343-351 (2011).
224. Sai, E., *et al.* Association between Myocardial Triglyceride Content and Cardiac Function in Healthy Subjects and Endurance Athletes. *Plos One* **8**(2013).
225. van der Meer, R.W., *et al.* The ageing male heart: myocardial triglyceride content as independent predictor of diastolic function. *Eur Heart J* **29**, 1516-1522 (2008).
226. Petritsch, B., *et al.* Age Dependency of Myocardial Triglyceride Content: A 3T High-Field 1H-MR Spectroscopy Study. *Rofo* **187**, 1016-1021 (2015).
227. Reybrouck, T. & Fagard, R. Gender differences in the oxygen transport system during maximal exercise in hypertensive subjects. *Chest* **115**, 788-792 (1999).
228. Hahn, V.S., *et al.* Endomyocardial Biopsy Characterization of Heart Failure With Preserved Ejection Fraction and Prevalence of Cardiac Amyloidosis. *JACC Heart Fail* **8**, 712-724 (2020).
229. Palstrom, N.B., Matthiesen, R., Rasmussen, L.M. & Beck, H.C. Recent Developments in Clinical Plasma Proteomics-Applied to Cardiovascular Research. *Biomedicines* **10**(2022).
230. Kim, C.X., *et al.* Sex and ethnic differences in 47 candidate proteomic markers of cardiovascular disease: the Mayo Clinic proteomic markers of arteriosclerosis study. *PLoS One* **5**, e9065 (2010).
231. Esterhammer, R., *et al.* Cardiac high-energy phosphate metabolism alters with age as studied in 196 healthy males with the help of 31-phosphorus 2-dimensional chemical shift imaging. *PLoS One* **9**, e97368 (2014).
232. Nathania, M., *et al.* Impact of age on the association between cardiac high-energy phosphate metabolism and cardiac power in women. *Heart* **104**, 111-118 (2018).

233. Katz, A.M. Is the failing heart energy depleted? *Cardiol Clin* **16**, 633-644, viii (1998).
234. Santos, M., *et al.* E/e' Ratio in Patients With Unexplained Dyspnea: Lack of Accuracy in Estimating Left Ventricular Filling Pressure. *Circ Heart Fail* **8**, 749-756 (2015).
235. Cremer, P.C., *et al.* Myosin Inhibition and Left Ventricular Diastolic Function in Patients With Obstructive Hypertrophic Cardiomyopathy Referred for Septal Reduction Therapy: Insights From the VALOR-HCM Study. *Circ Cardiovasc Imaging* **15**, e014986 (2022).
236. Pericas, P., *et al.* Impact of Sacubitril-Valsartan Treatment on Diastolic Function in Patients with Heart Failure and Reduced Ejection Fraction. *High Blood Press Cardiovasc Prev* **28**, 167-175 (2021).
237. Ito, H., *et al.* Cardiovascular magnetic resonance feature tracking for characterization of patients with heart failure with preserved ejection fraction: correlation of global longitudinal strain with invasive diastolic functional indices. *J Cardiovasc Magn Reson* **22**, 42 (2020).
238. Tschope, C., *et al.* The role of NT-proBNP in the diagnostics of isolated diastolic dysfunction: correlation with echocardiographic and invasive measurements. *Eur Heart J* **26**, 2277-2284 (2005).
239. Kostler, H., *et al.* Age and gender dependence of human cardiac phosphorus metabolites determined by SLOOP 31P MR spectroscopy. *Magn Reson Med* **56**, 907-911 (2006).
240. Stubbs, B.J., *et al.* On the Metabolism of Exogenous Ketones in Humans. *Front Physiol* **8**, 848 (2017).
241. Levy, J.C., Matthews, D.R. & Hermans, M.P. Correct homeostasis model assessment (HOMA) evaluation uses the computer program. *Diabetes Care* **21**, 2191-2192 (1998).
242. Abouezzeddine, O.F., *et al.* Myocardial Energetics in Heart Failure With Preserved Ejection Fraction. *Circulation: Heart Failure* **12**(2019).
243. Florian, J.P. & Pawelczyk, J.A. Non-esterified fatty acids increase arterial pressure via central sympathetic activation in humans. *Clin Sci (Lond)* **118**, 61-69 (2009).
244. Gosmanov, A.R., *et al.* Vascular effects of intravenous intralipid and dextrose infusions in obese subjects. *Metabolism* **61**, 1370-1376 (2012).
245. Hundertmark, M.J., *et al.* Assessment of Cardiac Energy Metabolism, Function, and Physiology in Patients With Heart Failure Taking Empagliflozin: The Randomized, Controlled EMPA-VISION Trial. *Circulation* **147**, 1654-1669 (2023).
246. Nielsen, R., *et al.* Cardiovascular Effects of Treatment With the Ketone Body 3-Hydroxybutyrate in Chronic Heart Failure Patients. *Circulation* **139**, 2129-2141 (2019).
247. Berg-Hansen, K., *et al.* Beneficial Effects of Ketone Ester in Patients With Cardiogenic Shock: A Randomized, Controlled, Double-Blind Trial. *JACC Heart Fail* **11**, 1337-1347 (2023).
248. Avogaro, A., *et al.* Myocardial metabolism in insulin-deficient diabetic humans without coronary artery disease. *Am J Physiol* **258**, E606-618 (1990).
249. Ho, K.L., *et al.* Increased ketone body oxidation provides additional energy for the failing heart without improving cardiac efficiency. *Cardiovasc Res* **115**, 1606-1616 (2019).
250. Schwartzenberg, S., *et al.* Effects of vasodilation in heart failure with preserved or reduced ejection fraction implications of distinct pathophysiologies on response to therapy. *J Am Coll Cardiol* **59**, 442-451 (2012).

251. Homilius, C., *et al.* Ketone body 3-hydroxybutyrate elevates cardiac output through peripheral vasorelaxation and enhanced cardiac contractility. *Basic Res Cardiol* **118**, 37 (2023).
252. McCarthy, C.G., *et al.* Ketone body beta-hydroxybutyrate is an autophagy-dependent vasodilator. *JCI Insight* **6**(2021).
253. Selvaraj, S., *et al.* Acute Echocardiographic Effects of Exogenous Ketone Administration in Healthy Participants. *J Am Soc Echocardiogr* **35**, 305-311 (2022).
254. Gambardella, J., *et al.* Ketone Bodies Rescue Mitochondrial Dysfunction Via Epigenetic Remodeling. *JACC Basic Transl Sci* **8**, 1123-1137 (2023).
255. Wallner, M., *et al.* HDAC inhibition improves cardiopulmonary function in a feline model of diastolic dysfunction. *Sci Transl Med* **12**(2020).
256. Jeong, M.Y., *et al.* Histone deacetylase activity governs diastolic dysfunction through a nongenomic mechanism. *Sci Transl Med* **10**(2018).
257. Mogensen, C.E., Christensen, N.J. & Gundersen, H.J. The acute effect of insulin on heart rate, blood pressure, plasma noradrenaline and urinary albumin excretion. The role of changes in blood glucose. *Diabetologia* **18**, 453-457 (1980).
258. Ranasinghe, A.M., *et al.* Glucose-insulin-potassium and tri-iodothyronine individually improve hemodynamic performance and are associated with reduced troponin I release after on-pump coronary artery bypass grafting. *Circulation* **114**, I245-250 (2006).
259. von Lewinski, D., Bruns, S., Walther, S., Kogler, H. & Pieske, B. Insulin causes [Ca2+]i-dependent and [Ca2+]i-independent positive inotropic effects in failing human myocardium. *Circulation* **111**, 2588-2595 (2005).
260. Glatz, J.F., Bonen, A., Ouwens, D.M. & Luiken, J.J. Regulation of sarcolemmal transport of substrates in the healthy and diseased heart. *Cardiovasc Drugs Ther* **20**, 471-476 (2006).
261. Luiken, J.J., *et al.* Insulin stimulates long-chain fatty acid utilization by rat cardiac myocytes through cellular redistribution of FAT/CD36. *Diabetes* **51**, 3113-3119 (2002).
262. Roden, M., *et al.* Mechanism of free fatty acid-induced insulin resistance in humans. *J Clin Invest* **97**, 2859-2865 (1996).
263. Arabi, Y.M., *et al.* Free Fatty Acids' Level and Nutrition in Critically Ill Patients and Association with Outcomes: A Prospective Sub-Study of PermiT Trial. *Nutrients* **11**(2019).
264. Challa, A.A. & Lewandowski, E.D. Short-Chain Carbon Sources: Exploiting Pleiotropic Effects for Heart Failure Therapy. *JACC Basic Transl Sci* **7**, 730-742 (2022).